ACTINIDE NUCLEAR DECAY SCHEMES

A thesis submitted for the Award of the Degree
of Doctor of Philosophy of the University of London

by

STEVEN PAUL HOLLOWAY

The Reactor Centre,
Imperial College of Science and Technology,
Silwood Park,
Ascot,
Berkshire.

May 1983

ABSTRACT

Measurements of the major ^{239}U β^- branching intensities populating levels below 200 keV in ^{239}Np have been made by comparing γ spectra obtained from ^{239}U β^- decay and ^{243}Am α decay. This method eliminated the need for accurate internal conversion coefficient data (which is usually the limiting factor on the accuracy of any β^- branching intensity measurement using accompanying γ decay data) and therefore the values of the ^{239}U β^- branching intensities are much more precise than those currently quoted in the literature. Absolute γ-ray intensities of major transitions following ^{239}U β^- and ^{243}Am α decay have also been determined and $^{243}Am(\alpha-\gamma)$ coincidence studies have confirmed the existence of several weak γ transitions within the ^{239}Np level scheme. Characteristic features of the ^{239}Np level structure have been interpreted using the Unified Model.

A study of the possible effect of chemical composition upon β^- decay transition probabilities has been carried out. It has been suggested that this effect is responsible for the current inconsistency between experimental measurements of the half-life of ^{241}Pu. The effect has been studied in the two β^- emitting isotopes ^{166m}Ho and ^{228}Ra which, unlike ^{241}Pu, produce measurable γ radiations which can be used to observe this effect. In neither case, within the limits of experimental uncertainty, was a correlation between chemical composition and β^- decay transition probability observed.

The nucleus $^{241}Np(T_{\frac{1}{2}} \sim 16m)$ decays by β^- emission to fissile ^{241}Pu. The reaction $^{238}U(\alpha,p)^{241}Np$ has been studied:-

(i) On-line in an attempt to examine the characteristics of the ^{241}Np level structure using $(p-\gamma)$ coincidence techniques, and

(ii) off-line to determine ^{241}Np decay properties and data on the level structure of ^{241}Pu.

The form of the excitation function for this reaction over an α particle energy range of 27 to 37 MeV was determined by the off-line γ-ray analysis of chemically separated Np. An estimate of the ^{241}Np half-life was obtained by γ-ray spectroscopy.

ACKNOWLEDGEMENTS

I should like to record my sincere gratitude to Dr. Brian Hooton, former group leader in Nuclear Physics Division at A.E.R.E. Harwell, for suggesting the programme of work which has formed the basis of this thesis and his many helpful discussions whilst it was carried out. I also wish to express my appreciation to Dr. Desmond MacMahon of the Imperial College Reactor Centre who, as my University supervisor, actively encouraged a close link between the University and A.E.R.E. Harwell and provided invaluable help and counsel during the course of the experimental measurements (performed both at Harwell and the Reactor Centre) and the subsequent data analysis.

I am greatly indebted to Mr. Adrian Talbot of the Neutron Systems Group in Nuclear Physics Division, A.E.R.E. Harwell for his technical assistance and advice throughout the complete duration of my research and to Mr. Frank Shipman and his engineering support staff for their prompt and meticulous construction of various items of equipment necessary to complete this work.

Mr. Gary Cuninghame and Dr. Howard Sims of Chemistry Division, A.E.R.E. Harwell were also extremely helpful during the course of a collaborative experiment involving the use of the Variable Energy Cyclotron and I am extremely grateful to Mr. Hedley Willis (also of Chemistry Division) for performing the necessary chemistry required in various experiments reported in this thesis.

Finally my thanks and appreciation to Mrs. Pamela Pullen and Miss Pamela Frost for the expert typing of this thesis and to the U.K.A.E.A. for financial support throughout the period of my research at A.E.R.E. Harwell.

CONTENTS

LIST OF FIGURES

LIST OF TABLES

CHAPTER 1. INTRODUCTION

1.1 Decay Scheme Data Requirements for the Actinide Nuclides

Many calculations dealing with the design and operation of nuclear fission reactors and associated nuclear plant require an accurate knowledge of the nuclear decay properties of the actinide nuclides (atomic number $Z \geq 89$) as well as the fission product nuclides produced during and after reactor operation. One particular field of reactor physics where nuclear data obtained from experimental observations of nuclear decay schemes is extremely important is in the calculation of the radioactivity levels[1], or heat generation, from the entire reactor, or an individual fuel element, at times ranging from a few seconds to years following shutdown of the reactor. For example, in order to cater for the depressurisation accident in gas-cooled reactors or the loss-of-coolant accident in water reactors it is necessary to know, with reasonable accuracy, the short-term heat generation from irradiated fuel in the reactor core; any emergency core-cooling system must be capable of removing this heat. A knowledge of long-term heat generation is also essential to achieve the safe storage of radioactive waste extracted from spent reactor fuel during reprocessing.

In recent years there has also been a need for the development of reliable techniques for the non-destructive detection and assay of fissionable materials[2]. Prompted principally by nuclear Safeguards requirements and the need of the nuclear industry for improved quality and inventory control methods, the development of reliable non-destructive detection techniques has expanded rapidly over the last ten years. Many of the techniques employed, for example in measuring uranium and plutonium in solid waste, require accurate actinide nuclear data in order to make a quantitative assessment of waste isotopic composition.

Both reactor heat generation calculations and the assaying of fissionable materials require a reliable and detailed data base of nuclear decay properties. The basic decay data requirements are listed in table 1.1. In parallel with these energy independent quantities is also a need for data on energy dependent quantities such as reaction cross-sections and neutron flux levels. The work presented in this thesis will be concerned primarily with the

experimental determination of specific actinide nuclear decay data (i.e. energy independent quantities).

Table 1.1 Decay Data Requirements

half-life
Q values
branching fractions
α decay data; energy and intensity
β decay data; energy, intensity and transition type
γ decay data; energy, intensity and internal conversion coefficients
Spontaneous fission decay data; mean number of neutrons per fission and continuous spectral data
Also included with the above data are their uncertainties

The actinide elements comprise one of several components responsible for heat generation in a reactor, the other components being fission product decay heat, neutron-induced reactions on structural and cladding material producing additional radioactive species which liberate decay heat, delayed neutron induced fission decay heat and the production of heat from spontaneous fission neutron induced reactions within the fuel constituents, fission products and cladding material following reactor shutdown.

During irradiation of natural uranium fuel, the nuclide ^{238}U undergoes neutron capture (n,γ) with the formation of the nuclides ^{239}U, ^{239}Np and ^{239}Pu. However these are not the only radioactive species produced as a result of neutron induced transmutations in the fuel since it is possible through (n,α), (n,γ) and $(n,2n)$ reactions and subsequent α and β decay to create numerous heavy elements and actinides during reactor operation. A number of these isotopes are themselves fissile with their own characteristic fission properties.

Hence, following reactor shutdown, there remain many radioactive species which arise as a result of neutron-induced transmutation of the fuel constituents. The radiation subsequently emitted, in the form of α, β and γ-rays, is an important component of reactor heat.

The relevance of actinide nuclear data to decay heat generation can be seen by considering a simple method of calculating the actinide component of decay heat in a uranium fuelled reactor. For times up to 10 days following shutdown, the principal nuclides responsible for the actinide component of decay heat are ^{239}U and ^{239}Np which have radioactive half-lives of 23.5 minutes and 2.35 days respectively.

Let R be the (constant) neutron absorption rate in ^{238}U (i.e. the maximum production rate of both ^{239}U and ^{239}Np). The number of atoms N_1 and N_2, of ^{239}U and ^{239}Np respectively, may be described by

$$\frac{dN_1}{dt} = R - \lambda_1 N_1 \tag{1.1}$$

$$\frac{dN_2}{dt} = \lambda_1 N_1 - \lambda_2 N_2 \tag{1.2}$$

where λ_1 and λ_2 are the radioactive decay constants of ^{239}U and ^{239}Np respectively.

Assuming that the ^{238}U is steadily replenished, or that its depletion may be neglected during an irradiation period T, then at a time t following shutdown the decay heat components H_1 and H_2, due to ^{239}U and ^{239}Np respectively, are given by

$$H_1 = E_1 R(1 - e^{-\lambda_1 T})e^{-\lambda_1 t} \tag{1.3}$$

$$H_2 = E_2 R\left\{\left[1 + \frac{(\lambda_2 e^{-\lambda_1 T} - \lambda_1 e^{-\lambda_2 T})}{(\lambda_1 - \lambda_2)}\right]e^{-\lambda_2 t} + \frac{\lambda_2}{(\lambda_1 - \lambda_2)}(e^{-\lambda_2 t} - e^{-\lambda_1 t})(1 - e^{-\lambda_1 T})\right\} \tag{1.4}$$

where E_1 and E_2 represent the total absorbable energy release (mean β plus mean γ) per disintegration of ^{239}U and ^{239}Np respectively.

The mean β energy per decay is defined as the average energy of all electron emissions and therefore includes β^-, conversion electrons

and Auger electrons whilst the total γ energy per decay includes all electromagnetic radiation such as γ-rays, X-rays, annihilation radiation and bremsstrahlung. Thus the parameters E_1 and E_2 are strongly dependent on the measured absolute fractional intensities per disintegration of the various radiations produced during de-excitation as well as their associated absolute energies.

Equations similar to those developed above are applicable to the evaluation of short-term decay heat in a uranium-thorium reactor system in which the thorium is used to breed fissile ^{233}U and the principal short-term actinide decay heat components are ^{233}Th and ^{233}Pa (with half-lives of 22.3 minutes and 27.1 days respectively). The production and subsequent decay (for example by α-emission or spontaneous fission) of other actinide isotopes requires the introduction of an additional term in order to calculate the total absorbable energy release; this term is the mean α energy per decay and is essentially the mean energy of all heavy particles including α particles, recoil nuclei, protons, neutrons and spontaneous fission fragments. In recent years the development of computers has enabled the calculation of actinide decay heat by a more rigorous treatment. The reactions normally considered in calculating the inventory during irradiation of each nuclide are its own radioactive decay and total neutron absorption, its production from α and β decay of parent nuclides and production from (n,γ) and $(n,2n)$ reactions in other species present. Such reactions lead, mathematically, to a linear system of coupled first-order differential equations which may be represented in matrix notation by

$$\frac{dN}{dt} = [A] \times \underline{N}$$

where N is the column vector of inventories and matrix [A] contains details of decay constants and reaction rates. Due to the complexity of the couplings in the case of the actinides the equations must be solved by numerical integration and therefore several computer codes have been developed to calculate the actinide contribution to total decay heat output. (See, for example, table 7 of Tobias[1] for details of actinide summation codes currently in use.) Each code must have access to a reliable library of actinide nuclear decay data in order to predict accurately the variation in actinide decay heat as a function of time.

As mentioned earlier, actinide nuclear decay data has also assumed an important role in fuel safeguards and accountancy measurements where, for example, passive γ-ray detection techniques used to assay and determine the isotopic composition of the fuel or radioactive waste requires a prior knowledge of accurate absolute γ-ray intensities.

Thus, in the last few years there has been an intense effort to evaluate decay data for the actinide and heavy elements. These efforts have been concentrated in France, the U.S.A. and the U.K.[3] and it is in response to requests from the U.K. Chemical Nuclear Data Committee for more reliable and accurate actinide decay data that much of the work presented in this thesis has been carried out.

1.2 Summary of Present Measurements

The work presented in this thesis has been concerned with:-

(i) Determining specific nuclear decay data for the actinide nuclides ^{239}U, ^{243}Am and ^{241}Np.

(ii) A study of the possible effect of chemical composition upon β^- decay transition probabilities.

A study of the γ decay from excited states in the daughter nucleus ^{239}Np has permitted the β^- branching intensities in the decay of the parent ^{239}U to be measured. The experimental method involved a comparison of γ-ray intensities resulting from the decay of ^{239}U produced by the $^{238}U(n,\gamma)^{239}U$ reaction with the intensities of the same γ-rays resulting from the α decay of ^{243}Am. In this manner it was possible to eliminate the requirement for accurate internal conversion coefficient data which is usually the major uncertainty component in any β^- branching intensity measurement performed using accompanying γ decay data. Absolute γ-ray transition intensities following ^{239}U β^- decay and ^{243}Am α decay were also determined and ^{243}Am $(\alpha-\gamma)$ coincidence studies confirmed the previously reported existence of several low energy, weak intensity γ-rays within the ^{239}Np level scheme. The β^- and γ data obtained for ^{239}U is directly relevant to the problem of predicting short-term decay heat production in a uranium fuelled reactor as discussed above.

The β^- emitting actinide ^{241}Np ($T_{\frac{1}{2}} \sim 16m$) has received little attention hitherto but an investigation of its decay characteristics

would provide information on the level structure of fissile ^{241}Pu, an important actinide produced mainly by successive neutron capture events in irradiated ^{239}Pu which, together with other Pu isotopes, tends to maintain the overall reactivity of a thermal reactor fuelled with natural or partially enriched uranium. Using the Harwell Variable Energy Cyclotron ^{241}Np was synthesised by the $^{238}U(\alpha,p)^{241}Np$ reaction and on-line (p-γ) coincidence measurements were performed in an attempt to examine the excited level structure of ^{241}Np itself whilst its associated decay properties were examined off-line by γ spectroscopy of chemically separated Np. The form of the excitation function for this reaction over an incident α particle energy range of 27 to 37 MeV was also determined by the off-line γ-ray analysis to enable selection of a suitable α beam energy which would maximise the ^{241}Np yield and simultaneously minimise interference from ^{239}Np and ^{240}Np also produced during the α particle bombardment of ^{238}U.

Despite the high accuracy attained in various experiments for the measurement of the half-life of ^{241}Pu the experimental data do not agree, one with another, sufficiently well[4]. It has been suggested that in addition to normal continuum β^- decay the probability for the bound state capture of an emitted β^- particle into a vacancy in an outer atomic shell of the daughter atom is greatly dependent on the chemical bonding and, under some conditions, can compromise a substantial part of the whole β^- decay probability. The magnitude of the effect, manifesting itself experimentally as a change in observed half-life, increases with decreasing β^- end-point energy and has been estimated theoretically to account for ~1% of the total β^- decay probability for tritium ($E_{\beta max}$ = 18.6 keV) and could be much larger in the case of ^{241}Pu ($E_{\beta max}$ = 20.8 keV). It is not easy to measure a variation in the β^- decay emission probability for ^{241}Pu since the final ^{241}Am nucleus has a long half-life and there are no direct observable γ-rays.

Therefore two different experimental methods have been applied to two low energy β^- emitting isotopes which result in measurable radiations (i.e. the emission of γ-rays) and where the effect may possibly be observed.

The first method consists of measuring the relative intensity of two radiations, one of which is expected to vary with chemical composition. It has been applied to the rare-earth isotope ^{166m}Ho (formed by the reaction $^{165}Ho(n,\gamma)^{166m}Ho$) where the two β^- branches lead to observable γ-rays and only one, the low energy β^- transition, is expected to be affected by the chemical composition.

The second method is based on an ingrowth measurement. If the transition probability for β^-'s is affected by chemical composition then the effect will be seen in a daughter product as a change in specific activity as the daughter approaches a new level of secular equilibrium. Experiments have been performed to detect a change in the 6 hour activity of ^{228}Ac after modifying the chemical state of the parent ^{228}Ra.

REFERENCES

1. A. Tobias, C.E.G.B. Report No. RD/B/N4611 (1979).

2. R. Sher and S. Untermeyer, The Detection of Fissionable Materials by Non-destructive means (The American Nuclear Society, 1980) ch. 5.

3. A. L. Nichols and M. F. James, Heavy element decay data; progress report for the I.A.E.A. coordinated Research programme on the measurement and evaluation of transactinium isotope nuclear decay data (May 1979), CNDC(79) P5.

4. Y. A. Ellis, Nucl. Data Sheets 23, 123 (1978).

CHAPTER 2. ^{239}U β^- DECAY

2.1 Current Status of Specific Nuclear Decay Data for ^{239}U

Following a series of United Kingdom Chemical Nuclear Data Committee (U.K.C.N.D.C.) and International Atomic Energy Agency (I.A.E.A.) coordinated research programme meetings on the measurement and evaluation of actinide isotope decay data it has been possible to compile a list of specific actinide decay properties which, because of their importance in nuclear technology and in various aspects of the nuclear fuel cycle, require further experimental measurement. Decay data for the uranium and plutonium isotopes maintain the highest priority on the U.K.C.N.D.C. and I.A.E.A. lists[1-3] which also provide recommendations for the required accuracies to be achieved in any future measurements.

In the case of ^{239}U β^- decay the I.A.E.A. has requested accuracies of the order of 1% for the ^{239}U half-life, 2% for the intensity of the major β^- branch feeding the 74.67 keV level in the ^{239}Np daughter and 2% for the accompanying major γ transition intensity which decays to the ^{239}Np ground state; the achieved accuracies to date, according to the most recent Table of Isotopes[4] and Nuclear Data Sheets[5], are of the order of 0.2% for the half-life and 10% for the major γ transition intensity. The intensities of the major β^- branches quoted in the literature[4,5] have been evaluated from β^- spectroscopy experiments and separate measurements of relevant γ-ray and internal conversion electron intensities; the γ and conversion electron data have been used to deduce the β^- branching intensities by considering the intensity balance requirements within the level scheme of the ^{239}Np daughter. Therefore, the major β^- branching intensities currently quoted are only as accurate as the existing β^-,γ and internal conversion electron data; for example, the current uncertainty in the intensity of the major β^- branch feeding the 74.67 keV level in ^{239}Np is of the order of 14%. Fig. 2.1 shows those levels in ^{239}Np fed strongly by ^{239}U β^- decay and table 2.1 lists the currently accepted values for the major β^- branching intensities together with their uncertainties.

The earliest measurements on the β^- branching intensities to the ground state and 74.7 keV level in ^{239}Np were performed by

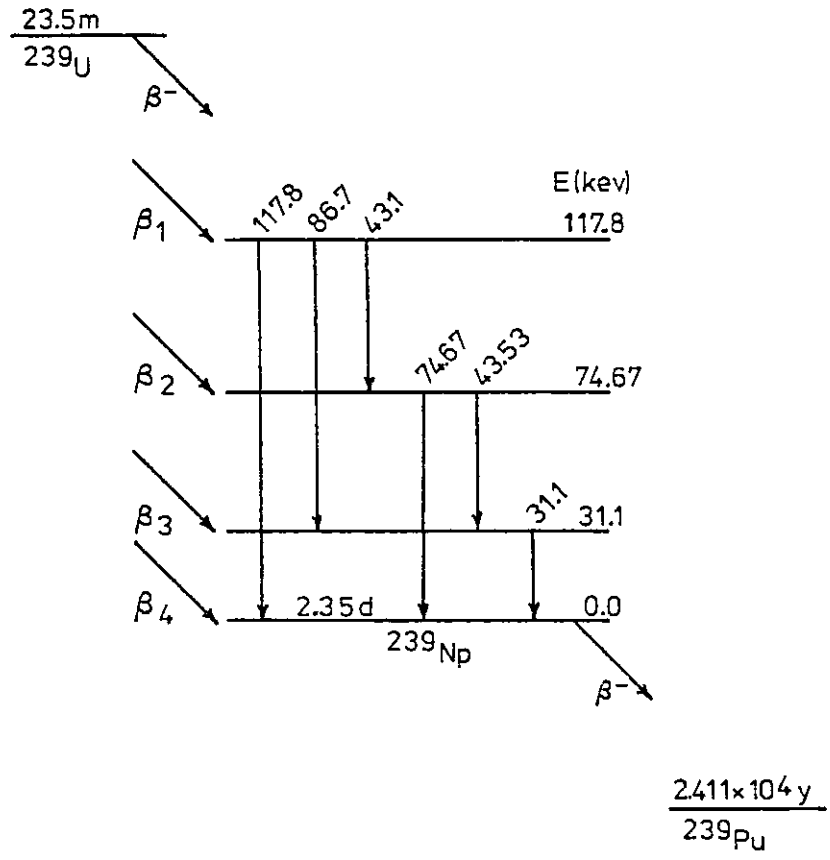

Fig. 2.1 ^{239}Np partial level scheme showing low energy states fed by major β^- branches from ^{239}U decay and accompanying low energy γ transitions. The subsequent β^- decay of ^{239}Np produces numerous γ transitions within the level scheme of ^{239}Pu

Blinowska et al.[6] who resolved a ^{239}U singles β^- spectrum into two components with end-point energies of 1285 and 1211 keV. The intensities of the two β^- branches were measured to be $I_{1285} = (20 \pm 4)\%$ and $I_{1211} = (80 \pm 4)\%$ although a $\beta^-\gamma$ coincidence experiment predicted $I_{1285} = (26 \pm 6)\%$. There was no experimental evidence for a significant β^- branch to the 31.1 keV level although an upper limit of a 10% β^- feed to this level and a 4% β^- branch to the 117.8 keV level were deduced from theoretical considerations. These direct β^- intensity measurements have subsequently been adjusted to take into account more recent γ and internal conversion electron data[7,8] and, from intensity balance considerations, it has been possible to arrive at the β^- branching intensities listed in table 2.1. The four β^- branches shown in fig. 2.1 account for 99% of all β^- transitions; the remaining 1% of β^- transitions are quoted[5]

as being divided approximately equally between lower energy β^- branches feeding levels at 662.3 (0.25%), 819.2 (0.27%), 844.1 (0.25%) and 964.4 keV (0.23%).

The currently accepted intensity of the 74.67 keV γ-ray is $(0.50 \pm 0.05)\gamma$ per decay[4,5], although two other unpublished values of (0.48 ± 0.02) and 0.593 (with no ascribed error) are also listed in the most recent Nuclear Data Sheets evaluation[5].

Therefore, because of the large uncertainties which currently exist in ^{239}U β^- and γ decay data, a series of experiments has been performed to determine the major β^- branch and γ transition intensities, paying particular attention to U.K.C.N.D.C. and I.A.E.A. recommendations regarding final experimental accuracies.

Table 2.1 Currently accepted ^{239}U major β^- branching intensities

(Taken from ref. 5)

β^- Branch	E_{β^-} (keV)	Absolute β^- Branch Intensity (%)
β_1	1168	≃ 2
β_2	1211	73 ± 10
β_3	1254	≃ 6
β_4	1285	18 ± 8

2.2 Measurement of ^{239}U β^- Branching Intensities

Since the measurement of a multiple branch β^- decay is extremely difficult by direct β^- spectroscopy because of the continuous energy spectrum characteristic of β^- decay, the most satisfactory method of determining β^- branching intensities is to calculate the data from the measured γ decay. However, γ emission is not the only process by which a nucleus may lose energy. A process which competes strongly with γ emission, especially in the heavy nuclei, is internal conversion. This is the general name given to the ejection of an atomic electron into a free (unbound) state; the electron will have a kinetic energy less than the γ transition energy by an amount equal to the binding energy of the atomic shell from which it was ejected. The total

internal conversion coefficient (ICC) for a particular transition is defined as the ratio of electron emission probability to γ emission probability. As the atom returns to the ground state the ejection of an Auger electron is a competitive process to the emission of characteristic X-rays[9]; in the actinides X-ray emission is the dominant process accompanying the ejection of an internal conversion electron. The high degree of internal conversion associated with the actinides results in the internal conversion electron data contributing significantly to the production of a comprehensive decay scheme and, therefore, any γ decay data must also be complemented by internal conversion electron data if values for absolute transition intensities (and hence β^- branching intensities) are to be accurately determined. However, because of the experimental difficulty in obtaining and resolving internal conversion electron data, the accuracy of any β^- branching intensity measurement is limited by the uncertainty in the experimental conversion electron data.

In the present work measurements of the major β^- branching intensities in the decay of ^{239}U to ^{239}Np have therefore been made by comparing γ spectra obtained from ^{239}U β^- decay and ^{243}Am α decay which both populate levels in ^{239}Np. This comparison method eliminates the need for accurate internal conversion coefficient data. Fig. 2.2 shows those levels in ^{239}Np populated by major β^- and α transitions from ^{239}U and ^{243}Am decay respectively.

To a first approximation (i.e. neglecting feeding from the decay of higher excited states) the measured intensity of a particular γ-ray in the decay scheme from ^{239}U β^- decay is given by

$$I_\gamma(\beta^-) = N_o(\beta^-)\beta_j F_\gamma \varepsilon_\gamma \qquad (2.1)$$

where $N_o(\beta^-)$ is the absolute β^- decay source strength, β_j is the unknown β^- branching intensity feeding the level j from which this γ transition originates, F_γ is the fraction of level decays which produce this particular γ-ray and ε_γ is the absolute γ-ray detection efficiency. To take into account the feeding of the level by the decay of higher excited states, correction terms (dependent upon internal conversion coefficient data) must be included in the

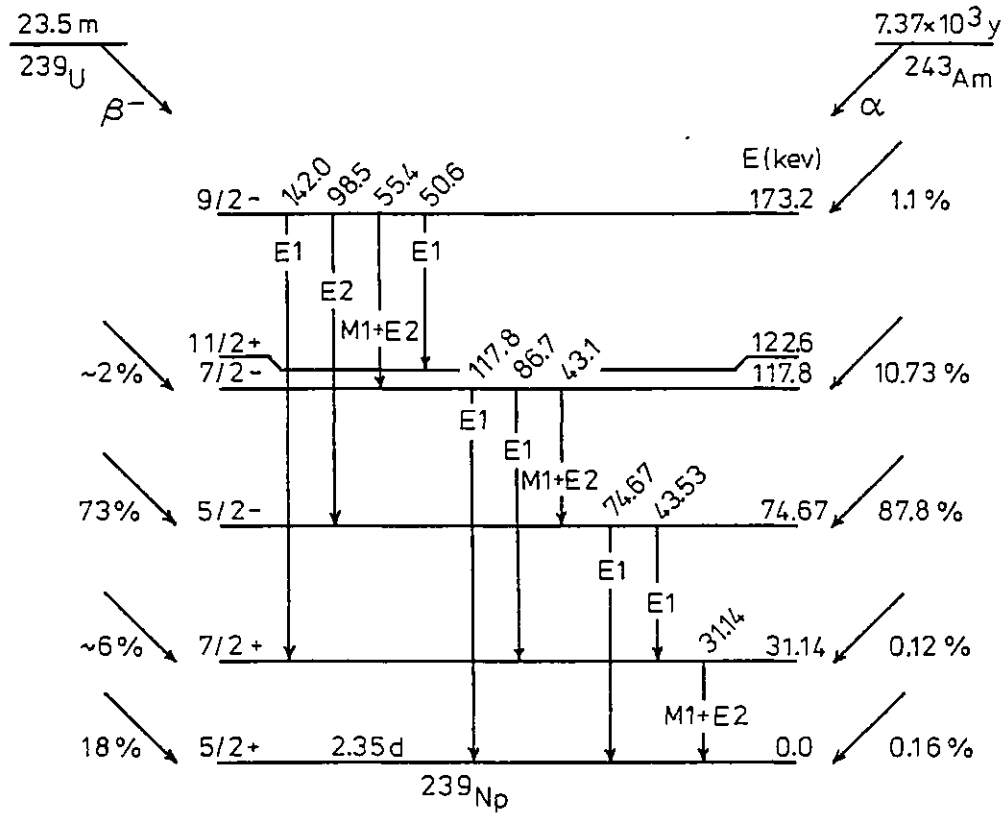

Fig. 2.2 ^{239}Np partial level scheme showing levels fed by major β^- and α branches from ^{239}U and ^{243}Am decay respectively

expression for $I_\gamma(\beta^-)$. In general F_γ in eqn. 2.1 is unknown because of internal conversion and γ branching but, since the mode of decay of the level is independent of the mode of formation, a similar experiment using ^{243}Am α decay would give

$$I_\gamma(\alpha) = N_o(\alpha)\alpha_j F_\gamma \varepsilon_\gamma \qquad (2.2)$$

where $N_o(\alpha)$ is the absolute α activity, α_j is the well-known α branching ratio and, again, terms due to feeding from the decay of higher states have been ignored in the approximate expression for $I_\gamma(\alpha)$. If these two measurements are combined then the full expression for β_j is given by

$$\beta_j = \frac{N_o(\alpha)\ I_\gamma(\beta^-)}{N_o(\beta^-)\ I_\gamma(\alpha)}\ \alpha_j + \text{terms resulting from decay of higher excited states}$$

and an independent measurement of $F_\gamma \varepsilon_\gamma$ is not required. The correction terms, to allow for the population of the level by the decay of higher excited states within the level scheme, do require a knowledge of the total internal conversion coefficients of those transitions which feed the level. Although the uncertainties in the internal conversion coefficients used in the correction terms may be large, the overall uncertainty in the calculated β^- branch intensity will be mainly due to the uncertainties associated with the leading term in the expression for β_j which is independent of internal conversion coefficient data. The intensity of the β^- branch feeding the ^{239}Np ground state is to be calculated by making all ^{239}U β^- transitions sum to 100%. The measured γ-ray intensity is to be determined only from those γ interactions which deposit their full incident energy in the detector (i.e. those which undergo either a single photoelectric absorption or multiple Compton scattering followed by photoelectric absorption within the detector) and is therefore characterised by the number of events per second entering the full energy (photoelectric) peak[10].

Hence, in order to determine the β^- branching intensities feeding the excited states in ^{239}Np a knowledge of the absolute β^- and α activities of the ^{239}U and ^{243}Am sources respectively is required together with measured γ-ray photopeak area data obtained from certain transitions within the level scheme of fig. 2.2 which are common to both α and β^- decay modes. The next three sections of this chapter are therefore concerned with:-

(i) The production of ^{239}U sources and the measurement of their absolute β^- activities and γ-ray photopeak areas,

(ii) the measurement of the ^{243}Am source absolute α disintegration rate and determination of γ-ray photopeak areas under identical experimental conditions as used in (i), and

(iii) the determination of the ^{239}U β^- branching intensities from the data obtained in (i) and (ii).

2.3 ^{239}U γ Spectroscopy and Disintegration Rate Measurements

2.3.1 Source preparation

^{239}U sources were produced by the reaction $^{238}U(n,\gamma)^{239}U$ using the Imperial College 100 kW research reactor. A few mg of uranium nitrate in solution (uranium content = 99.999% ^{238}U and typical concentration of 1 mg uranium per 0.1 ml of water) were irradiated in the reactor in a thermal neutron flux density of approximately 10^{11} neutrons cm^{-2} s^{-1} and where the fast/thermal flux density ratio was of the order of 6×10^{-2}. A low fast/thermal flux density ratio was necessary to reduce the possibility of fission product contamination of the ^{239}U source.

After the irradiation period (varying from 45 to 90 mins duration) a small volume of the active ^{239}U solution was placed on a thin (~ 15 μg cm^{-2}) film of VYNS metalised on both sides with an evaporated coating of gold (~ 10 μg cm^{-2} on each side) and then rapidly dried under an infra-red lamp before transferring to the counting position for γ-ray analysis. Since ^{239}U has only a 23.5 minute half-life it was essential that the source preparation stage following the end of the irradiation be completed quickly in order to obtain good counting statistics from the ^{239}U source and to reduce interference from the 2.35 day β^- emitting ^{239}Np daughter.

Five sources were prepared for γ-ray analysis and subsequent absolute β^- activity measurement. Each source was approximately 1 mm in diameter and the thin VYNS film on which each source was mounted allowed β^- emission into 4π geometry. Two stronger, extended sources were made and counted to determine relative γ-ray intensities and the purity of the ^{239}U; γ spectroscopy revealed no detectable radioactive contaminant which could not be accounted for in the background and all γ and X-ray peaks were identified as originating from either the parent ^{239}U or daughter ^{239}Np β^- decay.

2.3.2 ^{239}U γ spectroscopy

A large volume (15 cm^2 x 1 cm) planar intrinsic Ge detector suitable for low energy γ and X-ray spectroscopy was used to determine the photopeak areas of selected γ transitions occuring in the decay of ^{239}U. The pulse processing system consisted of a high resolution γ spectroscopy amplifier and a Canberra "Series 80"

multichannel analyser. Gamma spectra were recorded over 4096 channels corresponding to an energy range of approximately 0-410 keV and stored on floppy disc for subsequent analysis. The detector resolution was measured to be 0.75 keV full width at half maximum peak height (FWHM) at a γ-ray energy of 122 keV.

A 6 mm thick perspex absorber was used to stop the ^{239}U and ^{239}Np β^-'s entering the Ge detector and a source-detector distance of 105 mm was used to minimise γ-ray pile-up effects which can result in the loss of counts from the photopeak due to accidental summing of two (or more) γ transitions within the inherent resolving time of the detector or pulse processing system. For a resolving time τ_R following a typical signal pulse and a random pulse rate $r_s (r_s \tau_R << 1)$, the rate at which coincidences occur should be the fraction of all time which lies within τ_R of a preceding pulse (given by $r_s \tau_R$) multiplied by the rate of pulse arrival (r_s), or $r_{chance} = r_s^2 \tau_R$. Therefore the accidental (or chance) summing rate will be proportional to the square of the counting rate. The resolving time τ_R is normally set by the shaping time constant of the linear amplifier used in the pulse processing chain from the detector. Visual evidence for accidental pile-up is provided by the presence of sum peaks in the γ spectrum of interest corresponding to the sum of two (or more) full energy pulses. Pile-up corresponding to the summing of pulses from Compton scattered photons or Compton scattered photons plus full energy event pulses is less obvious since it results only in an increase in the continuous background spectrum level. Examination of the γ spectra obtained from each of the five effective point ^{239}U sources revealed no evidence of pile-up in the form of accidental sum peaks. However, evidence for accidental summing was provided by the two extended sources in which a sum peak at 149.4 keV (γ74.7 + γ74.7) was present in the γ spectra; using the expression for r_{chance} it was estimated that accidental summing was responsible for ~ 0.5% loss in counts from the intense 74.7 keV γ photopeak area for both these sources.

Fig. 2.3 shows a typical low-energy γ spectrum obtained from a ^{239}U source. The γ-rays at 31.14, 43.54, 74.69 and 86.75 keV are established transitions in ^{239}Np. The 117.8 keV ground-state γ transition in ^{239}Np is partially masked by the 117.49 keV Np $K\beta_2'$ X-ray and 117.26 Pu $K\beta_1'$ X-ray. Since the 43.1 keV transition

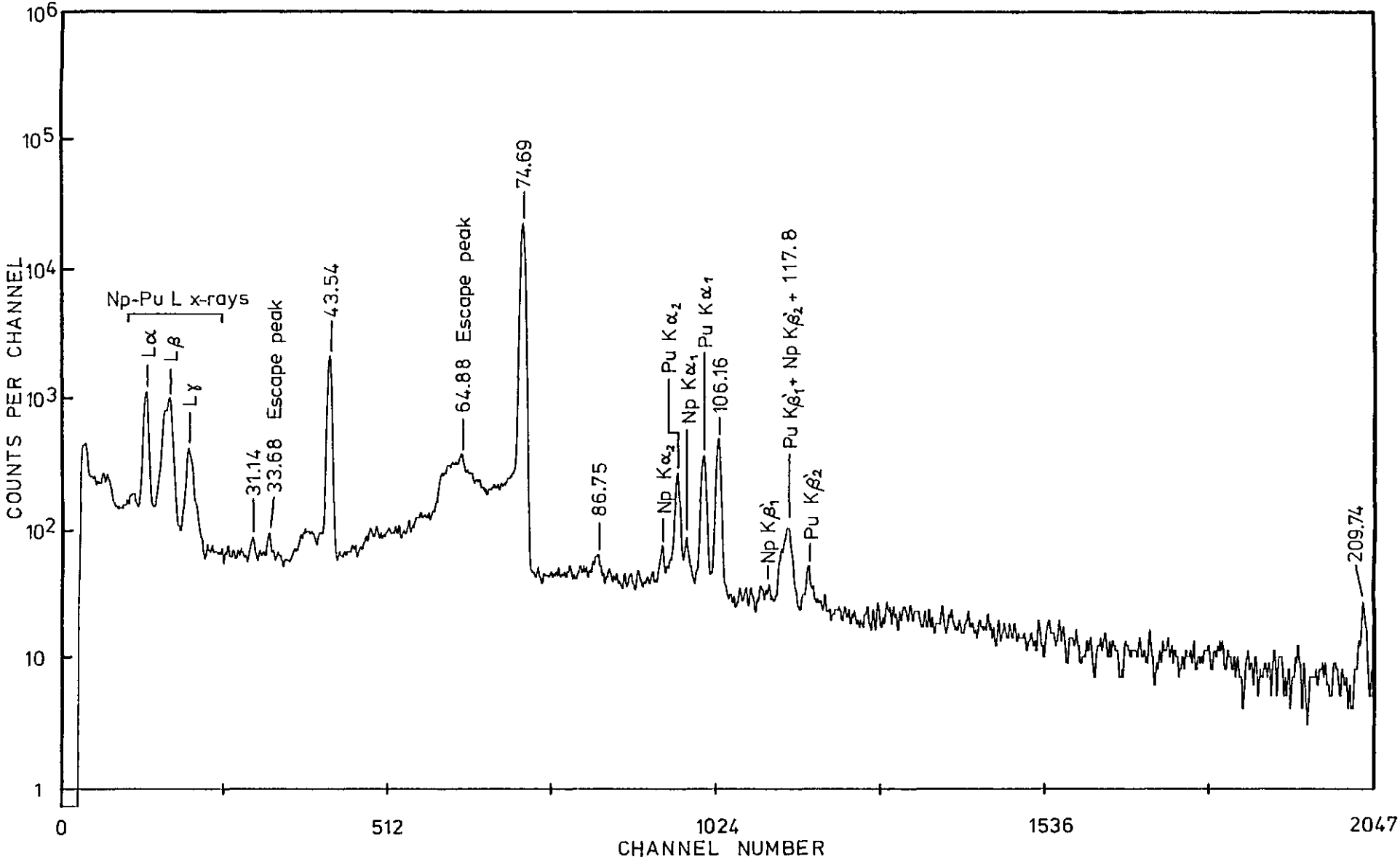

Fig. 2.3 Low energy ^{239}U γ-ray spectrum measured with 15 cm^2 x 10 mm Ge detector. Counting time 1000s

depopulating the 117.8 keV level in ^{239}Np (fig. 2.2) cannot be experimentally resolved from the 43.54 keV γ transition then a quantitative determination of the relative intensity of the members of this doublet is not possible, neither is it necessary; for the purpose of determining the β^- branch intensity feeding the 74.67 keV level in ^{239}Np it is possible to utilise the γ decay data from the accompanying 74.67 keV transition which depopulates this particular level rather than use the γ decay data of the 43.54 keV transition which also depopulates the 74.67 keV level, but whose measured intensity will contain a certain (unknown) fraction of events from the unresolved 43.1 keV transition which is populated by a different lower energy β^- branch. The γ-ray at 106.16 keV is a transition in the level scheme of ^{239}Pu resulting from the rapid growth of the ^{239}Np (2.35d) daughter in the source. The ^{239}Np daughter continues to grow into the source until its maximum activity level is reached $\simeq$ 2.8 hrs following the end of the reactor irradiation period and thereafter decays with its characteristic half-life. The peaks at 33.68 and 64.88 keV are identified as escape peaks of the 43.54 and 74.69 keV γ transitions; the escape of characteristic X-rays from germanium following photoelectric absorption can be significant for γ detectors with a large surface to volume ratio and result in a peak in the γ spectrum at 9.85 keV below the photopeak, with the energy difference corresponding to the characteristic K X-ray energy for germanium. The broad peaks at $\simeq$ 39 and 63 keV are the back-scattered peaks associated with the intense 43.54 and 74.69 keV γ transitions and are the result of Compton scattering of source γ-rays in the materials surrounding the detector.

Fig. 2.4 (upper trace) shows a γ spectrum obtained from the same source five hours after the end of the irradiation period; the ^{239}U initially present (see lower trace of fig. 2.4) has decayed sufficiently as to be no longer observable and therefore the upper spectrum is essentially the γ spectrum from the β^- decay of a ^{239}Np source. The γ-rays at 61.48, 106.16, 209.74, 228.16, 277.63, 285.30, 315.93 and 334.18 keV are major transitions in ^{239}Pu. The peaks at 241.7, 295.0 and 351.7 keV are also present in the background spectrum and are identified as intense transitions in the ^{238}U natural decay chain. Similarly, the background peaks at 238.6 and 338.4 keV are identified as belonging to the ^{232}Th natural decay chain.

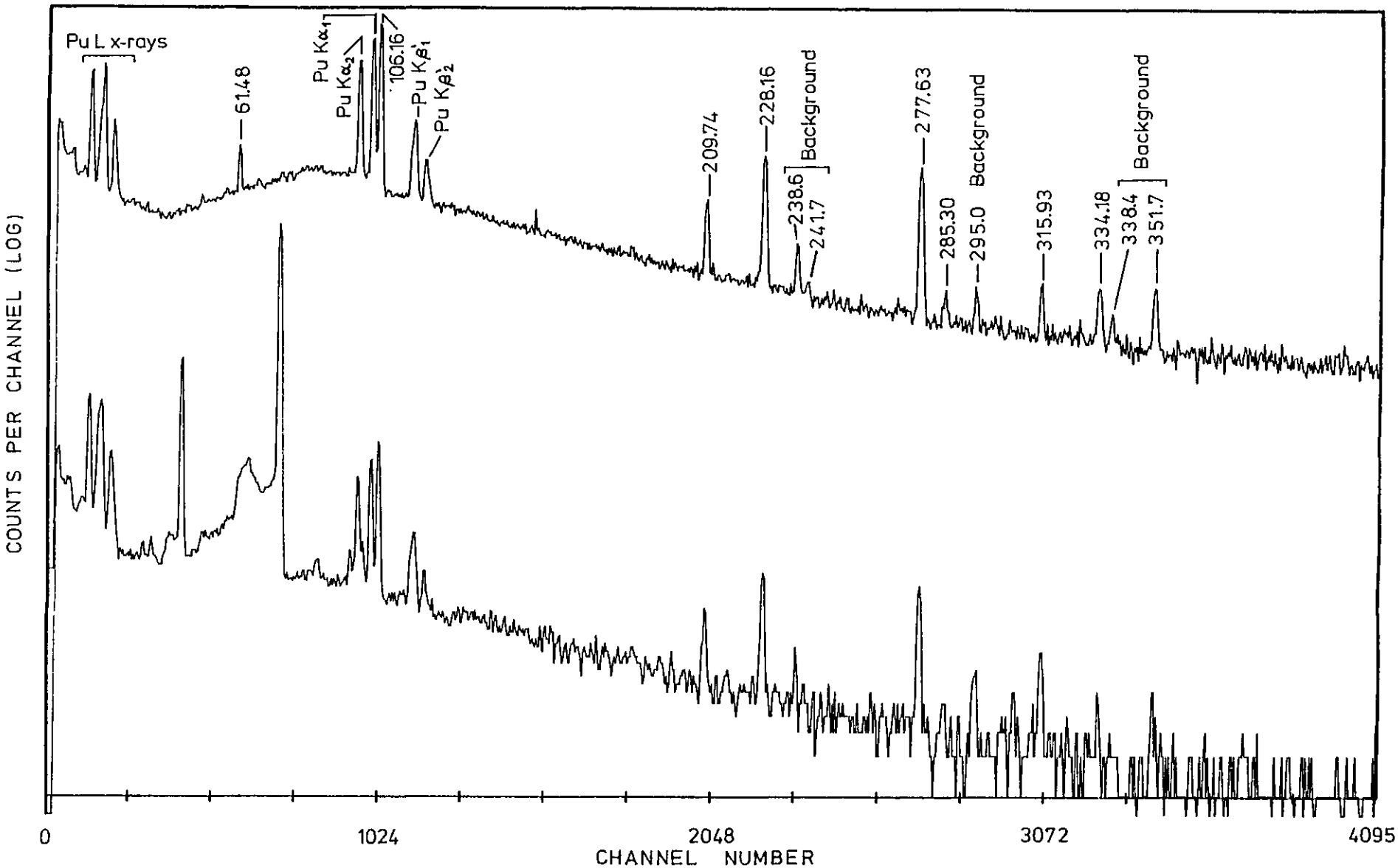

Fig. 2.4 ^{239}Np γ-ray spectrum (upper trace) following decay of ^{239}U parent (lower trace) measured with 15 cm^2 x 10 mm Ge detector. 20,000s ^{239}Np γ spectrum accumulation period

An analysis of the γ spectra obtained from each ^{239}U source revealed no signs of source impurity and all γ transitions could be attributed to either the parent ^{239}U β^- decay, the ^{239}Np daughter β^- decay or background decay.

2.3.3 Measurement of peak areas

The purpose of any peak analysis, manual or computerised, is to provide a representation of the area and position of a peak that is independent of the experimental conditions and spectral backgrounds. Therefore as long as the same method is used to represent the areas for the ^{239}U and ^{243}Am γ spectra (and later the detector efficiency calibration spectra used to determine absolute γ-ray intensities), it is not necessary to determine, or even define, a 'true' area since the value which is obtained for the area will depend upon the functional forms used to describe both the peak and the background. The review of Kokta[11] provides a general discussion of peak area measurement, and Helmer et al.[12] have made some quantitative comparisons of different peak fitting routines.

The method of peak area analysis used throughout this experiment involved representing the background by a linear function and determining the number of counts in a peak that were above the background level. The background level was determined by averaging the counts in a specified number of channels on either side of the peak to determine the average background levels and then fitting a straight line between these averaged values. The net peak area, A_p, is given by the expression

$$A_p = I - \frac{N}{2}(B_1 + B_2)$$

where

I = the total number of counts between the cursors located at channels u and v

$N = v - u + 1$ = the number of data channels

$B_1 = \frac{1}{k}\left[\sum_{a=u}^{u+k-1} X_a\right]$ = estimated height of the background on the left of the peak; X_a are the number of counts in channel a and k is the number of channels used to estimate the background on either side of the peak.

$$B_2 = \frac{1}{k}\left[\sum_{a=v-k+1}^{v} X_a\right]$$ = estimated height of the background on the right of the peak.

This is shown graphically, in fig. 2.5(a), for k = 3.

The uncertainty in the peak area (at the 1σ or 68% confidence level) is given by σA_p where

$$\sigma A_p = \{I + \left(\frac{N}{2k}\right)\left(\frac{N}{2}\right)(B_1 + B_2)\}^{\frac{1}{2}}$$

The value of k used to determine the average background level of a peak of energy E_o was set equal to the peak FWHM and the backgrounds B_1 and B_2 were determined from the intervals $\{E_o - 3k, E_o - 2k\}$ and $\{E_o + 2k, E_o + 3k\}$ respectively. (See fig. 2.5(b).)

Table 2.2 lists the raw peak area data obtained for the 31.1, 43.54, 74.67 and 86.75 keV γ transitions of the five point ^{239}U sources (source numbers 1 to 5) and the two extended ^{239}U sources (source numbers 6 and 7). Due to the variation in initial source activity and the length of time required to prepare a source for γ-ray analysis it was not always possible to provide peak area data on the very weak γ transitions for each source.

The measured γ-ray intensity, $I_\gamma(\beta^-)$, is then given by the expression

$$I_\gamma(\beta^-) = A_\gamma C \qquad (2.3)$$

where A_γ is the measured γ-ray peak area (taken from table 2.2) and C is a correction factor which takes into account the decay of the ^{239}U source during the γ-ray analysis counting period. C is given by

$$C = \frac{(1 - e^{\lambda_1 \Delta T})}{\Delta T(e^{-\lambda_1 T_L} - 1)}$$

where λ_1 is the decay constant for ^{239}U, T_L is the livetime counting period and ΔT is the difference between the corresponding elapsed time (T) and livetime count duration. $I_\gamma(\beta^-)$ therefore corresponds to the number of γ-rays per second entering the full-energy photopeak at the start of the γ-ray analysis period. For the case of a long-lived radionuclide in which the source activity can be said to remain constant during the γ counting period (i.e. $\lambda_1 T_L << 1$) the

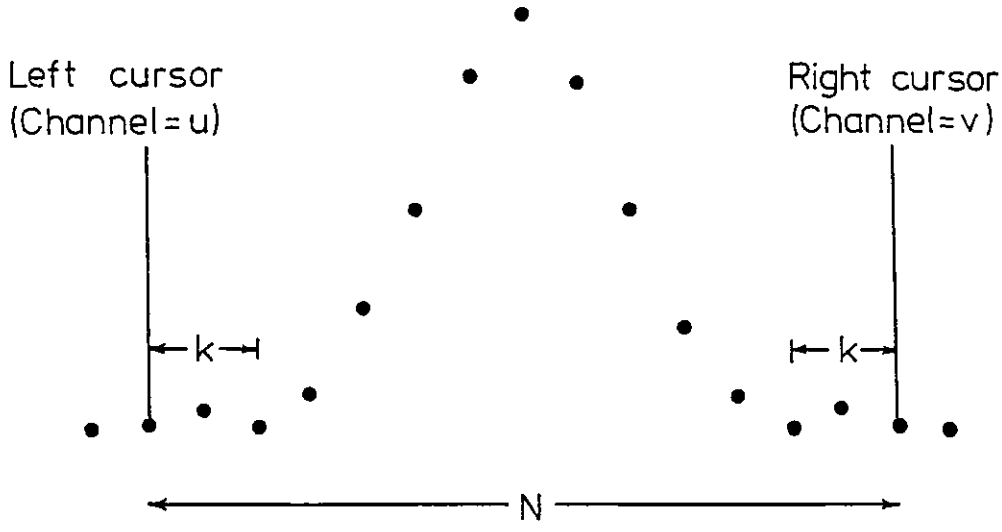

Fig. 2.5(a) Background parameters used to determine net peak area

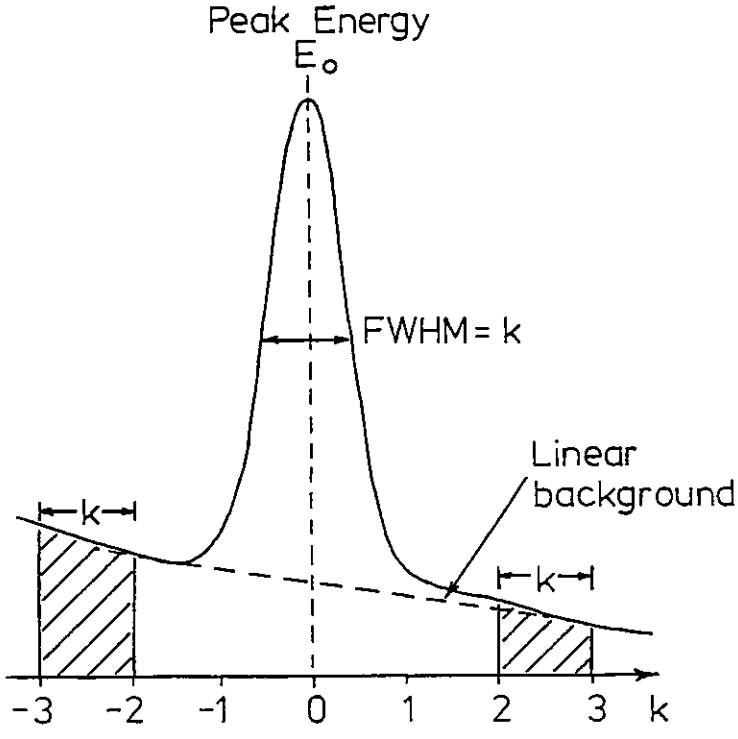

Fig. 2.5(b) Relation between γ-ray peak FWHM parameter (k) and background interval regions (shaded) used in peak area analysis

expression for $I_\gamma(\beta^-)$ reduces to A_γ/T_L, the γ-ray peak area divided by the livetime count period.

Table 2.3 lists the calculated values of C for sources 1 to 7; the ^{239}U half-life was taken to be (23.50 ± 0.05) mins[5]. Table 2.4 lists the corresponding values of $I_\gamma(\beta^-)$ for the peak energies and areas listed in table 2.2. The uncertainty in the measured γ-ray intensity, $\sigma I_\gamma(\beta^-)$, was calculated using the expression[13]

$$\sigma I_\gamma^2(\beta^-) = \sum_i \left(\frac{\partial I_\gamma(\beta^-)}{\partial P_i}\right)^2 \sigma P_i^2 \qquad (2.4)$$

where $\left(\frac{\partial I_\gamma(\beta^-)}{\partial P_i}\right)$ is the partial derivation of $I_\gamma(\beta^-)$ with respect to the i-th parameter and σP_i its associated absolute uncertainty. This expression is only valid when no correlation exists between the individual parameter uncertainties. The uncertainty $\sigma I_\gamma(\beta^-)$ was calculated using the uncertainty components for A_γ and λ_1.

Table 2.2 Peak area counts and associated statistical uncertainties[a] for selected γ transitions from the β^- decay of ^{239}U

Source number	γ Transition energy (keV)			
	31.1	43.54	74.67	86.75
1		8765 (1.4)	100071 (0.34)	
2		4085 (2.2)	46088 (0.51)	
3		5208 (2.1)	58666 (0.46)	
4	209 (32)	14014 (1.0)	161081 (0.26)	
5		8792 (1.3)	102257 (0.35)	
6	263 (27)	24866 (0.77)	274266 (0.20)	305 (17)
7	769 (13)	50992 (0.34)	563716 (0.14)	518 (15)

a The statistical uncertainties (in %) are the numbers in parentheses beside the peak area

Table 2.3 ^{239}U Source decay correction factors

Source number	Preset livetime count T_L (s)	Elapsed time T (s)	Correction factor C
1	2000	2010	7.874-4[b]
2	1000	1004	1.267-3
3	2000	2007	7.868-4
4	1000	1009	1.269-3
5	1000	1008	1.268-3
6	500	513	2.263-3
7	1000	1028	1.275-3

b Throughout this thesis the mathematical notations 7.874-4 ≡ 7.874e-04 ≡ 7.874 x 10^{-4} will be used

Table 2.4 Measured γ-ray intensities and associated uncertainties[c] for the transitions listed in Table 2.2

Source number	$I_{31.1}$ (s^{-1})	$I_{43.54}$ (s^{-1})	$I_{74.67}$ (s^{-1})	$I_{86.75}$ (s^{-1})
1		6.901+0 (1.40)	7.879+1 (0.35)	
2		5.176+0 (2.20)	5.840+1 (0.51)	
3		4.098+0 (2.10)	4.616+1 (0.47)	
4	2.651-1 (32.0)	1.778+1 (1.00)	2.043+2 (0.26)	
5		1.115+1 (1.30)	1.297+2 (0.33)	
6	5.952-1 (27.0)	5.627+1 (0.77)	6.207+2 (0.20)	6.902-1 (17.0)
7	9.802-1 (13.0)	6.499+1 (0.54)	7.185+2 (0.15)	6.602-1 (15.0)

c The uncertainties, $\sigma I_\gamma(\beta^-)$, are expressed in % in parentheses beside the measured γ-ray intensity

2.3.4 Source disintegration rate measurements

By considering the equations governing the build-up and subsequent decay of the parent and daughter radionuclides during and after the reactor irradiation period it can be shown that, as a function of time, the ratio of the parent to daughter activity is independent of neutron flux density and neutron capture cross-section data. Therefore the absolute activity of the parent can be deduced from a measurement of the daughter absolute activity and a knowledge of the parent-daughter activity ratio. In this manner the absolute β^- activity of a ^{239}U source was determined from a measurement of the daughter ^{239}Np β^- activity using the $4\pi\beta$-γ coincidence technique[14]; the short ^{239}U half-life precluded a direct measurement of the ^{239}U absolute β^- activity due to the build-up of the daughter ^{239}Np activity within the source. The build-up of ^{239}Pu activity ($T_{\frac{1}{2}} = 2.411 \times 10^4$ y) was assumed to be negligible.

The equations describing the time variation of the ^{239}U and ^{239}Np yields and specific activities during and after the reactor irradiation period are derived in detail in Appendix 1. Only the relevant equations are quoted here for brevity. After removal of a sample from the reactor the absolute β^- activities of the ^{239}U parent and ^{239}Np daughter are given by $A_1(t)$ and $A_2(t)$ respectively, where

$$A_1(t) = N_o\phi\sigma(1 - e^{-\lambda_1 T})e^{-\lambda_1 t} \qquad (2.5)$$

$$A_2(t) = \frac{N_o\phi\sigma}{(\lambda_2 - \lambda_1)}\left[(1 - e^{-\lambda_1 T})e^{-\lambda_1 t} - \frac{\lambda_1}{\lambda_2}(1 - e^{-\lambda_2 T})e^{-\lambda_2 t}\right] \qquad (2.6)$$

Here λ_1 and λ_2 are the decay constants for ^{239}U and ^{239}Np respectively, T is the length of the reactor irradiation period and t is the time elapsed since the removal of the sample from the reactor. N_o is the number of ^{238}U nuclei originally present in the sample, ϕ is the neutron flux and σ is the ^{238}U neutron capture cross-section.

The ^{239}U source β^- activity was required to be known at a time t_1 corresponding to the start of the γ-ray analysis. ($t = 0$ was

defined as the end of the reactor irradiation period.) This was determined by measuring the ^{239}Np β^- activity of the same source at t_2 by which time the parent ^{239}U had decayed sufficiently as to be no longer observable in any γ-ray analysis of the source and which would therefore produce a negligible contribution to the overall measured β^- activity; the minimum time allowed to elapse between the γ analysis of the ^{239}U source and the measurement of the resulting ^{239}Np daughter β^- activity was approximately 11 hours. For such times, t_2, used throughout this experiment (i.e. $\lambda_1 t_2 >> 1$) the ratio, R, of the ^{239}U β^- activity at time t_1 to the ^{239}Np β^- activity at time t_2 is given (using eqns. 2.5 and 2.6) by the expression

$$R = \frac{(\lambda_1 - \lambda_2)}{\lambda_1} \frac{(1 - e^{-\lambda_1 T})}{(1 - e^{-\lambda_2 T})} \frac{e^{-\lambda_1 t_1}}{e^{-\lambda_2 t_2}}$$

and is independent of neutron flux and neutron capture cross-section data. Table 2.5 lists the calculated values of R and their associated uncertainties, σ_R, for each of the five point sources. Four separate values of R are quoted for source 1 since the β^- activity of this source was measured four times (runs 1 to 4 inclusive). The ^{239}Np half-life was taken to be $(2.355 \pm 0.004)^5$ days; the ^{239}U half-life has been previously defined as (23.50 ± 0.05) mins. The uncertainties in T, t_1 and t_2 were estimated to be 60s, 30s and 30s respectively.

Table 2.5 ^{239}U/^{239}Np Activity ratios

Source No.	Run No.	T (mins)	t_1 (h.m.s.)	t_2 (h.m.s.)	R	σ_R	$\frac{\sigma_R}{R}$ (%)
1	1	45.0	01.18.30	12.10.07	9.135+0	0.174	1.9
	2			25.36.45	1.077+1	0.21	1.9
	3			38.58.59	1.269+1	0.24	1.9
	4			54.08.21	1.529+1	0.29	1.9
2		60.0	00.25.16	33.21.15	4.829+1	0.87	1.8
3		60.0	00.44.33	22.57.23	2.407+1	0.44	1.8
4		90.0	00.30.30	25.58.20	2.833+1	0.49	1.7
5		90.0	00.50.16	37.31.17	1.822+1	0.32	1.7

4πβ-γ Coincidence counting system

A 4πβ-γ coincidence counting system consisting of two 7.62- x 7.62-cm sodium iodide (NaI(Tl)) scintillation detectors placed above and below a pill-box type $4\pi\beta^-$ proportional counter was used to determine the ^{239}Np source disintegration rate. The coincidences between the β^- proportional counter and the scintillation detectors were counted along with the singles β^- and γ pulses using the coincidence assembly shown in the block diagram of fig. 2.6.

For a simple one-component β^- decay to an excited level, which subsequently decays by prompt γ-ray emission, the β^-,γ and coincidence counting rates are given to first approximation, respectively, by

$$N_\beta = N_o\varepsilon_\beta,$$
$$N_\gamma = N_o\varepsilon_\gamma,$$
$$N_c = N_o\varepsilon_\beta\varepsilon_\gamma.$$

The source disintegration rate, N_o, is then given by the relation

$$N_o = N_\beta N_\gamma / N_c$$

Here, ε_β and ε_γ are the efficiencies of the β^- proportional counter and the γ-ray scintillation detector, respectively. In these relations, it is assumed that N_β,N_γ and N_c have been corrected for dead-time, background and accidental coincidences and that the efficiency of the coincidence circuit is 100%. However, in the more general case of complex β-γ emission[14] involving multiple β^- branch transitions, it can be shown that

$$N_\beta = F(N_c/N_\gamma), \qquad (2.7)$$

$$N_\beta \to [F(1) = N_o] \text{ as } N_c/N_\gamma \to 1$$

where the function F is of unspecified general form and in practice defined simply as a polynomial in N_c/N_γ. Equation 2.7 or any equivalent may be taken as the practical coincidence formula used to

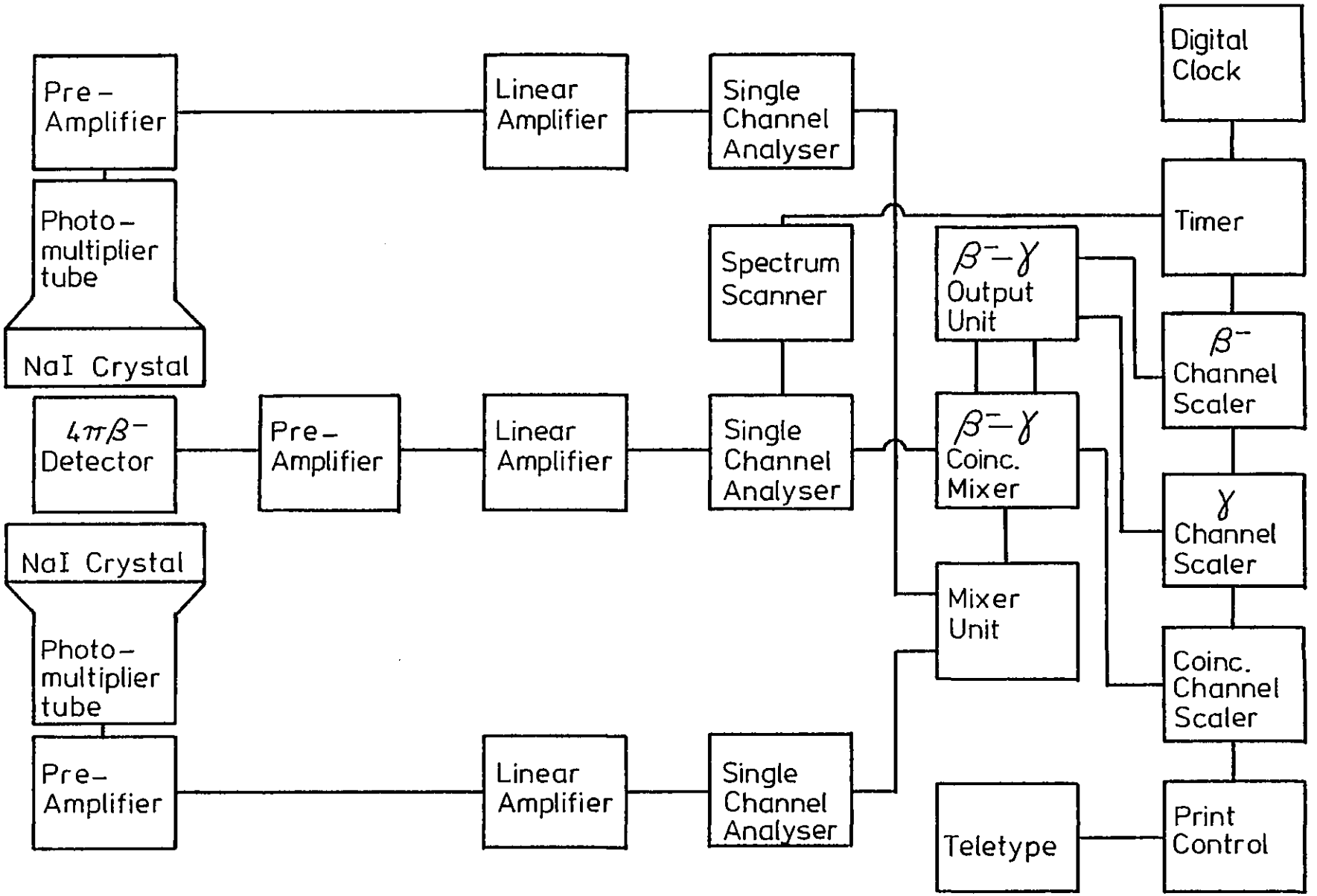

Fig. 2.6 Block diagram of 4πβ-γ coincidence system

evaluate N_o. The function F does not depend directly on decay scheme parameters and is determined experimentally by varying the β^- detection efficiency. The disintegration rate, N_o, is then taken to be the value N_β resulting when the ratio N_c/N_γ is extrapolated to unity (i.e. ε_β = 100%) using the lowest order polynomial (usually ≤ 3) which will provide an adequate fit to the data. The β^- efficiency is varied in the present study by adjusting the β^- discrimination threshold level.

The dead time, τ, in the β^- channel and the coincidence system resolving time, τ_R, were measured, using the method proposed by Baerg[15], by introducing periodic pulses at the β^- amplifier input in parallel to the detector; the β^- channel dead time was measured to be ≈ 2.4 μs and the coincidence circuit resolving time was measured to be 1.0 μs. The γ channel dead time was assumed to be equal to the β^- channel dead time, since the dead-time is imposed on the β^- and γ channels by the coincidence unit.

Sample decay rate measurements

Each of the five point ^{239}Np sources was counted in the $4\pi\beta$-γ system. The β^- activity of source 1 was measured four times together with single measurements for sources 2 to 5.

Although the detection of X-rays by the NaI(Tl) detectors following highly internally converted transitions further complicates the equations used in the analysis of $4\pi\beta$-γ data it has been shown, at least in the case of ^{233}Pa β^- decay[16], that no appreciable error in the measured disintegration rate is introduced by including the K X-rays in the γ channel counts. Therefore, a γ channel window centred on the intense 106.1 keV γ transition in the decay of ^{239}Np and including the Pu K X-rays (~ 100 keV) was used in the counting of each source. This γ window setting provided good counting statistics and gave a maximum value for the ratio N_c/N_γ (with the β^- discrimination threshold set to zero volts) of the order of 0.75. The β^- channel efficiency was varied automatically between preset upper and lower level threshold settings in sixteen equal steps covering a typical N_c/N_γ range of 0.4 to 0.75.

Data analysis

The equations used in the analysis of the data taken with the system are those given by Bryant[17]. The experimental data was evaluated by two methods in order to determine a reliable value for the source disintegration rate; first (i.e. linear) and second order polynomial functions were used to fit the data plotted in the form N_β vs. N_c/N_γ and in the more slowly varying form $N_\beta N_\gamma/N_c$ vs. N_γ/N_c. These two methods were used to search for systematic errors arising from the possibility that the polynomial function used was either inaccurate or unsuitable for extrapolation. The decay of the ^{239}Np source during the $4\pi\beta$-γ counting period was taken into account in the fitting programme used to determine the source disintegration rate. The measured disintegration rate was itself corrected back to the time 00.00.00 on the $4\pi\beta$-γ system digital clock.

Figures 2.7(a) and 2.7(b) show the best linear and quadratic fits to the data for source 1 (run 1) plotted in the forms N_β vs. N_c/N_γ and $N_\beta N_\gamma/N_c$ vs. N_γ/N_c, respectively. The linear and quadratic fits in fig. 2.7(b) appear, visually, to be much worse than the corresponding fits in fig. 2.7(a); this is due to the slower variation in the quantity $N_\beta N_\gamma/N_c$ compared with N_β, although both methods of data analysis should, theoretically, predict the same extrapolated value for the source disintegration rate. Plots of $N_\beta N_\gamma/N_c$ vs. N_γ/N_c tend to reveal any curvature in the data that is not apparent in a plot of the form N_β vs. N_c/N_γ. Similar plots were obtained for the other ^{239}Np sources.

Since the data from each source was non-linear it was assumed that the quadratic fits would predict a more reliable estimate for the source disintegration rate, N_o. However, because of the long extrapolation required to obtain N_o from the experimental data, it was evident that the quadratic fits were tending to overestimate the value of N_o to the same extent that the linear fits were underestimating N_o. Therefore a compromise was reached by rejecting (i) the lowest N_o predicted by the two linear fits and (ii) the highest N_o predicted by the quadratic fits; the source disintegration rate was then taken to be the mean N_o predicted by the remaining one linear and one quadratic fit. The value of N_o obtained by this method is found to be in good agreement with that obtained from the mean of

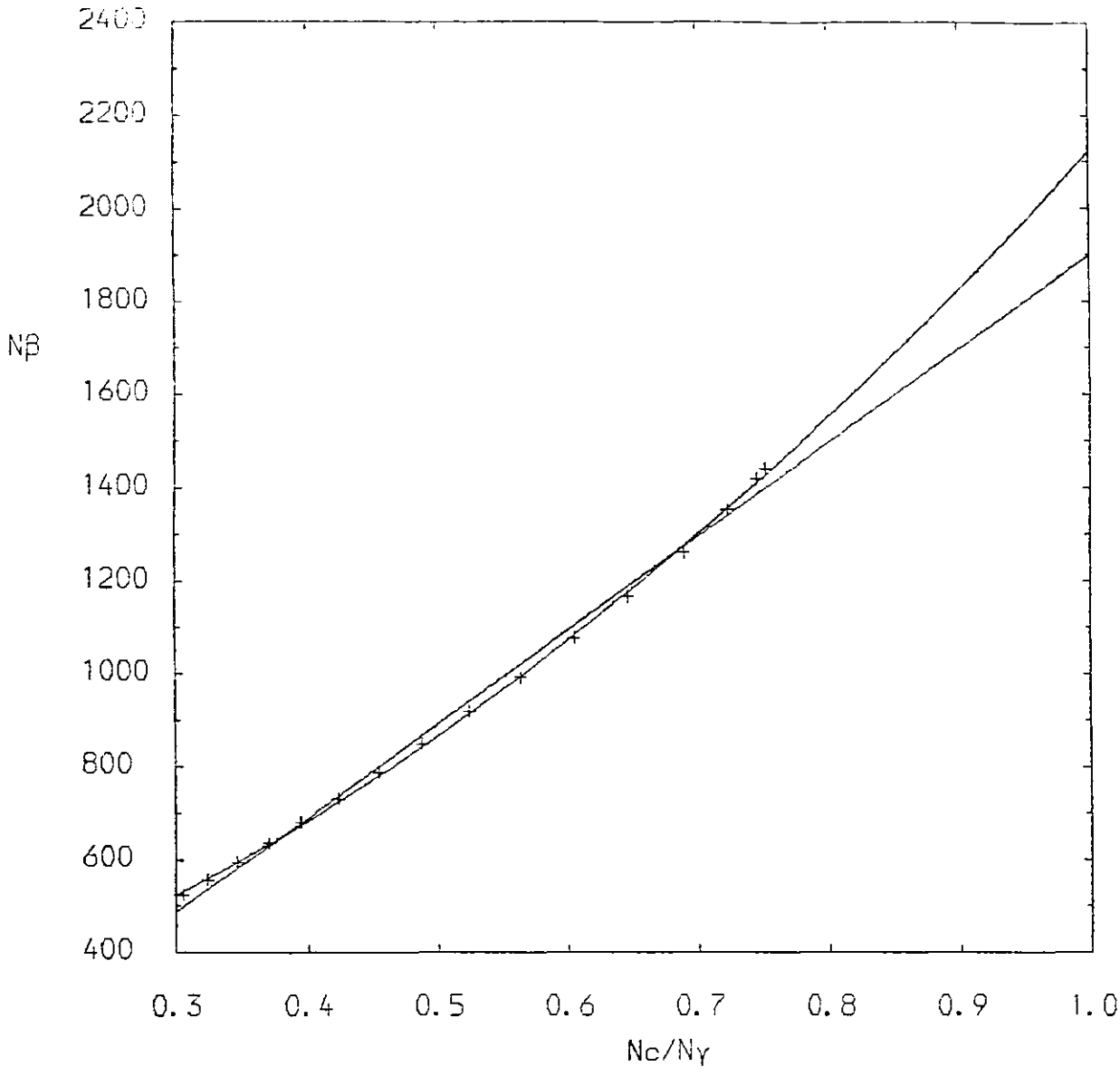

Fig. 2.7(a) Linear and quadratic fits to coincidence data of source 1 (Run 1), plotted in form N_β vs. N_c/N_γ

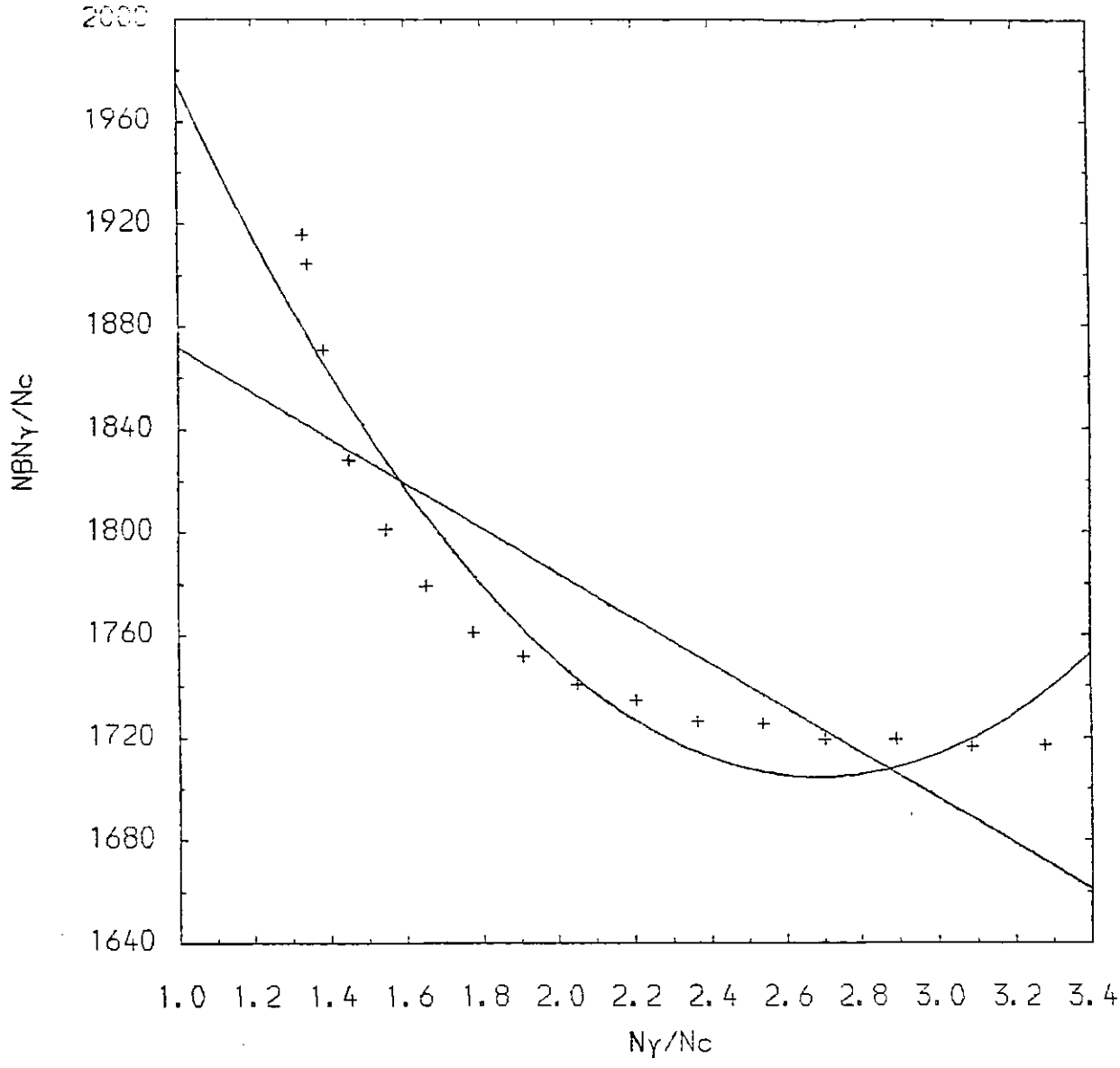

Fig. 2.7(b) Linear and quadratic fits to same coincidence data of fig. 2.7(a), plotted in form $N_\beta N_\gamma / N_c$ vs. N_γ / N_c

Table 2.6 ^{239}Np and ^{239}U Source Disintegration Rates

Source number	Run number	N_o (s^{-1}) <1 Linear + 1 Quadratic> 16 point data fit	N_o (s^{-1}) <1 Linear + 1 Linear> 11 point data fit	^{239}Np Disintegration rate (at time 00.00.00) (s^{-1})	^{239}Np Disintegration rate at time t_2 (s^{-1})	^{239}U Disintegration rate[a] at time t_1 (s^{-1})
1	1	1938 ± 43	1935 ± 59	1937 ± 51	1695 ± 45	1.548 + 4 (3.3)
	2	1988 ± 49	1984 ± 64	1986 ± 56	1474 ± 42	1.588 + 4 (3.4)
	3	2000 ± 51	1996 ± 70	1998 ± 61	1259 ± 38	1.598 + 4 (3.6)
	4	1988 ± 49	1989 ± 70	1989 ± 60	1041 ± 31	1.591 + 4 (3.5)
2		389.5 ± 8.1	389.3 ± 12.2	389.4 ± 10.2	260.0 ± 6.8	1.256 + 4 (3.2)
3		541.0 ± 9.1	540.7 ± 12.7	540.9 ± 10.9	410.3 ± 8.3	9.876 + 3 (2.7)
4		2144 ± 35	2129 ± 54	2136 ± 45	1563 ± 33	4.428 + 4 (2.7)
5		2538 ± 38	2522 ± 53	2527 ± 46	1605 ± 29	2.924 + 4 (2.5)

a. The figure in parentheses is the uncertainty (in %) in the calculated disintegration rate

the two linear functions used to fit a reduced data set of 11 experimental points, obtained by removing the first five data points (corresponding to the lowest N_c/N_γ values in the plot of N_β vs. N_c/N_γ) to minimise the curvature present in the original data. The final disintegration rate for each source was therefore taken to be the mean of the two N_o values predicted by the analysis of the complete (16 point) data and the reduced (11 point) data sets.

Column 5 of table 2.6 lists the final ^{239}Np source disintegration rates (as measured at time 00.00.00 on the $4\pi\beta$-γ clock) together with their uncertainties. The values quoted are the mean of columns 3 and 4, and the uncertainty in each source activity measurement is the statistical contribution from the unweighted least squares fit analysis. Finally, in column 6 of table 2.6, each source disintegration rate is corrected back to the time t_2 corresponding to the start of the $4\pi\beta$-γ counting period and in column 7 the corresponding ^{239}U β^- disintegration rate at time t_1 is derived using the ^{239}U/^{239}Np activity ratios, R, of table 2.5 and the results of column 6. The overall uncertainty in the ^{239}U β^- disintegration rate is determined from the uncertainties in R and the ^{239}Np β^- disintegration rate, combined in quadrature.

2.4 ^{243}Am γ Spectroscopy and Disintegration Rate Measurements

2.4.1 Source preparation

^{243}Am is produced by irradiating high purity ^{242}Pu in a high flux reactor to form ^{243}Pu which then decays by β^- emission with a 5 hr half-life to form ^{243}Am. The ^{242}Pu target material is itself produced by neutron irradiation of ^{239}Pu and ^{240}Pu which is then chemically purified to remove the main impurity, ^{241}Am, formed by the β^- decay of ^{241}Pu during the irradiation period.

The ^{243}Am source used in this experiment was prepared by Chemistry Division at A.E.R.E., Harwell using high purity ^{243}Am solution (americium content = 99.995% ^{243}Am) produced by the above method. The age of the solution since radiochemical separation was such that the daughter radionuclide ^{239}Np ($T_{\frac{1}{2}}$ = 2.355d) was present in secular equilibrium with the ^{243}Am parent ($T_{\frac{1}{2}}$ = 7370y). ^{243}Am was deposited at the centre of a 25.4 mm diameter x 0.5 mm thick stainless steel backing support by vacuum volatilisation to produce a thin,

uniform 7 mm diameter active area. The source was quoted as having a nominal α activity of 2.76×10^6 α disintegrations per minute ($\equiv$ 1.24 μCi) corresponding to a source thickness of $\sim$ 16 $\mu g\ cm^{-2}$.

2.4.2 ^{243}Am γ spectroscopy

The ^{243}Am source was counted at the same source-detector distance with the Ge detector-amplifier-MCA system used in the γ-ray analysis of the ^{239}U sources.

Fig. 2.8 shows a typical low-energy γ spectrum obtained from the ^{243}Am source. The peaks at 31.10, 43.53, 74.68, 86.74 and 141.84 keV are identified as transitions in ^{239}Np. The 117.8 keV ground-state transition in ^{239}Np is masked by the intense Pu $K\beta_1'$ X-ray peak. Similarly, the weak 98.5 keV transition depopulating the 173 keV level in ^{239}Np is masked by the Pu $K\alpha_2$ X-ray peak. Very weak γ-rays in the ^{239}Np level scheme (fig. 2.2) at 50.6 and 55.4 keV, previously observed by Van Hise[20] in ^{243}Am(α-γ) coincidence studies, are not observed in the present singles γ spectrum. The peaks at 49.45, 57.37, 61.47, 67.86, 106.12, 181.67 and 209.74 keV are transitions in the level scheme of ^{239}Pu. There is a weak 44.6 keV γ-ray in the decay of ^{239}Np which, with the resolution of the Ge detector, is not resolved from the 43.53 keV peak from ^{243}Am α decay. The peaks at 33.67 and 64.85 keV are Ge escape peaks of the intense 43.53 and 74.68 keV γ transitions.

At the source-detector distance employed in the γ-ray counting of the ^{243}Am source the effect of 'true' coincidence summing for γ-rays from ^{239}Np decay is very pronounced. ^{239}Np has many multiple cascade γ-rays in its decay and two (or more) γ-rays from a single decay are, in effect, emitted in coincidence. It is then possible for both γ-rays from a single decay to interact and deposit all of their energy within a time that is short compared with the response time of the detector or the resolving time of the following electronics. A 'sum peak' will be observable in the spectrum which occurs at a pulse height that corresponds to the sum of two individual γ-ray energies. Fig. 2.9, which includes the high energy portion of the ^{243}Am-^{239}Np γ spectrum displayed in fig. 2.8, shows sum peaks at 205.82 (γ106.12 + Pu $K\alpha_2$ X-ray), 223.32 (γ106.12 + Pu $K\beta_1'$ X-ray) and 383.69 (γ106.12 + γ277.64) keV. Sum peaks at 209.83

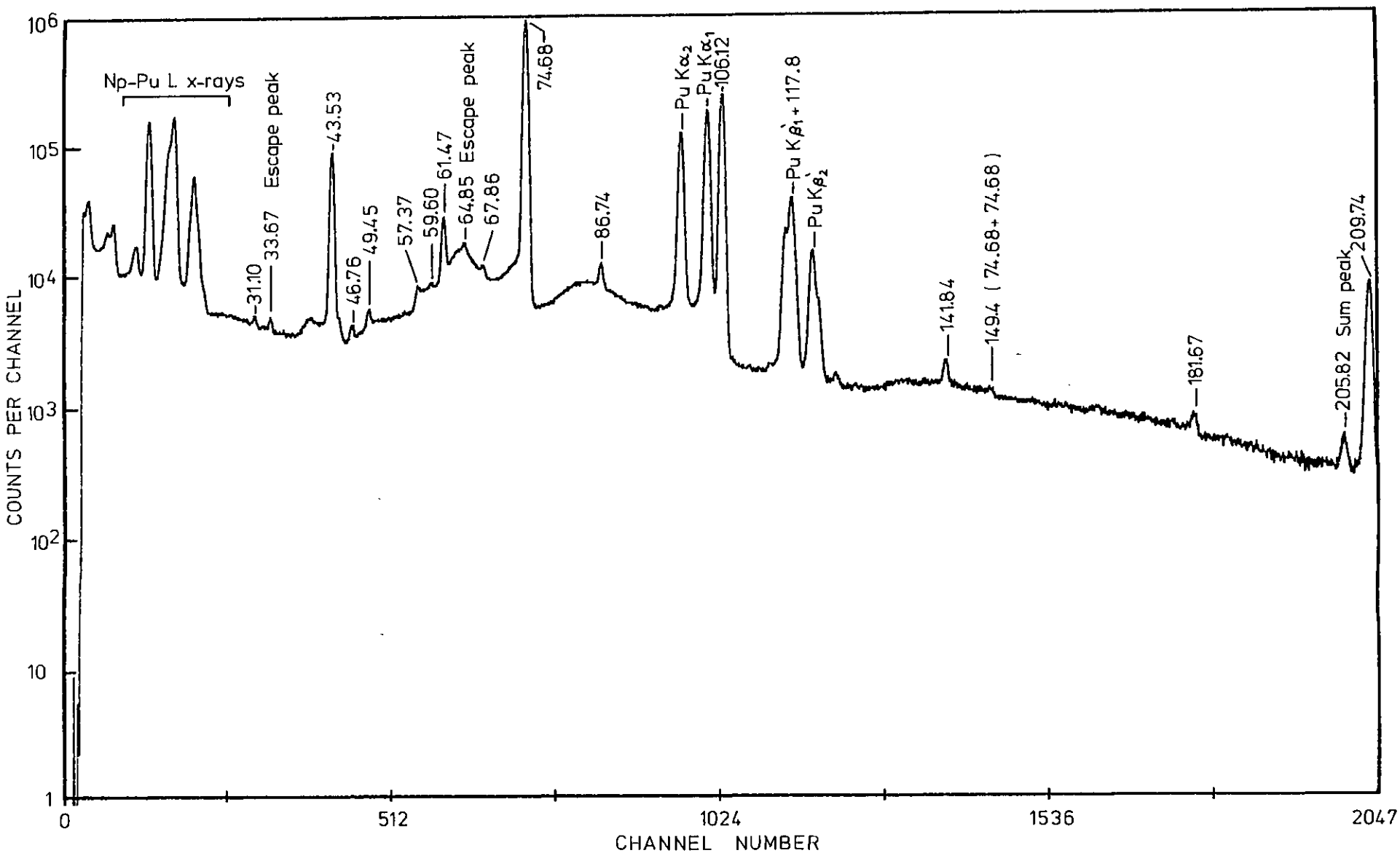

Fig. 2.8 Low energy ^{243}Am γ-ray spectrum measured with 15 cm^2 x 10 mm Ge detector. Counting time 20,000s

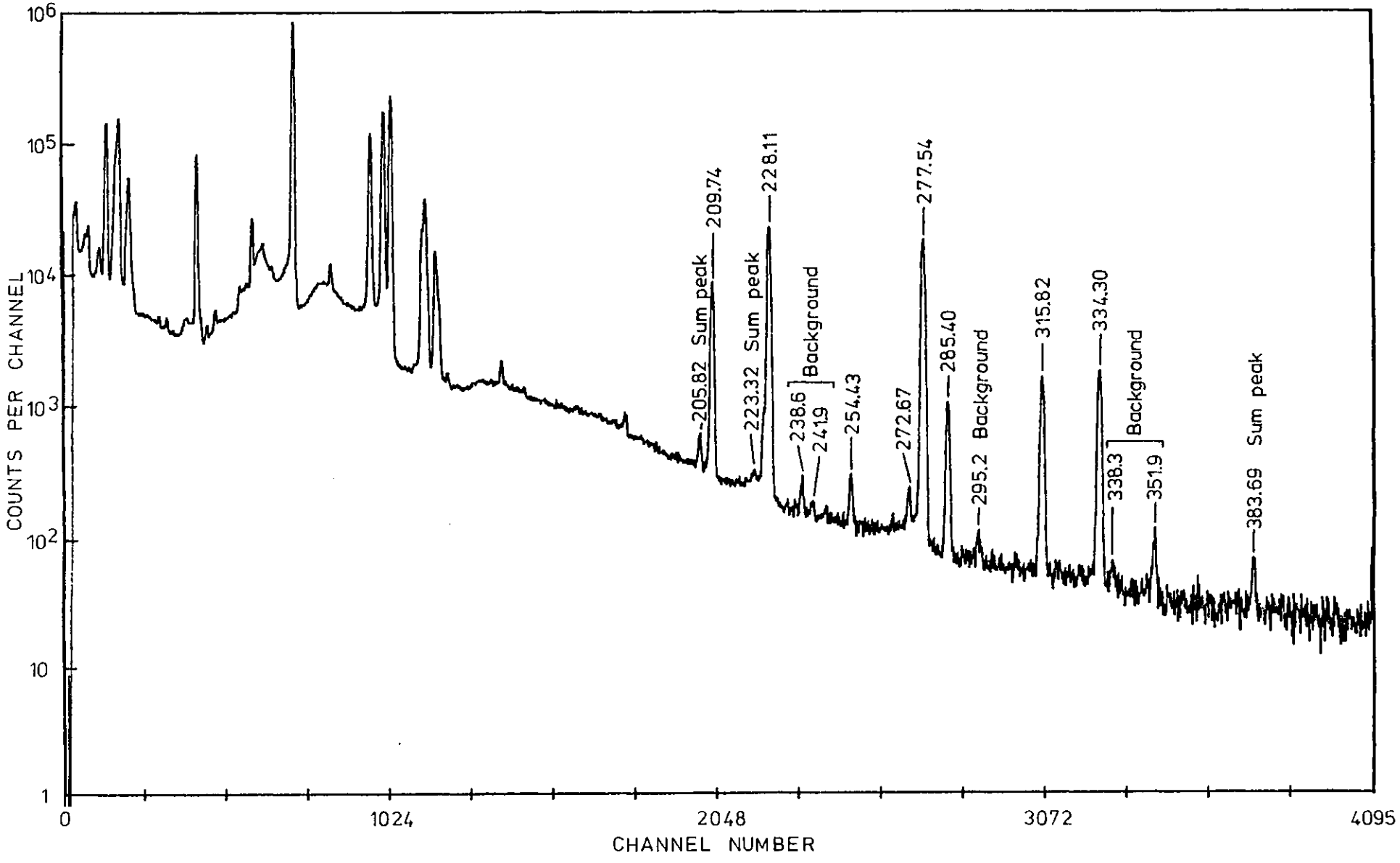

Fig. 2.9 High energy portions of ^{243}Am - ^{239}Np γ-ray spectrum

(γ106.12 + Pu $K\alpha_1$ X-ray), 226.71 (γ106.12 + Pu $K\beta_2'$ X-ray), 315.86 (γ106.12 + γ209.74) and 334.23 (γ106.12 + γ228.11) keV are also present in the spectrum but are unresolved from the main γ transitions at 209.74, 228.11, 315.82 and 334.30 keV respectively. In ^{243}Am α decay true coincidence summing occurs mainly between γ-rays and L X-rays and was reduced in the present experimental arrangement by the 6 mm perspex absorber which, as well as stopping β^-s entering the Ge detector, also attenuated the low energy X-ray photons.

Evidence for random coincidence summing in the spectrum of fig. 2.8 is provided by the 149.4 keV peak, the result of accidental summing of two 74.68 keV γ transitions. It is estimated that the random summing is responsible for ~ 0.5% reduction in the true peak area of the intense 74.68 keV transition.

The 46.76 keV peak in the ^{243}Am-^{239}Np γ spectrum (fig. 2.8) is not listed as a transition occurring in either ^{243}Am α decay or ^{239}Np β^- decay although it has been observed in previous studies of ^{243}Am α decay[18-20]. In the earliest of these studies[8] a 46.6 keV γ line was observed in the course of ^{243}Am gross (α-e^-) experiments (the coincidence γ spectrum was obtained by placing a Be absorber over the source) and was identified as being a possible transition between the 117.8 keV level in ^{239}Np and a level at 71.2 keV; however, previous ^{243}Am (α-γ) coincidence experiments[20] carried out by the author of ref. 8 did not reveal a γ transition of this energy in coincidence with any of the major ^{243}Am α groups and therefore the identification of the transition remained uncertain. Subsequent ^{243}Am-^{239}Np singles γ studies[18,19], in which a peak at 46.7 keV is clearly resolved, do not make any reference to the origin of this peak although extensive ^{239}Np (γ-γ) coincidence experiments[18] did not place the transition anywhere within the level scheme of ^{239}Pu either. Further ^{243}Am (α-γ) coincidence experiments described later (see section 3.6) provide evidence that the peak is in fact a γ transition between the $7/2^-$ level at 117.8 keV and the predicted $9/2^+$ member of the $5/2^+$ ground state rotational band* at ~ 71.2 keV. Conservation of angular momentum and parity lead to a proposed E1 multipole assignment for this transition.

*A discussion of the ^{239}Np level structure in terms of the rotational excitations of a deformed nucleus is given in section 2.6.

Since the 117.8 keV is also populated by ^{239}U β^- decay then the 46.7 keV γ transition should also be observed in a γ spectrum obtained from a ^{239}U source. However it is not possible to confirm the existence of this weak transition in any of the ^{239}U γ spectra obtained from those sources prepared by the ^{238}U $(n,\gamma)^{239}U$ reaction. This is due mainly to the expected low intensity of the transition and the restricted γ accumulation period necessary to reduce interference from the ^{239}Np daughter; the 117.8 keV level is fed by only $\simeq$ 2% of all β^- transitions from ^{239}U decay compared with $\simeq$ 11% of all α transitions from ^{243}Am decay and therefore the measured γ-ray intensity of the 46.76 keV transition will be a factor of $\sim$ 5 lower than the measured intensity from ^{243}Am α decay. Identification of this weak transition is also hindered by the presence of the backscatter peak (from the intense 74.69 keV transition) in the region of interest coupled with poor counting statistics due to the short γ counting time available.

The only sign of possible impurity in fig. 2.8 is the very weak γ-ray peak at 59.60 keV which indicates that the impurity is most likely to be ^{241}Am. The peaks at 238.6, 241.9, 295.2, 338.3 and 351.9 keV are present in the spectrum background.

Fig. 2.10(a) shows a low energy γ, X-ray spectrum of the ^{243}Am source obtained using a 12 mm^2 x 3 mm Si(Li) detector with 250 μm Be window. The superior energy resolution of the Si(Li) detector compared to the Ge detector allows the weak 44.6 keV γ transition in the decay of ^{239}Np to be resolved from the intense 43.53 keV transition (see fig. 2.10(b)) and hence it is possible to calculate that fraction of the total 43.53 keV peak area in the γ spectrum obtained using the Ge detector which is a direct result of the parent ^{243}Am α decay.

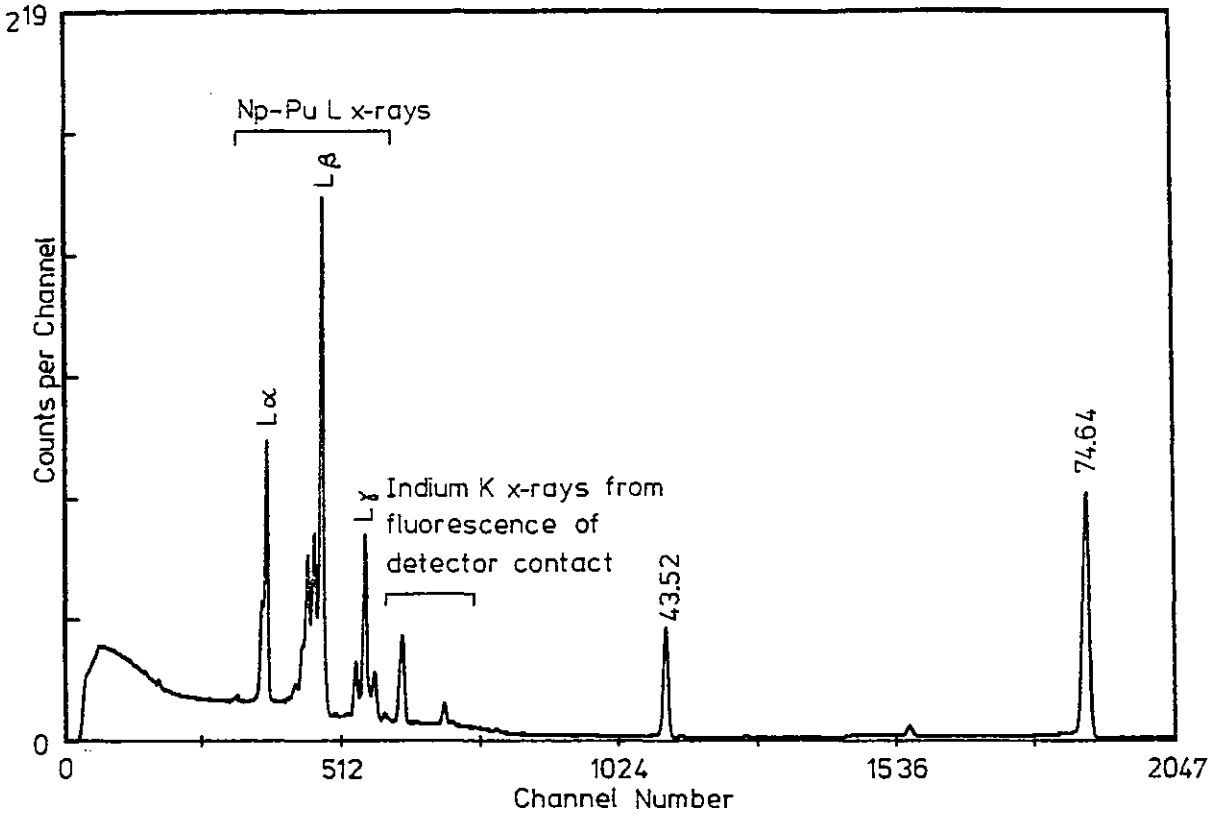

Fig. 2.10(a) Low energy ^{243}Am γ-ray spectrum measured with Si(Li) detector. Counting time 2.3 x 10^5s

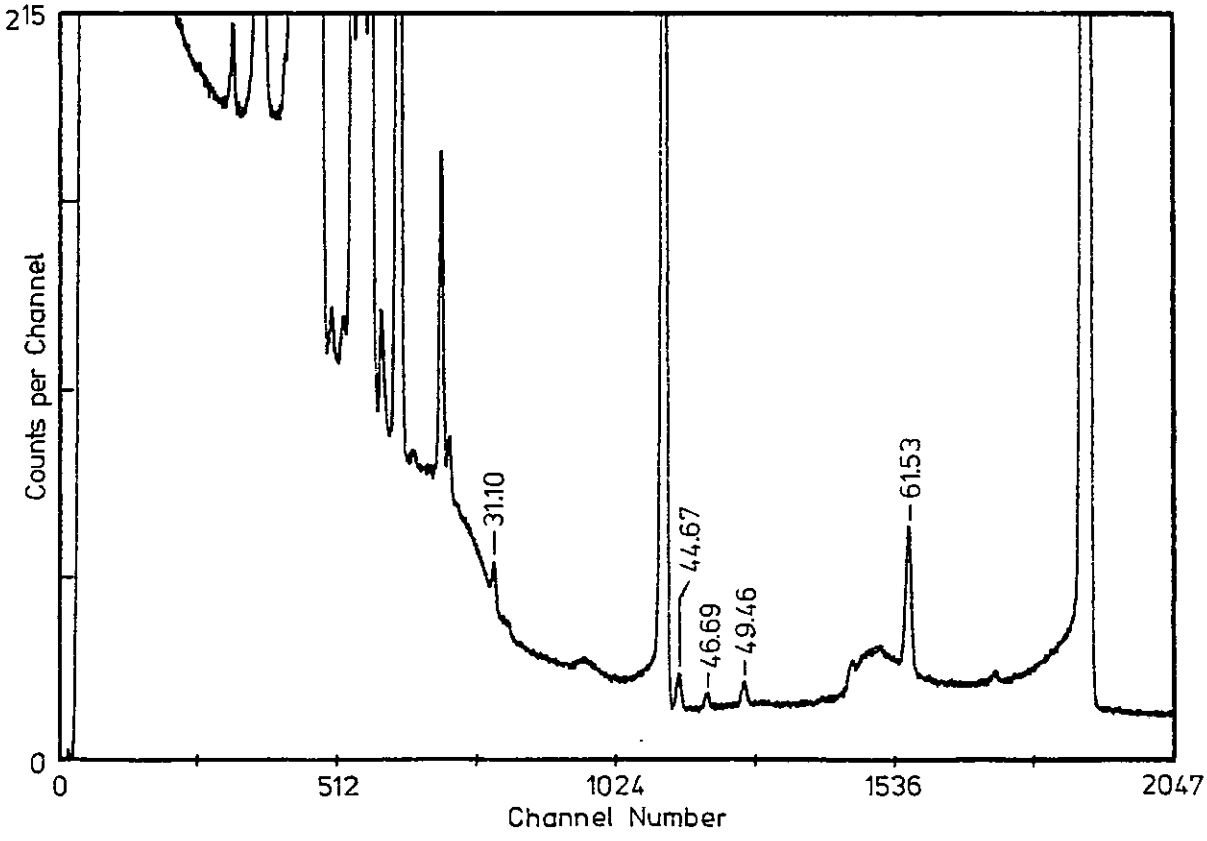

Fig. 2.10(b) γ-ray spectrum of fig. 2.10(a) with expanded vertical scale (linear) to show weak γ transitions occurring in ^{243}Am-^{239}Np decay

2.4.3 Measurement of peak areas

The peak areas of selected γ transitions occurring in the decay of ^{243}Am were determined using the method described in section 2.3.3. The correction to take into account the decay of the source during the γ counting period was negligible and the measured γ-ray intensities, $I_\gamma(\alpha)$, were calculated simply by dividing the peak area by the live-time count duration (i.e. the decay correction factor C of eqn. 2.3 was set equal to $1/T_L$).

Table 2.7 lists the peak areas of six transitions obtained from seventeen consecutive (20,000s livetime count)γ spectra; as well as providing peak area data for the same γ transitions listed in table 2.2, which are required to determine the β^- branching intensities β_1, β_2, β_3 (fig. 2.1), the table also contains peak area data for the 46.76 and 141.84 keV γ transitions so that a comprehensive set of relative γ transition intensities can be established for this particular decay scheme. These latter calculations require a knowledge of the Ge detector full-energy peak detection efficiency.

The uncertainty in the mean peak area for each transition in the table is the average deviation of the seventeen experiments. This uncertainty is of the same order of magnitude as the statistical deviation derived from the associated individual peak area uncertainties for the seventeen runs. The uncertainties in the measured γ-ray intensities listed at the end of table 2.7 are due solely to the observed spread in peak area data for the seventeen runs.

2.4.4 Source disintegration rate measurements

The absolute α activity of the ^{243}Am source was measured using a low-geometry system with accurately known solid angle for α particle detection. Using this technique only those α particles which are emitted (isotropically) into a solid angle Ω subtended by a circular aperture placed in front of the α detector are measured and the source disintegration rate is obtained by correcting the observed count rate by the geometry factor $4\pi/\Omega$. The accuracy of the activity measurement depends upon the certainty with which the geometry is known.

The problem of determining the solid angle subtended by an aperture at a source has been treated in many papers[21-23]. The fraction of the total solid angle subtended by the aperture is often

Table 2.7 γ-Ray Peak Areas and Intensities ($I_\gamma(\alpha)$) from ^{243}Am α Decay

Run Number	γ Transition energy (keV)					
	31.10	43.53	46.76	74.68	86.74	141.84
1	3847 (13)[a]	533329 (0.1)	4762 (11)	5900545 (.05)	27373 (3.4)	5257 (6.7)
2	4081	535277	4732	5905077	26921	5160
3	4079	531523	4804	5901726	27004	5147
4	3929	532957	4975	5899139	27097	5466
5	3698	534000	4369	5908087	27172	5956
6	3696	531751	4303	5901267	27600	5685
7	4024	534002	5091	5905264	27247	5568
8	4312	532243	4563	5903516	27582	5956
9	4110	533089	4418	5908432	26750	5531
10	3925	534128	4804	5896868	28745	5227
11	3503	532542	4539	5898689	28485	5716
12	4263	532520	4859	5904011	27337	5312
13	4021	532727	4910	5897319	27989	5367
14	3610	530849	4263	5893894	26950	5132
15	3620	532334	4715	5895870	27815	5348
16	4094	532762	4289	5895898	27756	5277
17	3872	531271	5210	5898560	26857	5234
Mean peak area	3923	532783	4683	5900833	27452	5438
Standard deviation of mean area	57	276	70	1058	137	64
Measured γ-ray intensity $I_\gamma(\alpha)$ (s^{-1})	1.962 - 1 (1.45)[b]	2.664 + 1 (0.05)	2.342 - 1 (1.49)	2.950 + 2 (0.02)	1.373 + 0 (0.50)	2.719 - 1 (1.17)

a. The figure in parentheses following the peak area is its associated statistical uncertainty (expressed in %). Similar uncertainties were obtained in the remaining 16 runs for each γ transition energy.

b. The figure in parentheses under the measured γ-ray intensity, $I_\gamma(\alpha)$, is its associated uncertainty (expressed in %) derived from the spread in the experimental data.

referred to as the 'geometry', G, of the aperture. In this experiment the geometry required is that of a circular aperture mounted coaxially with a uniformly spread circular source; in this case the geometry, denoted by Gs, is given by a sum of terms in an infinite series of the form

$$Gs = G\acute{p}\left\{1 - \frac{3b^2}{8D^4}zD(D+z) + \frac{5b^4}{16D^8}zD(D+z)(z^2 - 3/4\ a^2) - \ldots\right\} \qquad (2.8)$$

where a is the aperture radius, b is the source radius, z is the source-aperture separation distance, $D = (z^2 + a^2)^{\frac{1}{2}}$ and $G\acute{p}$ is the fraction of the solid angle subtended by the same aperture at a point source mounted coaxially at the same source-aperture separation;

$$G\acute{p} = \frac{1}{2}[1 - z/D] = \frac{1}{2}\left[\frac{a^2}{D(D+z)}\right] \qquad (2.9)$$

Low-geometry counting system

Fig. 2.11 shows a cross-section of the low-geometry system used to determine the absolute α activity of the ^{243}Am source. The system consisted of a source holder, solid-angle defining aperture and silicon surface barrier α detector mounted coaxially and placed within a cylindrical vacuum chamber of 38 mm inside diameter. The separation distance between the source and solid-angle defining aperture was controlled by three 5 mm diameter spacing rods of accurately machined length which also served to maintain the coaxial source-aperture-detector geometry. Three anti-scatter collimators were situated between the source and the aperture; the positions of these three collimators along the length of the chamber were adjusted to minimise the possibility of a single or multiple wall-scattered α particle entering the α particle detector and being counted above the α detection threshold level.

The diameter of the solid-angle defining aperture was chosen to stop any emitted α particle striking the extreme edge of the 50 mm^2 active area of the Si(Au) surface barrier detector and thereby registering only part of its full energy within the depleted region of the detector before escaping from the Si crystal. The reduced

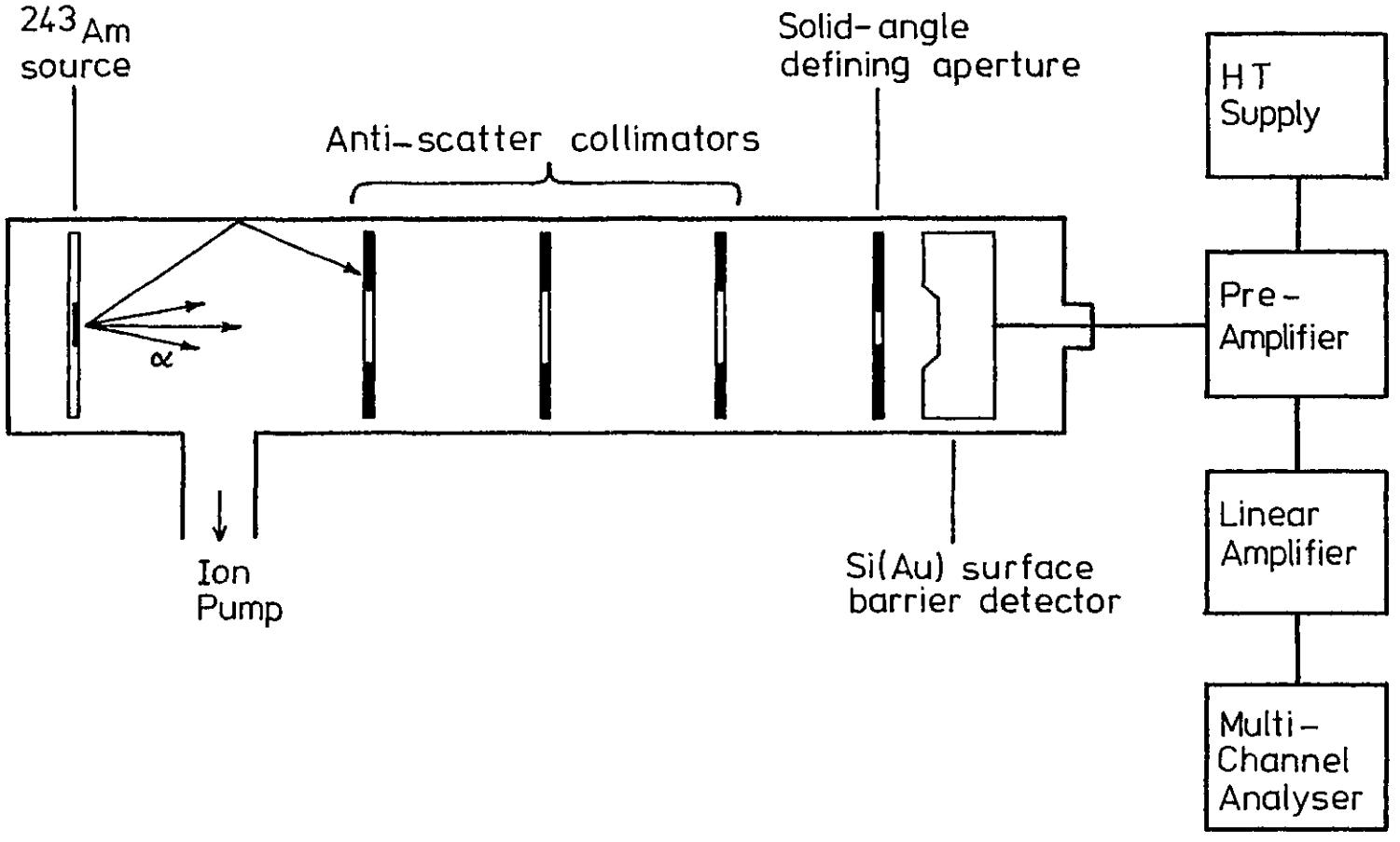

Fig. 2.11 Schematic cross-section of low geometry α counting system

pulse from this α event might then appear below the α detection threshold level and be lost (in the spectrum background) from the total α particle count.

After initially reducing the pressure in the experimental chamber by means of a diffusion-rotary pump combination the chamber was isolated and its pressure maintained at ~ 6 x 10^{-6} mbar using an ion pump.

After suitable signal amplification α spectra were recorded using an ADC conversion gain of 4096 channels.

Sample decay rate measurements

The absolute α decay rate of the ^{243}Am source was measured in two different source geometries by changing the source-aperture separation distance. The diameter of the solid-angle defining aperture (common to both geometries) was measured with a travelling microscope; the mean diameter of the aperture and its associated error were derived from a set of six measurements.

Table 2.8 lists the relevant source-aperture separations, aperture and source diameters used in eqns. 2.8 and 2.9 to determine the geometry factors Gs(1) and Gs(2), corresponding to the two source-aperture separations. The overall uncertainties in the Gs are determined mainly by the uncertainties in the aperture diameter and the source-aperture separation distance; this can be seen by considering that, for the source-aperture separations used in this experiment, a/z ~ b/z << 1 and eqns. 2.8 and 2.9 therefore reduce to

$$Gs \simeq G\acute{p} \qquad (2.10)$$

$$G\acute{p} \simeq a^2/4z^2 \qquad (2.11)$$

respectively. Hence the geometry Gs is independent of b and its associated uncertainty and can be well approximated by the geometry, $G\acute{p}$, of an effective point ^{243}Am source. Calculations, using eqns. 2.10 and 2.11, predict geometry factors which differ by only 0.005- and 0.009% from the tabulated values for Gs(1) and Gs(2) respectively. The final uncertainties in Gs(1) and Gs(2) are of the order of 0.41- and 0.42% respectively.

Table 2.8 Data used to determine Geometry Factors, Gs

	Geometry 1	Geometry 2
Source diameter (mm)	7.0 ± 0.1	
Aperture diameter (mm)	5.03 ± 0.01	
Source-aperture separation (mm)	550.48 ± 0.26	400.48 ± 0.26
Geometry factor Gs	(5.218 ± 0.021) - 6	(9.859 ± 0.041) - 6

Fig. 2.12(a) shows a typical ^{243}Am singles α spectrum obtained with the low-geometry system. The low energy α detection threshold level is set at ≃ 2 MeV in the well defined region separating the low energy spectrum tail (composed of β^-s and conversion electrons from ^{239}Np decay and conversion electrons from ^{243}Am decay) from the higher energy ^{243}Am α peaks. The advantage of using anti-scatter collimators to determine an accurate value for the low energy α cut-off is well illustrated in fig. 2.12(b) which shows an α spectrum obtained without the use of anti-scatter collimators; in this case it is difficult to assess which part of the pulses should be attributed to degraded α particles emitted originally into the measured solid angle, which part should be attributed to wall-scattered α particles with an originally 'wrong' direction, and at what level the threshold for β^- and conversion electron detection should be set so as to exclude these pulses from the measured α count.

Fig. 2.13 is an expanded region of fig. 2.12(a) showing the resolved ^{243}Am peaks. A resolution (FWHM) of 13.8 keV was obtained in the case of the intense α_{75}(Eα = 5276 keV) peak. The small peak at ~ 5485 keV was identified as an impurity of ^{241}Am. The ^{241}Am impurity content in the source was estimated to be less than 0.01%. The upper limit for ^{243}Am α particle detection was therefore set to exclude those counts from the α decay of the ^{241}Am impurity and the contribution to the total ^{243}Am α count from the low energy tail of the ^{241}Am impurity was assumed to be zero.

The low α count rates involved - ≃ 0.24 s^{-1} for Gs(1) and ≃ 0.45 s^{-1} for Gs(2) - excluded the possibility of random (α-α) summing effects within the detector.

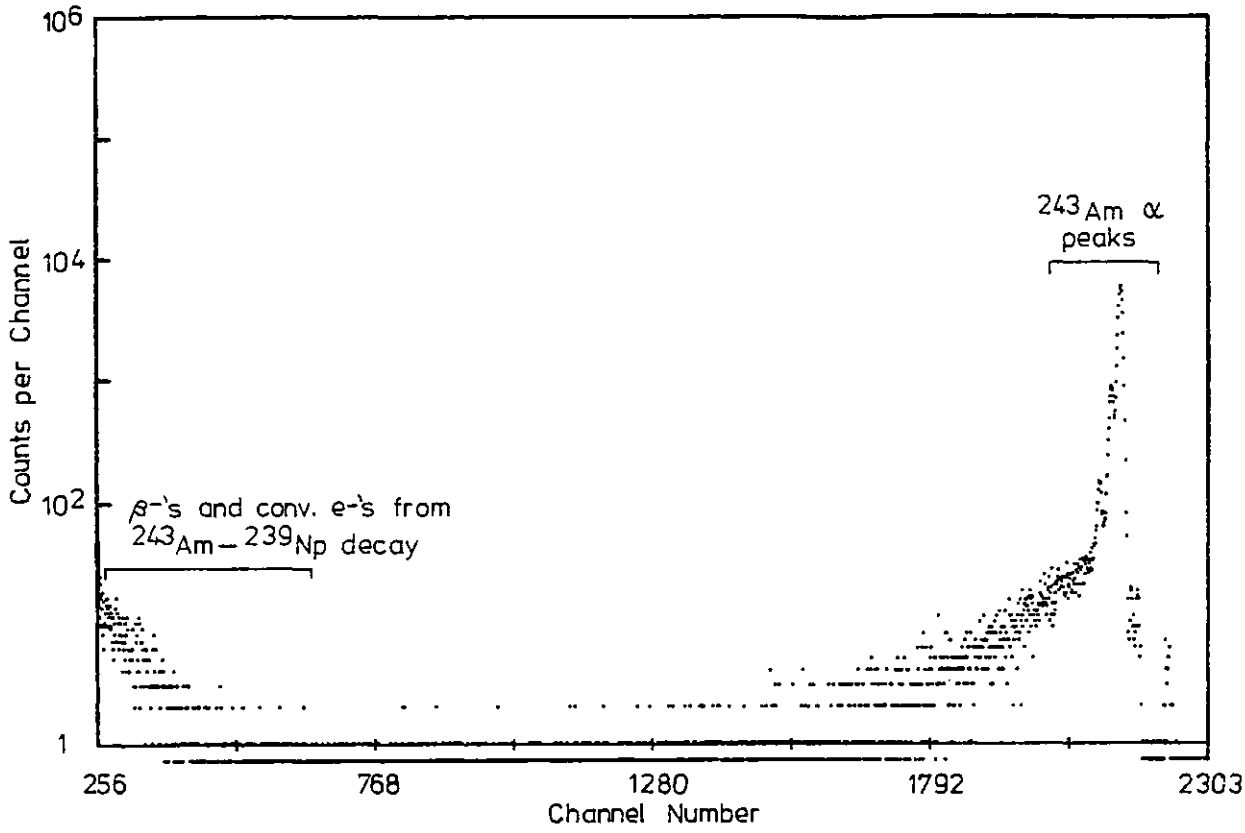

Fig. 2.12(a) ^{243}Am singles α spectrum obtained using anti-scatter collimators in low geometry counting system

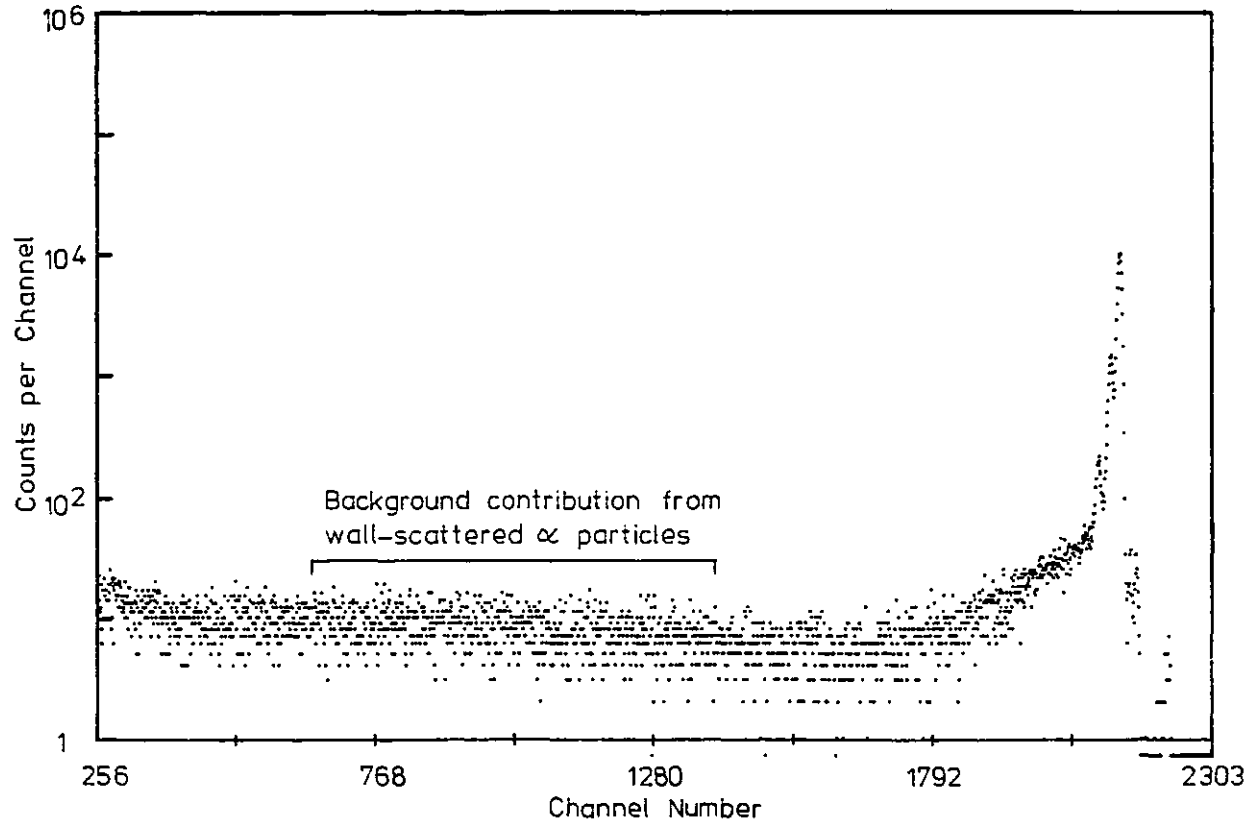

Fig. 2.12(b) ^{243}Am singles α spectrum obtained without anti-scatter collimators in low geometry counting system

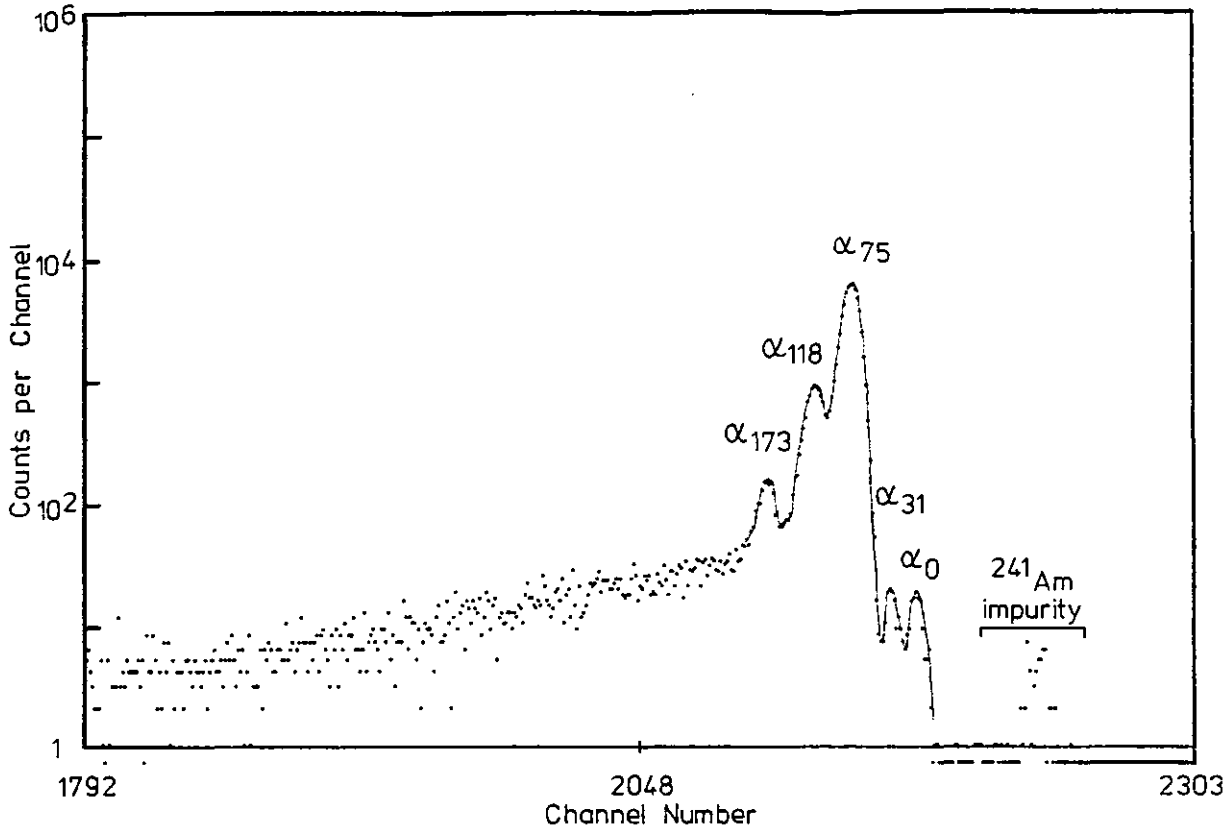

Fig. 2.13 Expanded region of fig. 2.12(a) showing resolved ^{243}Am α peaks and ^{241}Am impurity. ^{243}Am α peaks are labelled according to energy level populated in ^{239}Np

The error in the total α count due to the uncertainty in the lower level threshold setting was found to be negligible compared to the uncertainty component derived from the statistical fluctuations in the source.

Table 2.9 lists the mean α count rates and their associated statistical uncertainties for the geometries Gs(1) (15 measurements) and Gs(2) (44 measurements). The statistical uncertainties are found to be in good agreement with the standard deviations predicted from the observed spreads in the complete set of individual counting rate measurements for each geometry. The measured α decay rate of the ^{243}Am source is then obtained by a simple division of the observed α count rate by the appropriate geometry factor.

Table 2.9 Decay Rate Measurements for ^{243}Am Source

	Geometry 1	Geometry 2
Total counting period ($\times 10^3$s)	840	1133
Mean α count rate (s^{-1})	0.2382 ± 0.0007	0.4475 ± 0.0007
Measured α decay rate (s^{-1})	(4.565 ± 0.023) + 4	(4.539 ± 0.021) + 4
Final α decay rate corrected for backscattering (s^{-1})	(4.562 ± 0.023) + 4 ≡(1.233 ± 0.006)μCi	(4.536 ± 0.021) + 4 ≡(1.226 ± 0.006)μCi

The measured α decay rate is then corrected to take into account the effect of α particle backscattering from (i) the ^{243}Am source stainless steel backing support, and (ii) the gold window of the Si(Au) surface barrier detector. An approximate calculation, using the Rutherford differential scattering cross-section, to estimate the contribution to the measured α decay rate by α particle backscattering from the source support, has been performed in detail in Appendix 2; a decrease in the observed α decay rate of the order of 0.06% is predicted.

The correction for α particle backscattering from the gold window of the Si(Au) surface barrier detector can be calculated in the same manner using the Rutherford cross-section. Bambynek[24] obtained a 0.012% correction for the backscattering of 5 MeV α's from a 1 $mgcm^{-2}$ gold foil; since the thickness of the gold window on the surface barrier detector is ≃ 40 μgcm^{-2} then the correction for α particle backscattering from the detector window can be neglected.

Any uncertainty in the geometry factor, and hence the measured α decay rate, due to non-axial alignment of the source and aperture is assumed to be negligible; increases in the geometry factors Gs(1) and Gs(2) of the order of 0.002- and 0.004% respectively are predicted for a 2 mm shift off axis by the source (or aperture). The three source-aperture spacing rods used in the low-geometry counting system precluded any such movement of this magnitude.

The final corrected ^{243}Am absolute α decay rate obtained from each counting geometry is listed at the end of table 2.9. The overall uncertainty in each decay rate includes the contributions from the geometry factor and the α count rate combined in quadrature. Overall uncertainties of 0.50- and 0.45% in the ^{243}Am disintegration rate are thus obtained for the measurements carried out in geometries 1 and 2 respectively.

2$\pi\alpha$ Counting

An independent check on the measured ^{243}Am absolute α activity was made by counting the source in the proportional counter of the 4π β-γ coincidence system. The efficiency of the proportional counter for α particle detection was determined using a calibrated ^{241}Am source ($T_{\frac{1}{2}}$ = 432.2 years) of identical physical dimensions, construction and active area as the ^{243}Am source. The α disintegration rate of the ^{241}Am source was also measured in the coincidence counting system to verify the calibrated measurement. (A direct measurement of the ^{243}Am source absolute α disintegration rate using coincidence counting techniques was not possible because, unlike ^{241}Am which is a pure α emitter, ^{243}Am is both an α and β^- emitter - the latter arising from the decay of ^{239}Np present in equilibrium with the ^{243}Am - and therefore its decay scheme characteristics cannot be described in terms of the usual coincidence equations used to determine source disintegration rates.)

Since no α particles could escape through the ^{241}Am source stainless steel backing, the absolute α activity measurement was made under conditions of 2π geometry. It was also necessary to operate the proportional counter at a lower H.T. voltage of $\approx$ 1050V (compared with 1600V for 4π β-γ coincidence experiments) to prevent overloading of the spectroscopy amplifier in the α channel. The measured α disintegration rate of 5520 $\pm$ 25 disintegrations per second was found to be in close agreement with the calibrated measurement (corrected for source decay) of 5484 $\pm$ 39 disintegrations per second. Corresponding to the minimum α particle discrimination threshold used in the 2π α-γ coincidence counting the proportional counter was found to have a maximum α detection efficiency (N_c/N_γ) of 0.505 $\pm$ 0.002. This value implies that approximately 1% of the α's detected are due to backscattered events in the source support.

The ^{243}Am source was then counted at the same minimum setting of the α detection threshold to determine the mean number of α's per second emitted from the front face of the source. To check that no β^-'s from the decay of ^{239}Np were being counted in the α channel the ^{243}Am source was replaced by a ^{239}Np source produced by ^{239}U β^- decay; no counts were registered in the α channel above the minimum α detection threshold.

A mean α count rate of $(2.2895 \pm 4)s^{-1}$ (0.06% uncertainty) was obtained after correcting the observed count rate for dead-time effects. No corrections for background effects were applied because the reduced operational voltage of the proportional counter resulted in no background counts being observed in the α channel.

The ^{243}Am source α decay rate is obtained by dividing the measured α count rate by the α particle detection efficiency, producing a final disintegration rate of $\{(4.534 \pm 0.018) \pm 4)\}$ disintegrations per second ($\equiv 1.225 \pm 0.005$ μCi). This value is in good agreement with the two values predicted from the low-geometry α counting experiment. A final absolute α activity for the ^{243}Am source of (1.228 ± 0.004) μCi is obtained from a weighted calculation of the mean disintegration rate and its associated error using the two measurements from the low-geometry α counting and the single measurement from the 2πα counting. No correction has been applied to the final ^{243}Am source absolute α activity value to take into account the decay of the source during the seven month period required to perform the low geometry α counting, 2πα counting and γ-ray analysis since, over this period, the calculated decrease in the ^{243}Am source ($T_{\frac{1}{2}}$ = 7370y) α activity is only of the order of 0.006%.

2.5 Calculation of ^{239}U β^- Branching Intensities

The ^{239}U β^- branching intensities β_1, β_2 and β_3 feeding the 117.8, 74.67 and 31.14 keV levels in ^{239}Np respectively are given, using eqns. 2.1 and 2.2 and the decay scheme characteristics of fig. 2.2, by the following expressions;

$$\beta_1 = \frac{N_o(\alpha)}{N_o(\beta^-)} \frac{I_{87}(\beta^-)}{I_{87}(\alpha)} [\alpha_1 + \alpha_0 F_{55}]S \qquad (2.12)$$

$$\beta_2 = \frac{N_o(\alpha)}{N_o(\beta^-)} \frac{I_{74}(\beta^-)}{I_{74}(\alpha)} [\alpha_2 + \alpha_1 F_{43.1} + \alpha_0 (F_{98} + F_{55} F_{43.1})]S - [\beta_1 F_{43.1}] \qquad (2.13)$$

$$\beta_3 = \frac{N_o(\alpha)}{N_o(\beta^-)} \frac{I_{31}(\beta^-)}{I_{31}(\alpha)} [\alpha_3 + \alpha_2 F_{43.5} + \alpha_1 (F_{87} + F_{43.1} F_{43.5}) + \alpha_0 (F_{142} + F_{98} F_{43.5} + F_{55} F_{87} + F_{55} F_{43.1} + F_{55} F_{43.1} F_{43.5})]S - [\beta_1 (F_{87} + F_{43.1} F_{43.5}) + \beta_2 F_{43.5}] \qquad (2.14)$$

Here α_0, α_1, α_2 and α_3 are the α branching intensities to the 173.2, 117.8, 74.67 and 31.14 keV levels in ^{239}Np respectively and S is a correction factor to take into account the difference in solid angle subtended at the Ge detector by the extended (7 mm dia.) ^{243}Am source and the effective point (1 mm dia.) ^{239}U sources counted at the same source-detector distance. The subscripts on the measured γ-ray intensities $I_\gamma(\alpha)$, $I_\gamma(\beta^-)$ and the level branching fraction F_γ refer to particular γ transitions within the level scheme of fig. 2.2. All terms involving F_γ in the expressions for β_1, β_2 and β_3 are correction terms to allow for the population of the level by the decay of higher excited states. However, no corrections are made to allow for feeding from higher levels (populated by either α or β^- decay modes) not shown in fig. 2.2; this is a good approximation since the α branches shown in fig. 2.2 account for 99.9% of all α decays from ^{243}Am and the remaining 1% of β^- transitions from ^{239}U decay unaccounted for in fig. 2.2 populate (via γ decay) the 31.14 keV and ground state levels in the ratio 1:3 respectively with negligible feeding of the 117.8 and 74.67 keV levels.

2.5.1 ^{243}Am α branching intensities

^{243}Am α branching intensities recommended by the latest Nuclear Data Sheets[5] and Table of Isotopes[4] are given in columns 3 and 4 respectively of table 2.10. A third set of α branching intensities

has been proposed by Rogers[25] (column 5). Differences in the recommended values reflect the importance attached by the evaluator to each of the two existing complete sets of experimental ^{243}Am α branching intensity measurements by Hummel[26] and Baranov[27] (see columns 6 and 7); the Table of Isotopes quotes the more recent measurements of Baranov whilst Rogers takes the mean of the two sets of data for his recommended α_1 and α_2 intensities. Nuclear Data Sheets attaches more importance to the recent Baranov experimental data and the α_1, α_2 intensities quoted are in fact taken from an evaluation of transactinium α decay data by Baranov[28]. Although the quoted uncertainty in the intense α feed to the 74.67 keV level, α_2, is of the correct order of magnitude for an α branch intensity measurement using magnetic spectrometry techniques the quoted uncertainty in α_1 seems erroneous and is more likely to be of the order of $\pm$ 0.10 rather than $\pm$ 0.01. The α branching ratios used to calculate the ^{239}U β^- branching intensities in this work are those recommended by Nuclear Data Sheets.

Table 2.10 Recommended and Experimental Values of ^{243}Am α Branch Intensities

α Branch	E_α (keV)	^{243}Am α branch intensity (%)				
		Recommended intensities			Exptl measurements	
		Nuclear Data Sheets[5]	Table of Isotopes[4]	Rogers[25]	Hummel[26]	Baranov et al.[27]
α_0	5181	1.1	1.1	1.1	1.1	1.1
α_1	5233.5	10.73 $\pm$ 0.01	10.6	11.0	11.5	10.6
α_2	5275.4	87.8 $\pm$ 0.5	87.9	87.4	87.1	87.9
α_3	5321	0.12	0.12	0.12	0.16	0.12
α_4[a]	5350	0.16	0.16	0.18	0.17	0.16

a. α branch feeding ^{239}Np ground state included for completeness

2.5.2 Level branching fractions, F_γ

Table 2.11 lists the relevant data used to calculate the level branching fractions, F_γ, which are independent of the mode of formation of the level. The data is taken from the Nuclear Data Sheets[5] evaluation of ^{243}Am α decay data except that for the 46.7 keV transition which is taken from the results of this work. Assuming equal γ detection efficiency for the 46.7 and 86.7 keV γ transitions (this is later proved to be an extremely good approximation) then the ratio of the measured γ-ray intensity of the 46.7 keV transition to the 86.7 keV transition is 0.17 using the results of table 2.7. The intensity of the 46.7 keV transition is therefore 0.057γ/100α and is in good agreement with the value of 0.056γ/100α obtained by Engelkemeir[8]. Also, assuming an E1 type transition (total I.C.C. ~ 1) then the intensity of this transition is 0.114 ($\gamma + e^-$)/100α which is 1% of the total transition intensity from the 117.8 keV level. No value of total I.C.C. for the 43.1 keV transition appears in table 2.11 because of the experimental difficulty in determining the relative γ-ray intensity of this transition.

Table 2.11 Data used in Calculating Branching Fractions, F_γ

γ Transition energy (keV)	Transition type	Total I.C.C.	I_γ †	Total ($\gamma + e^-$)/ 100α decays
31.14	M1 + E2	≈170	0.11	≈12
43.1	M1 + E2	-	-	-
43.53	E1	1.16	8.4	12
46.7	E1	≈1	≈0.087	≈0.114
50.6	E1	0.78	0.004	0.0052
55.4	M1 + E2	≈114	0.015	≈1.17
74.67	E1	0.28	100	84
86.75	E1	0.19	0.51	0.40
98.5	E2	15.9	0.014	0.156
117.8	E1	0.086	0.84	0.60
142.0	E1	0.23	0.19	0.15

† For absolute intensity per 100α decays multiply by 0.66

Table 2.12 lists the level branching fractions, F_γ, for the transitions given in table 2.11. The total branching fraction from each level is, by definition, equal to 1.0.

Table 2.12 Branching Fractions from the 173.2, 117.8, 74.67 and 31.14 keV levels of ^{239}Np

γ Transition energy (keV)	Branching fraction F_γ
173.2 keV level	
142.0	0.136
98.5	0.142
55.4	0.717[a]
50.6	0.005
117.8 keV level	
117.8	0.052
86.7	0.035
46.7	0.010
43.1	0.903[a]
74.67 keV level	
74.67	0.875
43.53	0.125
31.14 keV level	
31.14	1.000

a. Determined by difference to make the sum of the branching fractions equal to unity

The total number of transitions depopulating the 173.2 keV level, according to table 2.11, is 1.48 $(\gamma + e^-)/100\alpha$ decays compared with a level populating (feeding) intensity of $1.1\alpha/100\alpha$ decays; this discrepancy reflects the experimental difficulty in determining the total I.C.C. and hence the total $(\gamma + e^-)$ transition intensity of the mixed multipolarity, highly internally converted, 55.4 keV transition. Therefore, the total intensity of the 55.4 keV transition has been

recalculated by making the total $(\gamma + e^-)/100\alpha$ decays for all transitions from the 173.2 keV level sum to 1.1 using the individual intensities of the 50.6, 98.5 and 142.0 keV transitions listed in table 2.11. (The intensities of the 50.6, 98.5 and 142.0 keV transitions are assumed to be accurate since the transitions are of pure multipole type and their I.C.C.'s are well known.) In this manner the 55.4 keV total transition intensity is calculated to be $0.789(\gamma + e^-)/100\alpha$, leading to the 173.2 keV level branching fractions listed in table 2.12. The 55.4 keV transition branching fraction is found to be in approximate agreement with a value of 0.688 calculated by Engelkemeir[8].

Using the calculated intensity of the 55.4 keV transition the total number of transitions depopulating the 117.8 keV level is found to be 11.52 $(\gamma + e^-)/100\alpha$, of which $10.41(\gamma + e^-)/100\alpha$ go via the highly internally converted 43.1 keV transition. The 43.1 keV transition branching fraction from the 117.8 keV level has been calculated by difference to make the sum of the 117.8, 86.7, 46.7 and 43.1 keV branching fractions equal to unity. (Again, the 117.8, 86.7 and 46.7 keV transition intensities are assumed to be accurate because of the pure multipole nature of these transitions.) This leads to a branching fraction of 0.903 for the 43.1 keV transition which is in good agreement with the value of 0.905 determined by Engelkemeir[8].

The total number of transitions populating the 74.67 keV level in ^{239}Np is then calculated to be 98.4 transitions/100α decays which agrees reasonably well with the sum of the 74.67 and 43.53 keV total transition intensities listed in table 2.11. More recent γ decay data[19] indicates that the relative γ intensity of the 43.53 keV transition compared to the 74.67 keV transition is 0.091 and therefore the total number of transitions depopulating the 74.67 keV level is increased to 97.0, in closer agreement with the calculated number of transitions populating this level.

Since the 31.14 keV level de-excites via one γ transition only then the branching fraction of this transition is equal to unity.

2.5.3 Solid angle correction factor, S

The fractional solid angle subtended at the Ge detector by the coaxially mounted 7 mm dia. ^{243}Am disc source is calculated to be 1.0478-2, compared with a fractional solid angle of 1.0486-2 for a coaxial 1 mm dia. ^{239}U source at the same source-detector distance. Therefore the solid angle subtended by the disc ^{243}Am source to that subtended by the ^{239}U 'point' source at the Ge detector, is calculated to be 0.9992.

Since a true point source subtends a fractional solid angle of 1.0487-2 at the same source-detector geometry then the variation in ^{239}U source diameter (0.5 to 1.2 mm) can be assumed to produce a negligible change in the fractional solid angle subtended at the detector.

Similarly, changes in the solid angle due to source being mounted off axis (relevant in the case of the ^{239}U sources where the ^{239}U solution was not always placed centrally on the thin VYNS film) are calculated to be negligible; the maximum off axis location of a ^{239}U source was 1.7 mm corresponding to a 0.03% decrease in the fractional solid angle subtended at the detector by a coaxially mounted ^{239}U source of the same diameter.

2.5.4 Intensity calculations

Branching intensity β_1

Data on the measured γ-ray intensity of the weak 86.7 keV γ transition from ^{239}U β^- decay is available only for the extended, high activity ^{239}U sources. (See table 2.4, sources 6 and 7.) β_1 is therefore determined by rearranging eqn. 2.12 into the form

$$\beta_1 = \frac{N_o(\alpha)}{I_{87}(\alpha)} \frac{I_{87}(\beta^-)}{I_{74}(\beta^-)} \frac{I_{74}(\beta^-)}{N_o(\beta^-)} [\alpha_1 + \alpha_o F_{55}] S$$

where the measured γ-ray intensity ratio of the 86.7 and 74.7 keV transitions is determined from the data obtained from sources 6 and 7 and the ratio of the measured γ-ray intensity of the 74.7 keV transition to the source β^- activity is taken to be the mean ratio calculated from the data for sources 1 to 5.

The data of tables 2.4 and 2.6 predict a mean value for the ratio $I_{74}(\beta^-)/N_o(\beta^-)$ of 4.672-3 (1.90% uncertainty). The experimental ^{243}Am source α disintegration rate measurement (section 2.4.4) and the measured γ-ray intensity of the 86.7 keV transition from ^{243}Am α decay (section 2.4.3) combine to give a value for the ratio $I_{87}(\alpha)/N_o(\alpha)$ of 3.015-3 (0.60% uncertainty). Sources 6 and 7 predict a value for $I_{87}(\beta^-)/I_{74}(\beta^-)$ of 1.01-3 (12.9% uncertainty). Hence, combining these results with the tabulated values of α_1, α_0 (table 2.10) and F_{55} (table 2.12), the absolute ^{239}U β^- branching intensity β_1 is calculated to be 1.80/100 β^- decays. The uncertainty in β_1 due to the uncertainties in the experimental measurements alone is calculated to be 13.0% (i.e. 0.60, 1.90 and 12.9% combined in quadrature).

A contribution to this uncertainty must now be made to allow for uncertainties in the tabulated values of α_0, α_1 and F_{55}. The uncertainty in the solid angle correction factor S is assumed to be small (i.e. less than 1%). The uncertainty in α_1 is assumed to be ten times larger than the value quoted in table 2.10 and is therefore of the order of 0.9%. Allowing 20.0% uncertainties in each of the total (γ + e^-) transition intensities of the 142.0, 98.5 and 50.6 keV transitions the overall uncertainty in F_{55} is calculated (using eqn. 2.4) to be of the order of 7.0%. Therefore, allowing for a 10% error in α branch intensity α_0, the overall uncertainty in β_1 is calculated to be 13.1%. The final uncertainty in β_1 is therefore relatively insensitive to large errors in the level branching fraction and the intensity of the higher feeding α branch. (Even allowing for a 5% uncertainty in α_1 increases the overall uncertainty in β_1 to only 13.8% and a factor-of-two error in F_{55} leads to only a 7% increase in the value of β_1.)

Branching intensity β_2

Beta branch β_2 is determined using eqn. 2.13. The value of $I_{74}(\beta^-)/N_o(\beta^-)$ has been determined previously and is set equal to 4.672-3 (1.90% uncertainty). The value of $I_{74}(\alpha)/N_o(\alpha)$ is calculated to be 6.493-3 (0.33% uncertainty). Using the value of β_1 determined in the previous section the absolute ^{239}U β^- branching intensity β_2 is calculated to be 69.1/100β^- decays. (1.93% uncertainty from experimental γ decay and source disintegration rate measurements.)

The uncertainty in $F_{43.1}$, assuming 20% uncertainties in the total ($\gamma + e^-$) intensities of the 117.8, 86.7 and 46.7 keV transitions, is calculated to be 1.4%. The uncertainty in F_{98} is assumed to be 20%. Therefore the overall uncertainty in β_2 (using the previously determined uncertainties in α_0(10%), α_1(0.93%), α_2(0.57%), F_{55} (7.0%) and β_1(13.1%)) is calculated, using eqn. 2.4, to be 2.1%.

The increase in overall uncertainty in β_2 (from 1.9 to 2.1%) is accounted for almost entirely by the accuracy to which α_2 is known and is again insensitive to much larger uncertainties in the level branching fractions and higher level α and β^- feeding intensities than used in the present calculation, although the present values are considered realistic.

Branching intensity β_3

In a similar manner to that used to calculate the β^- branch intensity β_1 the value of β_3 has been determined by utilising the 31.14 keV γ transition data obtained from sources 6 and 7 (of unknown β^- activity) as well as that from source 4 (see table 2.4). The expression for β_3 (eqn. 2.14) is therefore required in the form

$$\beta_3 = \frac{N_o(\alpha)}{I_{31}(\alpha)} \frac{I_{31}(\beta^-)}{I_{74}(\beta^-)} \frac{I_{74}(\beta^-)}{N_o(\beta^-)} [\alpha_3 + \alpha_2 F_{43.5} + ...]S -$$

$$[\beta_1(F_{87} + F_{43.1}F_{43.5}) + \beta_2 F_{43.5}]$$

A weighted mean calculation of $I_{31}(\beta^-)/I_{74}(\beta^-)$ for the three sources yields 1.29-3 (11.0% uncertainty). The value of $I_{31}(\alpha)/N_o(\alpha)$ is calculated to be 4.318-6 (1.49% uncertainty). The value of $I_{74}(\beta^-)/N_o(\beta^-)$ has been determined previously.

Using the calculated values of β_1 and β_2 and the tabulated level branching fractions and α branch intensities, the ^{239}U β^- branch intensity β_3 is calculated to be 10.2/100β^- decays. The uncertainty component in β_3 due to the uncertainties in the measured γ decay data and source absolute disintegration rates is calculated to be 11.3%. The value of β_3 is found to be in good agreement with the value of 10.1/100β^- decays determined from the γ and β^- activity data of source 4 alone.

For beta branch β_3 the overall uncertainty in the calculated β^- branch intensity is highly dependent upon the value of $F_{43.5}$; this is due to the fact that the α branch which directly feeds the 31.14 keV level is of weak intensity and, to a good approximation, all transitions populating the level proceed via the 43.53 keV transition which itself is fed by the most intense α branch (α_2 = 87.8%). Therefore, the correction terms involving F_γ which take into account feeding from higher levels, and which in the previous calculations of β_1 and β_2 have been small because the α and β^- branch intensities feeding these higher levels have themselves been small, now dominate the expression for β_3. Thus, whereas in the calculations of β_1 and β_2 the only other major source of uncertainty (apart from the experimental γ decay and source disintegration measurements) was the error in the α branch intensity populating the same level as the β^- branch under consideration, in the case of β_3 a large uncertainty in α_3 produces negligible change in the existing uncertainty component derived from the experimental γ and absolute activity measurements. Indeed a factor-of-two increase in the value of α_3 leads to only a 1.7% increase in the calculated value of β_3. The overall uncertainty in β_3 is therefore now dependent upon how well the value of $F_{43.5}$ is known.

An order of magnitude estimate for the uncertainty in $F_{43.5}$ is derived from the inbalance in the calculated number of transitions populating (98.4/100α decays) and depopulating (97/100α decays) the 74.67 keV level in ^{239}Np; if the discrepancy is due solely to errors in the measured γ and e^- (I.C.C.) data for the 43.5 keV transition then the error in $F_{43.5}$ is estimated to be of the order of 12%.

Alternatively, a more rigorous calculation of the uncertainty in $F_{43.5}$ can be made using the known uncertainties in the measured relative γ-ray intensity rate of the 43.53 and 74.67 keV transitions and their associated I.C.C.'s; assuming 7.0%[5] and 5.0% uncertainties in the γ-ray intensity ratio and the corresponding I.C.C. data for each transition respectively, the uncertainty in $F_{43.5}$ is calculated to be 6.7%. Therefore, using a compromise uncertainty in $F_{43.5}$ of 10%, the overall uncertainty in β_3 increases from 11.3 to 18.4%.

Branching intensity β_4

The value of the ^{239}U β^- branch intensity to the ^{239}Np ground state is determined from the expression

$$\beta_4 = 0.99 - (\beta_1 + \beta_2 + \beta_3)$$

where the value of 0.99 is used instead of 1.0 to take into account the observed 1% β^- feed to higher levels in ^{239}Np not shown in fig. 2.2. Hence the absolute β^- branch intensity β_4 is calculated to be 17.9/100β^- decays with an associated uncertainty of 13.3%.

Summary of ^{239}U β^- branch intensity calculations

Table 2.13 lists the calculated intensities of the ^{239}U β^- branches feeding the various energy levels, E, in the level scheme of fig. 2.2. Only the effect of true coincidence summing (see section 2.4.2) in the measured γ-ray intensity data from the ^{239}U and ^{243}Am sources has not been taken into account in calculating the beta branch intensities; however, the gross similarity in the structure of level feeding in ^{239}Np from either ^{239}U β^- decay or ^{243}Am α decay leads one to assume that such effects would be approximately the same in either decay mode and would therefore cancel out in the calculation of the beta branch intensities.

Table 2.13 Absolute β^- Branching Intensities from ^{239}U Decay

β^- Branch	E (keV)	Absolute β^- intensity (%)	
		This work	Nuc. Data Sheets[5]
β_1	117.8	1.80 ± 0.24	≈ 2
β_2	74.67	69.1 ± 1.4	73 ± 10
β_3	31.14	10.2 ± 1.9	≈ 6
β_4	0.0	17.9 ± 2.4	19 ± 8

The values of the β^- branch intensities obtained by this method are much more precise than the current published values with the uncertainty in the major β^- branch intensity reduced by approximately one order of magnitude; the uncertainty in the intensity of this

major β^- branch is also at the requested 2% accuracy level proposed by the I.A.E.A. The only major discrepancy between this work and the current published values is in the value of β_3; a possible explanation for this is the fact that β_3 is highly dependent upon the measured γ-ray intensity of the extremely weak 31.14 keV γ transition in ^{239}U β^- decay which, prior to the present work, has not been reported in any study of ^{239}U β^- decay.

2.6 Nuclear Levels and Transitions in ^{239}Np According to the Unified Model

Since the actinide nuclei lie in a region of large nuclear deformation where the nuclei are stabilised in a non-spherical shape under the influence of the coherent effects of many particles in unfilled shells, the strong-coupling Unified Model[29] may be expected to provide useful guidance in the interpretation of the level structure and characteristic features of the ^{239}Np decay scheme. In the region of deformed nuclei the Unified Model predicts a separation of the complete nuclear wave function, ψ, into three parts such that

$$\psi = \chi_{part} \cdot \phi_{vib} \cdot D_{rot}$$

Here χ represents the intrinsic motion of the nucleons which can be expressed in terms of the independent motion of the individual particles in the deformed field. The second factor ϕ_{vib} describes the vibrations of the nucleus around the equilibrium shape; while D_{rot} represents the collective rotational motion of the system as a whole. Since the energy associated with the excitation of the lowest-lying vibrational states is of the order of one MeV then that part of the complete ^{239}Np level structure shown in fig. 2.2 can be interpreted in terms of single particle and rotational motion only.

2.6.1 Single particle states in ^{239}Np

In the ordinary spherical shell model, the energies of individual particle states are calculated by the use of an isotropic potential intermediate between a square well and a harmonic oscillator; with the additional assumption of strong spin-orbit coupling, an order of levels is obtained which reproduces the observed points of major shell closures[30]. In the region of large nuclear deformation such as the actinide (and lanthanide) elements

similar calculations must take account of the fact that the binding field is non-spherical and is dependent upon the amount of deformation. This problem has been considered by several authors[31,32], but here only the results of Nilsson[31] are applied to the interpretation of the ^{239}Np level scheme. Fig. 2.14 is a reproduction of part of the Nilsson energy level diagram, plotted as a function of prolate deformation. In this representation each level is designated by the spin (Ω) and parity (π), the total oscillator quantum number N, and also by the quantum numbers n_z and Λ which are 'good' in the limit of large deformation; n_z and Λ are, respectively, the components of N and the particle orbital angular momentum ℓ along the symmetry axis. The value of Λ is equal to $\Omega \pm \frac{1}{2}$ and is even or odd as $N-n_z$ is even or odd. The Nilsson diagram of fig. 2.14(a) can be used to predict the spins of the ground state and low-lying states of the odd-A ^{239}Np nucleus. Moving vertically through the diagram at the known nuclear deformation (δ) each state is counted twice (each state is doubly degenerate) until the state corresponding to the last particle is reached. This state should then correspond to the observed ground state in spin and parity. The ^{239}Np nucleus has 93 protons (11 past the shell closure at 82) and a deformation δ in the region of 0.2 to 0.25; the above procedure leads to the level indicated by the designation $\Omega\pi\ [Nn_z\Lambda] = 5/2^+\ [642]$. A spin and parity of $5/2^+$ are in agreement with the experimental facts[34]. In addition the 74.67 keV excited level in ^{239}Np has a spin 5/2 and opposite parity to that of the ground state and is therefore assigned to the $5/2^-$ [523] level which lies immediately above the $5/2^+$ [642] level for a δ value of 0.25. Similarly, Fig. 2.14(a) predicts the same $5/2^-$ [523] level assignment for the ground state of ^{243}Am (Z = 95). The Nilsson level diagram of Fig. 2.14(b) assigns the $5/2^+$ [622] level to the ground state of ^{239}U (N = 147).

2.6.2 Rotational excitations in ^{239}Np

Upon each intrinsic structure (single particle state) in the odd-A nuclei is a series of levels with spin sequence I = K, K + 1, K + 2, ... all of the same parity as the single particle state; here K is the component of the total nuclear angular momentum I along the symmetry axis and is a 'good' quantum number in the region of large deformation (see fig. 2.15). This series of levels form a rotational band which is the result of the rotation of the deformed

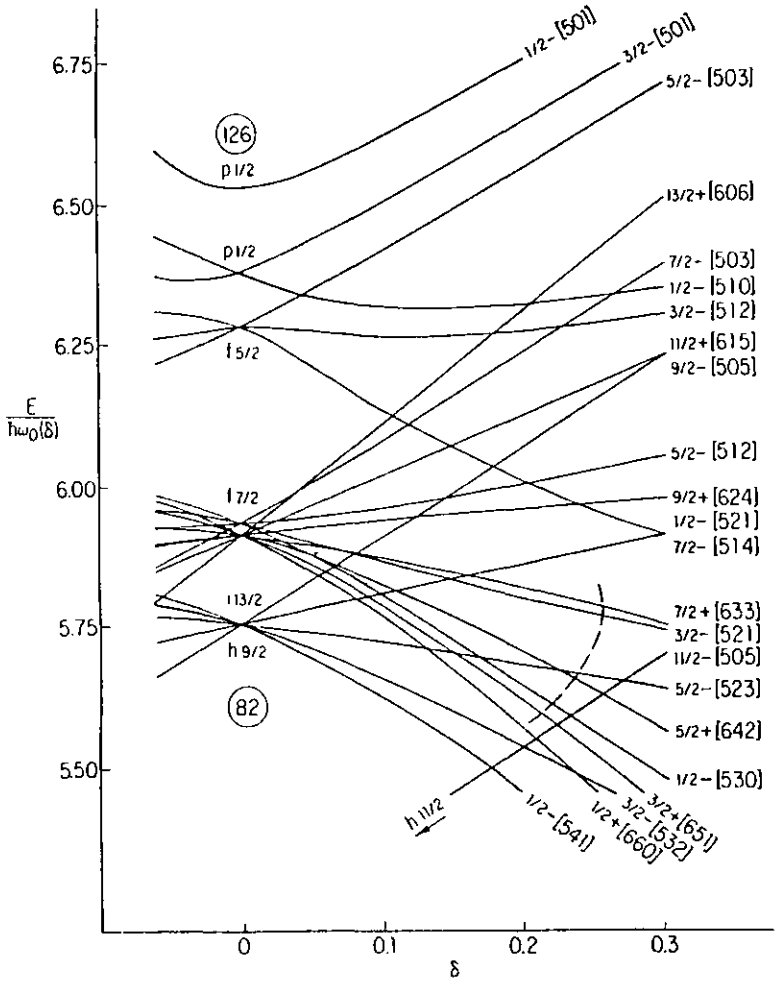

Fig.2.14(a) Energy level diagram for protons in the 82-126 shell as a function of prolate nuclear deformation given in terms of the parameter δ. Shell model assignments are given for the spherical case (δ = 0). For strong deformation each level is labeled with Ω and parity quantum numbers. In brackets the asymptotic quantum numbers [N, n_z, Λ] also are given. From MOTTELSON AND NILSSON.(Ref 33)

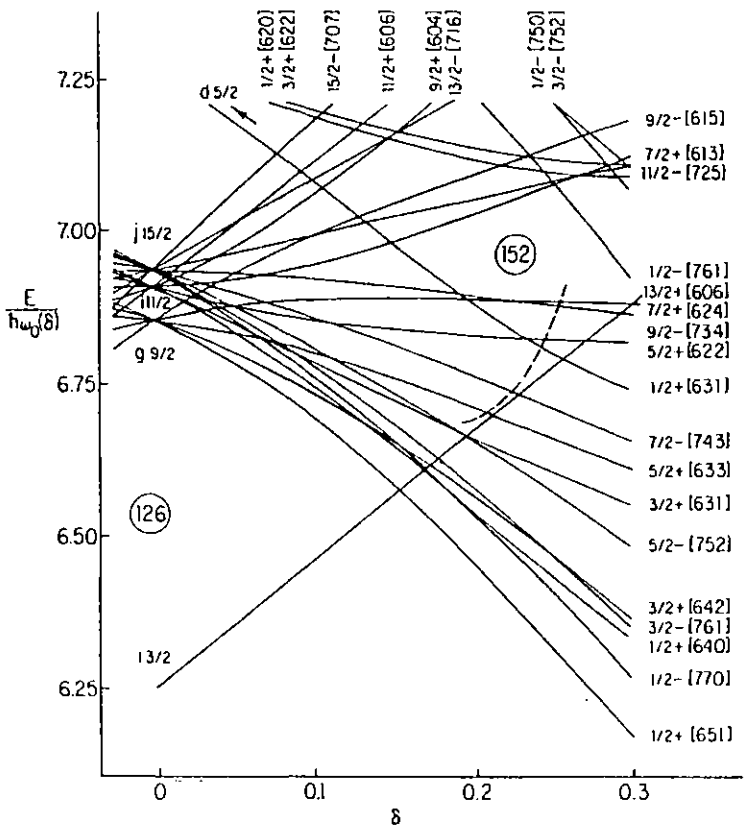

Fig.2.14(b) Energy level diagram for neutrons in the region $126 \leq N \leq 160$ as a function of prolate nuclear deformation. Shell model assignments are given for the degenerate levels in a spherical nucleus. For strong deformation each level is labeled with Ω, π and with the asymptotic quantum numbers [N, n_z, Λ]. The ordinate indicates the energy of the various levels. The dashed line indicates very roughly the deformations empirically found for nuclei with certain numbers of neutrons. From MOTTELSON AND NILSSON.(Ref 33)

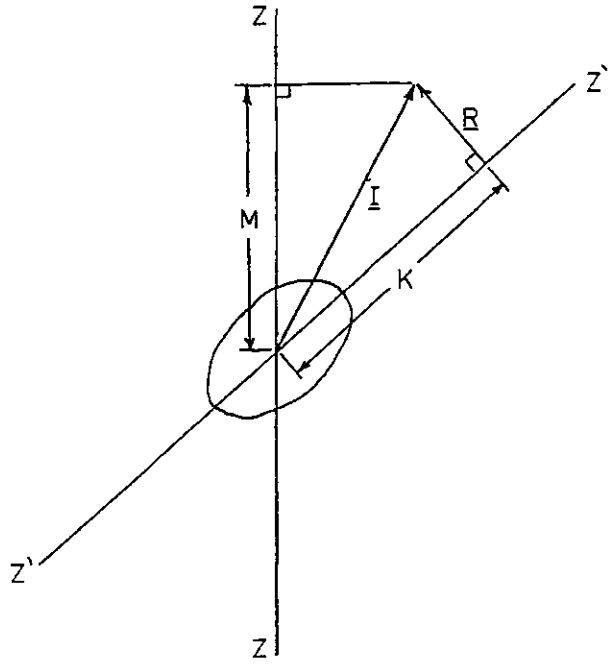

Fig. 2.15 Coupling scheme appropriate for deformed nuclei. $\underline{I}$ is the total angular momentum of the nucleus. K and M are projections of $\underline{I}$ on the axis of symmetry Z' and a space fixed axis Z, respectively. $\underline{R}$ is the collective rotational angular momentum. This vector is always perpendicular to Z'. For the ground state and for many low-lying states K is equal to Ω where Ω is defined as the projection of the total angular momentum of the intrinsic particle motion on the symmetry axis

nucleus with preservation of shape and internal structure. Since the rotational angular momentum is perpendicular to the symmetry axis, all members of a rotational band have the same quantum number K. The rotational energies are given by

$$E_I = \frac{\hbar^2}{2I_m}[I(I+1) - K(K+1)] + E_K \qquad (2.15)$$

except in the special case $K = \Omega = \frac{1}{2}$, I_m being the amount of inertia. In the low-lying levels encountered here, there is no vibrational excitation and so $K = \Omega$ where Ω is the angular momentum of the last unpaired particle.

Fig. 2.16 shows the energy levels of ^{239}Np with associated levels of rotational excitation; the energies of the levels are predicted from eqn. 2.15 for the two lowest states of intrinsic excitation, namely the ground state single particle level ($5/2^+$ [642])

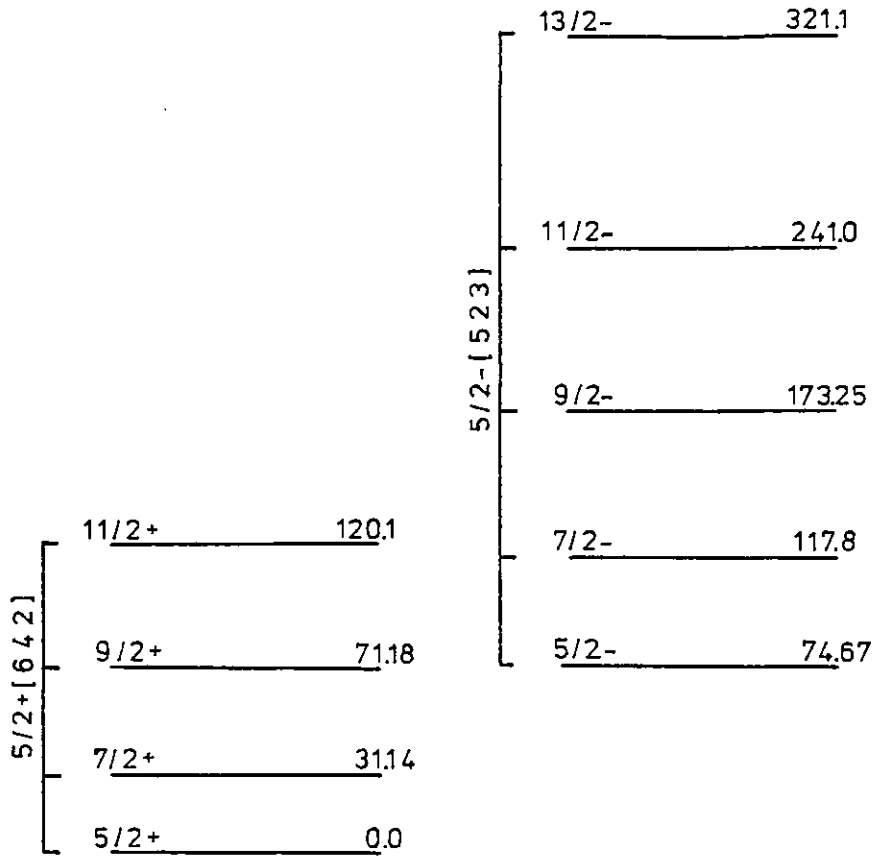

Fig. 2.16 The two lowest states of intrinsic excitation of ^{239}Np with associated levels of rotational excitation. Energies are given in keV at the right of each level, spin values to the left

and the 74.67 keV excited state single particle level ($5/2^-$ [523]). The predicted energies agree well, in general, with the experimental levels given in fig. 2.2; the only exception is the $11/2^+$ member of the ground state rotational band which, from experiment, is placed ~ 3 keV higher than the theoretical value. This discrepancy may be due to a rotational-particle interaction which can cause deviations from the I(I + 1) dependence of the energy level spacing[35].

In section 2.4.2 it was pointed out that the weak 46.7 keV γ transition observed in the singles γ spectra from ^{243}Am α decay was most likely to be a de-excitation of the 117.8 keV level, a fact which was confirmed by (α-γ) coincidence studies carried out in the course of this work (section 3.6). The transition would therefore lead to a new level at 71.1 keV, which agrees well with the predicted energy of the $9/2^+$ member of the ground state rotational band using eqn. 2.15.

The $11/2^-$ member of the rotational band built upon the 74.67 keV state in ^{239}Np is also confirmed by previous ^{243}Am (α-γ) coincidence studies[20] in which evidence was found for a weak 169 keV γ transition between a level at 241 keV (populated by $\sim 5 \times 10^{-3}$% of all α decays) and the predicted $9/2^+$ member of the ground state rotational band ($\Delta E = 241 - 71.2 = 169.8$ keV).

A level at 320 keV in ^{239}Np, populated by an extremely weak α branch[20] (2×10^{-3}%) has been tentatively assigned the $13/2^-$ member of the rotational band built upon the 74.67 keV level.

2.6.3 Consideration of β and γ transitions

The Unified Model also implies definite and simple relations governing the strengths of γ and β transitions within a rotational band, or those from a given nuclear state to the various members of a rotational band. Ratios of reduced transition probabilities for γ or β transitions of given multipolarity* to different members of a rotational band depend only upon a geometrical factor[36]:

$$\frac{B(L,\ I_i \rightarrow I_f)}{B(L,\ I_i \rightarrow I_f')} = \frac{\langle I_i L\ K_i (K_f - K_i) | I_f\ K_f \rangle^2}{\langle I_i L\ K_i (K_f - K_i) | I_f'\ K_f \rangle^2} \qquad (2.16)$$

where L is the multipolarity of the transition, f and f′ denote members of the same rotational sequence ($K_f = K_f'$), and the $\langle | \rangle$ are Clebsch-Gordan coefficients representing the vector addition of the angular momentum I_i and L to form I_f.

The ratio of γ-rays emission probabilities for a given multipolarity is then given by[36]

$$\frac{T(L,\ I_i \rightarrow I_f)}{T(L,\ I_i \rightarrow I_f')} = \left(\frac{E}{E'}\right)^{(2L+1)} \frac{B(L,\ I_i \rightarrow I_f)}{B(L,\ I_i \rightarrow I_f')} \qquad (2.17)$$

where T is the transition probability per second and E and E′ are the energies of the transitions populating the states f and f′ respectively.

*In the case of β transitions, the term multipolarity here refers to the total angular momentum of the electron and neutrino.

The reduced relative E1 transition probabilities for the 46.7, 86.7 and 117.8 keV transitions depopulating the $7/2^-$ member of the $5/2^-$ [523] rotational band and the 43.53 and 74.67 keV transitions depopulating the $5/2^-$ member of the same band, are given in table 2.14. The theoretical and experimental reduced transition probability ratios show good agreement despite the fact that the E1 transitions to the K = 5/2 ground state rotational band require changes $\Delta N = 1$, $\Delta n_z = 2$ and $\Delta\Lambda = 1$ which violate the asymptotic rates[37] for E1 transitions and hence are expected to be hindered. (If only the simple selection rule, $\Delta\Omega = 0,1$ parity change was allowable then the dashed lines of figs. 2.14(a) and (b) indicate places where the spin and parity values of near-lying states would permit E1 transitions; the region marked in fig. 2.14(a) includes the ^{239}Np single particle states under consideration here.) An anomalous I.C.C. is usually associated with a hindered γ transition; several examples of such anomalous I.C.C.'s have been found in neighbouring odd-A nuclei[38]. However, the degree of hindrance associated with the E1 γ transitions within the level scheme of ^{239}Np is a factor of 10^2-10^3 smaller than that experienced by neighbouring odd-A nuclei and the experimental I.C.C.'s for ^{239}Np do not deviate from the E1 I.C.C. values predicted by normal internal conversion theory[39,40].

Table 2.14 Reduced Relative E1 Transition Probabilities in ^{239}Np

	Experimental[a]	Theoretical[b]
B(7/2 → 5/2)/B(7/2 → 7/2)	0.66	0.54
B(7/2 → 5/2)/B(7/2 → 9/2)	0.60	0.55
B(7/2 → 7/2)/B(7/2 → 9/2)	0.92	1.02
B(5/2 → 5/2)/B(5/2 → 7/2)	2.36	2.50

a. Deduced from eqn. 2.17 using data of table 2.11.

b. From eqn. 2.16.

Selection rules for β decay of strongly deformed nuclei have been given by Alaga[41]. Beta transitions are classified as 'unhindered' and 'hindered' according to whether they obey or violate the following rules:

Allowed transitions: $\Delta I = 0,1$ no

$\Delta N = 0, \Delta n_z = 0, \Delta\Lambda = 0$

First forbidden transitions: (a) $\Delta I = 0,1$ yes

$\Delta N = 1, \Delta n_z = 0, \Delta\Lambda = 1$

$\Delta N = 1, \Delta n_z = 1, \Delta\Lambda = 0$

(b) $\Delta I = 2$ yes

$\Delta N = 1, \Delta n_z = 0, \Delta\Lambda = 1$

The analysis by Alaga[41] of β decay log ft values in the rare-earth element region has indicated that those β transitions which violate the asymptotic selection rules are in general retarded by about a factor of ten. Table 2.15 lists the experimental log ft values and the quantum number changes which occur in the four main ^{239}U β^- transitions leading to levels in ^{239}Np. The spin and parity changes are listed first to denote the general classification of the transition as allowed or forbidden. Then the changes in N, n_z and Λ are given.

Table 2.15 Analysis of ^{239}U β^- Transitions

Final state in ^{239}Np (keV)	$\Delta I, \Delta\pi$ Type	$\Delta N, \Delta n_z, \Delta\Lambda$	Asymptotic classification	Exptl.[a] log ft.
0.0	0 no, allowed	0 2 0	hindered	6.7
31.14	1 no, allowed	0 2 0	hindered	
74.67	0 yes, 1st forb.	1 0 1	unhindered	6.0
117.8	1 yes, 1st forb.	1 0 1	unhindered	

a. Taken from ref. 6.

The β^- transitions to the ground and 74.67 keV states therefore conform to the assignments of respectively ah (allowed, hindered) and 1u (1st forbidden, unhindered). Calculations of the theoretical log ft values for these two transitions, using the β^- branch

intensities determined in section 2.5.4 and taking no account of asymptotic selection rules for deformed nuclei, predict values of ~5.65 for the β^- transition to the ground state (allowed type classification) and ~5.70 for the transition to the 74.67 keV level (approximated by a 1st forbidden unique classification). The difference of ~1 between the experimental and theoretical log ft values for the ground state transition (equivalent to a factor 10 in the ratio of ft values) agrees well with the magnitude of the hindrance factor proposed by Alaga for β transitions which violate the asymptotic selection rules. The general agreement between the experimental and theoretical log ft values for the 74.67 keV transition confirms the unhindered classification of this transition according to the asymptotic selection rules.

The theoretical ratio of the reduced β^- transition probabilities to the $7/2^+$ and $5/2^+$ members of the ground state rotational band (assumed to be of L = 1 transition type) is calculated, from eqn. 2.16, to be 0.4. Thus the ratio of ft values is expected to be 2.5; using the log ft values quoted in Nuclear Data Sheets[5] ($\log(ft)_{31}$ = 7.1 and $\log(ft)_0$ = 6.6) the ratio is calculated to be 3.1 which is in fairly good agreement with the predicted value. Indeed, using $\log(ft)_{31}$ = 7.1 and $\log(ft)_0$ = 6.7 (i.e. using the experimental value of table 2.15), then the ratio is calculated to be 2.5 exactly; however, it is not certain from the literature[5] whether the log ft value for the β^- transition to the 31.14 keV level has been determined theoretically assuming a 6% β^- feed to this level or whether it has been determined from a knowledge of the experimental ground state log ft value combined with eqn. 2.16 which assumes the transition to be pure L = 1 type.

If the β^- transition to the ground state is not of pure L = 1 type then the ratio of ft values computed from 2.16 can only give a lower bound. The ground state of ^{239}U, which is obtained from an $i11/2$ state at zero nuclear deformation (see fig. 2.14(b)), contains an admixture of the $g9/2$ state at the large nuclear deformation in question ($\delta \sim 0.25$), and the ground state of ^{239}Np, which is obtained from $i13/2$ state at zero deformation contains admixtures of both $g9/2$ and $i11/2$ states at the same deformation; therefore it is possible that the β^- decay to the ground state can proceed by a weak L = 0 channel due to an admixture of j values other than the principal

values required for the transition to proceed via L = 1. The ratio of ft values obtained from Nuclear Data Sheets[5] may therefore reflect the possibility that the β^- transition to the ground state is not of pure L = 1 type. On the other hand, the ratio of ft values for the 31.14 keV and ground state transitions using the experimental β^- branching ratios determined in section 2.5.4 (i.e. $\beta_3 \sim 10\%$ and $\beta_4 \sim 18\%$) is calculated to be ~ 1.8 which is below the theoretical lower limit of 2.5 for pure L = 1 transitions; this may indicate that higher order multiples (L > 1) are influencing the β^- transition rates to members of the $5/2^+$ [642] rotational band.

The ratio of reduced β^- transition probabilities to the $7/2^-$ and $5/2^-$ members of the rotational band based upon the 74.67 keV level in ^{239}Np is calculated, using the currently quoted log ft values[5], to be ~ 30. The theoretical ratio of ft values (assuming the transitions to be pure L = 1 type) is again 2.5. There is therefore a much greater probability for the β^- transition to the 74.67 keV level to proceed by L = 0; this is reflected by the fact that at the large nuclear deformation in question the (h9/2) 74.67 keV level contains an admixture of h11/2 (6.1%). Thus there is ample mixing between the i11/2 and g9/2 states comprising the ^{239}U ground state and the h9/2 and h11/2 states of the $5/2^-$ [523] single particle level for the β^- transitions to the 74.67 keV level to proceed via L = 0. The experimental branching ratios of section 2.5.4 ($\beta_1 \sim 1.8\%$ and $\beta_2 \sim 69\%$) support this conclusion.

2.6.4 Consideration of α transitions

Particles occupying states which differ only in the sign of their projection of total angular momentum along the nuclear symmetry axis interact strongly due to the large overlap of their wave functions. Thus, the formation of an α particle from an independent particle system is expected to take place most easily from two such pairs of protons and neutrons. This type of α decay, which is characterised by the selection rules $\Delta K = 0$ and no change of parity, is referred to as a favoured α transition. In an odd-A nucleus the favoured α decays leave the last odd particle moving in the same orbital in the daughter as in the parent. Hence the most intense α transition occurring in the decay of ^{243}Am (ground state single particle level: $5/2^-$ [523]) is to the $5/2^-$ [523] level at

74.67 keV in ^{239}Np and the transitions to the ground state band are hindered.

The total emission probability for an α particle of a given orbital angular momentum ℓ is shared amongst several fine structure components in each rotational band in ^{239}Np. For a favoured α transition from a parent in a state I_i, K_i to a daughter in a state $I_f, K_f = K_i$, the transition probability is given by[42]

$$P = P_o(Z,E) \sum_{\ell} \frac{1}{F_\ell} \langle I_i \; \ell \; K_i \; O | I_f K_f \rangle^2 \qquad (2.18)$$

The quantity P_o is the transition probability calculated from spin-independent theory and is given by[42]

$$\log_{10} P_o(Z,E) = C - D/\sqrt{E} \qquad (2.19)$$

where E is the energy of the emitted α particle and C and D are constants for each element and vary regularly with Z. The coefficients F_ℓ in eqn. 2.18 are hindrance factors which determine the total reduced transition probability for a given ℓ and are obtained from the observed α intensities in the even-even nuclei where an α particle with given ℓ can populate only a single member of a rotational family. Only even values of ℓ are involved for favoured α transitions since the nuclear parity remains unaltered.

In table 2.16 the favoured ^{243}Am α branch intensities to the first three levels based upon the $5/2^-[523]$ band are calculated in accordance with eqns. 2.18 and 2.19 and compared with the experimental values. The calculations assume ℓ = 0 and ℓ = 2 transitions only and therefore neglect ℓ = 4 and higher contributions which would reduce the calculated α branch intensity to the $9/2^-$ member, bringing it closer into agreement with the experimental branching intensity. Overall, the rather good agreement between experimental and calculated α branching intensities, lends support to the validity of the K quantum number assignments in the ^{243}Am parent and ^{239}Np daughter nuclei.

Table 2.16 Analysis of α decay of ^{243}Am to members of favoured rotational band

Final state spin (K = 5/2)	Relative abundance uncorrected for energy		Energy correction factor	Summation (normalised) %	Experimental intensity %
	ℓ = 0	ℓ = 2			
$5/2^-$	1.0	0.214	1	86.9	87.8
$7/2^-$		0.285	1/1.81	11.3	10.7
$9/2^-$		0.100	1/3.84	1.86	1.1

Hindrance factors for ℓ waves deduced from α decay of ^{242}Pu and ^{244}Cm.

ℓ = 0 : F_0 = 1.0 (by definition)

ℓ = 2 : F_2 = 1.67

Eqn. 2.19: C = 52.491, D = 147.89 - taken from ref. 43.

Equation 2.18 can also be used for the unfavoured α decays which populate the ground state and 31.14 keV levels of the $5/2^+$ [642] rotational band in ^{239}Np. However, the hindrance factors, F_ℓ, are not well known because parity change requirements permit ℓ = 1,3,5 ... transitions only. Therefore the F_ℓ's for use in ^{243}Am must be estimated from the experimental hindrance factors of neighbouring odd-mass α emitters.

Assuming the α decays to the ground and 31.14 keV state to be of pure ℓ = 1 type then eqn. 2.18 predicts the relative α intensity 1:0.27 in favour of the ground state transition. (The unknown F_1 hindrance factors cancel in the expression.) This value is clearly inconsistent with the experimental data given in table 2.10 and predicts an admixture of higher (ℓ = 3,5, ...) terms.

By considering ℓ = 1,3 transitions only, and using the experimental α branch intensities of table 2.10, the ratio of hindrance factors F_1:F_3 is calculated to be of the order of 1:0.48 for ^{243}Am α decay. A similar calculation by Van Hise and Engelkemeir[20] yielded F_1:F_3 = 1:0.35 for experimental α branching intensities 0.22 and 0.19% respectively to the ground and 31.14 keV states in ^{239}Np.

2.6.5 Conclusions

The low level sequence of states in ^{239}Np (fig. 2.2) can, on the basis of the Unified Model, be interpreted as a result of rotational excitations of a deformed nucleus. Accordingly, many of the characteristic features of the ^{239}Np level scheme, including intrinsic state assignments, level spacings and γ-ray transition intensity ratios are consistent with the predictions of the Unified Model. The concept of favoured α decay to the rotational band based upon the 74.67 keV level and the predicted α branching intensities to members of this band are also found to be in excellent agreement with the previously measured intensities. Similarly, many of the gross features of β^- transition rates and the relative population of levels in ^{239}Np following ^{239}U β^- decay, can be interpreted using the asymptotic selection rules for β^- decay; however, unlike α decay, it is not possible to accurately predict the β^- transition intensities to several members of a rotational family of levels using the reduced transition probability ratios (eqn. 2.16) since the relative mixing of different angular momentum components for each transition are unknown from theory or experiment. Experimental determinations of the β^- branching intensities are therefore necessary and important in the construction of a consistent decay scheme.

REFERENCES

1. A. J. Fudge and A. L. Nichols, Report on the 2nd I.A.E.A. Advisory Group meeting on Transactinium Isotope Nuclear Data (Cadarache, 2-6 May 1979), CNDC(79) P4.

2. B. W. Hooton and A. L. Nichols, Beta and Conversion electron decay data requirements for heavy element nuclides, CNDC(79) P8.

3. A. J. Fudge and A. L. Nichols, 3rd I.A.E.A. Co-ordinated Research Programme meeting on the measurement and evaluation of Transactinium isotope nuclear decay data (Vienna, 12-13 June 1980), CNDC(80) P4.

4. C. M. Lederer and V. S. Shirley, Table of Isotopes (7th ed., Wiley, New York, 1978).

5. M. R. Schmorak, Nucl. Data Sheets 21, 153 (1977).

6. K. J. Blinowska, P. G. Hansen, H. L. Nielsen, O. Schult and K. Wien, Nucl. Phys. 55, 331 (1964).

7. D. R. MacKenzie and R. D. Connor, Nucl. Phys. A108, 81 (1968).

8. D. Engelkemeir, Phys. Rev. 181, 1675 (1969).

9. Detailed discussions of nuclear β^- decay, internal conversion and the Auger process are to be found in Alpha, Beta and Gamma-ray Spectroscopy (ed. K. Siegbahn, North Holland, Amsterdam, 1965).

10. G. F. Knoll, Radiation Detection and Measurement (Wiley, New York, 1979) ch.10.

11. L. Kokta, Nucl. Instr. and Meth. 112, 245 (1973).

12. R. G. Helmer, J. E. Cline and R. C. Greenwood, The Electromagnetic Interaction in Nuclear Spectroscopy (ed. W. D. Hamilton, North Holland, Amsterdam, 1975) ch.17.

13. P. R. Bevington, Data Reduction and Error Analysis for the Physical Sciences (McGraw-Hill, New York, 1969) ch.4.

14. A. P. Baerg, Metrologia 2, 23 (1966).

15. A. P. Baerg, Metrologia 1, 131 (1965).

16. R. J. Gehrke, R. G. Helmer and C. W. Reich, Nucl. Sci. and Engineering 70, 298 (1979).

17. J. Bryant, Intern. J. Appl. Radiation Isotopes 14, 143 (1963).

18. J. C. Pate, K. R. Baker and R. W. Fink, Z. Physik A272, 169 (1975).

19. I. Ahmad, Nucl. Instr. and Meth. 143, 9 (1982).

20. J. R. Van Hise and D. Engelkemeir, Phys. Rev. 171, 1325 (1968).

21. M. L. Curtis, J. W. Heyd, R. G. Olt and J. F. Eichelberger, Nucleonics 13, 38 (1955).

22. A. H. Jaffey, Rev. Sci. Instr. 25, 349 (1954).

23. A. K. Kovarik and N. I. Adams, Phys. Rev. 40, 718 (1932).

24. W. Bambynek, Standardisation of Radionuclides (I.A.E.A., 1967), 373.

25. F. J. G. Rogers, A.E.R.E. R-8005 (1976).

26. J. P. Hummel, UCRL-3456 (unpublished) 1956; data published in Phys. Rev. 98, 261 (1955).

27. S. A. Baranov, V. M. Kulakov and V. M. Shatinskii, Nucl. Phys. 56, 252 (1964).

28. S. A. Baranov, A. G. Zelenkov and V. M. Kulakov, Transactinium Isotope Nuclear Data Vol. III, IAEA-186 (1976). Review Paper B6.

29. A. Bohr and B. R. Mottelson, Dan. Mat. Fys. Medd. 27 No. 16 (1953).

30. M. G. Mayer, Phys. Rev. 75, 1969 (1949).

31. S. G. Nilsson, Dan. Mat. Fys. Medd. 29, No. 16 (1955).

32. K. Gottfried, Phys. Rev. 103, 1017 (1956).

33. B. R. Mottelson and S. G. Nilsson, Mat. Fys. Skr. Dan. Vid. Selsk. 1, No. 8 (1959).

34. F. Asaro and I. Perlman, Phys. Rev. 93, 1423 (1954).

35. A. Kerman, Dan. Mat. Fys. Medd. 30, No. 15 (1955).

36. G. Alaga, K. Alder, A. Bohr and B. R. Mottelson, Dan. Mat. Fys. Medd. 29, No. 9 (1955).

37. G. Alaga, Nucl. Phys. 4, 625 (1957).

38. F. Asaro, F. S. Stephens, J. M. Hollander and I. Perlman, Phys. Rev. 117, 492 (1960).

39. J. H. Hamilton, Internal Conversion Processes (Academic Press, New York, 1966).

40. R. S. Hager and E. C. Seltzer, Nucl. Data A4, 1 (1968).

41. G. Alaga, Phys. Rev. 100, 432 (1956).

42. A. Bohr, P. O. Fröman and B. R. Mottelson, Dan. Mat. Fys. Medd. 29, No. 10 (1955).

43. E. K. Hyde, I. Perlman and G. T. Seaborg, The Nuclear Properties of the Heavy Elements, Vol. I (Prentice-Hall, New Jersey, 1964) ch.4.

CHAPTER 3. ABSOLUTE INTENSITIES OF γ-RAYS IN THE DECAYS OF ^{239}U AND ^{243}Am

3.1 The Need for Accurate Absolute γ-Ray Intensities

The uncertainty in the absolute γ-ray intensity of the major 74.67 keV transition from ^{239}U β^- decay is currently of the order of 10%[1]. The intensity of the same transition occurring in ^{243}Am α decay is currently quoted as (66 ± 3)γ/100α (i.e. ~4.5% uncertainty[1]) although more recent measurements have yielded values of (59.1 ± 4.0)[2], (60 ± 4)[3] and (68 ± 2)[4] γ/100α decays.

Therefore if reactor heat calculations are to accurately predict the ^{239}U γ contribution to short term decay heat production, the uncertainty in the measured absolute intensity of the 74.67 keV γ-ray needs to be reduced from the present level.

Americium-243 is also an important actinide in that, together with ^{241}Am, it lies on a main route to the formation of higher mass actinides following successive neutron capture events in irradiated ^{239}Pu. (See fig. 3.1.) In particular, neutron capture in ^{241,243}Am leads to the production of the ^{242,244}Cm isotopes which, through spontaneous fission, contribute more than 95% of the neutron emissions during storage and reprocessing of spent fuel[5]. If the ^{243}Am neutron capture cross-section is well known then it is possible to predict the relative build-up and decay of the higher mass actinides as a function of time. (Similar calculations can be performed for the case of ^{241}Am, assuming the neutron capture cross-section is known.) If the amount of ^{243}Am at any given time is also known then it is also possible to quantify the higher mass actinides, in particular the important ^{242,244}Cm isotopes. One method of assaying the amount of ^{243}Am is to utilise the absolute γ-ray intensity of the 74.67 keV transition under circumstances in which the γ self-absorption properties are known from experimental or theoretical considerations. Therefore the smaller the uncertainty in the measured absolute intensity of the 74.67 keV γ transition from ^{243}Am α decay, the more accurate the prediction of higher mass actinide contributions to long term decay heat output and radiation levels.

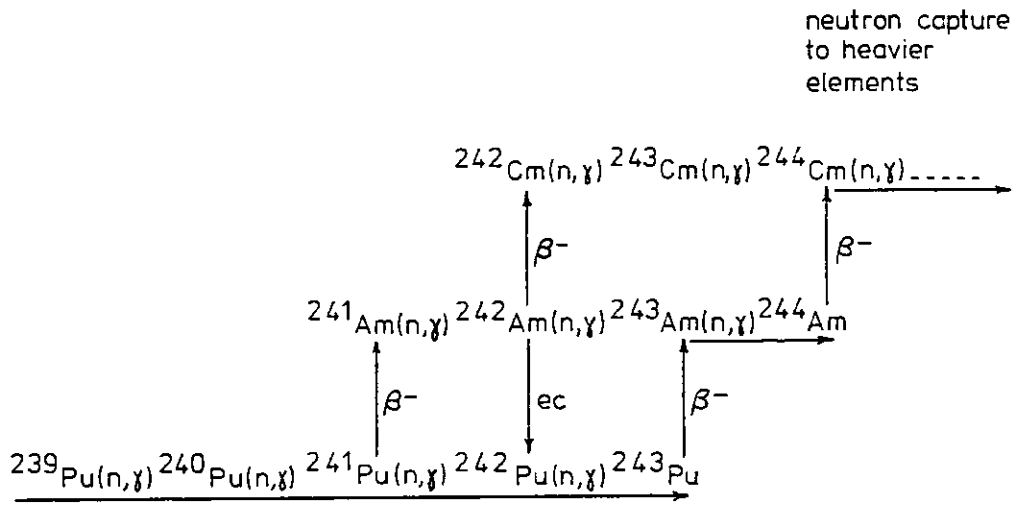

Fig. 3.1 Sequence of neutron-capture reactions starting with ^{239}Pu and leading to the synthesis of heavier elements via $^{241,243}Am$

3.2 Measurement of γ Detection Efficiency

In order to determine the absolute γ-ray intensities of the 74.67 keV γ transitions from ^{239}U β^- decay and ^{243}Am α decay (as well as the other γ transitions shown in fig. 2.2) it is necessary to know the energy dependent peak detection efficiency of the Ge detector used throughout this series of measurements as well as the individual ^{239}U and ^{243}Am source absolute disintegration rates. Here the term 'efficiency' is the full energy (photoelectric) peak (FEP) efficiency and is defined, for a particular γ transition, as the ratio of the number of counts in the full energy peak to the number of γ-rays emitted by the source.

3.2.1 Efficiency calibration using γ-ray intensity standards

The efficiency of the Ge detector was measured using a series of different radioactive sources, each with a known disintegration rate and emitting γ-rays of known absolute intensity. The γ spectra from these calibrated γ standard sources, obtained by counting for a preselected livetime period, were measured at the same source-detector distance as used in the γ counting of the ^{239}U and ^{243}Am sources and analysed to determine the appropriate peak area count rates; the γ-ray peak areas of selected transitions from the

standard sources were determined in the manner outlined in section 2.3.3, that is, by following the procedure used for the 'unknown' ^{239}U and ^{243}Am sources.

The experimental absolute FEP γ detection efficiency, ε_γ, is defined by the equation

$$\varepsilon_\gamma = \frac{I_\gamma}{N_o P_\gamma} \qquad (3.1)$$

where I_γ is the measured γ-ray intensity of the standard source peak, P_γ is the known absolute γ-ray intensity of the same transition and N_o is the absolute disintegration rate of the source at the start of the γ counting period, corrected where necessary to take into account the decay of the source during the elapsed interval since the initial calibration measurement.

In order to define the curvature of the efficiency versus energy below 100 keV (where there exist only a few well resolved γ-ray lines of known intensity) it was necessary to include in the experimental data efficiency values for (a) the peak at 81.0 keV in the decay of ^{133}Ba which is a doublet consisting of a low intensity γ-ray peak at 79.62 keV and an intense peak at 81.00 keV ($P_{81}/P_{80} \sim 14$) and (b) the combined (unresolved) Ba $K\alpha_1$ + $K\alpha_2$ X-ray peaks occurring in ^{137}Cs decay, centred at ~ 32.1 keV. In the case of the 81.0 keV doublet a visual estimate of the peak 'start' and 'finish' channels was sufficient to yield a value for the combined peak area. The number of counts in the peak region of the Ba $K\alpha_1$ + $K\alpha_2$ X-ray peak were summed up in a broader interval than used for the γ-ray peaks to take into account the tails of the Lorentzian distribution[6] used to describe the natural line shape of an X-ray peak. Correspondingly, the backgrounds for the X-ray peak were also taken from higher and lower channel number regions than normally used for the γ-ray peaks.

Measured γ-ray intensities, I_γ, for the γ standard sources ^{57}Co, ^{133}Ba, ^{137}Cs and ^{241}Am are listed in table 3.1 together with the relevant data required to calculate the corresponding FEP detection efficiencies. The listed I_γ are the mean values determined from a set of five measurements. The uncertainties in the values of I_γ quoted in the table are calculated from the observed spread in the experimental peak area data, and agree well with the estimated mean

Table 3.1 Uncorrected full-energy peak γ detection efficiencies[a], ε_γ

Source	N_o (s^{-1})	E_γ (keV)	P_γ[b]	I_γ (s^{-1})	ε_γ
^{57}Co {$T_{\frac{1}{2}} = (270.9 \pm 0.6)d^{9}$}	9.172 + 3 (1.70)	122.06	0.856 (0.47)	5.668 + 1 (0.06)	6.818 - 3 (1.77)
		136.47	0.111 (2.70)	6.063 (0.22)	5.624 - 3 (3.20)
^{133}Ba {$T_{\frac{1}{2}} = (10.5 \pm 0.1)y^{10}$}	2.918 + 4 (2.31)	53.16	0.0216 (2.60)	6.145 (0.34)	9.749 - 3 (3.49)
		81.00	0.3408[c] (1.71)	9.624 + 1 (0.06)	9.677 - 3 (2.87)
		276.4	0.0701 (2.14)	3.215 (0.31)	1.572 - 3 (3.17)
		302.9	0.181 (1.94)	6.958 (0.19)	1.317 - 3 (3.02)
		356.0	0.620 (1.61)	1.780 + 1 (0.11)	9.836 - 4 (2.82)
^{241}Am {$T_{\frac{1}{2}} = (432.2 \pm 0.5)y^{11}$}	3.934 + 4 (1.70)	26.35	0.024 (4.17)	7.815 (0.26)	8.272 - 3 (4.51)
		59.54	0.357 (1.40)	1.463 + 2 (0.04)	1.042 - 2 (2.20)
^{137}Cs {$T_{\frac{1}{2}} = (30.174 \pm 0.034)y^{12}$}	4.202 + 4 (2.00)	32.1	0.0566[d] (3.53)	2.132 + 1 (0.14)	8.966 - 3 (4.06)

a The % uncertainties in N_o, P_γ and I_γ which contribute to the overall uncertainty in ε_γ are given in parentheses below their respective tabulated values.

b Taken from Ref. 7, except that for ^{137}Cs which was taken from Ref. 8.

c Doublet; $P_{79.62} = 0.0234$, $P_{81.00} = 0.3174$. Uncertainty in quoted P_γ based on 2.90% and 1.82% uncertainties in intensities of 79.62 and 81.00 keV γ-ray peaks respectively.

d Ba $K\alpha_1 + K\alpha_2$ X-ray peak.

uncertainty derived from the associated statistical uncertainties in the peak areas.

Corrections to measured γ-ray intensities to take into account source decay during individual γ counting periods and also during the series of five repeated measurements have been calculated and found to be negligible in all cases; the largest correction was for ^{57}Co ($T_{\frac{1}{2}}$ = 270.9d) where the source activity at the end of the complete γ-ray analysis period was calculated to be 0.999 of its initial value, corresponding to a 0.1% decrease in source activity.

The uncertainties in the individual source disintegration rates, N_o, include contributions from the calibration measurements and a source decay correction factor combined in quadrature. The overall uncertainties in the FEP detection efficiencies, ε_γ, include the uncertainties in N_o, P_γ and I_γ combined in quadrature. (All uncertainties in table 3.1 are estimated 1σ, or 68% confidence level, values.)

3.2.2 Corrections to peak efficiencies

Corrections to measured FEP γ-ray intensities (or peak areas) produce changes in the experimental FEP detection efficiencies, ε_γ. The major correction to the measured peak area is due to coincidence summing.

The effect of random coincidence summing (discussed in section 2.3.2) in the γ spectra from the standard sources was reduced to a negligible level by judicious selection of appropriate source activities for the fixed source-detector geometry under consideration. In this manner, analyser dead times were kept low, less than ~ 2%, and were therefore comparable with the dead times produced by the ^{239}U and ^{243}Am sources. The standard source γ spectra showed no direct evidence, in the form of sum peaks, for random coincidence summing events.

Calculations of, and corrections for, real coincidence summing effects (discussed in section 2.4.2) were made for each γ-ray intensity listed in table 3.1. A detailed description of the method used to determine the summing corrections for the measured peak areas is given in Appendix 3, together with the final calculated % coincidence summing corrections. The specific features included in these

calculations were as follows:

(a) all γ-rays of significant intensity were included in the calculations,

(b) the K (or L) X-rays following internal conversion were included where significant,

(c) the angular correlation factor (including those for triple γ cascades) were calculated for all γ-γ cascades. The finite size of the Ge detector was also taken into account to provide an angular correlation coefficient averaged over the solid angle subtended by the detector.

In this study the coincidence summing corrections were found to be typically 1%, with the major source of uncertainty arising from the calculated value of the total γ detection efficiency. Assuming an (arbitrary) overall 20% uncertainty in the summing correction, then the relative contribution of this term in the computation of the total uncertainty in the corrected FEP intensity was ~ 0.2%.

The measured FEP γ-ray intensities from the standard sources were also corrected to take into account γ absorption within the 0.5 mm polystyrene window surrounding each active source. (Unlike the γ standard sources, the ^{239}U and ^{243}Am sources were unsealed.) This correction was performed as part of the overall coincidence summing correction calculations and is described in detail in Appendix 3, section A3.5. The γ-ray transmission of an identical polystyrene window used in the manufacture of the γ standard sources was measured as a function of incident γ-ray energy. The transmission was also calculated from the tables of Storm and Israel[13]. The two approaches agreed within ~ 0.5%. An error of 0.5% was therefore assigned to this particular correction which was added in quadrature to the existing uncertainty in the FEP γ detection efficiency.

The escape of Ge X-ray radiation from the detector (see section 2.3.2) is dependent solely upon the geometrical size and shape of the Ge crystal; the magnitude of the effect, at a given γ-ray energy, is therefore identical for both calibrated and unknown sources and can be ignored for the purpose of absolute γ-ray intensity measurements assuming, of course, that any γ-ray peak of interest does not contain an escape peak from a γ-ray transition of higher energy.

Table 3.2 lists the corrected FEP γ detection efficiency values and their associated uncertainties, $\sigma\varepsilon_\gamma$, calculated using the standard source window γ transmission factors of table A3.4 and the coincidence summing correction data of table A3.6, both given in Appendix 3. No coincidence summing correction was necessary for the Ba X-ray peak from the ^{137}Cs standard source.

Table 3.2 Corrected full-energy peak γ detection efficiencies

Source	E_γ (keV)	ε_γ	$\sigma\varepsilon_\gamma$	$\sigma\varepsilon_\gamma/\varepsilon_\gamma$ (%)
^{241}Am	26.35	8.508-3	0.386-3	4.54
^{137}Cs	32.1	9.130-3	0.373-3	4.09
^{133}Ba	53.16	9.936-3	0.351-3	3.53
^{241}Am	59.54	1.053-2	0.238-3	2.26
^{133}Ba	81.00	9.817-3	0.286-3	2.92
^{57}Co	122.06	6.885-3	0.127-3	1.85
^{57}Co	136.47	5.649-3	0.181-3	3.24
^{133}Ba	276.4	1.611-3	0.519-4	3.22
^{133}Ba	302.9	1.344-3	0.413-4	3.07
^{133}Ba	356.0	9.974-4	0.286-4	2.87

3.2.3 Functional form of absolute efficiency curve

Various empirical functions describing the γ detection efficiency as a function of energy were investigated. These included various polynomials of ε_γ and $\log_e\varepsilon_\gamma$ in terms of E_γ, E_γ^{-1} and $\log_e E_\gamma$. None of these proved adequate for describing the shape of the efficiency curve over the entire energy range without the necessity for using splines to join fits of the above type over portions of the energy range. This failure led to the use of an analytical function which approximated the physical behaviour of the detector to enable interpolation from the experimental efficiency data for an arbitrary energy.

The FEP detection efficiency was represented using an analytical form proposed by Mowatt[14] involving the Ge photoelectric (τ) and Compton (σ) absorption cross-sections, namely

$$\varepsilon_\gamma = K\exp(-\sum_i \mu_i x_i) \left\{ \frac{(\tau + f\sigma)}{(\tau + \sigma)} \right\} [1 - \exp(-(\tau + \sigma)d)] \qquad (3.2)$$

Here the constant K is the fractional solid angle subtended by the detector. The term $\exp(-\sum_i \mu_i x_i)$ represents the probability that a γ-ray reaches the sensitive volume of the detector (with its energy unchanged) and is therefore equivalent to the γ-ray attenuation in the materials between the source and the intrinsic region of the detector, each material being of thickness x_i and possessing associated mass attenuation coefficient μ_i. The term [ ] represents the fraction of those γ-rays reaching the detector which interact in the intrinsic region of the Ge detector of thickness d. The factor f denotes the probability that, following a Compton interaction, the remaining energy (of the scattered photon) is totally absorbed in the Ge crystal by further multiple Compton scattering followed by a photo-electric event; thus a certain fraction, $(\tau + f\sigma)/(\tau + \sigma)$, of the initial γ-flux for a particular energy will contribute to the corresponding FEP. It was proposed by Freeman and Jenkin[15] that for a γ-ray energy E_γ, the fraction f have the form

$$f = A\exp(-BE_\gamma) \qquad (3.3)$$

where the constant A is related to the volume of intrinsic region of the Ge detector.

Combining eqns. 3.2 and 3.3 gives a final functional representation of the efficiency curve of the form

$$\varepsilon_\gamma = a_1 \exp(-\sum_i \mu_i x_i) \exp(-\mu_{Ge} a_2)\, x$$

$$[\{\tau + \sigma a_3 \exp(-a_4 E_\gamma)\}/(\tau + \sigma)]\, x$$

$$[1 - \exp(-\mu_{Ge} a_5)] \qquad (3.4)$$

where the a_i are parameters which are allowed to vary to obtain the best fit to the experimental data and the values of τ, σ, μ_{Ge} and μ_i (for perspex and Be) are interpolated accurately between tabulated values[13] by expressing as analytical functions of the form

$$\log_e \mu = \sum_i A_i (\log_e E_\gamma)^i \qquad (3.5)$$

using a least-squares fitting procedure. Here μ_{Ge} is the absorption coefficient (including coherent scattering) at energy E_γ and the A_i's in eqn. 3.5 are polynomial coefficients. The summation term includes two contributions from the 6 mm perspex β^- absorber and the 0.56 mm Be window of the Ge detector. The term $\exp(-\mu_{Ge} a_2)$ in eqn. 3.4 is included to take account of any possible dead-layer beneath the electrode contact at the upper (window) surface of the Ge crystal in which charge collection is inefficient.

3.2.4 Fitting of experimental data

Equation 3.4 was fitted to the experimental data $\varepsilon_{\gamma i}$ using a weighted version of Marquardt's[16] non-linear least-squares algorithm. In minimising chi-squared, i.e.

$$\chi^2 = \sum_i \frac{[(\varepsilon_{\gamma i} - \varepsilon_\gamma(\mathrm{FIT})_i]^2}{\sigma\varepsilon_{\gamma i}^2} \qquad (3.6)$$

the contributions were weighted with the squares of the experimental uncertainties at each point, taken from table 3.2. The resultant fit is shown in fig. 3.2 and the resulting parameter values in table 3.3.

Table 3.3 Values of eqn. 3.4 parameters determined by least-squares fitting

Parameter	i	a_i
Solid angle	1	(1.080 ± 0.016)-2
Dead layer	2	(6.24 ± 4.27)-4 cm
Multiple scatter components	3	(1.57 ± 0.57)
	4	(2.98 ± 0.88)-3 keV^{-1}
Depletion depth	5	(0.77 ± 0.05) cm

The fit is visually good and the reduced chi-squared has the value of 0.58; the mean of the moduli of deviations between experimental and theoretical points is 1.34%.

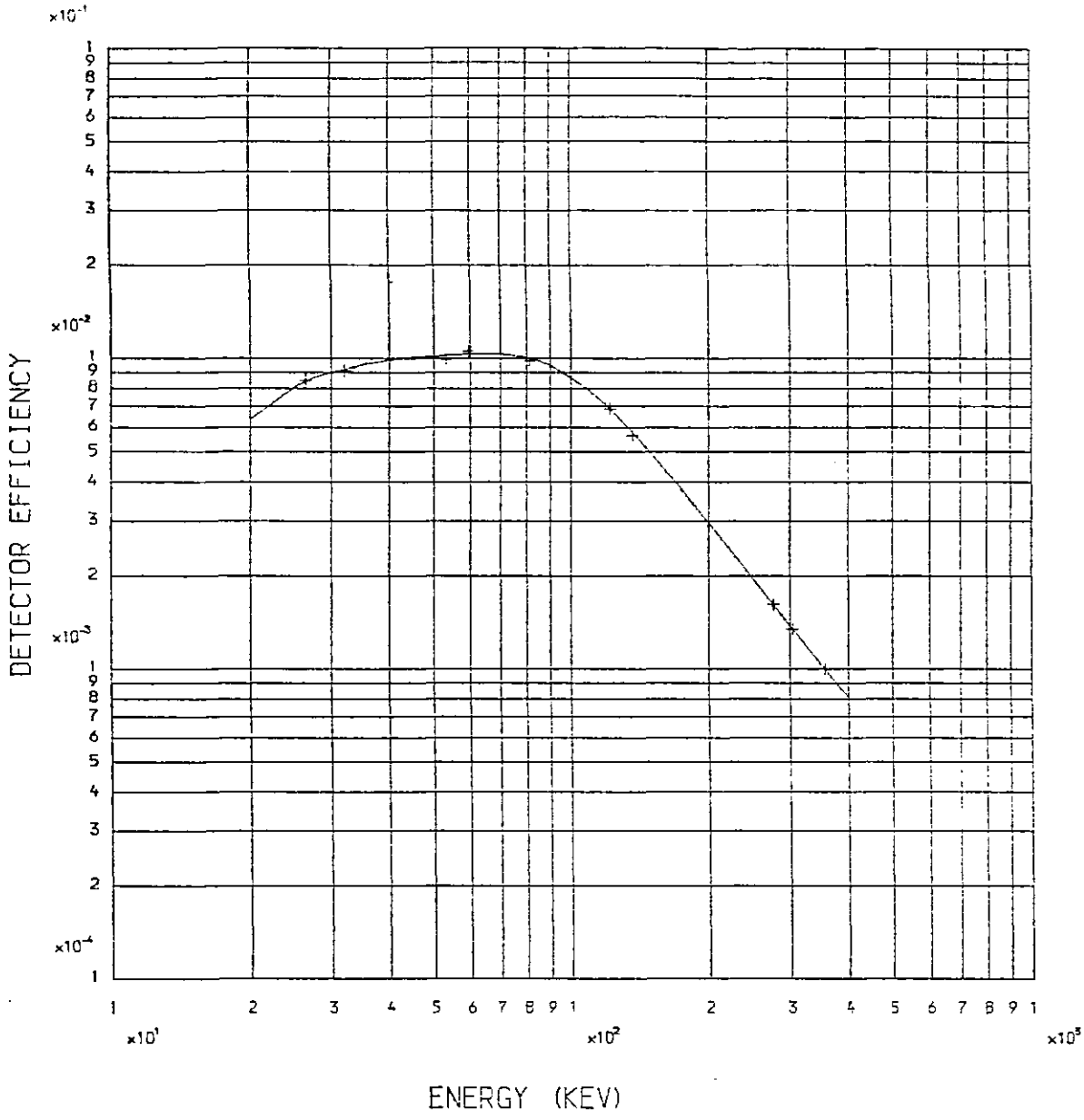

Fig. 3.2 Measured efficiency data for Ge detector (table 3.2) fitted with 5-parameter function of eqn. 3.4

The fitted value of the solid-angle parameter, a_1, agrees well with the calculated solid-angle of ~1.05-2, although the fitted effective intrinsic depth of the Ge crystal of ~7.7 mm (parameter a_5) is lower than the detector manufacturer's quoted depth of 10 mm. The overall fit is insensitive to large errors in parameter a_2 where a dead-layer thickness of the order of μm is predicted.

The values of f (eqn. 3.3) derived using the fitted values of a_3 and a_4 are (1.48 $\pm$.54) and (0.48 $\pm$ 0.24) for γ-ray energies of 20 and 400 keV respectively. The absolute value of f at low energy is therefore higher than expected from theory (i.e. $f_{max} = 1.0$) although the large uncertainty in f reflects the correspondingly increased probability for interaction via the photoelectric effect in this energy region where the photoelectric cross-section is two or three orders of magnitude greater than the Compton cross-section at the same γ energy.

Since the deviations between measured and fitted points are all less than the experimental errors it was decided that the five parameter model of eqn. 3.4 was suitable for interpolation of γ detection efficiencies at arbitrary energy values.

The Marquardt algorithm generates the covariances $\sigma^2 a_{ij}$ in the various parameters, affording estimates of the error in any interpoluted efficiency via

$$\sigma^2 \varepsilon_\gamma = \sum_{\substack{i=1 \\ j=1}}^{N} \frac{\partial \varepsilon_\gamma}{\partial a_i} \frac{\partial \varepsilon_\gamma}{\partial a_j} \sigma a_{ij}^2 \qquad (3.7)$$

where a_{ij} are parameters from the fit, and the partial derivatives of the efficiency ε_γ are evaluated at energy E_γ. Equation 3.7 is a more general form of eqn. 2.4. It transpires that the parameters are not uncorrelated and so the cross-terms in eqn. 3.7 are quite necessary. While these errors are not to be regarded as exact, they are superior to errors estimated by visual examination of the experimental efficiency curve.

Table 3.4 lists the fitted ε_γ and their uncertainties $\sigma\varepsilon_\gamma$ for the γ standard sources. Table 3.5 lists the interpolated ε_γ values for the transitions shown in fig. 2.2 including the previously

unplaced 46.7 keV γ transition; coincidence summing corrections have been calculated according to the procedure outlined in Appendix 3 using the interpolated efficiency values, and the corrected (final) FEP γ detection efficiencies are listed in columns 6 and 8 for transitions arising from ^{239}U β^- decay or ^{243}Am α decay, respectively. The uncertainties in the final corrected FEP efficiencies are derived from the interpolated uncertainties of column 3 and an arbitrary 20% uncertainty in each summing correction term, combined in quadrature.

Table 3.4 Fitted full-energy peak γ detection efficiencies

Source	E_γ (keV)	Fitted ε_γ	Fitted $\sigma\varepsilon_\gamma$	$\frac{\sigma\varepsilon_\gamma}{\varepsilon_\gamma}$ (%)
^{241}Am	26.35	8.417-3	0.265-3	3.15
^{137}Cs	32.1	9.266-3	0.170-3	1.83
^{133}Ba	53.16	1.023-2	0.131-3	1.28
^{241}Am	59.54	1.031-2	0.137-3	1.33
^{133}Ba	81.00	9.995-3	0.109-3	1.09
^{57}Co	122.06	6.825-3	0.797-4	1.17
^{57}Co	136.47	5.768-3	0.710-4	1.23
^{133}Ba	276.4	1.604-3	0.303-4	1.89
^{133}Ba	302.9	1.349-3	0.200-4	1.48
^{133}Ba	356.0	9.974-4	0.211-4	2.11

The general agreement of the magnitudes of the summing correction terms for major γ transitions populated by both α and β^- decay modes support the argument proposed in section 2.5.4 that coincidence summing effects cancel each other out in the calculations of the ^{239}U β^- branching intensities.

Table 3.5 Interpolated FEP efficiencies corrected for true coincidence summing effects

E_γ (keV)	Interpolated		Coinc. summing correction (%)		Corrected FEP efficiency			
	ε_γ	% Error	^{239}U Decay	^{243}Am Decay	^{239}U Decay		^{243}Am Decay	
					ε_γ	% Error	ε_γ	% Error
31.14	9.163-3	1.97	+ 0.36	+ 0.61	9.196-3	1.97	9.219-3	1.97
43.53	9.985-3	1.22	+ 0.25	+ 0.28	1.001-2	1.22	1.001-2	1.22
46.7	1.009-2	1.23	0	+ 0.02	1.009-2	1.23	1.009-2	1.23
50.6	1.018-2	1.26	-	0	-	-	1.018-2	1.26
55.4	1.026-2	1.30	-	+ 0.66	-	-	1.033-2	1.31
74.67	1.023-2	1.22	+ 0.01	+ 0.03	1.023-2	1.22	1.023-2	1.22
86.7	9.675-3	1.00	+ 0.23	+ 0.25	9.697-3	1.00	9.699-3	1.00
98.5	8.804-3	0.99	-	+ 0.10	-	-	8.813-3	0.99
117.8	7.185-3	1.14	- 0.17	- 0.15	7.173-3	1.14	7.174-3	1.14
142.0	5.400-3	1.30	-	+ 0.23	-	-	5.412-3	1.30

3.3 Gamma-ray Transition Intensities

Tables 3.6 and 3.7 list the relative intensities of the major γ transitions from ^{239}U β^- decay and ^{243}Am α decay respectively. The absolute intensity of the major 74.67 keV γ transition common to both ^{239}U and ^{243}Am decay is also given for each decay mode. Relative transition intensities were determined using the measured γ-ray intensities of tables 2.4 (^{239}U β^- decay) and 2.7 (^{243}Am α decay) and the interpolated efficiency values of table 3.5. The absolute intensity of the 74.67 keV γ transition was determined for each decay mode by utilising the previously calculated ratios of $I_{74}(\beta^-)/N_o(\beta^-)$ and $I_{74}(\alpha)/N_o(\alpha)$ given in section 2.5.4.

As well as including the various contributions from the measured γ-ray intensities, interpolated efficiency values and source activities to the uncertainties in the resulting absolute γ-ray intensities, a contribution from the lack of reproducibility of the source geometry was also included in the overall uncertainty calculation; by ensuring a reproducible source position of $\pm$ 0.25 mm for the source-detector distance of 105 mm, the error component in the γ detection efficiency

due to change in solid angle was maintained at a level of ~0.5%. The non-axial location of the ^{239}U sources has been discussed in section 2.5.3; changes in detection efficiency (i.e. solid angle) were found to be negligible and do not lead to an increase in the overall error assignment for the absolute γ-ray intensity of the 74.67 keV transition from ^{239}U decay.

The change in detection efficiency due to the variation in the size of the γ standard sources used for efficiency calibration purposes and the 'unknown' ^{239}U and ^{243}Am sources was calculated and found to be negligible; the maximum change occurred in the ratio of the solid angle subtended by the 7 mm diameter ^{243}Am source to that subtended by a 1 mm diameter γ standard source at the Ge detector, which was calculated to be 0.9992, indicating ≤ 0.1% change in solid angle and hence detection efficiency.

Table 3.6 γ-ray intensities from ^{239}U β^- decay

E_γ (keV)	Relative γ-ray intensity	
	This work	Nuclear Data Sheets[1]
31.14	0.144 ± 0.016	-
43.53	9.04 ± 0.17	8.9 ± 0.3
74.67	100	100
86.7	0.107 ± 0.014	0.12
117.8	0.29 ± 0.08	0.29
Absolute $P_{74.67}$ = 0.457 ± 0.010 This work = 0.50 ± 0.05 Nucl. Data Sheets[1]		

Table 3.7 γ-ray intensities from ^{243}Am α decay

E_γ (keV)	Relative γ-ray intensity	
	This work	Nuclear Data Sheets[1]
31.14	0.074 ± 0.002	0.11 ± 0.01
43.53	9.04 ± 0.16	8.4 ± 0.6
46.7	0.081 ± 0.002	0.09 ± 0.01*
74.67	100	100
86.7	0.491 ± 0.008	0.51 ± 0.05
117.8	1.12 ± 0.24	0.84 ± 0.12
142.0	0.174 ± 0.004	0.19 ± 0.02
Absolute $P_{74.67}$ = 0.635 ± 0.009 This work		
= 0.66 ± 0.03 Nucl. Data Sheets[1]		

*Not listed in Nuclear Data Sheets, but taken from ref. 17 upon which the NDS evaluation is based

3.3.1 Discussion of γ-ray intensities from ^{239}U β^- decay

The intensity of the 117.8 keV γ transition was determined by subtracting the PuKβ_1' X-ray peak contribution from the total peak area. (The contribution of the NpKβ_2' X-ray peak to the total area was assumed negligible upon consideration of the relative size of the NpKβ_1' X-ray peak in the spectrum of fig. 2.3.) The PuKβ_1' contribution was calculated from the known PuKα_1/PuKβ_1' intensity ratio which, from the γ spectrum of fig. 2.4 was calculated to be (2.8 ± 0.1), and from tabulated X-ray intensities[13], was taken to be 2.9. The residual peak area - attributed to the 117.8 keV γ transition - yielded the relative intensity value quoted in table 3.6. The large uncertainty in the intensity of the 117.8 keV γ transition - of the order of 28% - reflects the small contribution by the transition to the overall peak area.

There is clearly a lack of experimental data with which to compare the measured absolute γ-ray intensity of the 74.67 keV transition from ^{239}U β^- decay; the evaluated absolute intensity of (0.50 ± 0.05) $\gamma_{74.7}$ per source decay seems to be based on a normalised absolute intensity of 0.51 $\gamma_{74.7}$ per ^{239}U decay calculated to make all ^{239}U transitions sum to 100%[18]; since only γ data from three

transitions - namely those at 31.14, 43.53 and 74.67 keV - were used in this calculation then the quoted intensity value can be considered as only an upper limit of the 74.67 keV absolute γ-ray intensity. Two other unpublished values of (0.48 ± 0.02) and 0.59 $\gamma_{74.7}$ per ^{239}U decay are also listed in the Nuclear Data Sheets evaluation[1]; the first of these values is based upon the measured absolute γ-ray intensity of the 277.6 keV transition in ^{239}Np β^- decay, which is quoted as (0.141 ± 0.004)γ_{277} per ^{239}Np decay. The origin of the second measurement is unknown. A reported intensity of 0.62 $\gamma_{74.7}$ per ^{239}U decay[19] is erroneous since it takes no account of the competing 43.53 keV γ transition which depopulates the same level as the 74.67 keV transition.

The absolute intensity of the 74.67 keV γ transition determined in this work is within the uncertainty limits ascribed to the current evaluation of this intensity but is low compared to both this value and the unpublished value of (0.48 ± 0.02). It is apparent that further experimental measurements of the intensity of this γ transition are required. However the uncertainty in the intensity measured in this work is now at the 2% level requested by the I.A.E.A. nuclear data committees.

3.3.2 Discussion of γ-ray intensities from ^{243}Am α decay

The relative intensity of the 43.53 keV γ transition was determined by subtracting that contribution to the total peak area resulting from the unresolved 44.6 keV γ transition occurring in ^{239}Np β^- decay. From the γ spectrum obtained using the Si(Li) detector (see fig. 2.9) in which the 43.53 and 44.6 keV transitions are clearly resolved, the ratio $P_{44.6}/P_{43.53}$ was calculated to be (0.020 ± 0.002), in good agreement with previously determined values of (0.021 ± 0.003)[17] and (0.021 ± 0.002)[4], and hence the 43.53 keV transition was reckoned to account for 98% of the total γ-ray peak area.

The calculated relative intensity of the 43.53 keV γ transition is at variance with the currently quoted value of (8.4 ± 0.6) per 100 $\gamma_{74.7}$, although two measurements performed subsequent to this latest evaluation have yielded values of (8.8 ± 2.0)[3] and (9.12 ± 0.44)[4] per 100 $\gamma_{74.7}$, in closer agreement with the value obtained in this work.

Ignoring, for the moment, the effect of the highly internally converted 43.1 keV γ transition upon the measured intensity of the 43.53 keV γ transition, it is expected that the intensity of this γ transition (relative to that of the 74.67 keV γ transition) be the same irrespective of whether the 74.67 keV level in ^{239}Np is populated by α or β^- decay. However, for a given total I.C.C. for the 43.1 keV transition, the fraction of the combined 43.1 + 43.53 keV peak area due to unconverted 43.1 keV γ-rays from ^{243}Am α decay will always be larger than the corresponding fraction for ^{239}U β^- decay (because of the different relative α and β^- feedings to the 117.8 keV level compared to the 74.67 keV level) and therefore it is expected that the relative intensity of the 43.53 keV γ-ray or, to be more precise, the combined 43.1 + 43.53 keV γ-rays, from ^{243}Am decay be greater than or equal to the combined relative intensity of the same γ-rays occurring in ^{239}U decay depending upon the magnitude of α_T for the 43.1 keV transition; the larger the value of α_T for this transition the closer the agreement in the relative intensities of the 43.53 keV γ-rays from both α and β^- decay.

Assuming a total ICC α_T ~140 for the 43.1 keV transition (based upon previous experimental internal conversion data[20]; α_M ~ 31, $\alpha_M/(1+\alpha_T)$~0.23) it is estimated that, in the case of ^{239}U β^- decay, the contribution to the total 43.53 keV γ peak area by the 43.1 keV γ transition is of the order of ~0.3%, and is ~1.1% for ^{243}Am α decay; therefore it is expected that the intensities of the 'total' 43.53 keV γ transitions from ^{239}U and ^{243}Am decay differ by no more than ~0.8%. The experimental relative γ intensities obtained in this work support this general conclusion, although the absolute values tend to indicate an $\alpha_T > 140$ for the 43.1 keV transition.

An estimate of the relative intensity of the 117.8 keV γ transition was determined in the same manner as the corresponding transition from ^{239}Uβ^- decay by using the expression

$$\frac{P_{117.8}}{P_{74.7}} = \left(\frac{I_{117.8}}{I_{PuK\alpha_1}}\right)\left(\frac{\varepsilon_{PuK\alpha_1}}{\varepsilon_{117.8}}\right)\left(\frac{P_{PuK\alpha_1}}{P_{74.7}}\right)$$

where the ratio $I_{117.8}/I_{PuK\alpha_1}$ was derived by difference from the experimental ratio $I(PuK\beta_1' + \gamma_{117.8})/I_{PuK\alpha_1}$ obtained from ^{243}Am decay

and the mean ratio $I_{PuK\beta_1'}/I_{PuK\alpha_1}$ obtained from four ^{239}Np sources. It was estimated, on the basis of the small ICC for the 142.0 keV γ transition in ^{243}Am α decay, that the $NpK\beta_2'$ X-ray contribution to the total peak area was negligible (< 0.02%) and could be neglected in estimating the relative intensity of the 117.8 keV γ-ray transition. The ratio $P_{PuK\alpha_1}/P_{74.7}$ was derived from the previous experimental data of this ratio[4,17,21] which gave a weighted mean value of (0.312 $\pm$ 0.007). The ratio $I_{117.8}/I_{PuK\alpha_1}$ was calculated to be (0.032 $\pm$ 0.007). Assigning a FEP efficiency of (8.30-3) for the $PuK\alpha_1$ X-ray then the value of $P_{117.8}/P_{74.7}$ was calculated to be (1.12 $\pm$ 0.24) per 100 $\gamma_{74.7}$.

Although the intensity of the 117.8 keV γ transition obtained from the ^{243}Am single γ spectra does not agree well with the currently quoted value of (0.84 $\pm$ 0.12), it is in closer agreement with more recently published values of (1.17 $\pm$ 0.17)[3] and (1.04 $\pm$ 0.07)[4*] per 100 $\gamma_{74.7}$.

The absolute intensity of the 74.67 keV γ transition from ^{243}Am α decay is again low compared with the evaluated intensity listed in table 3.7, although it is still within the error limits ascribed to the evaluated intensity. A consideration of more recent measurements of the 74.67 keV γ transition intensity (see table 3.8) show that the absolute intensity obtained in this work is situated midway between sets of measurements centred around ~0.60 and 0.67 $\gamma_{74.7}$ per α decay.

Table 3.8 Intensity of 74.67 keV γ-ray from ^{243}Am α decay

Absolute intensity (%)	Reference
66 ± 3	1
59.1 ± 4.0	2
60 ± 4	3
68 ± 2	4

*This value has been extracted from the measured $PuK\beta_5$ + γ117.8 intensity of ref. 4 assuming a $PuK\beta_5/PuK\beta_1$ intensity ratio of 0.04 (Ref. 13).

It is interesting to note that the measurements belonging to each group involve the same author or group of authors.

The ratio of experimental 74.67 keV transition intensities from ^{243}Am α decay and ^{239}U β^- decay is calculated to

$$\frac{P_{74.7(\alpha)}}{P_{74.7(\beta^-)}} = 1.39 \pm 0.03$$

This ratio is independent of γ detection efficiency. Using the evaluated intensities of ref. 1 the ratio is given by

$$\frac{P_{74.7(\alpha)}}{P_{74.7(\beta^-)}} = \frac{(0.66 \pm 0.03)}{(0.50 \pm 0.05)} = 1.32 \pm 0.14$$

while substitution of (0.48 $\pm$ 0.02) for the ^{239}U 74.67 keV γ transition intensity produces a reduced ratio of (1.38 $\pm$ 0.08) which is in closer agreement with the present experimental value. It therefore appears, on the evidence of the present work, that the unpublished value of (0.48 $\pm$ 0.02) $\gamma_{74.7}$ per ^{239}U decay provides a more realistic estimate of the intensity of the 74.67 keV γ transition rather than the currently quoted value of (0.50 $\pm$ 0.05) $\gamma_{74.7}$ per ^{239}U decay. If this assumption is correct, the remaining differences in absolute transition intensities are due to unaccounted systematic errors in γ-ray detection efficiencies.

3.4 γ-Ray Intensities from ^{239}Np β^- Decay

There currently exists a large discrepancy in the measured γ-ray intensity ratio of the two major γ transitions following ^{239}Np β^- decay; a survey of the literature, summarised in table 3.9, shows that the ratio of the 106.13 and 277.6 keV γ transition intensities varies according to whether the measurements are made using a mixed ^{243}Am - ^{239}Np source or a pure β^- emitting ^{239}Np source formed by the reaction ^{238}U(n,γ)^{239}U(β^-). There is no evidence for a 106 keV γ-ray directly from ^{243}Am α decay which could be responsible for the increased P_{106}/P_{277} ratio observed in the ^{243}Am - ^{239}Np singles γ spectra and the subsequent decay of the ^{239}Pu daughter ($T_{\frac{1}{2}}$ = 2.411 x 10^4 y) does not give rise to measurable interfering γ or X-ray peaks in the region of 106 keV. The presence of small ^{241}Am impurities usually found in such ^{243}Am-^{239}Np sources are also not responsible for the discrepancy in intensity ratios.

Table 3.9 Absolute γ-ray intensities for 106.1 and 277.6 keV transitions following ^{239}Np β^- decay

Source	^{243}Am - ^{239}Np				^{239}Np
Author	Ahmad and Wahlgren[21] (1972)	Pate et al.[17] (1975)	Starozhukov et al.[2] (1977)	Ahmad[4] (1982)	Nuclear Data Sheets[1] (1977)
$P_{277.6}$ (%)	14.5 ± 0.4	-	15.0 ± 0.5	14.5 ± 0.4	14.1 ± 0.4
$P_{106.1}$ (%)	27.8 ± 0.9	-	26.6 ± 1.0	26.4 ± 0.8	22.7 ± 0.6
$P_{106.1}/P_{277.6}$	1.92 ± 0.08	1.85 ± 0.25[a]	1.77 ± 0.09	1.82 ± 0.07	1.61 ± 0.08

a Only relative measurement reported

Measurements of the absolute γ-ray intensities of the 106.13 and 277.6 keV γ transitions have therefore been made by utilising the known absolute disintegration rates of the ^{239}Np sources determined by 4πβ-γ coincidence counting (see section 2.3.4). The ratio of transition intensities was then compared with the same ratio determined from the mixed ^{243}Am - ^{239}Np source. It was not possible to determine absolute values for the 106.13 and 277.6 keV γ transition intensities using the ^{243}Am - ^{239}Np source for the reasons discussed in section 3.4.1.

The results of the absolute intensity measurements and intensity ratio calculations are shown in table 3.10. The uncertainties in the absolute γ-transition intensities represent one standard deviation. The errors in the intensities include contributions from β^- activity counting, measured γ-ray intensities, the γ-ray standards and interpolated absolute efficiencies. Corrections were also applied for true coincidence summing. The effect of random coincidence summing was ignored in calculating the relative γ-ray intensity ratio of the two major transitions since it was assumed that all peaks within a γ spectrum were affected to the same extent by this effect; indeed the ^{239}Np γ spectra following ^{239}U β^- decay revealed no detectable presence of random sum peaks and therefore the absolute γ-ray intensities were regarded as final.

The absolute intensities listed in table 3.10 are mean values obtained from the γ decay data of two ^{239}Np sources. The transition intensity ratio $P_{106.1}/P_{277.6}$, from both pure ^{239}Np β^- decay and

mixed ^{243}Am - ^{239}Np decay, agree well with one another and are in general agreement with the ratio quoted in Nuclear Data Sheets[1] which is based upon the γ decay data from a pure β^- emitting ^{239}Np source. The absolute transition intensities from ^{239}Np β^- decay also compare favourably with values of $P_{106.1} = 22.78\%$ and $P_{277.8} = 14.08\%$ determined by Ewan et al.[22]. The discrepancy in the ratio $P_{106.1}/P_{277.6}$ (table 3.9) is therefore due to large differences in the measured absolute intensity of the 106.1 keV γ transition from ^{243}Am - ^{239}Np decay.

Table 3.10 Experimental $P_{106.1}/P_{277.6}$ measurements

Source	^{239}Np	^{243}Am - ^{239}Np
$P_{277.6}$ (%)	13.8 ± 0.7	-
$P_{106.1}$ (%)	22.6 ± 0.7	-
$P_{106.1}/P_{277.6}$	1.64 ± 0.06	1.66 ± 0.04

3.4.1 Measured ^{239}Np γ and Pu X-ray transition intensities from the mixed ^{243}Am - ^{239}Np source

A detailed analysis of the same ^{243}Am - ^{239}Np γ spectra used to determine the measured γ-ray intensities following ^{243}Am α decay revealed a systematic increase in the measured intensities (i.e. peak areas) of all γ and Pu X-ray peaks arising from the β^- decay of ^{239}Np within the ^{243}Am source; during the four day counting period required to obtain the seventeen ^{243}Am - ^{239}Np γ spectra of table 2.7, each peak associated with ^{239}Np decay exhibited a ~5% increase in peak area. The releative intensities of these transitions, however, remained constant throughout the counting period and it was therefore possible to determine relative γ or X-ray intensities from the experimental data, but not absolute transition intensities. The ^{239}Np daughter ($T_{\frac{1}{2}} = 2.355d$) was expected to be in secular equilibrium with the parent ^{243}Am ($T_{\frac{1}{2}} = 7370y$) and therefore, like the measured γ-ray peak areas from ^{243}Am α decay, the γ-ray peak areas from ^{239}Np β^- decay were expected to remain constant throughout the counting interval.

Since the measurements of γ-ray intensities following ^{239}Np decay were not a major aim of this work - the measurements were not required to determine the ^{239}U β^- branching ratios - and because the initial

examination of the ^{243}Am - ^{239}Np γ spectra revealed nothing unusual (i.e. the measured γ-ray intensities from the parent ^{243}Am decay were constant in time) the increasing ^{239}Np peak area anomaly was not discovered until the later stages of this work. Further experimental investigation was therefore not possible and only a consideration of possible causes for this effect can be expounded here; these may be summarised under the following headings.

(i) Changes in γ detection efficiency

Changes in detection efficiency due to either movement of source position or inherent changes in the Ge detector itself and/or associated pulse processing system can be excluded as a possible cause since all these effects would also lead to systematic changes in the measured γ-ray intensities from ^{243}Am α decay; such effects were not observed. The time independent γ background did not reveal the presence of interfering γ-ray lines of unknown origin.

Following ^{243}Am α particle emission it is possible for ^{239}Np recoils (typical energy ~100 keV) to escape from the surface of the ^{243}Am source. In vacuum the recoil atoms can travel several cms before being stopped, usually in the vacuum chamber wall, thus changing the effective solid angle subtended by the ^{239}Np source at the detector. Such a process, if collection of ^{239}Np recoils on surfaces close to the γ detector window takes place, would lead to an observed increase in the ^{239}Np activity as a function of time. However, the range of recoil atoms in air is of the order of μm and therefore no deposition of ^{239}Np nuclei in the vicinity of the detector window is expected; hence no change (in time) of γ-ray intensities following ^{239}Np β^- decay is expected.

(ii) Source decay properties

There is no evidence that ^{243}Am decays by any mechanism other than α decay and therefore it is not possible to populate the levels in ^{239}Pu by a different intermediate radionuclide which has not yet attained secular equilibrium with the parent ^{243}Am. It is interesting to note however that such a decay mechanism exists in the case of ^{241}Pu which proceeds through β^- decay (99.998%) to ^{241}Am or α decay (0.002%) to ^{237}U, and then

both daughter nuclei decay to ^{237}Np; a consideration of the closed decay energy cycle for ^{239}Pu, ^{243}Am, ^{243}Cm and ^{239}Np shows that it is not possible for ^{243}Am to undergo β^- decay to form ^{243}Cm although ^{243}Cm does populate the levels of ^{239}Pu by α emission.

To date there has also been no evidence, experimental or theoretical for the existence of an isomeric state in ^{239}Np.

In conclusion, no satisfactory explanation can be offered to account for the experimental facts.

3.5 Conclusions

A comparison of absolute γ-ray transition intensities populated by different decay modes and studied under identical experimental conditions has been carried out for selected major γ transitions in ^{239}U, ^{243}Am and ^{239}Np; under such conditions employed here, the intensity ratios are independent of γ detection efficiency and are therefore more accurate than those determined from the currently quoted absolute γ intensities. Relative γ-ray intensities from ^{239}U β^- decay (table 3.6) and ^{243}Am α decay (table 3.7) are in broad agreement with the published data and the ratio $P_{106.1}/P_{277.6}$ obtained from the mixed ^{243}Am - ^{239}Np source is consistent with the value obtained from the pure ^{239}Np source, despite the unexplained increase (with time) in the peak areas of γ and Pu X-ray transitions following the decay of ^{239}Np within the parent ^{243}Am source.

3.6 ^{243}Am (α-γ) Coincidence Studies

To confirm the existence of several low energy γ transitions reported by Van Hise and Engelkemeir[23], but not revealed in previous ^{243}Am - ^{239}Np singles γ studies (section 2.4.2), weak γ transitions in the level scheme of ^{239}Np were measured in coincidence with α's to eliminate interference from the 2.3d β^- emitting ^{239}Np daughter.

3.6.1 (α-γ) coincidence arrangement

(α-γ) coincidences were studied using an Ortec 50 mm^2 Si(Au) surface barrier detector and the same 15 cm^2 x 10 mm deep planar intrinsic Ge γ detector used in previous ^{239}U and ^{243}Am singles γ studies. The Si(Au) detector gave a resolution full width at half-maximum of ~14 keV for α's. A fast-slow coincidence technique was employed to determine those γ transitions in coincidence with selected

^{243}Am α groups; fig. 3.3 shows the modular system used to obtain the coincidence data in which a 'slow' amplitude branch was used to select only those fast timing pulses that corresponded to events of a predetermined amplitude (i.e. those of a particular α group) set by the SCA window. The measured resolving time of the fast coincidence circuit was ~20 ns.

A 1 cm diameter, 0.93 μCi ^{243}Am source deposited on a 50 μm aluminium backing foil was used for all coincidence measurements. The source was mounted inside an evacuated chamber at a distance of 16.5 mm from the α detector. The Ge detector was placed at 180° and at a distance of 44 mm from the source for all α group-γ coincidence studies. The low Z of the source backing ensured minimum attenuation of low energy γ and X-rays before subsequent detection in the Ge detector.

The γ side was calibrated using known γ-ray standards and the absolute efficiency of the Ge detector was determined using the procedure outlined in section 3.2; typical interpolation efficiencies were uncertain to ~3%, including a 2% contribution from the uncertainty in source-detector geometry.

3.6.2 Results

Figures 3.4(a) and (b) show the effect of random coincidence summing upon the gross (α-γ) coincidence spectra taken at source-γ detector separations of 104 and 44 mm respectively. Although intended primarily for orientation purposes, these γ spectra (corrected for chance background) revealed that the 46.7 keV γ transition, previously observed in ^{243}Am - ^{239}Np singles γ spectra, is a transition within the ^{239}Np level scheme. Also in coincidence are the escape peaks of the 43.53 and 74.67 keV γ transitions.

The α group-γ coincidence measurements were taken in a series of runs in order to study the γ-rays in coincidence with the three most intense α groups populating the 173.2, 117.8 and 74.67 keV levels in ^{239}Np. In the case of the (α_{173}-γ) coincidence experiment a second run was performed using a 0.2 gm/cm^2 Al absorber inserted between the source and the Ge detector to reduce the intensity of the Np L X-ray peaks and so prevent random coincidence summing of Np L X-rays with higher energy γ transitions, in particular the intense 74.67 keV γ transition.

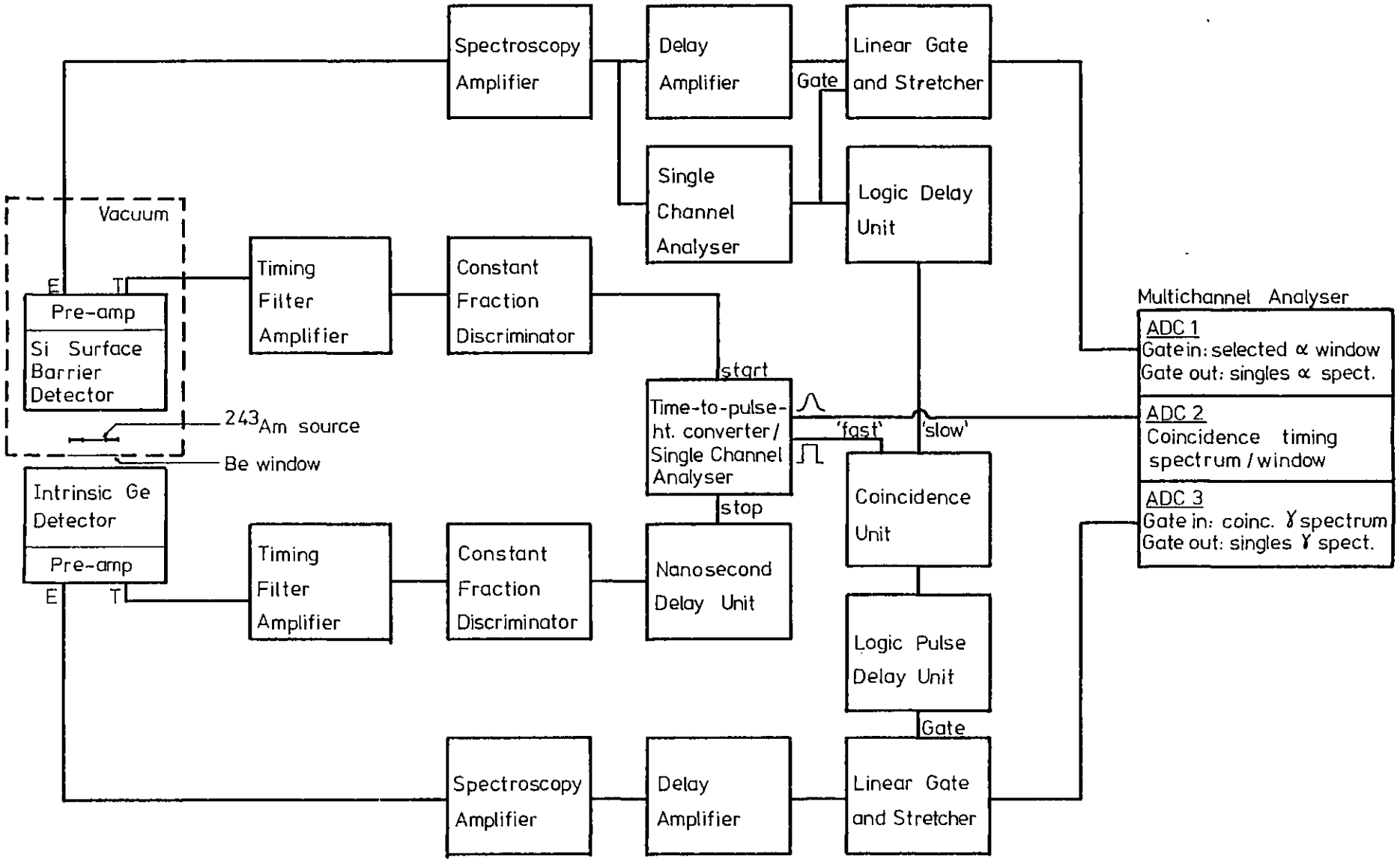

Fig. 3.3 Fast-slow coincidence system used for ^{243}Am (α-γ) studies

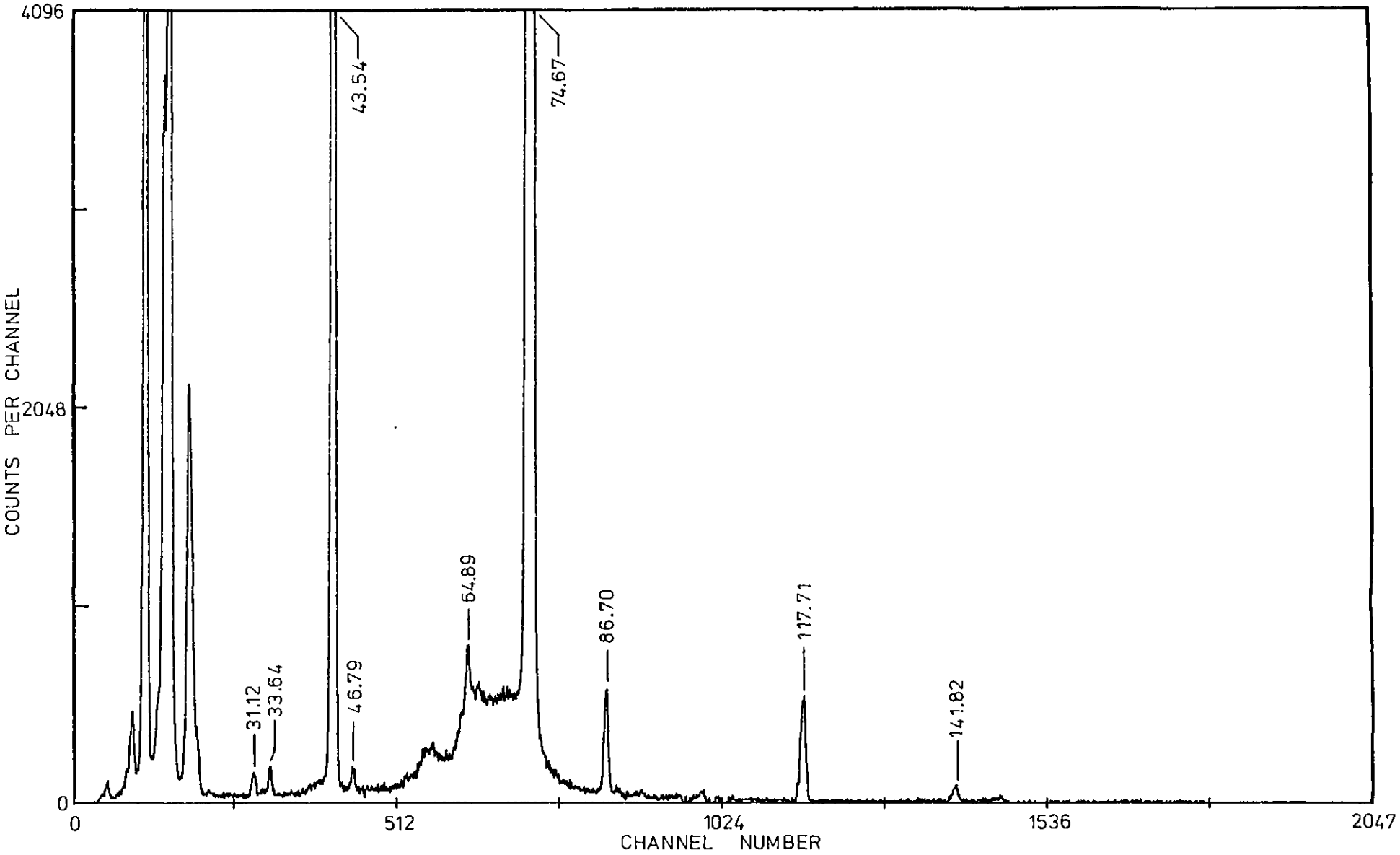

Fig. 3.4(a) Gross (α-γ) coincidence spectrum; 104 mm source-γ detector separation

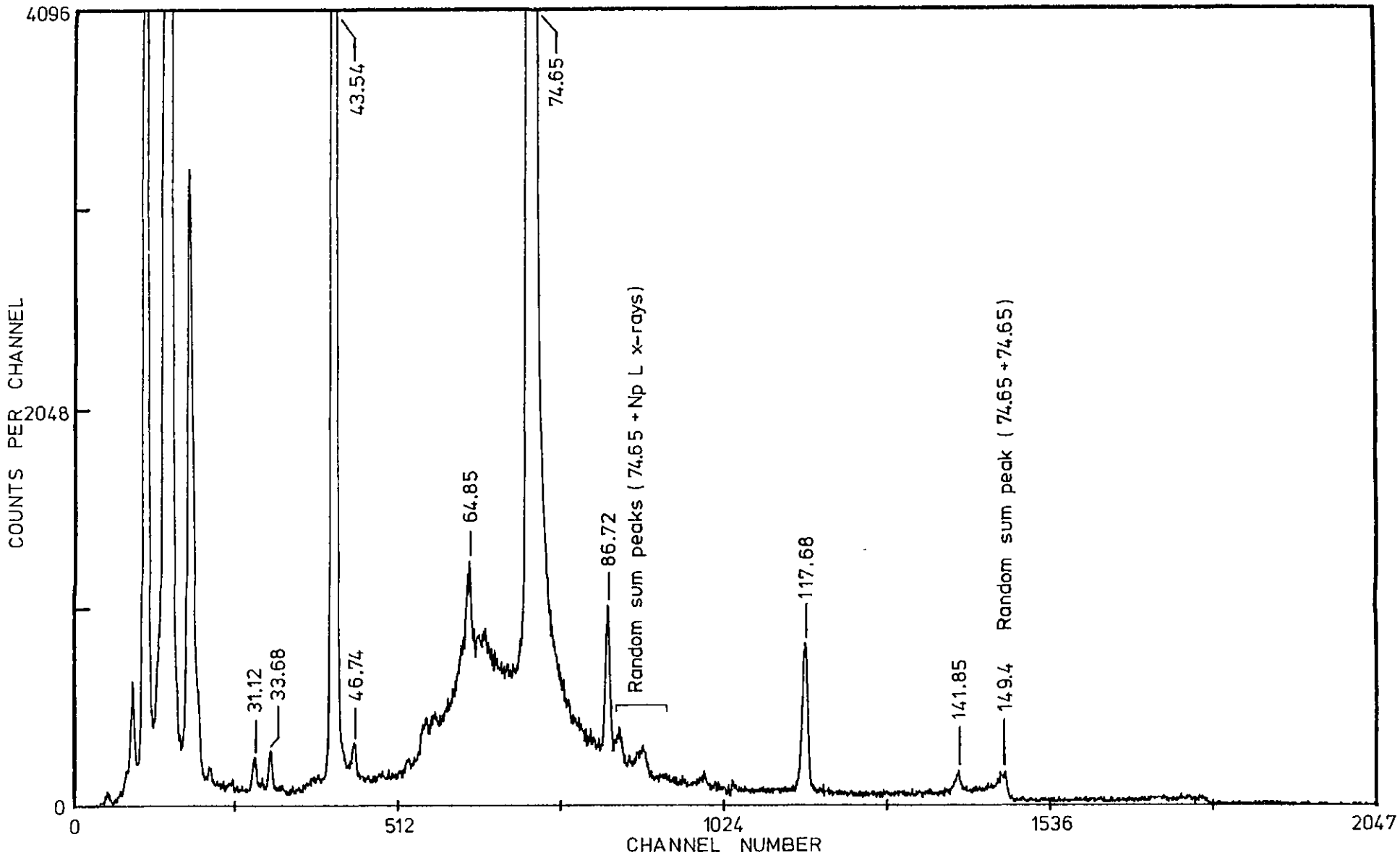

Fig. 3.4(b) Gross (α-γ) coincidence spectrum; 44 mm source-γ detector separation

$(\alpha_{75}-\gamma)$

The γ-ray spectrum in coincidence with α_{75} is shown in fig. 3.5(a). The γ-rays at 31.10, 43.53 and 74.67 are in true coincidence. Chance rates were evaluated and subtracted from the spectrum by inserting a 100 ns delay in one side of the fast coincidence circuit.

$(\alpha_{118}-\gamma)$

The $(\alpha_{118}-\gamma)$ spectrum of fig. 3.5(b) shows not only those transitions originating from the 117.8 keV level (i.e. those at 46.74, 86.72 and 117.63 keV) but also transitions from the 74.67 keV level which is strongly populated by the 43.1 keV transition. Since the relative contribution of the α_{75} group to the total α_{118} window rate was unknown it was not possible to correct the 31.10, 43.53 and 74.67 keV γ intensities for counts due to coincidences between these and the tail of the α_{75} group; because this is a general correction that must be applied whenever a γ is also in coincidence with a higher energy α, the determination of level branching fractions or total I.C.C.'s from the experimental coincidence data (except for the $(\alpha_{75}-\gamma)$ coincidence run) was not possible and the data analysis was restricted to a comparison of γ-ray intensities for all transitions depopulating a common level.

$(\alpha_{173}-\gamma)$

The spectrum in coincidence with α_{173} is shown in fig. 3.5(c). Transitions at 50.48, 55.12, 98.25, 101.78 and 141.75 keV are found in coincidence with α_{173} as well as those previously observed in $(\alpha_{75}-\gamma)$ and $(\alpha_{118}-\gamma)$ coincidence runs. Since the 117.8 keV level is strongly populated by the 55.12 keV transition there are no transitions within the spectrum which are characteristic only of the $(\alpha_{118}-\gamma)$ spectrum and which permit subtraction of an appropriate fraction of the $(\alpha_{118}-\gamma)$ spectrum to give the spectrum of transitions from the 173.2 keV level alone.

The peaks at 50.48, 55.12 and 98.25 keV are assumed to be the previously reported[20,23] 50.6, 55.4 and 98.5 keV γ transitions respectively. The previously unobserved 101.78 keV peak is identified as a γ transition between the 173 keV level and the proposed $9/2^+$ member of the ground state rotational band at 71.2 keV (i.e. the same

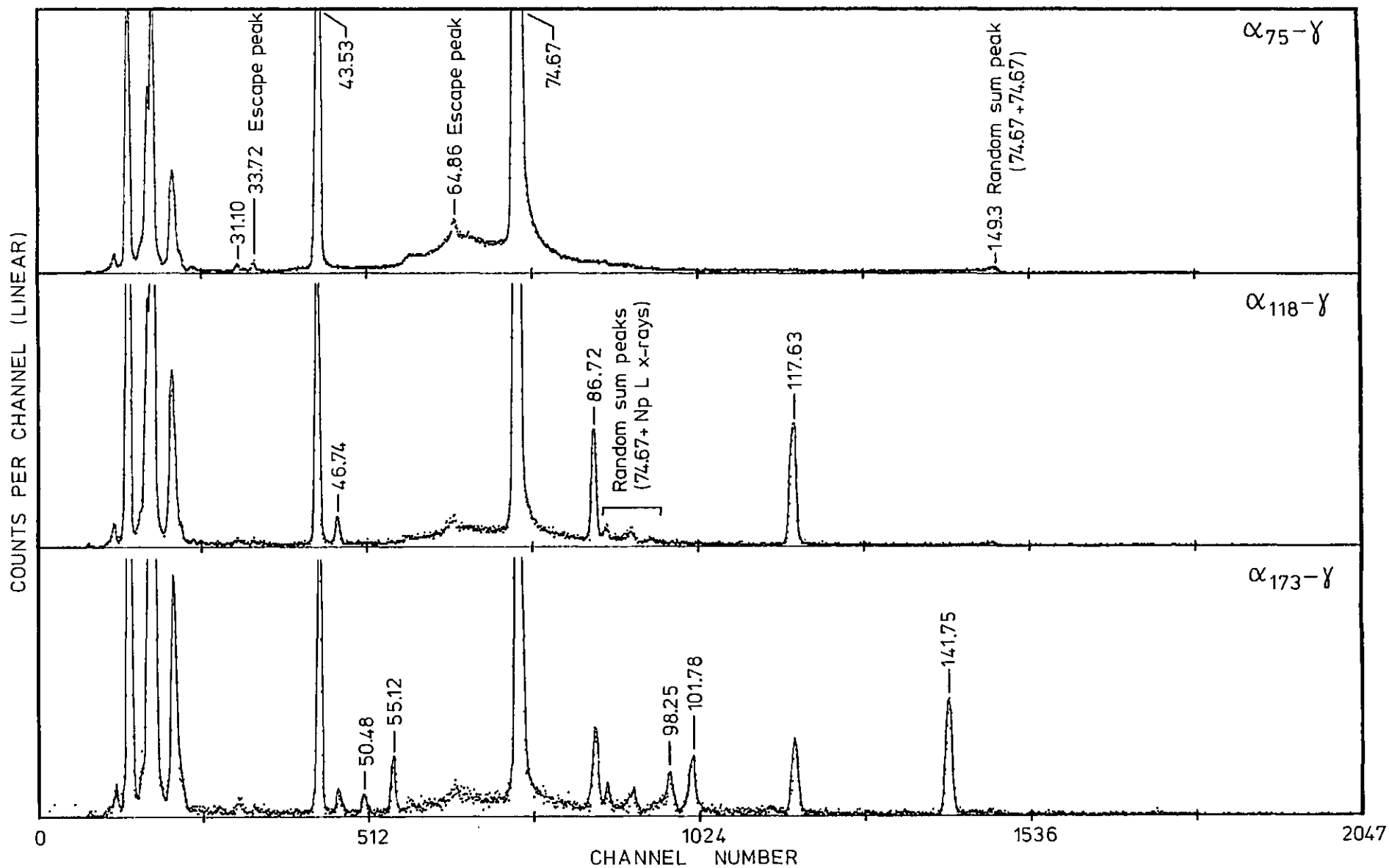

Fig. 3.5 ^{243}Am γ spectra in coincidence with selected α groups (a) (α_{75}-γ), (b) (α_{118}-γ), (c) (α_{173}-γ)

level as fed by the 46.7 keV γ-ray). Spin and parity selection rules favour an E1 multipole assignment for this transition. There is no evidence in the spectrum of fig. 3.5(c) for a de-excitation of the 71.2 keV level to either the 31.1 keV level or ^{239}Np ground state. The 101.78 keV peak area is expected to contain a contribution from the unresolved NpKα_1 X-ray peak (E ~ 101.1 keV) arising from the internal conversion of the 141.75 keV γ-ray; the accompanying NpKα_2 X-ray transition (E ~ 97.1 keV) is masked by the (74.67 + NpLγ) sum peak which can be seen as a low energy tail contribution to the 98.25 keV peak.

Fig. 3.6 shows the (α_{173}-γ) coincidence spectrum obtained using an Al absorber to remove (74.67 + NpL X-ray) random sum peaks from the spectrum region ~90-100 keV. In this spectrum the NpKα_2 X-ray peak (97.00 keV) is clearly resolved from the 98.29 keV γ transition and the relative contribution of the NpKα_1 X-ray peak to the 101.72 keV γ peak area can be estimated from the known relative intensity ratio of the Kα_1 and Kα_2 X-ray peaks.

There is a slight suggestion of a very weak transition at ~40 keV in the spectrum of fig. 3.6; this could be a transition between the 71.2 keV level and 31.1 keV level, which is expected to be mixed M1 + E2 and therefore highly internally converted.

Table 3.11 shows the relative intensity ratios of transitions depopulating the 74.67, 117.8 and 173.2 keV levels in ^{239}Np determined from the (α-γ) coincidence data, corrected for chance rates and γ detection efficiencies. In addition, the 98.2 and 101.8 keV γ-ray peak areas have been corrected for the presence of NpK X-rays from the internal conversion of the 142 keV γ transition assuming α_K = 0.174; NpKα_1 X-rays were calculated to account for ~20% of the total 101.8 keV peak area, with a similar contribution by the NpKα_2 X-ray peak to the 98.3 keV total peak area. A comparison has been made, where possible, with intensity ratios determined from a similar study of ^{243}Am (α-γ) coincidences by VanHise and Engelkemeir[23].

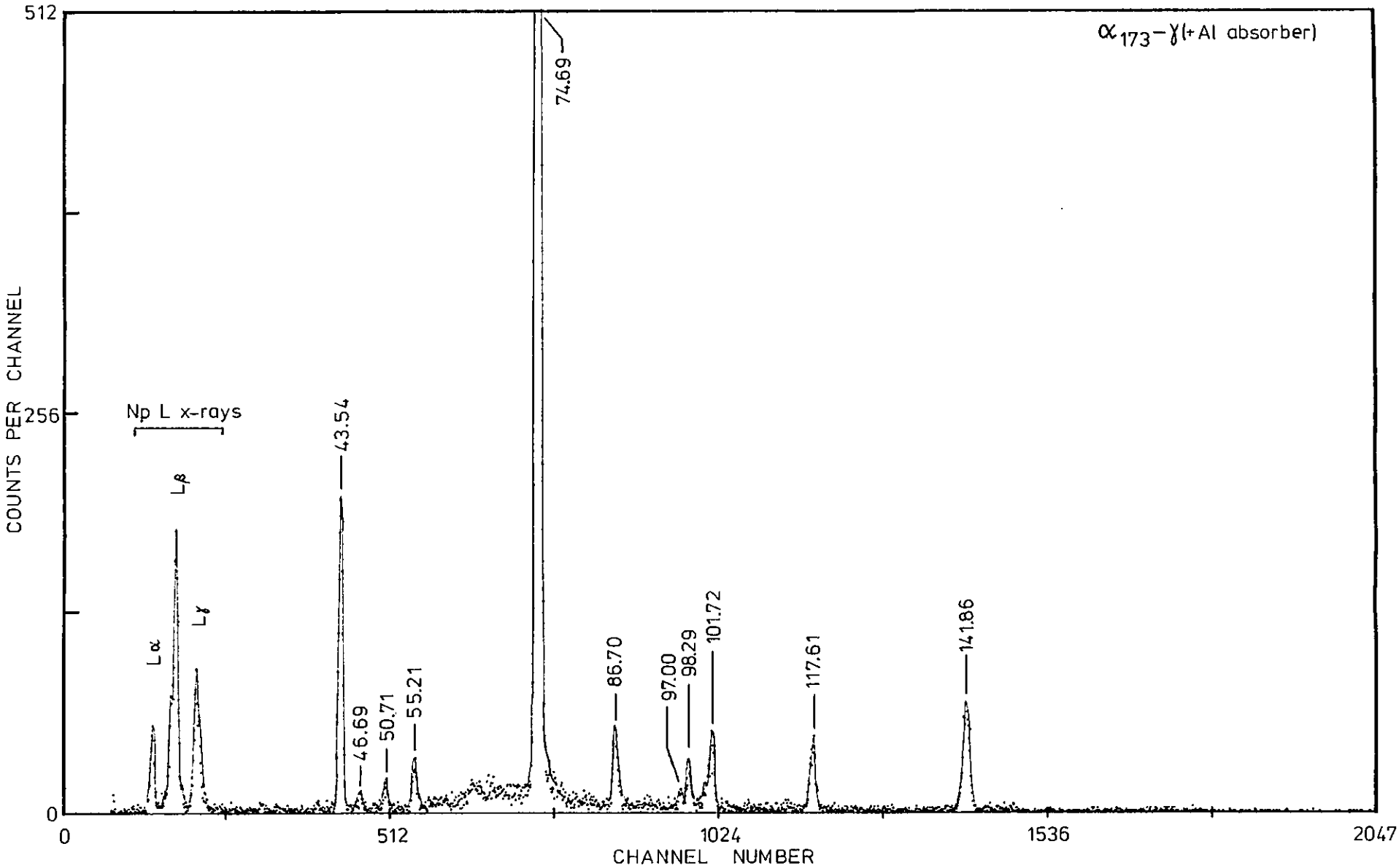

Fig. 3.6 ^{243}Am (α_{173}-γ) coincidence spectrum; 0.2 gm/cm^2 Al absorber

Table 3.11 γ Intensity ratios from ^{243}Am (α-γ) coincidence runs

γ Intensity Ratio	$(\alpha_{74}-\gamma)$		$(\alpha_{118}-\gamma)$		$(\alpha_{173}-\gamma)$	
	This work	Van Hise	This work	Van Hise	This work	Van Hise
43.5/74.7	.107 ± .005	.090	.094 ± .004	.081	.092 ± .004	.074
86.7/117.8			.53 ± .03	.53	.59 ± .05	.60
46.7/117.8			.11 ± .01	-	.14 ± .02	-
50.6/142					.06 ± .01	.02
55.2/142					.16 ± .01	.07
98.2/142					.14 ± .02	.07[a]
101.8/142					.27 ± .03	-

a Taken from ref. 1

α-γ Angular correlation effects

The change in the relative intensity ratio of the 43.53 and 74.67 keV γ transitions between coincidence runs gating on different α groups clearly illustrates the effect of perturbed angular correlations in ^{243}Am.[24,25] The perturbation arises from the high atomic recoil energy of the daughter (~ 100 keV) which results in the atom travelling many atomic radii through the source material where it can experience considerable electric field gradients; the (α-γ) angular correlation $W_{\alpha:\gamma}(\theta)$ must then be expressed in the form

$$W_{\alpha:\gamma}(\theta) = \sum_k G_k A_k P_k(\mathrm{Cos}\theta)$$

where G_k is an attenuation coefficient ($0 \leq G_k \leq 1$) which expresses the influence upon the angular correlation of interaction between extranuclear fields, and the electric and magnetic moment of intermediate-state nuclei. In the case of the $(\alpha_{118}-\gamma)$ coincidence run, where the 43.53 and 74.67 keV radiations are part of a triple (α-γ-γ) cascade with unobserved intermediate radiation, it is expected that a relatively strong perturbation of the triple correlation will occur[26] (i.e. $G_k \sim 0$) due to excitation of the electron shell associated with conversion of the unobserved radiation. The angular distribution of the 43.53 and 74.67 keV radiations will then be isotropic and the intensity ratio for these two transitions should equal that obtained from the ^{243}Am

singles γ data. The experimental data of table 3.11 broadly supports this statement. The ratio $\gamma_{43.5}/\gamma_{74.7}$ obtained from the $(\alpha_{75}\text{-}\gamma)$ coincidence run is also consistent with calculated A_2 coefficients of -0.38 and +0.12 for the 74.67 and 43.53 keV γ radiations respectively.

Similar arguments can be applied to other transitions within the decay scheme which are fed by more than one α branch.

Relative intensities of weak γ transitions

The $\gamma_{86.7}/\gamma_{117.8}$ ratio from the $(\alpha_{173}\text{-}\gamma)$ coincidence run and the singles γ measurement of the relative intensity of the 86.7 keV γ transition (table 3.7) combine to yield a value of $(0.83 \pm 0.07)\gamma_{117.8}/100\gamma_{74.7}$. This is consistent with the relative intensity of $(0.8 \pm 0.12)\gamma_{117.8}/100\gamma_{74.7}$ currently quoted in Nuclear Data Sheets[1] and agrees well with (0.88 ± 0.39) as reported by Aleksandrov et al.[27], but differs somewhat from the reported value of 1.2 obtained by $(\alpha\text{-}\gamma)$ coincidence measurements[23] and the value derived from the ^{243}Am singles γ data of this work. (See section 3.3.2.) The coincidence measurement of the intensity of the 117.8 keV γ transition is preferred over that derived from the singles data since it involves no large-scale corrections due to interference from neighbouring PuK X-ray peaks.

The relative intensities of the 50.6, 55.2 and 98.2 keV γ transitions with respect to the 141.9 keV transition are at variance with the experimental ratios determined from the coincidence data of Van Hise and Engelkemeir[23] (see table 3.11). It is interesting to compare the present experimental intensity ratios $\gamma_{50.6}/\gamma_{142}$ and $\gamma_{101.8}/\gamma_{142}$ with those derived using the expression 2.17 in which all transitions are assumed to be of E1 type. The theoretical ratios $\gamma_{50.6}/\gamma_{142}$ and $\gamma_{101.8}/\gamma_{142}$ are calculated to be 0.063 and 0.30 respectively and are therefore in good agreement with the experimental ratios determined in the course of this work. (It is assumed here that angular correlation effects are highly perturbed and all radiation distributions from the 173.2 keV level are isotropic). The experimental γ intensities of the 50.6 and 101.8 keV transitions therefore support the E1 assignments for these transitions.

Total I.C.C. for the 31.1 keV transition

From the (α_{75}-γ) coincidence run, in which there are no interfering tails from the higher energy α groups, the ratio $\gamma_{31.1}/\gamma_{43.5}$ is calculated to be 7.9-3; thus, from intensity balance coinsderations, and assuming no angular correlation effect upon the measured γ-ray peak intensities, the total I.C.C. of the 31.1 keV γ transition is calculated to be ~270. A similar value (~ 250) is obtained from the singles γ data of table 3.9 where it is assumed ~95% of the 31.1 keV transitions are populated by the preceeding 43.53 keV γ transition.

Both values are higher than the currently quoted[1] total I.C.C. of ~173. The discrepancy reflects the difference in measured γ-ray intensities for the 31.1 keV transition (see table 3.7).

3.6.3 Conclusions

The ^{239}Np level scheme of fig. 3.7 is proposed on the basis of the γ singles and (α-γ) coincidence data obtained from ^{243}Am α decay studies. Two new γ transitions, of energy 46.7 and 101.8 keV, have been placed within the level scheme which confirm the assignment of the $9/2^+$ member of the ground state rotational band at 71.2 keV. There is also slight evidence for a de-exciting transition from this level to the level at 31.1 keV in ^{239}Np.

3.7 ^{243}Am (α-e^-) Coincidence Studies

In order to obtain further experimental data on the I.C.C.'s of the low energy transitions within the ^{239}Np level scheme of fig. 2.2, attempts were made to measure conversion e^- spectra in coincidence with α's to eliminate interference from the ^{239}Np daughter.

3.7.1 (α-e^-) coincidence arrangement

Internal conversion e^- spectra were measured with a 25 mm^2 x 150 μm deep Si(Au) surface barrier detector with nominal 40 μg/cm^2 gold window. It was necessary to compromise on the active area (count rate) of the e^- detector and thickness (γ background) in order to achieve minimum total capacitance (noise). The detector was also cooled using liquid nitrogen to reduce detector leakage current and so optimise the extremely low e^- to noise signal ratio. A conventional Ortec pre-amplifier situated outside the vacuum chamber was used for pulse processing to provide suitable energy and timing signals. The energy loss in the Au window of the detector was calculated to be about

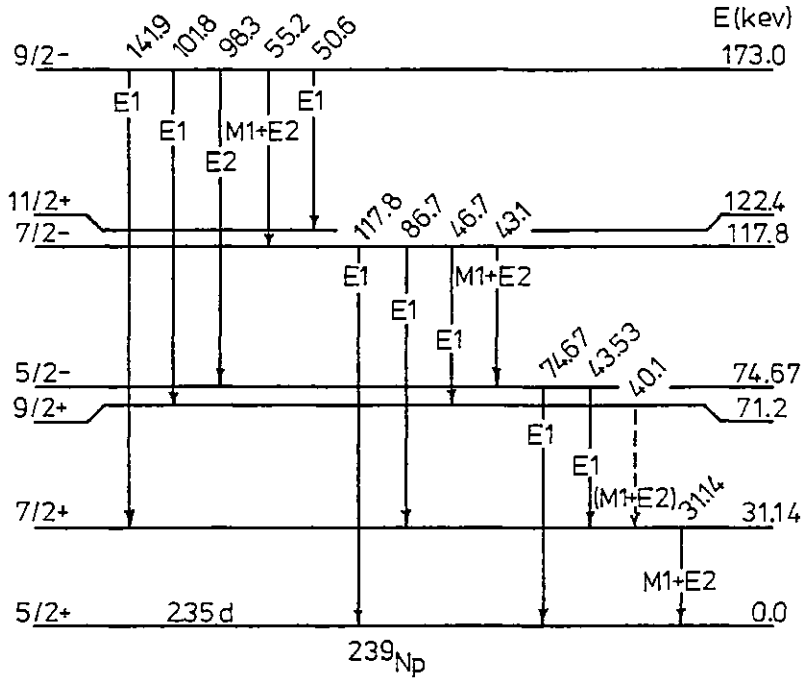

Fig. 3.7 Proposed partial ^{239}Np level scheme based upon γ decay data from ^{243}Am α decay

0.35 keV at 20 keV, decreasing to about 0.08 keV at 100 keV electron energy. Since 100 keV e^-'s have a range of ~60 μm in Si there was no way to discriminate against the α's from ^{243}Am decay.

A 150 mm^2 Si(Au) surface barrier detector, mounted at 90° to the e^- detector, provided the gating α pulse. The resolution of the detector (~ 14 keV for 5.3 MeV α's) enabled windows to be positioned on the three main ^{243}Am α groups. The ^{243}Am source, the same one as used in the (α-γ) coincidence runs, was mounted at 45° with respect to the normal axes of the e^- and α detectors and at a distance of 14 mm from the e^- detector and 45 mm from the α detector to maximise the coincidence efficiency.

The modular electronics system used to observe the ^{243}Am (α-e^-) coincidences was essentially that shown in fig. 3.3, except that further amplification of the pre-amp pulses from the e^- detector was required in order to disperse the e^- pulse height spectrum across the

largest number of channels to obtain suitable resolution of individual electron peaks. At the amplifier gain required to observe structure within the e^- spectrum (i.e. when operating at maximum gain) the e^- spectroscopy amplifier was in fact operating under continual overload conditions since there was no way to discriminate against the (much higher energy) ^{243}Am α pulses.

3.7.2 Results

Fig. 3.8 shows a singles e^- spectrum obtained from the ^{243}Am-^{239}Np source used for orientation and energy calibration of the ^{243}Am (α-e^-) coincidence spectra. The majority of peaks can be identified as conversion e^-'s from ^{239}Np β^- decay superimposed on a continuous β^- spectrum background. The expected positions of the e^- peaks from the internal conversion of the major 74.67 keV γ transition are indicated in the figure, although the (L_1 + L_2) and L_3 e^- peaks are unresolved from the M and N e^- peaks respectively arising from the internal conversion of the 57.26 keV γ transition following ^{239}Np β^- decay; although the I.C.C. of the 74.67 keV transition is not high ($\alpha_T \sim 0.28$) it is still expected that e^- lines from this transition will dominate any singles ^{243}Am conversion e^- spectrum. The only singlet peaks in the spectrum of fig. 3.8 are the K e^- lines of the 228.2 and 277.6 keV γ transitions following ^{239}Np decay; the resolution of the e^- detector was measured to be ~3.4 keV in the energy interval ~100 to 150 keV.

The e^- spectra in coincidence with the three major α groups are shown in figs. 3.9(a), (b) and (c). Owing to poor e^- detector resolution, individual e^- lines from a single transition (e.g. the 74.67 keV de-excitation) are not resolved and the detailed features of previous (α-e^-) studies[20], obtained using a Si(Li) e^- detector, are not revealed in the present work.

The spectrum in coincidence with α_{75} shows only transitions originating from the 74.67 keV level. The expected e^- lines from the conversion of the 31.1 keV transition which is populated by the 43.53 keV transition do not appear in the spectrum because it was not possible to detect coincidences between α's and low energy electrons (less than ~30 keV); the lower level discriminator in the fast e^- channel was set to exclude the noise contribution in which the low energy e^- signals were buried.

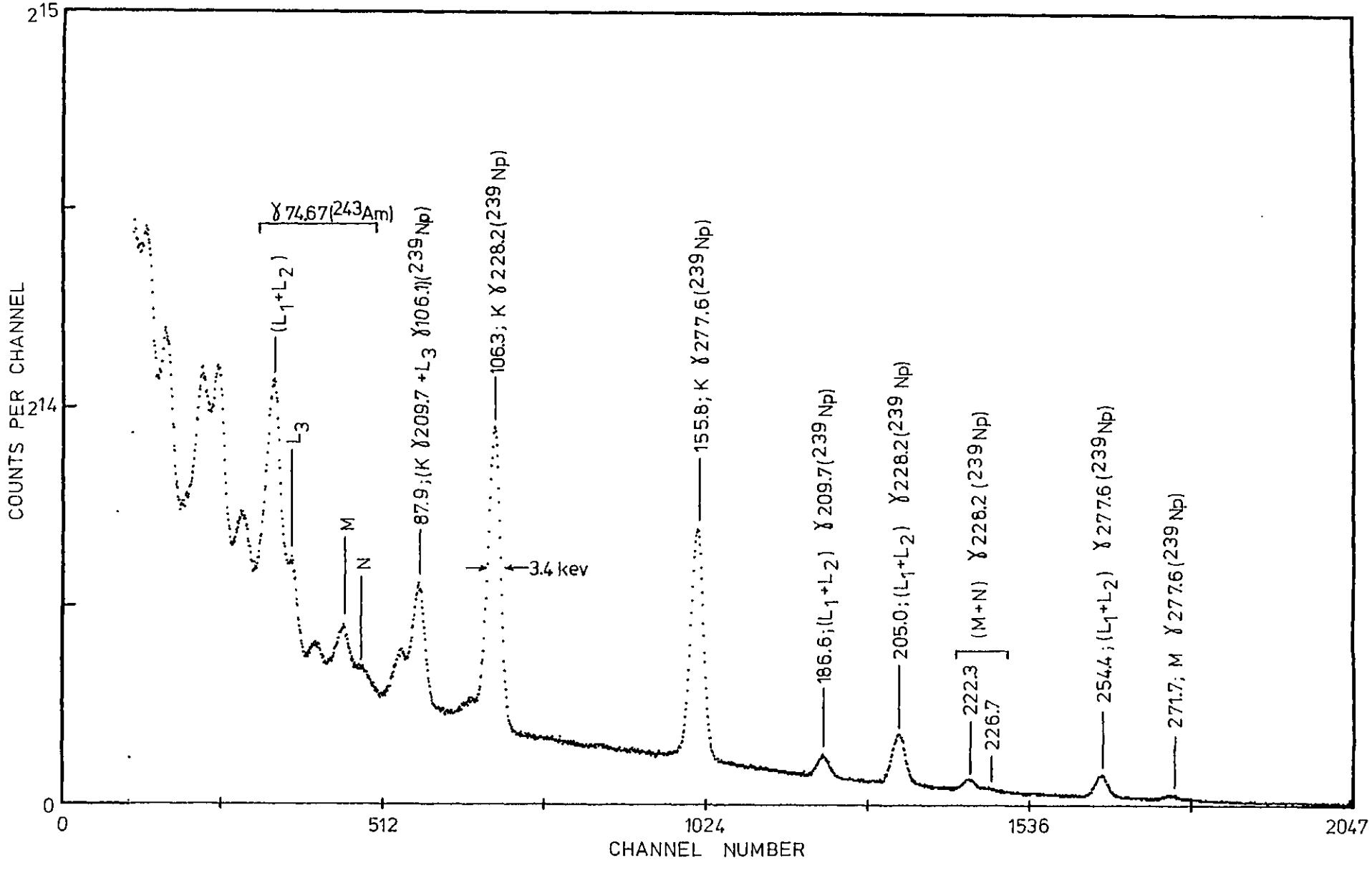

Fig. 3.8 Singles e^- spectrum from ^{243}Am-^{239}Np source obtained using a 25 mm^2 Si surface barrier detector

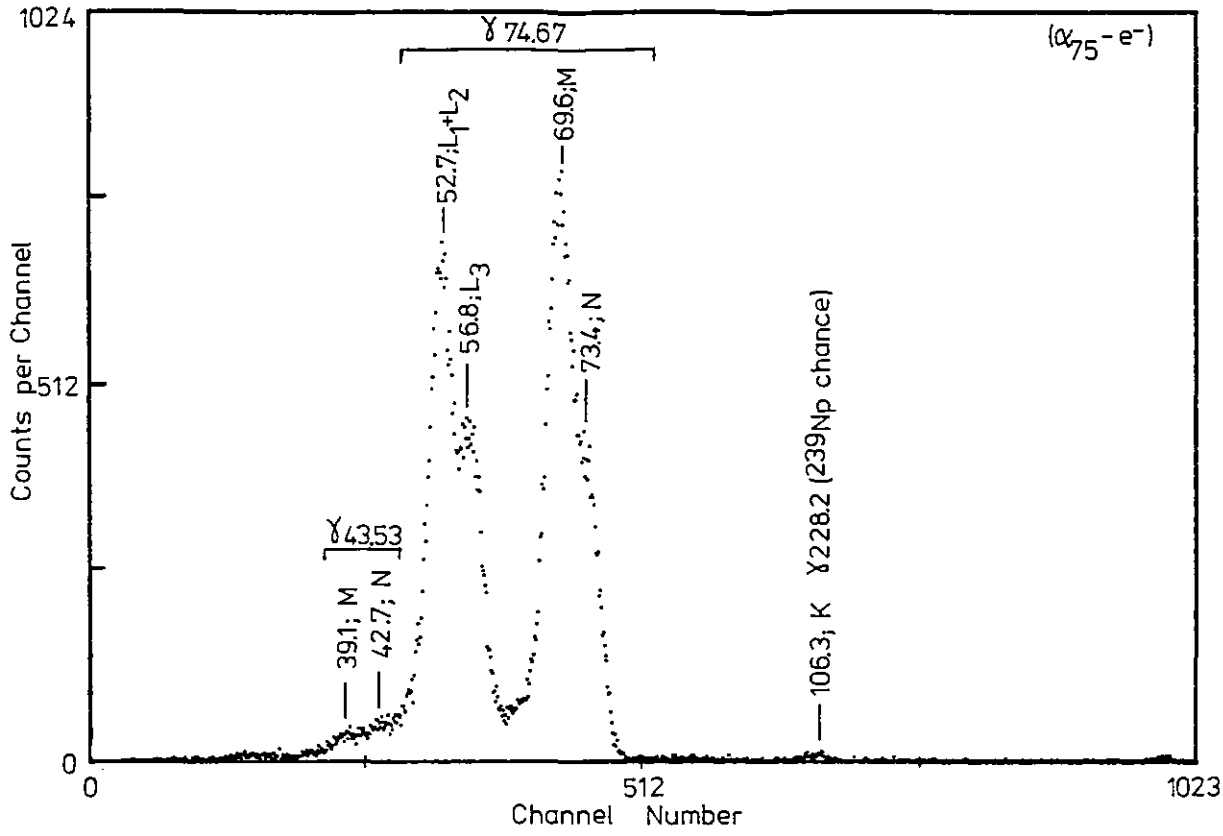

Fig. 3.9(a) ^{243}Am (α_{75}-e^-) coincidence spectrum

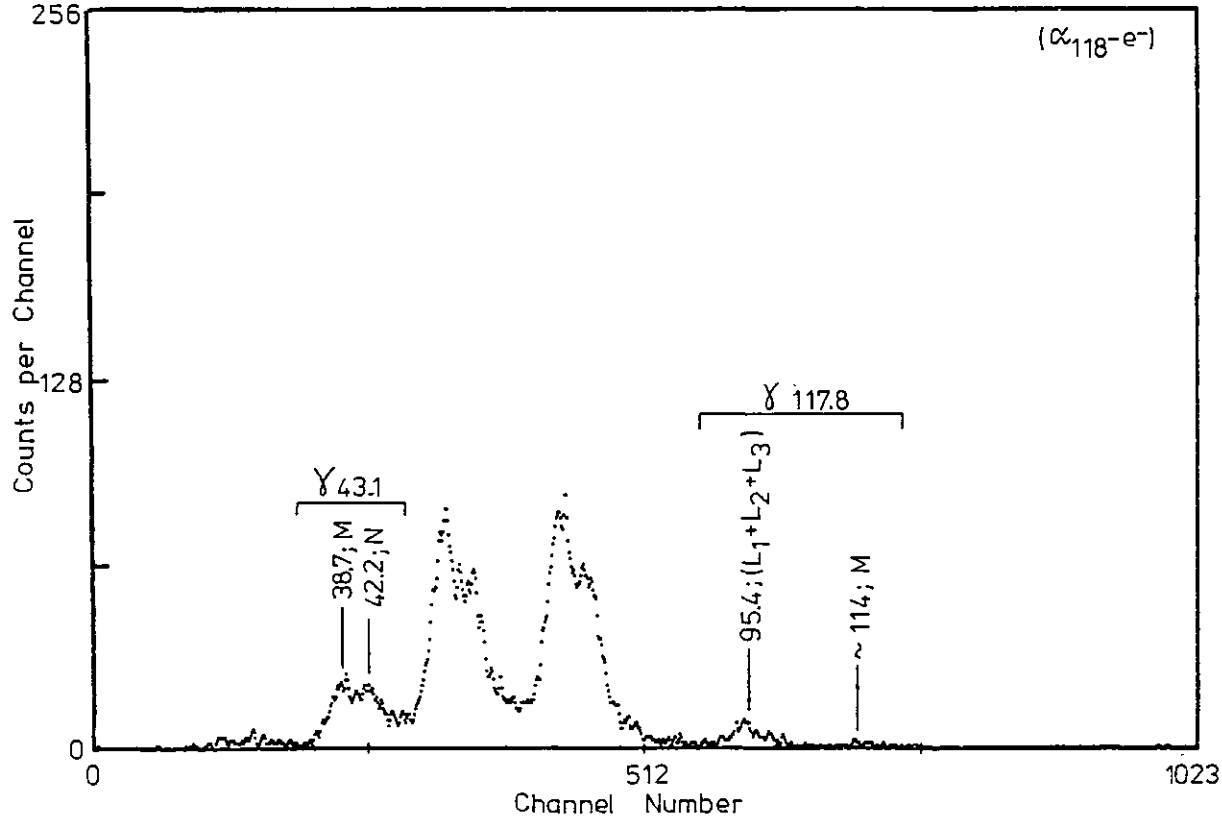

Fig. 3.9(b) ^{243}Am (α_{118}-e^-) coincidence spectrum

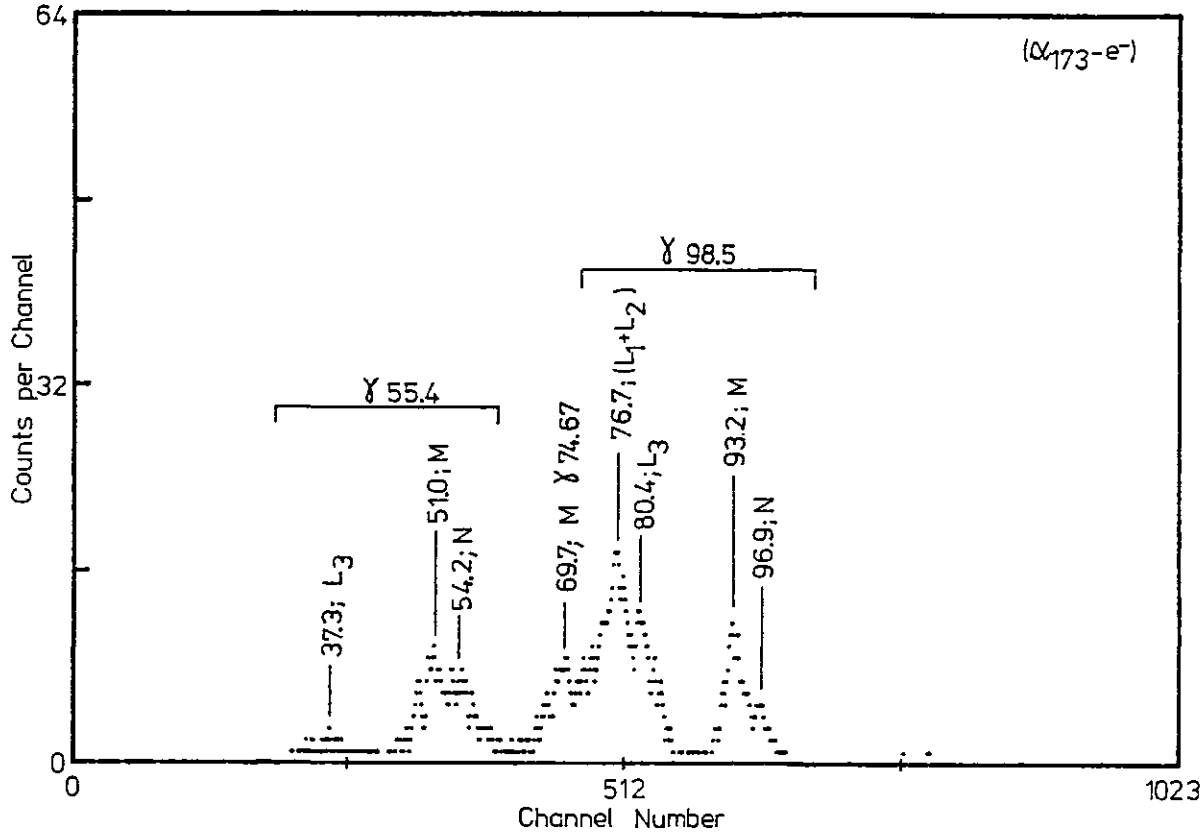

Fig. 3.9(c) ^{243}Am (α_{173}-e^-) coincidence spectrum

The (α_{118}-e^-) spectrum shows not only transitions originating from the 117.8 keV level but also transitions from the 74.67 keV level which is strongly populated by the 43.1 keV transition. A proportion of the lines characteristic of the (α_{75}-e^-) spectrum present in the (α_{118}-e^-) spectrum of fig. 3.9(b) are due to coincidences between e^-'s and the tail of the higher energy α_{75} group. There is slight evidence for conversion lines from the 86.7 keV transition on the high energy side of the 74.67 keV transition Ne^- peak ($\gamma_{86.7}$; Me^- = 82.3 keV, Ne^- = 85.7 keV) although the (L_1 + L_2) and L_3 e^- lines from the same transition are masked by the intense M e^- line of the 74.67 keV transition ($\gamma_{86.7}$; (L_1 + L_2) e^- = 66.8 keV, L_3 e^- = 69.1 keV). Despite the poor counting statistics of the (α_{173}-e^-) coincidence run it is possible to identify peaks arising from the internal conversion of those transitions with the largest I.C.C.'s, namely the 55.4 (α_T ~ 114) and 98.5 (α_T ~ 15.9) keV transitions.

3.7.3 Conclusions

The present poor e^- detector resolution, coupled with unknown variation in e^- detection efficiency and low peak area statistics makes a quantitative analysis of relative e^- line intensities, and hence the determination of relative partial or total I.C.C.'s for transitions de-exciting a common level in ^{239}Np, extremely difficult. The effect of the variation in e^- detection efficiency as a function of incident e^- energy can be seen most clearly in fig. 3.9(a) where L and (M + N + ...) shell internal conversion coefficients of 0.21 and 0.07 respectively for the 74.67 keV transition[28] imply a relative intensity of the L to (M + N + ...) e^- peaks of the order of 3; clearly this is not the case here, where the L and (M + N + ...) e^- peak areas are approximately equal, indicating a factor of three decrease in e^- detector efficiency in going from an e^- energy of ~ 70 keV to ~ 55 keV. A calculated $\alpha(L)/\alpha(M + N + ...)$ ratio of ~ 2.6 for the 98.5 keV transition[28] reflects more closely the experimental intensity data shown in fig. 3.9(c) for this particular transition, thus indicating an approximately constant e^- detection efficiency over the energy range ~ 80 to 100 keV. Unsealed ^{241}Am and ^{109}Cd sources would provide useful low energy e^- lines suitable for e^- efficiency calibration purposes.

To achieve $\lesssim$ 1 keV resolution on e^- peaks in the energy range studied here (i.e. $\simeq$ 20 to 100 keV) and hence be able to resolve individual e^- lines and obtain conversion coefficients for specific e^- shells, it is necessary to improve the e^- detector pre-amplifier stage. Operation of the input field-effect transistor of the pre-amplifier at the reduced temperature afforded by the e^- detector liquid nitrogen cooling system - by attaching the F.E.T. stage directly to the Si(Au) detector - would help minimise noise, as well as reducing stray capacitance associated with the long cables required to connect the e^- detector to the externally mounted pre-amplifier in the existing system.

REFERENCES

1. M. R. Schmorak, Nucl. Data Sheets 21, 153 (1977).

2. D. I. Starozhukov, Yu. S. Popov and P. A. Privalova, At. Energy 42, 319 (1977).

3. Yu. S. Popov, D. I. Starozhukov, V. B. Mishenev, P. A. Privalova and A. I. Mischenko, At. Energy 46, 111 (1979).

4. I. Ahmad, Nucl. Instr. and Meth. 193, 9 (1982).

5. A. L. Nichols, AEEW R-1251 (1979).

6. K. Debertin and W. Pessara, Nucl. Instr. and Meth. 184, 497 (1981).

7. C. M. Lederer and V. S. Shirley, Table of Isotopes (7th ed., Wiley, New York, 1978).

8. J. Legrand, J. P. Perolat, F. Lagoutine and Y. LeGallic, Table de Radionucleides (Laboratoire de Metrologie des Rayonnements Ionisants, 1975).

9. R. L. Auble, Nucl. Data Sheets 20, 327 (1977).

10. E. A. Henry, Nucl. Data Sheets 11, 495 (1974).

11. Y. A. Ellis, Nucl. Data Sheets 23, 123 (1978).

12. R. L. Bunting, Nucl. Data Sheets 15, 335 (1975).

13. E. Storm and H. Israel, Nucl. Data Tables A7, 565 (1970).

14. R. S. Mowatt, Nucl. Instr. and Meth. 70, 237 (1969).

15. J. M. Freeman and J. G. Jenkin, Nucl. Instr. and Meth. 43, 269 (1966).

16. R. Fletcher, AERE-R 6799 (1971).

17. J. C. Pate, K. R. Baker and R. W. Fink, Z. Physik A272, 169 (1975).

18. K. J. Blinowska, P. G. Hansen, H. L. Nielsen, O. Schult and K. Wien, Nucl. Phys. 55, 331 (1964).

19. D. R. MacKenzie and R. D. Connor, Nucl. Phys. A108, 81 (1968).

20. D. Engelkemeir, Phys. Rev. 181, 1675 (1969).

21. I. Ahmad and M. Wahlgren, Nucl. Instr. and Meth. 99, 333 (1972).

22. G. T. Ewan, J. S. Geiger, R. L. Graham and D. R. MacKenzie, Phys. Rev. 116, 950 (1959).

23. J. R. VanHise and D. Engelkemeir, Phys. Rev. 171, 1325 (1968).

24. J. M. R. Hutchison, Phys. Rev. 157, 1093 (1967).

25. F. Falk, S. Tornkvist, J. E. Thun, H. Snellman, K. Siegbahn and F. Asaro, Z. Physik 198, 106 (1967).

26. E. Flamm and F. Asaro, Phys. Rev. 129, 290 (1963).

27. B. M. Aleksandrov, O. I. Grigor'ev and N. S. Shimanskaya, Yad. Fiz. 10, 14 (1969).

28. Y. A. Ellis-Akovali, Nucl. Data Sheets 33, 79 (1981).

CHAPTER 4. THE EFFECT OF CHEMICAL COMPOSITION ON THE HALF-LIFE FOR β^- DECAY, WITH SPECIAL REFERENCE TO ^{241}Pu

4.1 Current Status and Importance of ^{241}Pu Half-life in the Nuclear Fuel Cycle

Accurate calculations to determine ^{241}Am and ^{242}Cm inventories depend upon the half-life of ^{241}Pu (see fig. 3.1), particularly when irradiated fuel is stored for a long period of time before being recycled. Upon reirradiation the build up of ^{242}Cm, a major neutron source, needs to be accurately known. Waste storage calculations and Pu assay measurements for nuclear safeguards also require an accurate ^{241}Pu half-life. However, in spite of the high accuracy achieved in various experiments for measuring the half-life of ^{241}Pu, the available data do not agree sufficiently closely with each other.[1,2] The existing scatter in the experimental data, although not large in absolute terms, is important with respect to the above applications of the ^{241}Pu half-life.

Between 1950 and 1970 measurements of the half-life ranged from 13.3 to 15.37y (typical uncertainty $\sim \pm$ 0.25y) and in the period 1971 to 1980 measurements ranged from 14.24 to 15.16y(typical uncertainty $\lesssim \pm$ 0.10y). In 1975 the American National Standards Institute[3] recommended a value of 14.35y for the ^{241}Pu half-life and in 1979 the International Nuclear Data Committee[4] increased this to (14.7 $\pm$ 0.4)y. This recommended value is the evaluated mean of previous data coupled to an uncertainty that covers the wide range of measured values; the associated uncertainty ($\sim$ 3%) is large compared with existing uncertainties in nuclides with similar half-lives (e.g. ^{244}Cm (18.1y), ^{250}Cf(13.1y), ^{252}Cf(2.64y), ^{238}Pu(87.7y)) which are all known to better than 1%.[4]

More recent measurements have yielded values of (14.44 $\pm$ 0.06),[5] (14.38 $\pm$ 0.03)[6] and (14.33 $\pm$ 0.02)[7]y for the ^{241}Pu half-life. Despite the closer agreement in these more recent measurements (and even greater assumed accuracy) there is no reason to discount the earlier measured values which were all careful measurements carried out by competent laboratories; this is perhaps the most important reason why the discrepancies between the measured ^{241}Pu half-life values should be resolved and attempts made to explain such large differences without, however, merely resorting to adding another "careful" measurement of the ^{241}Pu half-life to the existing set of data.

It has already been reported[8] that there is no conclusive evidence, experimental or theoretical, for the existence of an isomeric state in ^{241}Pu with a similar half-life of ~ 14.7y which could account for the observed facts. The work carried out in this chapter has therefore been based upon a mechanism which hitherto has received little attention in the literature but, as shown in sections 4.3 and 4.4, can be subjected to experimental investigation and an overall assessment made as to whether the model predictions can successfully account for the current discrepancy in the measured half-life of ^{241}Pu. The proposed mechanism (section 4.2) is concerned with bound state β^- decay which is directly dependent upon the chemical environment of the nuclide undergoing β^- decay.

4.2 The Effect of Chemical Composition on β^- Decay Transition Probabilities

It has been suggested[9] that the mechanism of bound state β^- decay,[10,11] in which (classically) an emitted β^- particle is captured in an outer atomic vacancy, can lead to a change in the half-life of a β^- emitting nuclide. The ratio of 'captured' to normal continuum decays is largest for low energy end-point β^- emitters and the probability for β^- decay into a bound state depends strongly on the electron environment or chemical composition of the daughter nucleus; for tritium ($E_{\beta max}$ = 18.6 keV) this probability can represent up to 1% of the total decay probability and predicts a half-life for ionised tritium ~ 0.3% larger than the half-life for neutral tritium. A large effect has also been suggested for ^{187}Re(12) where the β^- decay end-point is only ~ 2 keV and the bound electron mode of decay may amount to ~ 50% of the total decay.

In the particular case of ^{241}Pu, which proceeds by β^- decay to ^{241}Am (99.998%) with an $E_{\beta max}$ of 20.8 keV, it has been calculated[13] that the upper limit of the fraction of decays accompanied by β^- capture into (say) the $7s_{\frac{1}{2}}$ state of the daughter could be as high as 50%. Clearly, if the fraction of decay by this mode is as large as this, the chemical state of ^{241}Pu will show the effect by a variation in half-life with composition very clearly and could account for the observed differences in half-life measurements for ^{241}Pu.

However, it is not easy to measure a variation in the β^- decay emission probability for ^{241}Pu since the final ^{241}Am nucleus has a

long lifetime (~ 432y). Furthermore, ^{241}Pu β^- decays directly to the ^{241}Am ground state and therefore there are no direct γ-rays to observe.

It has been pointed out[14] that there are several other low energy β^- emitters which result in measurable γ radiations and where the effect of chemical composition on β^- decay transition probabilities may possibly be observed. Two general experimental methods have also been proposed[14] to observe chemical composition effects; these methods have been applied to ^{166m}Ho (section 4.3) and ^{228}Ra (section 4.4) which are both low energy β^- emitters.

4.3 The Relative Intensity Method

This method consists of measuring the relative intensity of two radiations, one of which is expected to vary with chemical composition. It is applicable to the case of ^{166m}Ho (E_β ~ 32 keV (18.7%), 73 keV (80.3%)) where a change in the β^- decay half-life (1.2 x 10^3y) will be observed as a change in the ratio of two observed γ transition intensities, one of which depopulates the nuclear level fed by the low energy (18.7%) β^- branch, and whose intensity is therefore expected to vary with chemical composition, and the other of which depopulates the level fed by the higher energy (80.3%) β^- branch, which is expected to remain unaffected.

Fig. 4.1 shows the energies of the γ transitions directly depopulating the nuclear levels fed by the two main β^- branches following ^{166m}Ho decay. A change in β^- transition probability of the low energy β^- branch will be reflected by a departure from unity for the ratios

$$\frac{(I_{451}/I_{411})C_1}{(I_{451}/I_{411})C_2} \quad \text{and} \quad \frac{(I_{752}/I_{712})C_1}{(I_{752}/I_{712})C_2} \qquad (4.1)$$

where I_γ is the measured γ-ray intensity of a particular energy transition and the subscripts C_1, C_2 refer to different chemical compositions of ^{166m}Ho for which the γ-ray intensity ratio is being calculated. The method is independent of the γ-ray detection efficiency although suitable source-detector distances must be employed to reduce the effect of random coincidence summing in the measured γ spectra which could lead to a false positive identification of the effect of chemical composition upon β^- decay half-lives.

Gamma-ray self absorption effects within the source must also be taken into account in the final analysis of the measured γ-ray intensity ratios.

4.3.1 Experimental Method

Milligramme quantities of high purity ^{165}Ho (holmium content = 99.99% ^{165}Ho) in the form of metal, oxide and sulphate powder were irradiated at the Imperial College Reactor Centre to produce ^{166m}Ho by the $^{165}Ho(n,\gamma)^{166m}Ho$ reaction. An initial cooling period of several months was allowed to remove interference from the 26.8 hr ^{166}Ho isotope produced during the irradiation period before beginning γ-ray analysis of the ^{166m}Ho sources. Other chemical forms of ^{166m}Ho, namely holmium chloride and nitrate, were produced from the active ^{166m}Ho metal powder by dissolving equal portions in concentrated hydrochloric (HCl) and nitric (HNO_3) acid, respectively.

The ^{166m}Ho sources, sealed in small 1 cm diameter polythene containers, were counted using a large volume (100 cm^3) Ge(Li) detector; the resolution of the γ detector was measured to be 1.95 keV (FWHM) at 1.332 MeV (^{60}Co).

Gamma spectra (4096 channels) from each source type were recorded in a series of runs (table 4.1); positions '3' and '5' refer to 3 cm and 5 cm source-detector separations, respectively. The average peak drift during the three month period required to obtain all the γ spectra was approximately 0.7 channels (i.e. less than a 0.1% shift in the lowest energy γ-ray peak of interest) indicating the excellent stability of the multichannel analyser and associated pulse processing electronics over the prolonged counting period.

Table 4.1 List of ^{166m}Ho Runs

Counting Position	Source Composition				
	Metal	Oxide	Sulphate	Nitrate	Chloride
3	18x* 25,000	14x 25,000	16x 25,000	-	-
5	11x 50,000	16x 50,000	16x 50,000	13x 80,000	13x 80,000

*Number of spectra x Livetime γ accumulation period(s)

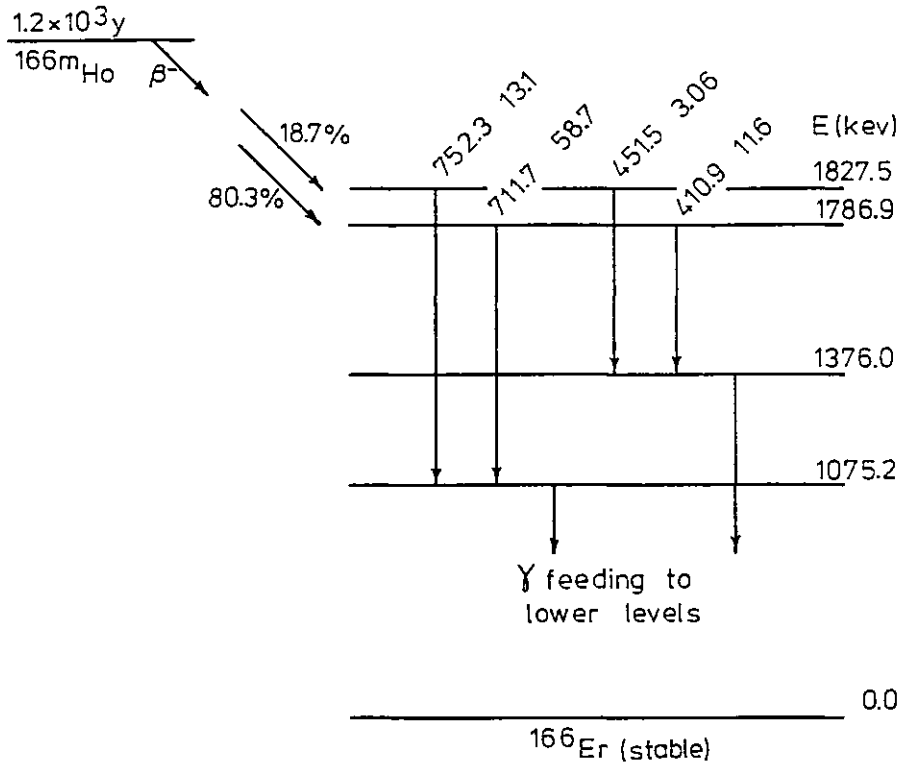

Fig. 4.1 Partial level scheme showing γ transitions used to observe a change in the low energy (18.7%) β^- branch transition probability following ^{166m}Ho β^- decay

Analyser dead times were kept within the limits 0.2% (source position 5) to 0.5% (source position 3) for all runs. No data were taken for the ^{166m}Ho chloride and nitrate sources in counting position '3'.

4.3.2 Results

Fig. 4.2 shows a typical γ spectrum obtained from a ^{166m}Ho metal source. Labelled peaks are those used to determine either (a) γ-ray intensity ratios used to identify possible effects of chemical composition upon the β^- decay half-life or (b) γ-rays used to calculate γ self-absorption effects in the source material; the intensities of these latter γ-ray peaks, populated by intermediate γ transitions which are fed by both the high and low energy β^- branches, are expected to remain constant even in the presence of true chemical composition effects upon the low energy β^- branch intensity because of the dominating influence of the unperturbed high energy β^- branch upon the total measured γ-ray intensity.

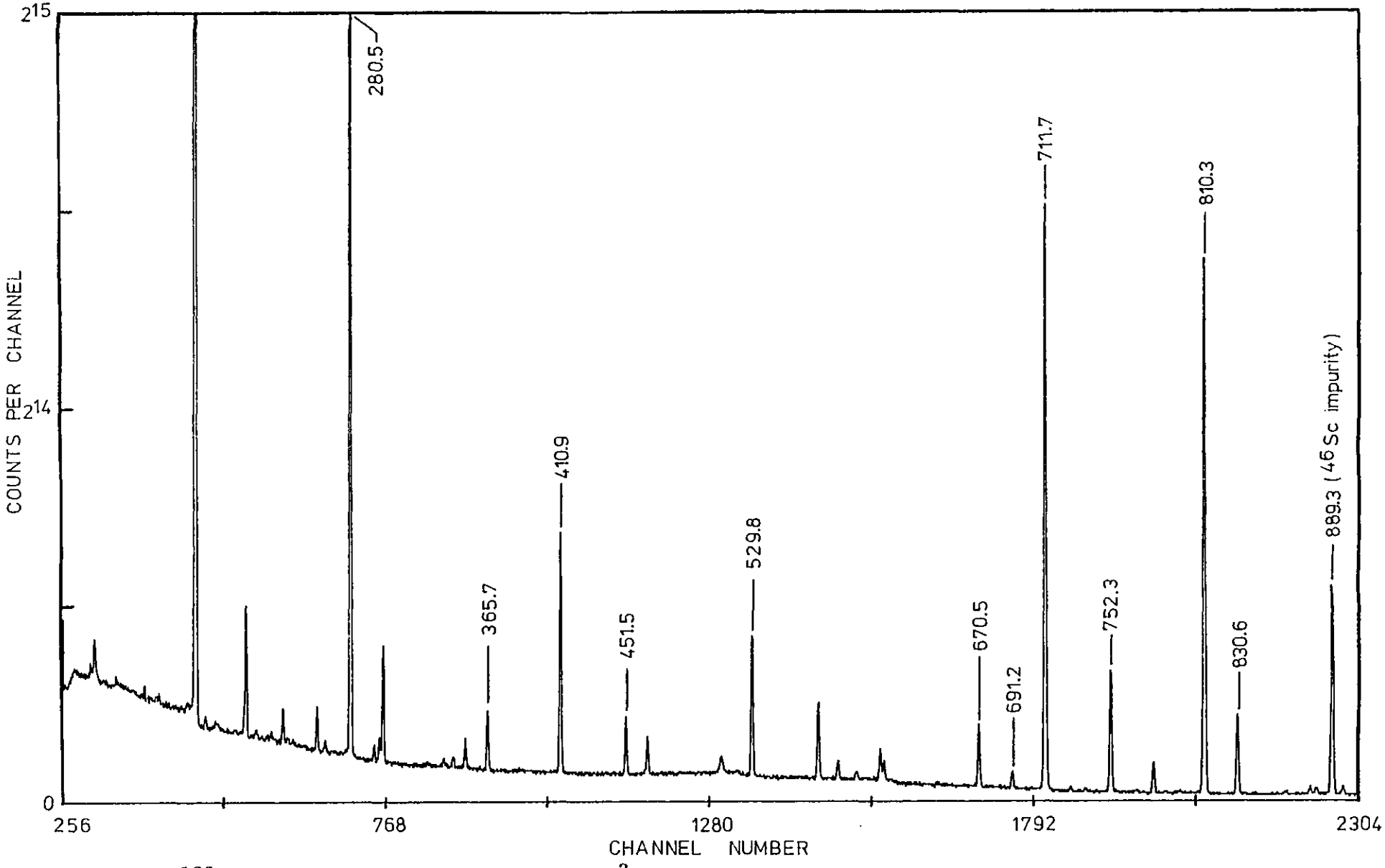

Fig. 4.2 ^{166m}Ho γ spectrum measured with 100 cm^3 Ge(Li) detector. Labelled peaks (in keV) used in γ data analysis (section 4.3.1)

An analysis of the high energy region of the γ spectrum (not shown in fig. 4.2) reveals the presence of impurity peaks, mainly from ^{46}Sc, ^{152}Eu and ^{160}Tb; however, these impurities do not give rise to further intense impurity peaks at the γ-ray energies used for investigation of chemical composition effects or for γ self-absorption corrections. Furthermore, the relative intensity ratios of the γ-ray peaks shown in fig. 4.2 (taking into account γ detection efficiency) are found to be in good agreement with the current published values and thus are assumed free from unresolved impurity peaks of the same γ-ray energy.

Similar impurities were identified in the γ spectra from the ^{166m}Ho oxide, sulphate, chloride and nitrate sources, although they varied in concentration (i.e. peak intensity) between sources.

Mean γ-ray peak areas and their associated uncertainties were derived from the mean and standard deviation in the mean of the complete set of γ-ray peak area data for each source type and counting position. The uncertainty obtained by this method was comparable, or slightly less than, the uncertainty obtained by considering the standard statistical deviation in the peak areas from the complete set of γ-ray spectra belonging to a particular run. Table 4.2 lists the mean peak areas and their associated uncertainties obtained from the various runs (table 4.1).

Data Analysis

For the parent ^{166m}Ho source in chemical state C_1, the measured intensity of the 451 keV γ-ray, $(I_{451})C_1$, is given by

$$(I_{451})C_1 = (No\ B_1 F_{451} \varepsilon_{451} S_{451})C_1 \qquad (4.2)$$

where
- No = absolute β^- activity of the ^{166m}Ho source
- B_1 = absolute intensity of low energy (32 keV) β^- branch
- F_{451} = fraction of level decays which produce γ_{451}
- ε_{451} = absolute full-energy peak detection efficiency for the 451 keV γ transition
- S_{451} = γ self-absorption factor due to finite source thickness.

Table 4.2 Mean γ-ray peak areas and uncertainties[a] from various ^{166m}Ho compounds

E_γ (keV)	Counting Position '3'			Counting Position '5'				
	Metal	Oxide	Sulphate	Metal	Oxide	Sulphate	Nitrate	Chloride
280.5	107315 (0.085)	152658 (0.082)	94563 (0.093)	129589 (0.142)	168133 (0.072)	111219 (0.125)	208408 (0.105)	128504 (0.071)
365.7	6717 (0.543)	9447 (0.513)	5839 (0.740)	8226 (0.521)	10648 (0.524)	6987 (0.520)	13072 (0.363)	8011 (0.782)
410.9	27496 (0.230)	38755 (0.179)	24126 (0.224)	34041 (0.263)	44150 (0.210)	29045 (0.201)	54223 (0.179)	33426 (0.203)
451.5	6466 (0.677)	9160 (0.568)	5697 (0.623)	7978 (0.946)	10440 (0.467)	6787 (0.787)	12746 (0.431)	7700 (0.345)
529.8	17837 (0.251)	25049 (0.215)	15653 (0.305)	22049 (0.289)	28548 (0.238)	18883 (0.254)	35309 (0.212)	21750 (0.385)
670.5	8258 (0.570)	11517 (0.366)	7200 (0.307)	10079 (0.626)	13017 (0.359)	8628 (0.384)	16103 (0.275)	9855 (0.489)
691.2	2376 (1.19)	3450 (1.18)	2169 (1.03)	2684 (1.16)	3489 (0.759)	2278 (1.18)	4371 (1.20)	2696 (1.57)
711.7	82250 (0.072)	116014 (0.089)	72055 (0.086)	98785 (0.086)	128805 (0.131)	84519 (0.111)	160031 (0.122)	98406 (0.063)
752.3	16993 (0.203)	24078 (0.251)	14848 (0.286)	20609 (0.238)	26775 (0.173)	17609 (0.180)	33312 (0.202)	20556 (0.246)
810.3	76999 (0.083)	108620 (0.080)	67369 (0.112)	92493 (0.172)	120342 (0.085)	79200 (0.109)	149613 (0.105)	92224 (0.080)
830.6	12113 (0.279)	17004 (0.281)	10494 (0.337)	14827 (0.364)	19305 (0.224)	12673 (0.333)	23817 (0.245)	14677 (0.336)
950.9	3380 (0.614)	4768 (0.573)	2945 (0.673)	3977 (0.990)	5144 (0.508)	3400 (0.557)	6456 (0.812)	4025 (0.767)

a. The figure in parentheses under the mean γ-ray peak area is its associated uncertainty (expressed in %) derived from the spread in the experimental data.

Similarly, the measured intensity of the 411 keV γ-ray in the same chemical state, $(I_{411})C_1$, is given by

$$(I_{411})C_1 = (No\ B_2\ F_{411}\ \varepsilon_{411}\ S_{411})C_1 \qquad (4.3)$$

where B_2 is the absolute intensity of the high energy (73 keV) β^- branch.

For the parent ^{166m}Ho source in chemical state C_2 the analogous expressions are

$$(I_{451})C_2 = (No\ B_1\ F_{451}\ \varepsilon_{451}\ S_{451})C_2 \qquad (4.4)$$

$$(I_{411})C_2 = (No\ B_2\ F_{411}\ \varepsilon_{411}\ S_{411})C_2 \qquad (4.5)$$

Since the parameters F_{451}, F_{411}, ε_{451}, ε_{411} and B_2 are independent of the chemical state of the parent ^{166m}Ho (i.e. assuming that only the low energy β^- branch, B_1, is a function of the source chemical composition) then eqns. 4.2 and 4.4 combine to give

$$\frac{(I_{451})C_1}{(I_{451})C_2} = \frac{(No\ B_1\ S_{451})C_1}{(No\ B_1\ S_{451})C_2} \qquad (4.6)$$

Similarly, eqns. 4.3 and 4.5 yield

$$\frac{(I_{411})C_1}{(I_{411})C_2} = \frac{(No\ S_{411})C_1}{(No\ S_{411})C_2} \qquad (4.7)$$

Equations 4.6 and 4.7 combine further to yield the expression

$$\left\{\frac{(I_{451})C_1}{(I_{451})C_2}\right\} \Big/ \left\{\frac{(I_{411})C_1}{(I_{411})C_2}\right\} \times \left\{\frac{(S_{411})C_1}{(S_{411})C_2}\right\} \Big/ \left\{\frac{(S_{451})C_1}{(S_{451})C_2}\right\} = \frac{(B_1)C_1}{(B_1)C_2} \qquad (4.8)$$

An identical expression to eqn. 4.8 is obtained for the $\gamma_{752} - \gamma_{712}$ pair.

In the absence of the effect of chemical composition upon the β^- decay transition probability then the ratio $(B_1)C_1/(B_1)C_2$ is equal to unity; any measurable departure from unity will therefore indicate an alteration of the low energy β^- branch decay probability, attributable to the difference in ^{166m}Ho source chemical composition. If γ self-absorption effects are negligible then eqn. 4.8 reduces to the simple expression of eqn. 4.1; these effects were minimised in the case of the ^{166m}Ho metal, sulphate and oxide powder samples by presenting a thin, uniform source distribution parallel to the Ge(Li) detector face during γ-ray analysis.

The relative γ self-absorption ratios of eqn. 4.8 were interpolated from the best fit to the experimental peak area ratios, plotted as a function of energy, for those γ transitions which are assumed to remain unaffected by chemical composition effects. Although the relative γ self-absorption between different chemical states of ^{166m}Ho is expected to follow a simple exponential law, the plots of peak area ratio versus γ-ray energy did not exhibit any gross curvature over the energy range considered (280-950 keV). Therefore both exponential and linear functions were used to fit the experimental data using a generalised weighted least squares fitting routine (Harwell library subroutine VB01A)[15]. Both functions produced identical results in terms of fitted and interpolated relative self-absorption ratios, although the uncertainties derived from the exponential fit (from the variance-covariance matrix) were between two and three times larger than those derived from the linear fit. The uncertainties obtained from the linear fit (in general of the order of ~ 0.1% at the 1σ confidence level) were combined with those for the mean peak areas of the 411, 451, 712 and 752 keV γ transitions (table 4.2) to yield the $(B_1)C_1/(B_1)C_2$ ratios listed in tables 4.3 to 4.6 inclusive, where all uncertainties are again quoted at the 1σ level.

Table 4.3 $(B_1)C_1/(B_1)C_2$ ratios for γ_{451}-γ_{411} pair; source position '5'

C_1	$\frac{(B_1)C_1}{(B_1)}$ metal	$\frac{(B_1)C_1}{(B_1)}$ oxide	$\frac{(B_1)C_1}{(B_1)}$ sulphate	$\frac{(B_1)C_1}{(B_1)}$ nitrate
Oxide	1.009±0.011	-	-	-
Sulphate	0.997±0.013	0.989±0.010	-	-
Nitrate	1.002±0.011	0.994±0.007	1.005±0.010	-
Chloride	0.982±0.011	0.974±0.007	0.985±0.009	0.980±0.006

Table 4.4 $(B_1)C_1/(B_1)C_2$ ratios for γ_{752}-γ_{712} pair; source position '5'

C_1	$\frac{(B_1)C_1}{(B_1)}$ metal	$\frac{(B_1)C_1}{(B_1)}$ oxide	$\frac{(B_1)C_1}{(B_1)}$ sulphate	$\frac{(B_1)C_1}{(B_1)}$ nitrate
Oxide	0.996±.003	-	-	-
Sulphate	0.999±.004	1.003±.004	-	-
Nitrate	0.997±.004	1.001±.004	0.998±.004	-
Chloride	1.000±.004	1.005±.004	1.002±.004	1.004±.004

Table 4.5 $(B_1)C_1/(B_1)C_2$ ratios for γ_{451}-γ_{411} pair; source position '3'

C_1	$\frac{(B_1)C_1}{(B_1)\text{ metal}}$	$\frac{(B_1)C_1}{(B_1)\text{ oxide}}$
Oxide	1.006±.009	-
Sulphate	1.005±.010	0.999±.009

Table 4.6 $(B_1)C_1/(B_1)C_2$ ratios for γ_{752}-γ_{712} pair; source position '3'

C_1	$\frac{(B_1)C_1}{(B_1)\text{ metal}}$	$\frac{(B_1)C_1}{(B_1)\text{ oxide}}$
Oxide	1.005±.004	-
Sulphate	0.998±.004	0.993±.004

It is calculated that the relative γ self-absorption ratios have a very small effect upon the $(B_1)C_1/(B_1)C_2$ ratios of tables 4.3 to 4.6, where they are responsible for no more than a 0.1% change in the magnitude of the ratios obtained using eqn. 4.1.

Despite the fact that the (B_1) chloride/$(B_1)C_2$ ratios of table 4.3, obtained using the γ_{451}-γ_{411} pair, tend to support the existence of a chemical composition effect, the corresponding ratios obtained using the more intense γ_{752}-γ_{712} pair (table 4.4) clearly do not. All other possible $(B_1)C_1/(B_1)C_2$ ratios in tables 4.3 - 4.6 also lend support to the general conclusion that, within the limits of experimental uncertainty, there is no positive evidence for a change in the ^{166m}Ho β^- transition probability for the low energy β^- branch varying with chemical composition. In this particular experimental arrangement the source-detector separation has little effect upon

the evaluated $(B_1)C_1/(B_1)C_2$ ratios.

The reduced (B_1) chloride/$(B_1)C_2$ ratios for the γ_{451}-γ_{411} pair can be attributed to either (a) an increase in the measured peak area of the 411 keV γ transition in the chloride source or (b) a decrease in the measured γ-ray intensity of the 451 keV γ transition in the same source. It is worth considering possible causes for such effects.

The most likely cause for an increase in the measured intensity of the 411 keV γ transition is the existence of an impurity peak at the same energy. However, since the chloride, nitrate and metal samples were all derived from the same original metal source then any impurity effect on the measured intensity of the 411 keV γ transition would tend to cancel out in the calculated $(B_1)C_1/(B_1)C_2$ ratios using the peak area data available for the nitrate, chloride and metal sources. This is clearly not the case here.

A detailed analysis of the available data (table 4.2) shows that option (b) is correct in that the ratio of the 451 keV peak area for the chloride source to the peak area of the same transition from the other sources is smaller than the corresponding ratios determined for nearby peaks. However, since the 752 keV γ transition depopulating the same nuclear level is not affected to the same extent, it is difficult to assign the reduced intensity of the 451 keV γ transition in the chloride source as being due to chemical composition effects. Indeed, as stated previously, the results for the γ_{752}-γ_{712} pair do not lend support to the existence of chemical composition effects upon β^- decay transition rates.

4.4 The Ingrowth Method

If the transition probability for β^- decay is affected by chemical composition then this effect will be seen as a change in the specific activity of the daughter product as it approaches a new level of secular equilibrium. This method is applicable to ^{228}Ra ($T_{\frac{1}{2}}$ = 5.76y; E_β ~ 14 keV (40%), 39 keV (60%)) where the ^{228}Ac daughter ($T_{\frac{1}{2}}$ = 6.13 hr) is present in secular equilibrium. After modifying the chemical state of ^{228}Ra, any perturbation of the β^- decay probability will be observed as a change (as a function of time) of the measured γ-ray peak intensity of the major 911 keV transition from ^{228}Ac decay, following a ~ 6 hr half-life as the ^{228}Ac approaches a new equilibrium level; see fig. 4.3. This method does not rely on the relative

intensity of two γ-rays remaining constant for different samples; however, it is essential that the source-detector geometry remain constant throughout the γ counting period in order to isolate those effects due solely to a change in the chemical state of the ^{228}Ra parent.

Since ^{228}Ra has only one common valence state the measurement must be designed to observe the difference between the metallic and the 2^+ ion. ^{228}Ra is a daughter of ^{232}Th ($T_{\frac{1}{2}} = 1.41 \times 10^{10}$ y) and metallic thorium should contain metallic radium. The experiment consists of dissolution of thorium metal and a search for a time variation of the specific activity of ^{228}Ac. It is essential that the ^{228}Ra remains in solution during the γ counting period in order that the effective solid angle for detection of the 911 keV radiation remains constant; precipitation of the ^{228}Ra out of solution could lead to a change in the measured intensity of the 911 keV γ transition (as a result of the change in effective solid angle) which might mask any real effect due to the change in chemical composition of the radium or, conversely, be falsely attributed as positive evidence for the existence of chemical effects upon the β^- decay half-life.

4.4.1 Experimental Method

Two runs were performed using 4g and 16g quantities of ^{232}Th metal foil. The age of the foil since the original chemical separation of the ^{232}Th was such that the daughter ^{228}Ra had grown into the foil over a period of several years and was therefore now present in sufficient quantity to allow accurate monitoring, at (say) one hourly intervals, of the 911 keV γ-ray peak intensity from the daughter ^{228}Ac decay. The 16g quantity of thorium in the second run was used purely to obtain increased peak area statistics and corresponding reduced statistical uncertainty in the measured γ-ray peak area so that any possible effect of chemical composition could be extracted more easily from the experimental peak area data.

The foil used in each run was dissolved in a quantity of nitric acid (HNO_3) - 25 ml in the case of the 4g foil - containing a few drops of ammonium fluorosilicate solution ($(NH_4)_2\ SiF_6$); this solution was used to dissolve the insoluble black residue formed when HNO_3 (or HCl) alone is used to dissolve thorium metal, leaving only a small residue of thorium oxide in the clear solution. The final solution

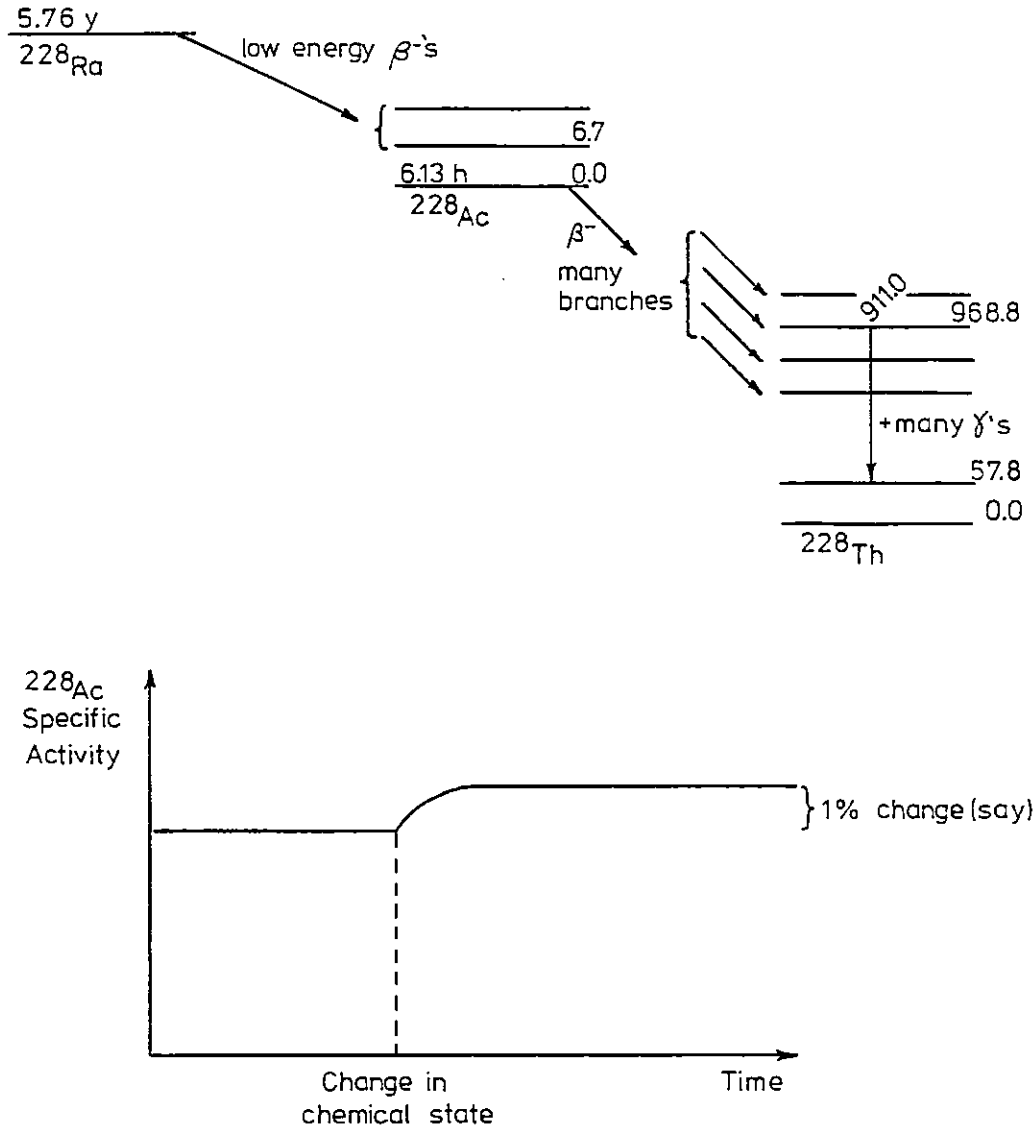

Fig. 4.3 A change in the low energy β^- transition probability following a change in the chemical state of ^{228}Ra will be observed as a change in the daughter ^{228}Ac specific activity, monitored as a function of time by observing the intense 911 keV γ-ray peak area following ^{228}Ac β^- decay

was centrifuged to remove this residue, poured into a 55 mm diameter x 9 mm deep polythene cell (: 15mm deep in the case of the 16g sample in which approximately twice the volume of acid was required to dissolve the thorium) and sealed inside a thin PVC bag in case of leakage. The dissolution process was completed in 20 mins. in the case of the 4g ^{232}Th sample, and in 40 mins. for the 16g sample; because of the relatively short times required to complete this process (i.e. much less than the ^{228}Ac half-life) it was not expected that the finite duration

of the dissolution period should introduce any marked effective increase in any possible time variation of the 911 keV γ transition.

To ensure maximum counting efficiency the cell was mounted as close to the Ge(Li) detector face as possible with only a 3 mm Pb absorber sandwiched between the detector and cell to reduce the intensity of low energy γ radiations entering the detector; coupled with a high lower level discriminator setting to remove unwanted low energy pulses, analyser dead times were kept low - ~ 3% for the 4g thorium sample and ~ 4% for the 16g sample - during the monitoring of the 911 keV γ-ray peak intensity. Periodic observations of the cell solution throughout the γ-ray analysis period revealed that the dissolved metal remained in solution.

4.4.2 Results

Figs. 4.4(a) and (b) show plots of the 911 keV γ-ray peak area (proportional to the ^{228}Ac specific activity) as a function of elapsed time since the ^{232}Th chemical dissolution process for the 4g and 16g ^{232}Th samples respectively. Each data point corresponds to a livetime γ counting period of one hour; for this counting duration the statistical uncertainties associated with the peak areas are of the order of 0.3 and 0.2% respectively for the 4g and 16g samples. Peak channel drifts were limited to 0.2 channel (in 2320 channel) during the 18 and 22 hr γ spectrum accumulation periods for the 4g and 16g ^{232}Th samples, respectively.

Within the limits of experimental uncertainty, neither plot shows evidence for an increase (with time) of the specific activity of the ^{228}Ac daughter following ^{228}Ra β^- decay.

4.5 Conclusions

Within the limits of experimental error, the results from the relative intensity and ingrowth methods show no evidence for a change in the β^- decay half-life as a function of chemical composition. Assuming the magnitude of the proposed effect of bound state electron capture upon the ^{166m}Ho, ^{228}Ra and ^{241}Pu β^- decay half-lives is comparable for all three nuclides then it therefore appears, on the basis of the present work, that the predicted ratio of bound to continuum β^- decays for ^{241}Pu is an overestimate and that the mechanism of bound state decay - and its dependence upon chemical composition -

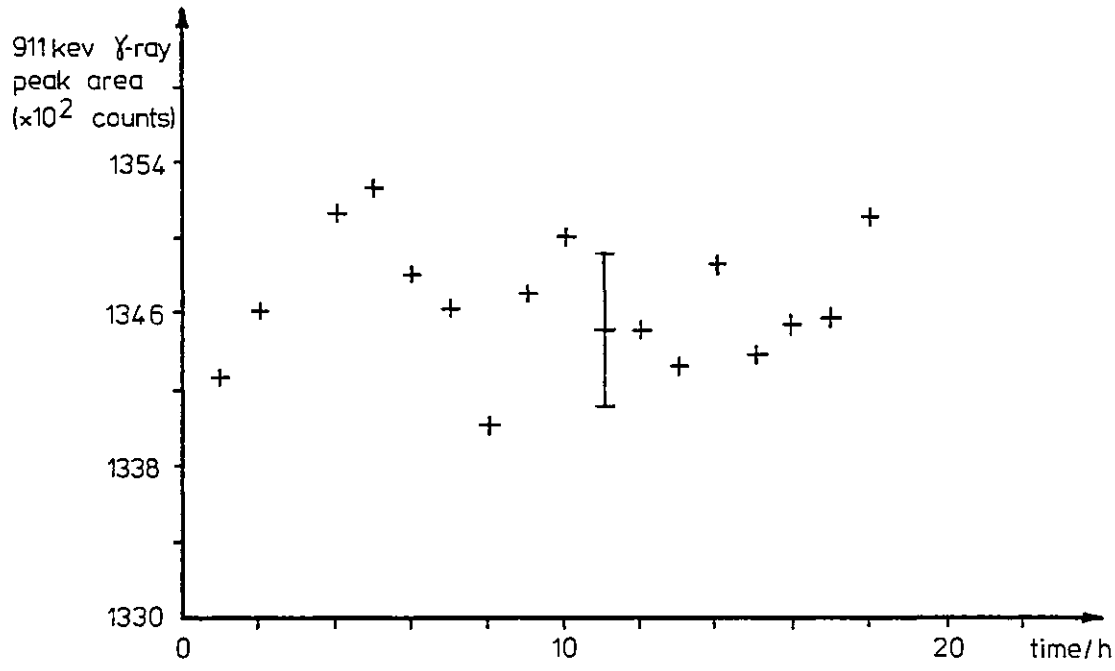

Fig. 4.4(a) Dissolved 4g ^{232}Th sample; Plot of 911 keV γ-ray peak area as a function of elapsed time since chemical dissolution process

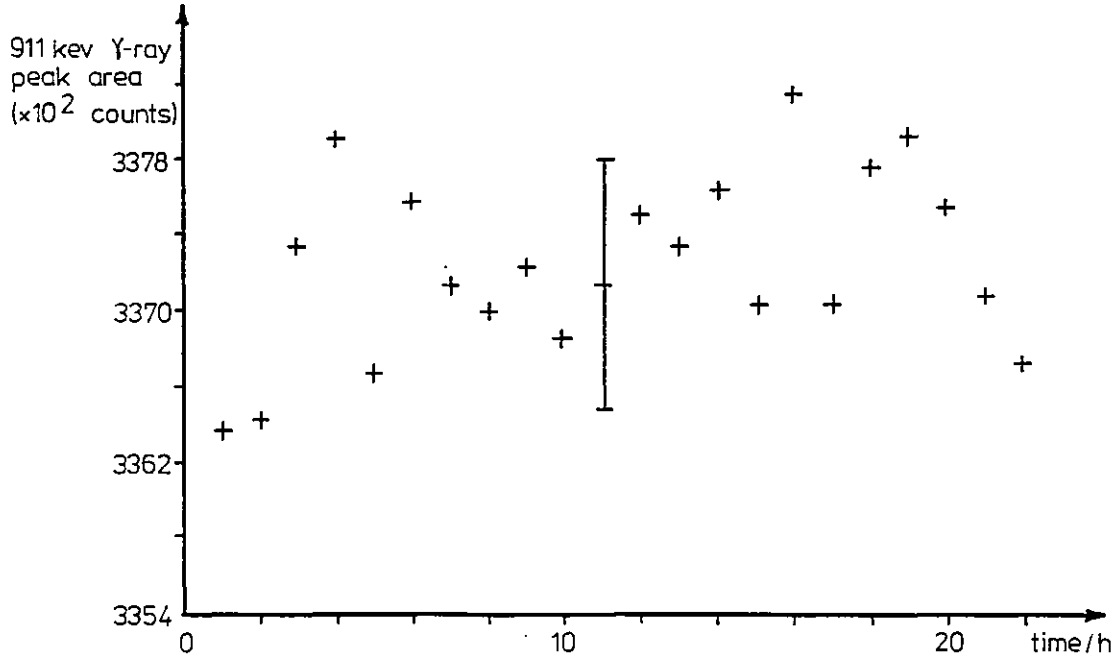

Fig. 4.4(b) Dissolved 16g ^{232}Th sample; Plot of 911 keV γ-ray peak area as a function of elapsed time since chemical dissolution process

cannot fully account for the current large spread in available ^{241}Pu half-life data.

It should be stated here, for clarity, that a large bound to continuum ratio does not necessarily imply a large and therefore easily detectable change in the total β^- decay transition probability; it is the variation in the bound to continuum decay ratio between different chemical states (i.e. different orbital e^- configurations) that is responsible for a change in the total β^- transition probability and this may, or may not, lend itself to experimental measurement. It is difficult to make an accurate calculation of the expected change in β^- decay half-life in all but the simple case of ^3H β^- decay where, as stated in section 4.2, a 0.3% change in half-life is predicted between ionised and neutral tritium. However, the probability of a chemical environment effect upon the β^- decay half-life is certainly increased when the predicted bound to capture ratio is large and, according to Tikhonov and Chukreev[13], may be significant for ^{241}Pu ions.

A recalculated estimate of the ratio of bound to continuum β^- decays for ^{241}Pu has been carried out in Appendix 4; again, electron capture into the $7s_{\frac{1}{2}}$ state has been considered in order that a comparison be made with the value obtained by Tikhonov and Chukreev.[13] The final calculated ratio is expressed as a fraction of the bound to continuum decay ratio for ^3H; however, because the results of various calculations[11,13,16] of this ratio are also in poor agreement - due either to misprints in publications or to inaccuracies on the part of the authors - a full derivation of the bound to continuum decay ratio for ^3H has also been performed in Appendix 4.

On the evidence of the calculations carried out in Appendix 4, and assuming a bound to continuum β^- decay ratio for tritium of ~ 1%, the corresponding bound to continuum ratio for ^{241}Pu is also estimated to be no larger ~ 1%; this value is two orders of magnitude smaller than that determined by Tikhonov and Chukreev[13] (who obtained a bound to continuum β^- decay ratio of ~ 100%) and therefore does not support their general conclusion that the upper limit of the fraction of ^{241}Pu β^- decays accompanied by electron capture may be 50%. Therefore it appears that the importance of bound state electron capture following ^{241}Pu β^- decay has been overestimated and the mechanism may not provide the complete solution to the current discrepancy in the

half-life of ^{241}Pu. Indeed, in the light of the present estimates of the magnitude of bound state β^- decay for the two low-energy β^- emitters, ^{3}H and ^{241}Pu, it is perhaps not surprising that the experiments carried out on ^{166m}Ho and ^{228}Ra did not show any evidence for a significant change in the β^- decay half-life as a function of chemical composition; the effect can be assumed to be small and the present experimental arrangements are not sensitive enough to detect the small changes (say $< 0.1\%$ for all but ^{3}H) in β^- decay half-life that the theory predicts.

However, although the role of bound state β^- decay in laboratory ^{241}Pu sources may not be totally responsible for the current large spread in ^{241}Pu half-life measurements, it may possibly assume greater significance within a reactor core where the atoms present have an increased probability for exhibiting inner shell ionisation effects due to the continual presence of a high density flux of ionising radiation. Since the overlap of an inner shell electron with the nucleus is greater than an outer shell electron, the probability of bound state β^- decay is increased (see eqn. A4.9, Appendix 4) and this may produce a much larger effect in the variation of β^- transition probability between different chemical states than is experienced in a laboratory source where only the configuration of the outermost electrons (i.e. those having smallest overlap with the nucleus) differ from one chemical state to another.

4.5.1 Other mechanisms affecting β^- decay transition probabilities

Several other mechanisms affecting β^- decay transition probabilities and which may be relevant to the current spread in ^{241}Pu half-life measurements have been proposed in the literature.[17,18] These mechanisms all involve the effect of the atomic electrons on the total decay rate and since all decay processes that depend on the presence of atomic electrons can, in principal, be modified by chemical means that affect the electronic wavefunctions, then it is expected that these effects may also be responsible for changes in β^- decay transition rates as a function of chemical environment. Two of the mechanisms are discussed here; Crasemann[17] provides a useful discussion of other aspects of atomic effects in nuclear transitions.

(i) Effect of Screening on the Fermi function

The screening of the nuclear charge by the atomic electrons can lead to a change in the integrated Fermi function (eqn. A4.2); for β^- emission $f(Z,W_o)$ is reduced and screening effects give rise to a 4%

change in the uncorrected $f(Z,W_o)$[17]. Alder et al.[19] have also computed the fractional change in the β^- decay constant as a function of Z and β^- end-point energy produced by a screening potential change which might typically result from variations in chemical environment. The effects are shown to become largest for low Z and low β^- end-point energy; for the low energy (18.6 keV) transition $^3H \rightarrow {}^3He$ a $\Delta\lambda/\lambda \sim 3\%$ is predicted. However, for large Z($\sim$ 90) and an $E_{\beta max}$ of $\sim$ 20 keV, the predicted $\Delta\lambda/\lambda$ is only $\sim 6 \times 10^{-5}$. Hence in the case of ^{241}Pu the effect of screening on the Fermi function produces a negligible change in the ^{241}Pu β^- decay half-life.

(ii) Imperfect atomic wavefunction overlap

The wavefunctions of the atomic electrons of the daughter atom are not quite the same as those in the parent atom because they are eigenfunctions of a different Hamiltonian. For example, in tritium β^- decay, the single electron in the Bohr orbit appropriate for a Z = 1 atom suddenly finds itself in an atom with Z=2. It need not remain in its ground state; that is

$$\int \psi^*_{1s}(He)\psi_{1s}(H)d^3\underline{r} < 1$$

which is meant by "imperfect overlap". Furthermore the wavefunctions for excited states of the daughter atom are not quite orthogonal to the ground state wavefunction of the parent; this circumstance can give rise to occasional excitation or ionisation of the daughter.

Imperfect overlap is expected to hinder the β^- transition rate. Bahcall[20] calculated the effect of the change in nuclear charge and showed that the β^- end-point energy was shifted by an average excitation energy, $\bar{E}_{ex}$, of the final atomic states. The total decay rate λ for β^- emission is given by

$$\lambda = \lambda_o(1 + \lambda_1/\lambda_o)$$

where the fractional change $\lambda_1/\lambda_o \sim -\bar{E}_{ex}/E_{\beta max}$. For ^{241}Pu the ratio λ_1/λ_o is calculated[20] to be $\sim$ 2%, but for most decays it is less than a few parts in a thousand.

Thus, as the above examples show, there exist other mechanisms beside bound state β^- decay which can lead to a dependence of β^- decay transition probability upon the chemical environment. It may be that only when all possible effects resulting in a change in the β^- decay constant are taken into account can the current discrepancy in the ^{241}Pu half-life be completely resolved.

REFERENCES

1. Y.A. Ellis, Nucl. Data. Sheets 23, 123 (1978)

2. S.K. Aggarwal and H.C. Jain, Phys. Rev. C21, 2033 (1980)

3. American National Standards Institute, Inc. ANSI N15.22-1975, 5 June 1975

4. Proposed Recommended list of Transactinium Isotope Decay data. Part 1. Half-lives (ed. A. Lorenz) INDC(NDS) - 108/N

5. S.K. Aggarwal, S.N. Acharya, A.R. Parab and H.C. Jain, Phys. Rev C23, 1748 (1981)

6. S.F. Marsh, R.M. Abernathy, R.J. Beckman and J.E. Rein, Int. J. Appl. Radiat. Isot. 31, 629 (1980)

7. P. DeBievre, M. Gallet and R. Werz, INDC(EUR) 016/G

8. B.W. Hooton, AERE - R9631 (1980)

9. V.N. Tikhonov and F.E. Chukreev, "Beta-decay of tritium into bound chemical states, and its effect on the accuracy of calorimetric measurements", INDC(CCP) - 151/NE (1980)

10. P.M. Sherk, Phys. Rev. 75, 789 (1949)

11. J.N. Bahcall, Phys. Rev. 124, 495 (1961)

12. C.J. Wolf and W.H. Johnston, Phys. Rev. 125, 307 (1962)

13. V.N. Tikhonov and F.E. Chukreev, "Comment on the half-life of ^{241}Pu", INDC(CCP) - 151/NE (1980)

14. B.W. Hooton, Private Communication

15. M.J. Hopper, AERE - R9185 (4th ed, 1981)

16. V.N. Andryushin, Sov. J. Nucl. Phys. 17, 171 (1973)

17. B. Crasemann, Nucl. Instr. and Meth. 112, 33 (1979)

18. K.P. Dostal, M. Nagel and D. Pabst, Z. Naturforsch. 32A, 3 (1977)

19. K. Alder, G. Bauer and U. Raff, Helv. Phys. Acta 44, 514 (1971)

20. J.N. Bahcall, Phys. Rev. 129, 2683 (1963)

CHAPTER 5. STUDIES OF THE REACTION $^{238}U(\alpha,p)^{241}Np$

5.1 Level Structure and Decay Scheme Investigations of ^{241}Np produced by Charged Particle Reaction Techniques

It was pointed out in the introductory chapter to this thesis that the β^- decay of $^{241}Np(T_{\frac{1}{2}} \sim 16m)$ leads to the production of ^{241}Pu, a key actinide in the production of higher mass actinides during reactor operation. The importance of these heavier actinides, particularly in terms of their contribution to overall heat output and radiation levels during spent fuel reprocessing and storage, has been previously discussed in section 3.1. However, in a typical reactor flux density of $\sim 10^{12}$ neutrons cm^{-2} s^{-1}, the formation of ^{241}Np by successive neutron capture in ^{239}Np gives rise to an insignificant ^{241}Pu yield compared to the amount of ^{241}Pu produced by successive neutron capture events in ^{239}Pu and therefore, for actinide inventory calculation purposes, the ^{241}Np β^- decay route to ^{241}Pu production can be ignored. Similarly the ^{241}Np contribution to decay heat and radioactivity levels following reactor shutdown can be assumed negligible.

From a nuclear structure viewpoint however, decay scheme data for ^{241}Np assumes an important role in helping to elucidate the excited level structure of ^{241}Pu; further experimental measurements of ^{241}Np decay scheme characteristics, in particular γ and β^- branch energies and intensities, would complement both recent ^{245}Cm α decay studies of the ^{241}Pu level structure and previous ^{241}Np β^- decay measurements. (See section 5.2 for a discussion of these earlier measurements). Furthermore, to date there exists no experimental data on the excited level structure of ^{241}Np itself. Because of its short half-life, ^{241}Np is not available as a standard laboratory source and must therefore be synthesised by a reaction mechanism which permits rapid access to, and analysis of, the ^{241}Np produced during the reaction.

The initial aims therefore of this particular section of work were to investigate the level structure of ^{241}Np, produced by the reaction $^{238}U(\alpha,p)^{241}Np$, by performing on-line (in-beam) $(p-\gamma)$ coincidence studies during α particle bombardment of ^{238}U target material, whilst also examining the decay of ^{241}Np by off-line measurements. For the first part irradiations were carried out using the Variable Energy Cyclotron (VEC) available in Chemistry Division, A.E.R.E., Harwell and attempts made to view on-line γ spectra in

coincidence with the emitted protons using an intrinsic Ge γ detector and a silicon surface barrier proton detector. However, because of practical problems associated with the proton detector (which was mainly one of ascertaining the positive registration of a proton from the $^{238}U(\alpha,p)^{241}Np$ reaction) greater importance became attached to the off-line measurements; these tended to follow the form of an experimental investigation to establish the best irradiation parameters for the production of ^{241}Np by chemical separation of Np from irradiated ^{238}U targets, followed by low energy (0-600 keV) X-ray and γ-ray spectrometry. In this manner it was possible to determine an approximate excitation function for the production of ^{241}Np by the $^{238}U(\alpha,p)$ reaction and hence establish the optimum α beam energy for future on-line (p-γ) coincidence studies once a suitable and reliable method of identifying the protons has been found.

5.2 Current Status of ^{241}Np Decay Data

The earliest reported studies on the production and mode of decay of the isotope ^{241}Np were performed by Vandenbosch[1], and Lessler and Michel[2]. In both studies thin uranium foils were bombarded with α particles, ranging in energy from 32 to 48 MeV, to search for ^{241}Np which may be produced by the $^{238}U(\alpha,p)^{241}Np$ reaction.

Vandenbosch[1] was able to resolve β^- decay curves, obtained from chemically separated Np samples, into individual 16m, 60m and 2.3d components attributable to the decays of ^{241}Np, ^{240}Np and ^{239}Np respectively. No γ-rays or X-rays (resulting from internal conversion) were observed which could be attributed to the 16m activity, thus providing possible evidence for an intense β^- transition to the ^{241}Pu ground state with no intermediate observable radiations. However, the complex spectrum of γ transitions, particularly in the low energy region, from the decay of the 60m ^{240}Np and 2.3d ^{239}Np could have masked any low intensity transitions from ^{241}Np decay and a weaker β^- branch feeding a low-lying level in ^{241}Pu could not be excluded.

Lessler and Michel[2], using time-of-flight mass separation techniques on a chemically separated neptunium fraction, identified 16m and 3.3h components at mass 241. Another mass separated sample, first counted 3.7h after the end of the irradiation period, showed only a single decay period of ~ 3.5h. They attributed this activity as strong evidence of an isomeric transition in ^{241}Np, with a 3.4h

half-life, although the possibility that the activity could be an ionised fission product, unseparated from the neptunium by chemistry, could not be entirely discounted.

Qaim[3], using the same reaction mechanism as the earlier studies, also obtained a ^{241}Np half-life of (16.0 ± 0.2)m from β^- decay measurements, and two γ-ray peaks at 135 and 175 keV were found to decay with a (18 ± 2)m half-life; an accurate estimate of the half-life of the two peaks could not be made due to the presence of interfering γ radiation from the other Np isotopes. However, it was proposed that these two transitions were in fact the same transitions as the 132 and 172 keV γ-rays observed by Asaro et al.[4] in ^{245}Cm α decay studies, thus indicating both α and β^- feeding to a common level in ^{241}Pu at ~175 keV. (This situation is analogous to the common intense feeding of the 74.67 keV level in ^{239}Np following ^{243}Am α decay and ^{239}U β^- decay). Qaim found no evidence for the existence of a ~ 3h isomer in ^{241}Np.

More recent studies by Dickens and McConnel[5] of the level structure of ^{241}Pu by analysis of γ spectra from ^{245}Cm α decay have yielded relative γ-ray intensity data for several strong γ transitions within the ^{241}Pu level scheme; the intensity of the 133.0 keV γ transition relative to that of the major 174.94 keV γ transition is quoted as 0.29. Both these transitions are assumed to depopulate the same 174.94 keV level in ^{241}Pu, a fact that is confirmed by the experimental evidence for a weak 41.95 keV γ transition (= 174.94 - 133.0) decaying directly to the ^{241}Pu ground state.

The most recent study of ^{241}Np β^- decay was performed by Parekh et al.[6]; this author and his team of co-workers have been responsible for a series of recent reported measurements of decay scheme data for neutron rich ^{240}Np, ^{240m}Np, ^{242}Np and ^{242m}Np isotopes. (See refs. 6 and 7 and references contained therein). In their study of ^{241}Np, sources were produced by the ^{244}Pu(n,p3n)^{241}Np reaction, using 30-160 MeV neutrons, and by the ^{238}U(α,p)^{241}Np reaction, using 32 MeV α particles, followed by intensive chemical separation procedures. The intensity of the 133 keV γ transition relative to the 175 keV γ transition was measured to be 0.28, in good agreement with the value of 0.29 derived from the previous ^{245}Cm α decay studies of Dickens and McConnel[5]. The absolute γ-ray

intensity of the 133 keV transition was determined using γ-ray spectroscopy and $4\pi\beta^-$ counting techniques, and is quoted as $(0.86 \pm 0.05)\gamma_{133}$/100 source decays. However, γ-ray analyses of the ^{241}Np sources used to determine the absolute γ-ray intensity of the 133 keV transition revealed the presence of longer-lived ^{239}Np and ^{240}Np isotopes and it is difficult to ascertain from the published account of this work whether a correction has been applied to take into account the relative ^{239}Np and ^{240}Np contributions to the overall total β^- emission rate. Such a correction would necessarily involve following the decay of the source over an extended period of time to enable accurate subtraction of the ^{239}Np and ^{240}Np β^- decay rates from the total source decay rate; decay corrections were applied by the authors to the $4\pi\beta^-$ and γ decay data but it is not clear whether the measured β^- activities have been corrected for both the decay of the ^{241}Np source during the $4\pi\beta^-$ counting interval and the presence of ^{239}Np and ^{240}Np in the source. If the latter corrections have not been applied then the quoted intensity of the 133 keV γ transition is necessarily a lower limit for the intensity of this particular γ-ray.

The half-life of ^{241}Np was also derived from a least squares decay analysis of the 175 keV γ-ray peak; two decay components were required to fit the experimental data since ^{240}Np ($T_{\frac{1}{2}} \sim 60$m) is also reported to produce a γ-ray of the same energy. A value of (13.9 ± 0.2)m was thus obtained for the ^{241}Np half-life which is smaller than the previously measured values of 16m[1,2,3].

5.3 On-line Studies of the Level Scheme of ^{241}Np

5.3.1 Experimental Method

Fig. 5.1 shows the experimental arrangement within the target chamber used to observe in-beam (p-γ) coincidences during α particle bombardment of ^{238}U. The 450 mm^2 x 1mm deep silicon surface barrier proton (p) detector and 15 cm^2 x 10mm Ge γ detector were placed at 90° to the incident beam and as close as possible to the depleted uranium target in order to maximise the coincidence efficiency. For the target - detector separations used here, the fractional solid angles subtended by the p and γ detector were ~ 0.09 and 0.15 respectively. The Be entrance window of the Ge detector was covered with a 0.13mm thick Cu sheet to reduce the intensity of low energy ($\lesssim$ 100 keV) γ and X-ray radiation, and the body of the detector wrapped in 5mm thick

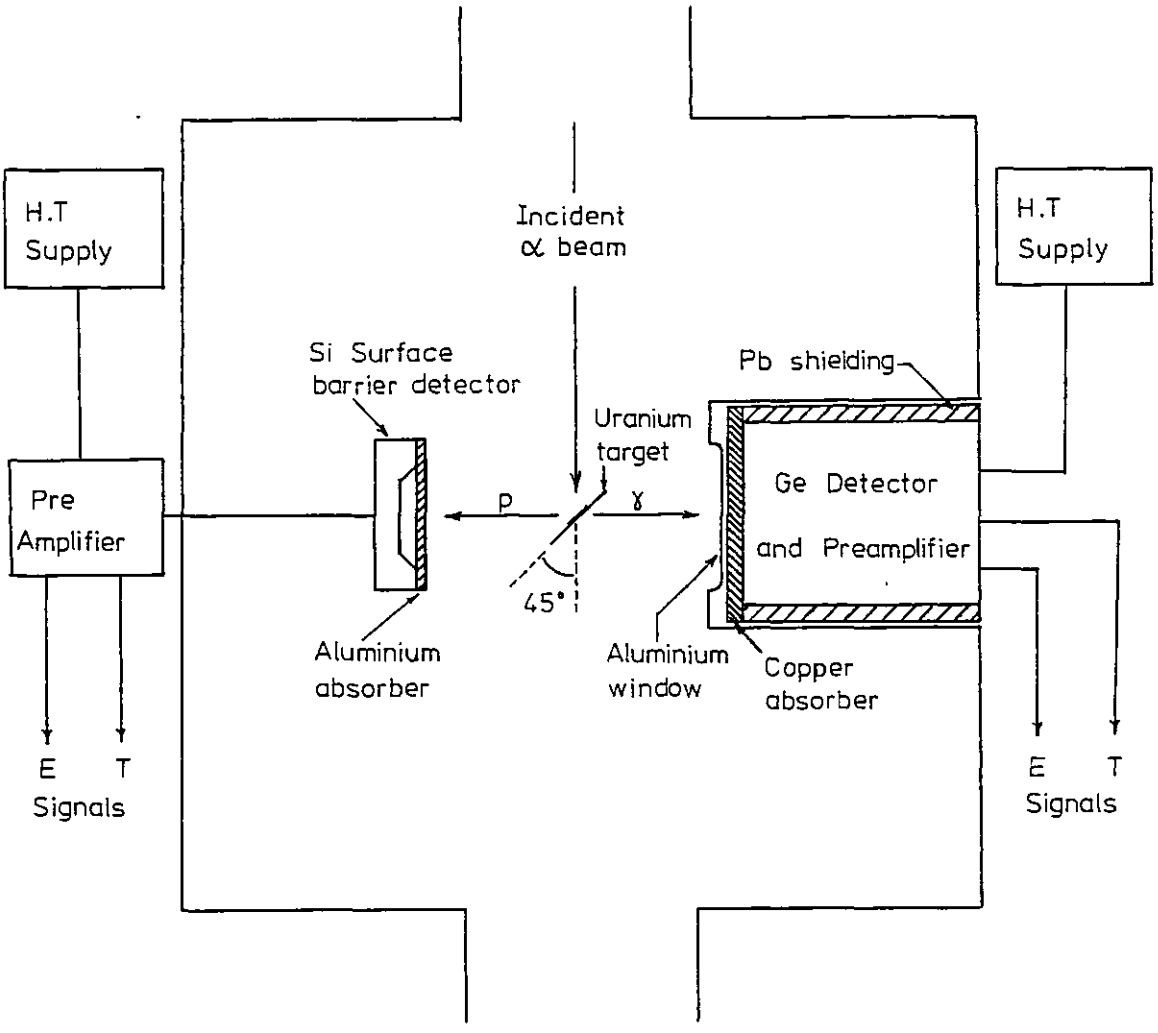

Fig. 5.1 Detector assembly arrangement within V.E.C. target chamber

Pb shielding to reduce background radiation from the VEC. A 140 mg cm^{-2} Al absorber was used to stop scattered α particles reaching the p detector; for this particular absorber thickness α particles with energies up to ~ 36 MeV will be stopped from entering the p detector, but protons with emergent energies $\gtrsim$ 9 MeV will still have sufficient energy after travelling through the absorber to be registered in the active volume of the silicon surface barrier p detector. The fast-slow coincidence pulse processing electronics system used to observe the (p-γ) coincidences was identical to the arrangement used in previous $^{243}Am(\alpha\text{-}\gamma)$ and $^{243}Am(\alpha\text{-}e^{-})$ coincidence studies and is shown in fig. 3.3.

Table 5.1 lists the results of kinematic calculations used to determine the energy of the emitted proton from the reaction

$$^{238}_{92}U + ^{4}_{2}He \rightarrow ^{241}_{93}Np + ^{1}_{1}p \; ; \; Q = -11.86 \text{ MeV}.$$

as a function of incident α particle beam energy and laboratory angle θ of p emission, measured from the axis defined by the α particle beam direction; these calculations assume a final excitation energy for the ^{241}Np nucleus of ~ 2 MeV which, upon de-excitation, may lead to the emission of sufficient γ-rays in coincidence with the outgoing protons to enable an experimental determination of the excited level structure of ^{241}Np. The results of table 5.1 show that there is little variation in emitted proton energy across the silicon surface barrier detector acceptance angle.

Since a 1mm thick Si detector is only capable of stopping protons up to ~ 12 MeV in energy then, above an α beam energy of ~ 35 MeV, additional absorbing material (above the 140 mg cm^{-2} Al already present) will be required to (i) stop the higher energy scattered α particles reaching the detector and (ii) reduce the energy of the emitted proton still further in order that complete registration of the remaining full peak energy within the detector active volume is still possible.

Table 5.1 Calculated energies of emitted protons from $^{238}U(\alpha,p)^{241}Np$ reaction assuming population of a 2 MeV excited level in ^{241}Np.

Incident α beam Energy (MeV)	Emitted Proton Energy(MeV)		
	$\theta_{lab} = 45^{o}$	$\theta_{lab} = 90^{o}$	$\theta_{lab} = 135^{o}$
26	11.84	11.64	11.43
30	15.82	15.57	15.32
34	19.78	19.48	19.18
38	23.74	23.39	23.05
42	27.71	27.31	26.90

5.3.2 Results

Preliminary runs using 30 MeV α particles and ~ 5 mg cm^{-2} depleted uranium targets showed that accelerator beam currents would have to be limited to less than a few nA in order to prevent serious dead-time and pulse pile-up problems associated with the extremely high γ count rates (> 65,000 s^{-1}) entering the Ge detector. At such low beam currents the total count rate in the Si surface barrier detector was of the order of 100 s^{-1} indicating that irradiation periods of several hours, at least, would be required in order to build up sufficient peak area statistics in the coincident γ spectrum. Indeed, if all the counts registered by the Si detector were protons from the $^{238}U(\alpha,p)^{241}Np$ reaction then, assuming an average of one accompanying γ-ray emission per proton emission, the expected number of coincidences per second is given by (100 x 0.15) = 15.0 s^{-1} assuming unity γ detection efficiency. However, this calculated value provides only an upper limit to the expected coincidence rate since the emission of a single proton following α particle bombardment of ^{238}U is only one of several possible exit channels available for this particular reaction, many of which also involve the emission of protons; previous studies[8] of helium-ion induced reactions in ^{238}U have yielded cross-section data for (α,pn), (α,p2n), (α,p3n) and (α,αn) reactions, but no data is currently available for the $^{238}U(\alpha,p)^{241}Np$ cross-section. Furthermore, these spallation reactions involving the production of similar heavy

element radionuclides are themselves in competition with α induced fission reactions which tend to dominate the reaction total cross-section. Therefore protons registered by the Si detector may originate from a series of different competing spallation reactions, and the small fraction of total protons due to the (α,p) reaction may be masked by the much larger proton contribution derived from the other competing reactions.

Particle spectra obtained during the course of prolonged α particle irradiations of ^{238}U did not reveal any definite structure from which it was possible to identify or select a particular energy window within which only protons from the (α,p) reaction could be presumed to provide the majority, if not all, of the registered counts, and which could be used as gating signals in order to obtain coincident γ spectra. Therefore coincident γ spectra were obtained by using all particle pulses above a preselected lower level discriminator setting as gating signals. Fig. 5.2 shows the essential features of a typical particle spectrum obtained during the α particle bombardment of a ^{238}U target.

Several coincident γ spectra revealed only the presence of a single low intensity γ-ray at ~ 198 keV, superimposed on a high continuous background. This transition was assumed to be the known 197 keV γ transition originating from a competing $^{16}O(\alpha,p)^{19}F$ reaction in an oxide layer formed on the uranium target. This particular γ transition is known to decay directly to the ^{19}F ground state.

Kinematic calculations, identical to those performed for the $^{238}U(\alpha,p)^{241}Np$ reaction, were carried out for the $^{16}O(\alpha,p)^{19}F$ reaction (Q =-8.11 MeV). Table 5.2 lists the energies of the emitted protons (at 90° to the incident α beam) as a function of the incident α beam energy assuming that the final ^{19}F nucleus is excited to only a few hundred keV. At low incident α beam energies, less than ~ 30 MeV, there is little difference between the emitted proton energies from the uranium target reaction (table 5.1) and those from the oxygen

Table 5.2 Calculated Energies of Emitted Protons (for $\theta_{lab} = 90^{o}$) from $^{16}O(\alpha,p)^{19}F$ reaction assuming Population of 200 keV Excited Level in ^{19}F

Incident α Beam Energy (MeV)	Emitted Proton Energy (MeV)
26	11.58
30	14.51
34	17.56
38	20.56
42	23.54

target reaction; only above an incident α particle energy of ~ 38 MeV does the difference in emitted proton energy become large enough to apply some form of practical energy discrimination and so prevent protons from the $^{16}O(\alpha,p)$ reaction entering the detector. For example, for an incident 42 MeV α particle beam energy, an Al absorber thickness of ~ 770 mg cm^{-2} is required to reduce the proton energy from the uranium reaction to ~ 10 MeV, suitable for subsequent complete detection by the 1mm thick Si detector; at this same α particle beam energy the $^{16}O(\alpha,p)$ protons have an energy of ~ 23.5 MeV, equivalent to a range of ~ 780 mg cm^{-2} in Al. Thus, by using (say) an 800 mg cm^{-2} Al absorber it should be possible to remove all the protons from the oxygen reaction leaving only those protons from the uranium reaction with enough energy to be subsequently registered in the Si detector.

Fig. 5.3 shows the essential features of a particle spectrum obtained using such energy discrimination techniques at an incident α beam energy of 45.2 MeV. There is now slight evidence for a discontinuity in the particle spectrum compared with that shown in fig. 5.2; it is possible that those counts above the discontinuity are protons from the $^{238}U(\alpha,p)^{241}Np$ reaction, although there is no conclusive evidence to support this statement. It is calculated that protons from the (α,pn), (α,p2n),... type reactions involving both proton and neutron emission will be absorbed by the Al absorber because of the larger -Q values associated with these particular reactions which result in lower emitted proton energies. The measured count

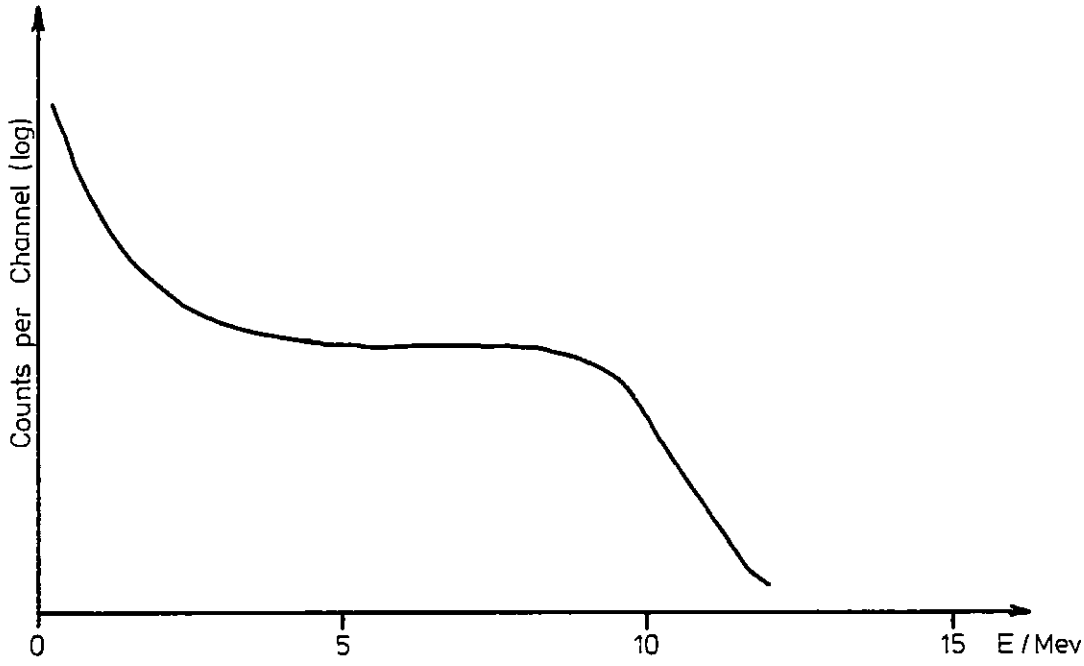

Fig. 5.2 Diagram showing basic shape of a typical particle spectrum obtained for an incident 34 MeV α particle energy and using a 400 mg cm^{-2} Al absorber to stop scattered α particles entering the Si surface barrier detector

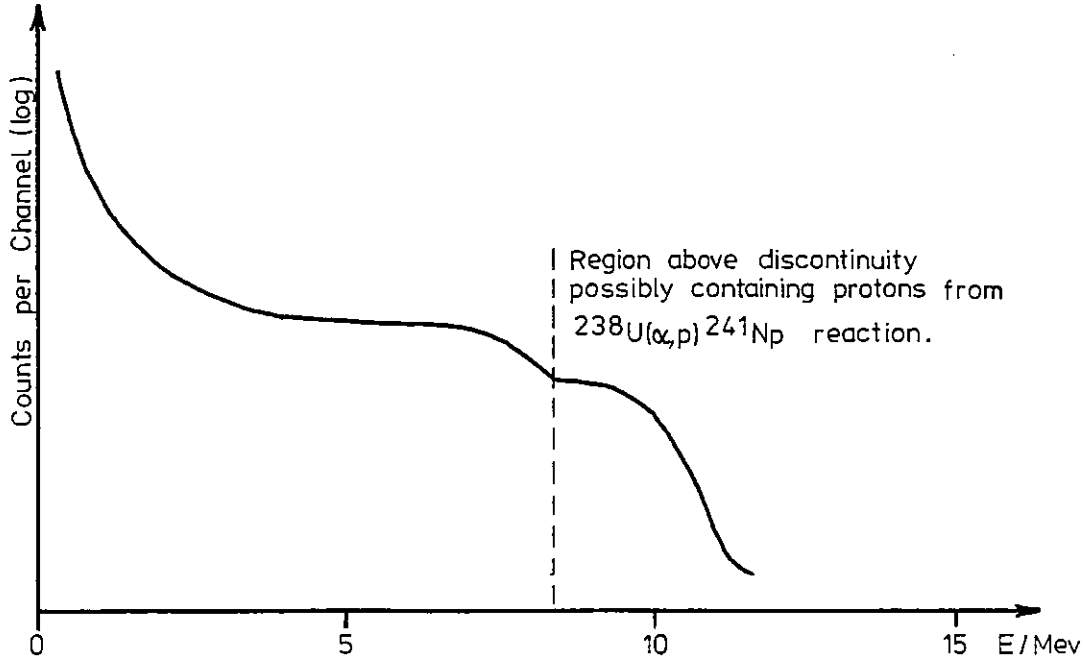

Fig. 5.3 Essential form of particle spectrum obtained using a 940 mg cm^{-2} Al absorber to stop protons from $^{16}O(\alpha,p)^{19}F$ reaction entering the Si surface barrier detector for an incident 45.2 MeV α particle energy

rate in the region above the discontinuity in the particle spectrum was ~ 10 s^{-1} and would therefore necessitate a prolonged irradiation period in order to accumulate useful coincidence γ data. A coincidence γ spectrum obtained over a 26,000s livetime count duration did not reveal any γ rays in coincidence with the selected particle window, assumed to contain those protons from the $^{238}U(\alpha,p)^{241}Np$ reaction.

Off-line singles γ spectra obtained from the active ^{238}U target material did not reveal any evidence for γ-ray peaks at 133 and 175 keV which could be attributed to the decay of ^{241}Np; indeed, the positive identification of any γ-ray in the measured spectra was extremely difficult because of the very low peak to continuum background ratio.

5.3.3. Conclusions

Unless a comprehensive interpretation of the particle spectra obtained during the course of α particle bombardment of ^{238}U can be deduced from the available experimental data then the present on-line measurement techniques cannot be used, with any degree of certainty, in an attempt to investigate the level structure of ^{241}Np. Indeed, an interpretation of the present particle spectra may be further complicated by (α,p) reactions in the Al absorber covering the Si detector due to target scattered α particles and the production of 'knock-on' protons due to the abundance of hydrogen present in the Al absorber and surrounding target chamber materials. It is therefore difficult to draw any positive conclusions from the present on-line measurement techniques, but a more successful investigation of the level structure of ^{241}Np may necessarily involve any combination of the following three proposals.

(i) To reduce interference from the competing $^{16}O(\alpha,p)^{19}F$ reaction the depleted ^{238}U target must be prepared and stored in an inert atmosphere which prevents the formation of an oxide layer.

Visual inspection of the present target surface also revealed a coarse grain structure unsuitable for achieving a well resolved proton signal; a carefully prepared thin, uniform target (of a few $\mu g\ cm^{-2}$ thickness rather than ~ 5 mg cm^{-2}) would help to reduce severe degradation of the proton resolution due to energy loss effects within the sample thickness.

(ii) It has been suggested[8] that at incident α beam energies greater than ~ 40 MeV, the (α,p), (α,pn) and $(\alpha,p2n)$ reactions are most likely

to occur by a direct reaction mechanism (rather than by the formation of a compound nucleus) involving the emission of protons, deuterons and tritons, respectively. Thus, by using particle identification techniques[9] at high incident α beam energies then it should be possible to detect those protons from the $^{238}U(\alpha,p)^{241}Np$ reaction. Particle identification can be achieved here by employing a thin transmission detector (of thickness t) in front of the present 1mm thick Si surface barrier detector. Any particle produced by the α bombardment of ^{238}U will lose an energy (-dE/dx)t in the transmission detector and the remainder in the thick detector. The pulse height from the transmission detector is proportional to (dE/dx), and by adding the outputs from both detectors one obtains a pulse height proportional to E. Then by using the approximate expression

$$\frac{dE}{dx} \propto \frac{MZ^2}{E}$$

where M is the mass of the particle and Z its atomic number, electronic multiplication of the pulse heights proportional to (-dE/dx) and E give a product pulse proportional to MZ^2 (which is 1,2,3 and 16 for protons, deuterons, tritons and α particles respectively). These two resultant signals, one containing information on the particle energy, the other proportional to MZ^2, can then be used to obtain (simultaneously) separate energy spectra of all particle types.

(iii) Other possible charged particle reactions which should be considered as alternative routes to the formation of ^{241}Np, and for which the ^{241}Np yield may be far greater than the present $^{238}U(\alpha,p)^{241}Np$ reaction yield, are the triton stripping reaction

$$^{238}_{92}U + ^{7}_{3}Li \rightarrow ^{241}_{93}Np + ^{4}_{2}He \quad (Q = +5.5 \text{ MeV})$$

and the proton pick-up reaction

$$^{242}_{94}Pu + ^{2}_{1}H \rightarrow ^{241}_{93}Np + ^{3}_{2}He \quad (Q = +1.39 \text{ MeV})$$

Since the ^{7}Li nucleus may loosely be described as a bound state of a triton and an α particle then the first of these reactions may in fact give rise to a high cross-section for ^{241}Np production by the

triton stripping mechanism. The second of these reactions could be performed using the Harwell Tandem Van de Graaff accelerator which has superior incident beam energy resolution compared to that obtained from the Variable Energy Cyclotron. Again, counter telescopes utilising both E and dE/dx detectors could be used in both reactions for particle identification. However the use of a Pu target in the second proposed reaction demands stringent safety precautions.

5.4 Off-Line Studies of ^{241}Np β^- Decay

5.4.1 Experimental Method

Because of the competing fission and spallation reactions occurring during the α particle bombardment of ^{238}U, it was decided that a chemical separation procedure would be required to isolate any ^{241}Np or other Np isotopes produced by the reaction from the accompanying fission products before an investigation of the decay scheme characteristics of ^{241}Np, using γ-ray spectroscopy, could be carried out. Since ^{241}Np has a short half-life ($\sim$ 16m) it was essential that the chemical separation be completed quickly following the end of the irradiation period.

The separation of Np isotopes from the irradiated depleted ^{238}U targets (performed by Chemistry Division, A.E.R.E. Harwell) was carried out by eluting the fission products from an anion exchange column containing the dissolved uranium target and a small volume of ^{237}Np tracer solution using 12M HCl acid; any Np isotopes remaining were then brought off the column with 4M HCl and 0.1M HF, diluted with $\sim$ 10 cc of water and sealed in a thin plastic vial suitable for low energy X and γ-ray analysis.

The fixed quantity of ^{237}Np tracer solution introduced during every chemical separation provided reference peaks in the γ-ray spectra obtained from the final separated solution which could be used to determine R, a quantity proportional to the (α,p) cross-section for ^{238}U; R is a function of E_α, the incident α beam energy, and is given by the expression

$$R(E_\alpha) = \left\{ \frac{(\text{Area of } ^{241}\text{Np } \gamma\text{-ray peak})}{(\text{Area of } ^{237}\text{Np } \gamma\text{-ray peak})} \right\}_T \qquad (5.1)$$

where the γ-ray peak areas are corrected to a time T corresponding to the end of the irradiation period to take into account differences in time intervals between the end of the irradiation period and the start of the γ-ray analysis for runs performed at different incident α beam energies. Substitution of ^{240}Np γ-ray peak areas into the numerator of eqn. 5.1 will yield quantities proportional to the (α,pn) cross-section for ^{238}U.

Since previous studies have only revealed the existence of two particularly intense γ-ray transitions at 133 and 175 keV following ^{241}Np β^- decay, then the presence of these two transitions in the present γ spectra, each decaying with ~ 16m half-life, would indicate the successful production of ^{241}Np. The decay of the well resolved 103.76 keV PuKα_1 X-ray peak with a 16m component would add further support to this conclusion, assuming internal conversion of presently unobserved low intensity ^{241}Np γ transitions. The peak area data obtained from these transitions would then be used to determine the values of $R(E_\alpha)$.

A series of four 15m irradiations were carried out at incident α particle beam energies of 27.87, 29.88, 32.17 and 37.01 MeV using 10-20 mg cm^{-2} ^{238}U targets in order to determine the form of the excitation function $R(E_\alpha)$. The length of the irradiation period was chosen so as to maximise the ratio of ^{241}Np to ^{239,240}Np production. Two further irradiations using an α beam energy of 29.97 MeV were carried out in an attempt to obtain increased peak statistics for the 133 and 175 keV γ transitions from which a more accurate ^{241}Np half-life could be extracted. Because no on-line measurements were involved in these particular irradiations, accelerator beam currents in the range 1 to 2 μA were used to enhance the ^{241}Np yield during the short irradiation period. All chemical separations were carried out and the sample solution positioned for counting within 15 m following the end of the irradiation period; however, the relatively short time constraint placed upon the chemical separation procedure by the short ^{241}Np half-life, did result in some breakthrough of fission product activity into the final solution.

Following each irradiation and chemical separation procedure, γ spectra were obtained during consecutive 4 min. intervals over a period of approximately 75 min. in order to identify any ~ 16 min. component attributable to the decay of ^{241}Np. Gamma spectra from

the last two irradiations (at 29.97 MeV) were obtained during consecutive 4 min. intervals over a period of ~ 60 min. followed by consecutive 15 min. intervals over a further period of ~ 4 hours in order to assess accurately that component present under the 175 keV and PuKα_1 X-ray peaks due to the β^- decay of ^{240}Np ($T_{\frac{1}{2}}$ measurements in the range 60 to 67 mins.).

Although earlier measurements on ^{240}Np β^- decay failed to place the 175 keV transition within the ^{240}Np decay scheme, the most recent study of ^{240}Np β^- decay[7] tentatively assigns this γ-ray (with measured energy 175.4 keV) as a transition between levels at 1177.4 and 1001.9 keV in ^{240}Pu. Therefore it is expected that a two-component fit, with the longer component represented by a half-life of ~60m, will be required to extract the ^{241}Np half-life from the total decay date of the 175 keV peak, assuming that other γ-ray peaks from the decay of ^{240}Np are also present in the spectra. The relative amounts of ^{241}Np and ^{240}Np present in the 175 keV γ-ray peak area will depend upon the form of each individual excitation function and therefore upon the incident α beam energy used in the ^{238}U irradiation.

5.4.2 Results

Typical low energy γ-ray spectra from the sample solutions produced at the highest and lowest α beam energies are shown in fig. 5.4. The corresponding high energy portions of these spectra are shown in fig. 5.5. The γ-ray energies (in keV) are given for those peaks identified as transitions from the decay of the separated Np isotopes and for those fission product peaks whose identifications are confirmed, in the main, by either the presence of at least one other accompanying γ-ray from the decay of the same parent or from a consideration of their decay half-lives. There is no conclusive evidence that any of the remaining unlabelled peaks (excluding the PuKα and PuKβ X-ray peaks in the regions ~98 to 105 and ~ 115 to 122 keV respectively) are due to the decay of other possible actinides produced during the α particle bombardment of ^{238}U and are therefore all assumed to arise from fission product decay.

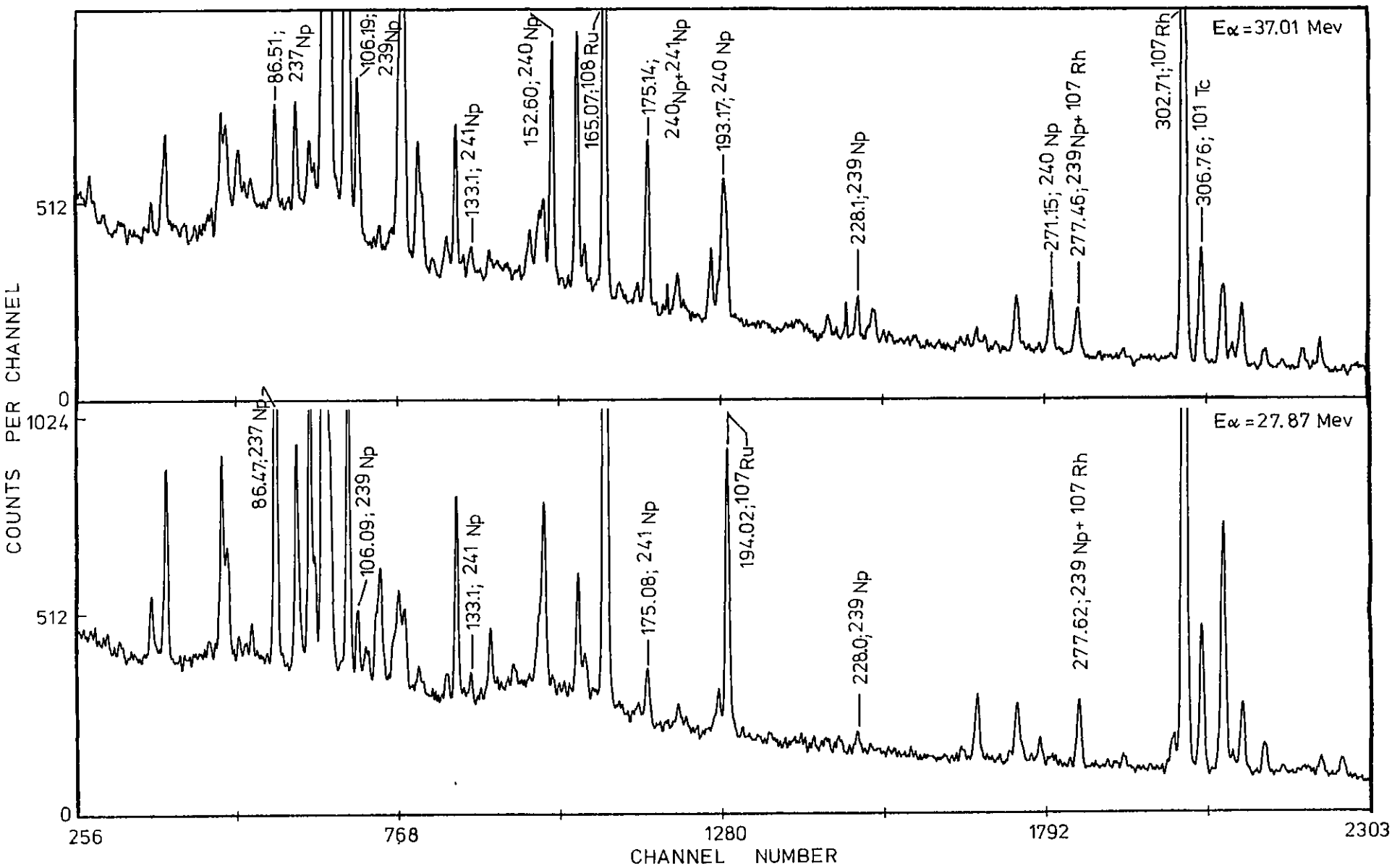

Fig. 5.4 Low energy γ spectra obtained from separated fractions of dissolved ^{238}U targets irradiated at 37.01 MeV (upper trace) and 27.87 MeV (lower trace). Time elapsed since completion of irradiation ~ 25m

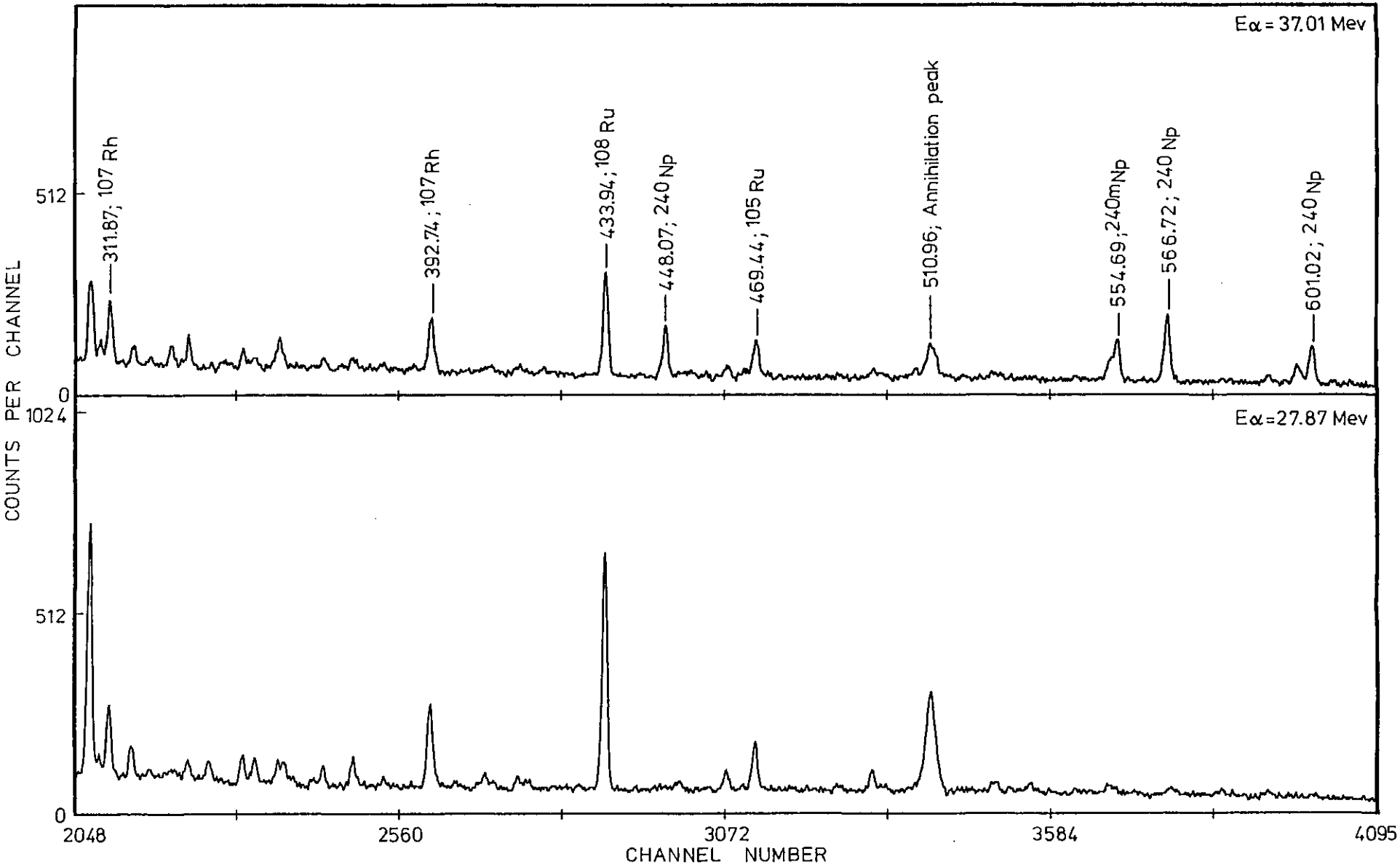

Fig. 5.5 Corresponding high energy portions of γ spectra shown in fig. 5.4

It is evident, from a consideration of the known relative γ-ray intensity ratios for the major transitions from ^{239}Np and ^{240}Np decay, that a number of these transitions in the measured γ-ray spectra of fig. 5.4 are unresolved from fission product peaks of the same energy. Table 5.3 lists the relative intensities of particular sets of γ-ray lines observed in ^{239}Np and ^{240}Np decay; the intensity ratios corrected for detector efficiency (column 3 of table 5.3) are only approximate since they are derived from efficiency data obtained using 1mm dia. standard γ sources, rather than sources of the same physical size and form as the unknown sample. Nevertheless, the corrected intensity ratios of table 5.3 are useful for identifying major fission product contamination peaks of the same energy as the Np isotope peaks.

Table 5.3 Predicted γ-ray Intensity Ratios for Selected Transitions from ^{239}Np and ^{240}Np Decay Observed in the γ spectra of Figs. 5.4 and 5.4

Isotope	γ Intensity Ratio	Tabulated Relative γ-Ray Intensity Ratio	Intensity Ratio corrected for Detection Efficiency
^{239}Np	$I_{106}/I_{228}/I_{277}$	1.0/0.47/0.62[a]	1.0/0.15/0.12
^{240}Np	$I_{153}/I_{175}/I_{193}$	1.0/0.70/0.84[b]	1.0/0.55/0.55
^{240}Np	$I_{448}/I_{566}/I_{601}$	1.0/2.06/1.49[b]	1.0/1.37/0.89

a Taken from ref. 10

b Taken from ref. 7

For example, visual estimates of the intensity of the 277.6 keV γ-ray from ^{239}Np decay relative to the 106.1 and 228.1 keV γ-rays (see fig. 5.4, E_α = 27.87 MeV) do not agree with the predicted intensity ratios of table 5.3; thus there is evidence that a much stronger contamination peak is masking the 277.6 keV γ-ray from ^{239}Np decay.

Fig. 5.6 follows the decay of 133 and 175 keV γ-ray peaks obtained from an irradiation using 29.97 MeV α particles and assumed to originate from the β^- decay of ^{241}Np.

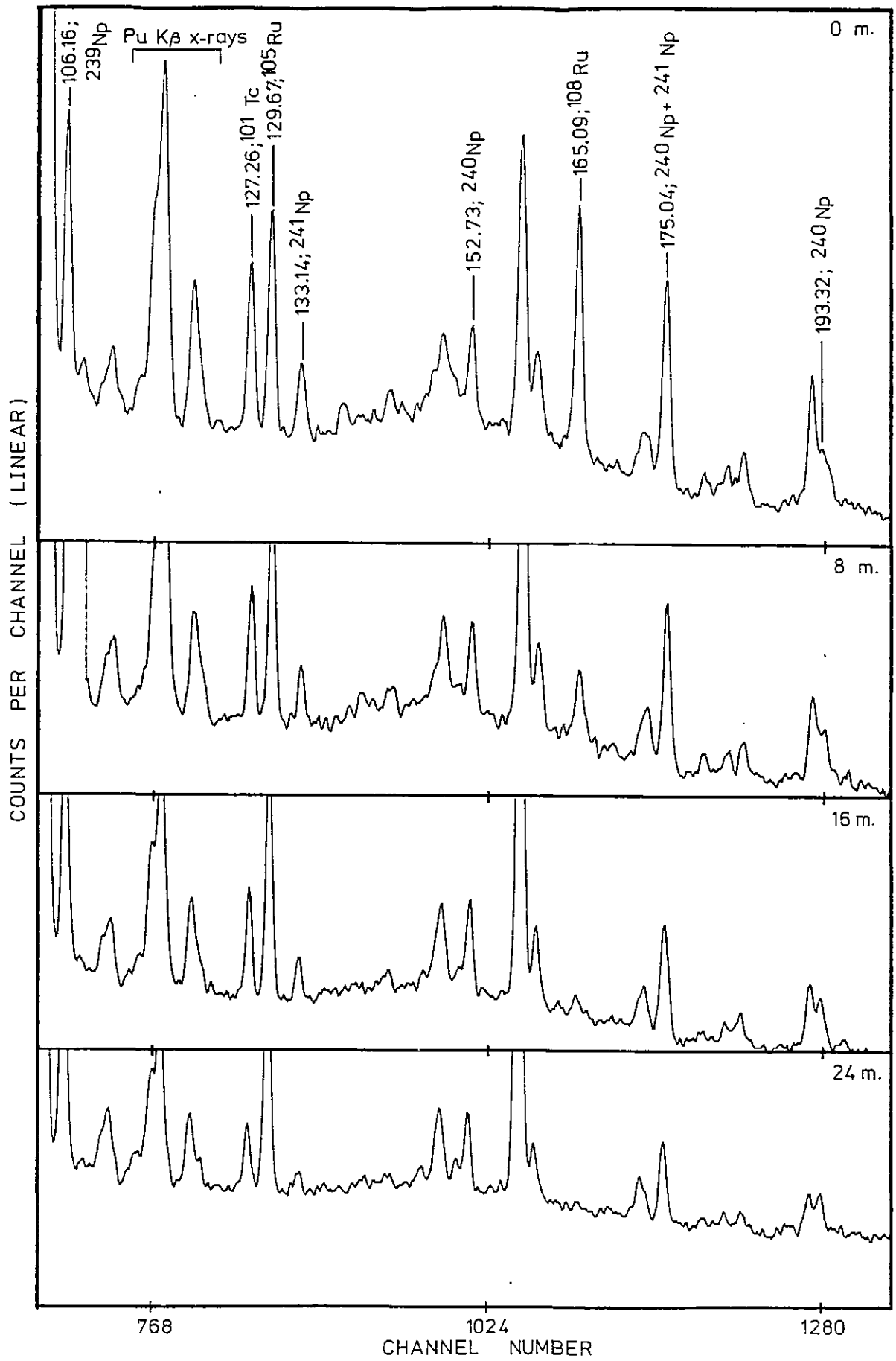

Fig. 5.6 γ spectra following decay of 133.1 and 175.0 keV γ-ray transitions occurring in ^{241}Np β^- decay

The most general conclusion that can be drawn from the spectra of figs. 5.4 - 5.6 (and also from the γ spectra obtained at intermediate α beam energies, but not shown here) is that, measured relative to the ^{237}Np tracer peak at 86.5 keV, the peak areas associated with the isotopes ^{239}Np, ^{240}Np and ^{241}Np all show an effective increase with increasing α beam energy, indicating an increase in the ^{238}U(α,p), (α,pn) and (α,p2n) cross-sections over the energy range considered here.

Despite poor peak area statistics it is also evident - from the measured intensities of the 106.1 and 228.1 keV transitions in the spectrum of fig. 5.4 - that the cross-section for the production of ^{239}Np at the lowest incident α beam energy used here is greater than that for the production of ^{240}Np; the peaks at 448.6 and 566.7 keV following ^{240}Np decay, which are found in samples obtained using higher incident α beam energies, are not present at the lowest α beam energy used in this particular experiment (i.e. E_α = 27.87 MeV).

5.4.3 Data Analysis

The raw spectrum data from each run was initially corrected for background and then smoothed using a 5-point data smooth programme incorporated in the multichannel analyser; because of the generally low counting statistics available in all γ peaks of interest, the smoothing procedure reduces the rapid point-to-point fluctuation in the raw data and leads to an improvement in peak limit definition required for peak area analysis. All peak area data were further corrected for analyser dead-time effects.

Analysis of peak area information from the γ spectra obtained at different incident α beam energies, consisted of the use of a least squares fitting programme to determine

(i) a value for the ^{241}Np half-life using peak area decay data from the Pu$K\alpha_1$ X-ray, 133 and 175 keV γ-ray peaks, where sufficient peak area statistics made such an analysis feasible, and

(ii) extraction of extrapolated peak area counts from the γ-rays following ^{240}Np and ^{241}Np decay in order to determine the form of the excitation functions for the (α,p) and (α,pn) reactions using eqn. 5.1.

The function used to fit the data in the least squares fitting routine consisted of a series of exponential terms of the form

$$f(t_i, \underline{v}, \underline{\lambda}) = \sum_{j=1}^{n} v_j e^{-\lambda_j t_i} \qquad (5.2)$$

where n specifies the number of half-life components required to fit the data and v_j and λ_j are parameters which can remain fixed or be allowed to vary (depending on user requirements) in order to obtain the best fit to the experimental data. v_j and λ_j are the peak area intercept (corresponding to $t_i = 0$) and decay constant respectively for the jth component required to fit the data. The best fit is interpreted as the values of $\underline{v}$ and $\underline{\lambda}$ which minimise

$$S = \sum_{i=1}^{m} w_i \left[y_i - f(t_i, \underline{v}, \underline{\lambda}) \right]^2$$

where $y_1, y_2 \ldots y_m$ are a set of experimental peak area observations of the function $f(t_i, \underline{v}, \underline{\lambda})$ for values of t equal to $t_1, t_2 \ldots t_m$ and where $w_1, w_2 \ldots w_m$ are the experimental weighting factors provided by the user. All data points were weighted according to the statistical uncertainty, σ_i, in the measured peak area (i.e. $w_i = 1/\sigma_i^2$). The reduced chi-square or variance ratio, χ_r^2, is determined from the weighted sum of squares S by dividing this quantity by the number of degrees of freedom, equal to m minus the number of free adjustable parameters.

Corrections to peak area data to take into account the decay of the source whilst γ counting is in progress require that $f(t_i, \underline{v}, \underline{\lambda})$ be replaced by the complete expression

$$f'(t_i, \underline{v}, \underline{\lambda}) = \sum_{j=1}^{n} \frac{v_j}{\lambda_j} \left[e^{-\lambda_j t_i} - e^{-\lambda_j t_{i+1}} \right]$$

$$= \sum_{j=1}^{n} v_j e^{-\lambda_j t_i} \left(\frac{1 - e^{-\lambda_j \Delta T_i}}{\lambda_j} \right) \qquad (5.3)$$

where ΔT_i is the preselected γ counting interval beginning at time t_i. For $T_i \ll (T_{\frac{1}{2}})_j$, where $(T_{\frac{1}{2}})_j = \log_e 2/\lambda_j$, eqn. 5.3 reduces to

$$f'(t_i, \underline{v}, \underline{\lambda}) \simeq \sum_{j=1}^{n} \left[v_j \Delta T_i e^{-\lambda_j t_i} \right]$$

and for equal ΔT_i used throughout the complete γ counting period then

$$f'(t_i,\underline{v},\underline{\lambda}) = \Delta T_i f(t_i,\underline{v},\underline{\lambda}). \qquad (5.4)$$

Hence, $f'(t_i,\underline{v},\underline{\lambda})$ and $f(t_i,\underline{v},\underline{\lambda})$ are equivalent apart from a constant factor (ΔT_i) which implies that both functions should predict identical fitted half-life components using the same initial data. In the case of the two runs performed at E_α = 29.97 MeV where unequal intervals ΔT_i of 4 and 15m were used throughout the γ counting period, eqn. 5.3 was used to fit the experimental data. In all other runs (using constant ΔT_i) both eqns. 5.2 and 5.3 were used to fit the experimental data; within the uncertainty limits predicted by the fitting routines, both functions were found to produce identical fits in accordance with eqn. 5.4.

Table 5.4 lists the results of fitted ^{241}Np half-life values for the PuKα_1 X-ray and 133 and 175 keV γ-ray peaks determined by weighted least squares analysis. Except at the lowest incident α beam energy used here, three exponential decay components were used to fit the peak area decay data for the PuKα_1 X-ray peak (to take into account the presence of ^{239}Np, ^{240}Np and ^{241}Np) and two components were used to fit the 175 keV γ-ray peak area data (to take into account the presence of ^{240}Np and ^{241}Np); at the lowest α beam energy, where there was no evidence for the production of ^{240}Np, the number of components required to fit the PuKα_1 X-ray and 175 keV γ-ray peak area data were reduced by one accordingly. Where sufficient peak area statistics allowed, the 133 keV γ-ray peak area decay data was expected to follow a simple exponential decay.

Table 5.4 Fitted ^{241}Np Half-life values (m)

Peak (keV)	E_α(MeV)				
	27.87	29.88	29.97*	32.17	37.01
103.76 (PuKα_1)	16.3±1.4	14.8±1.0	12.9±3.7 12.7±1.1	14.1±0.8	21.3±5.7
133	-	12.0±1.5	- 12.9±2.2	13.8±2.9	-
175	13.7±2.9	12.5±3.4	12.1±1.7 13.3±3.3	22.5±4.0	13.5±3.2

*Two runs performed at this energy.

The most consistent set of half-life data was obtained from the two runs performed at E_α = 29.97 MeV in which the longer lived Np components present in the case of the 175 keV γ and PuKα_1 X-ray peaks were followed over a much longer γ counting period than was possible for all other runs. However, the simultaneously fitted ^{240}Np half-life values predicted by the programme for the same runs (i.e. E_α= 29.97 MeV) ranged from 48 to 54m, each with an associated uncertainty of ~ $\pm$ 10m. These half-life values are consistently lower than the most recently determined ^{240}Np half-life of 61.9m[7]. By imposing fixed ^{240}Np half-life values of between 60 and 67m (i.e. by covering the existing range of ^{240}Np half-life measurements) the least squares analysis yielded fitted ^{241}Np half-life values ranging from 11.5 to 14.1m, each with an associated uncertainty of ~ $\pm$ 2m. Thus the mean ^{241}Np half-life, whether determined by fixing the longer-lived ^{240}Np component (where applicable) or by allowing it to vary, is determined from the data obtained at E_α = 29.97 MeV to be of the order of 12.8m with an overall uncertainty of ~ 2m derived from the mean of the uncertainties quoted in table 5.4. This value is low compared with previously determined 16m measurements of the ^{241}Np half-life, but is in reasonable agreement with the most recent[6] 13.9m measurement of this particular half-life.

The majority of the remaining fitted ^{241}Np half-life values of table 5.4 are in broad agreement with the mean value determined from the γ decay data taken at E_α = 29.97 MeV. However, one grossly discrepant result is that obtained using 32.17 MeV α particles where, despite a predicted ~ 14m half-life from the 133 keV γ-ray and PuKα_1 X-ray peak area data, the 175 keV γ-ray peak area data is best fitted by a 22.5m component. No explanation can be offered to account for this result. Similarly the predicted 21.3m half-life using the PuKα_1 X-ray peak area data obtained at E_α = 37.01 MeV is high compared with other fitted half-life values determined from other PuKα_1 X-ray data. This discrepancy may be due to the fact that ^{240m}Np($T_{\frac{1}{2}}$ ~7m) is present at this particular value of E_α(and is also evident in the γ spectrum of fig. 5.4) which makes an accurate prediction of the ^{241}Np component more difficult because of the increased number of parameters required to fit the data. At all other incident α beam energies there is no evidence for the production of ^{240}Np.

The internal consistency of the set of fitted half-life values obtained from the 133 keV peak area decay data is not matched by the results obtained from the analysis of the PuKα_1 X-ray peak data where a large spread in absolute fitted values is observed despite the small errors quoted on individual fitted half-life values. This large spread is most likely due to the fact that the 75m γ accumulation period used in all runs except those at 29.97 MeV α beam energy was not long enough to allow the fitting routine to accurately deduce the relative contribution of the longer-lived components to the total peak area. Excluding the fitted value of 21.3m, then the remaining five predicted half-life values obtained from the analysis of the PuKα_1 X-ray peak area data yield a mean ^{241}Np half-life of ~ 14.2m; an overall uncertainty of ~ 1.5m in this mean value is derived from the mean of the quoted individual uncertainties listed in table 5.4.

Thus, from the data of table 5.4 (but excluding the fitted half-life values of 23.1 and 22.5m) the PuKα_1 X-ray, 133 keV γ-ray and 175 keV γ-ray yield mean ^{241}Np half-life values of (14.2 $\pm$ 1.5), (12.9 $\pm$ 2.2) and (13.0 $\pm$ 2.0)m respectively. These values are in reasonable agreement with the most recent ^{241}Np half-life measurement of (13.9 $\pm$ 0.2)m but are all low compared with the three previously reported half-life measurements of ~ 16m.

Fitted ^{240}Np half-life values of (76.7 $\pm$ 12.6) and (73.7 $\pm$ 12.3)m were obtained from an analysis of the γ decay data from the 271.1 and 448.1 keV γ transitions, respectively, produced at E_α = 37.01 MeV. Thus, taking into account the previously determined ^{240}Np half-life values of ~ 50m (from multiple decay curve analysis) and the present single decay components of ~ 75m, then the data could possibly be interpreted as being distributed about a mean ^{240}Np half-life of approximately 63m, which is in broad agreement with the currently published ^{240}Np half-life of 61.9m. The large spread in ^{240}Np half-life values observed in the course of this work undoubtedly reflects the fact that much longer γ accumulation periods, extending over many half-life periods, are required if an accurate estimate of the longer-lived decay constants is to be deduced from the available experimental data.

Peak area intercepts, corresponding to the values of extrapolated peak areas at the common reference time T of eqn. 5.1 (T being defined

here as the end of the irradiation period) are listed in table 5.5 for certain transitions arising from the decay of ^{237}Np, ^{240}Np and ^{241}Np.

Table 5.5 Fitted peak area Intercepts

Isotope	Peak (keV)	E_α(MeV)			
		27.87	29.88	32.17	37.01
^{241}Np	103.76 ($PuK\alpha_1$)	3769±116	5460±141	9958±211	5950±119
^{241}Np	175.4	660±52	797±88	1855±104	1048±108
^{240}Np	566.7	-	96±46	414±79	985±99
^{237}Np	86.5	4283±136	2033±68	2158±70	668±85

Table 5.6 lists the experimental $R(E_\alpha)$ values for the (α,p) and (α,pn) reactions determined using eqn. 5.1 and the data of table 5.5. For comparison purposes the two sets of R values for the (α,p) reaction have been normalised to unity at E_α = 27.87 MeV. In general there is good agreement between the $R(E_\alpha)$ values determined from the 175 keV γ-ray and $PuK\alpha_1$ X-ray peaks despite the fact that the value of $R(E_\alpha$ = 37.01 MeV), determined using the $PuK\alpha_1$ X-ray peak area data, may be erroneous because the corresponding fitted ^{241}Np half-life was previously found to be larger than expected.

The $R(E_\alpha)$ values for the two different reactions cannot be compared directly and only provide an estimate of the variation in individual reaction cross-sections as a function of E_α. The mean of the two sets of R values from the (α,p) reaction is plotted against E_α in fig. 5.7; the form of the excitation function for the $^{238}U(\alpha,p)^{241}Np$ reaction is thus approximately linear over the energy range 27 to 37 MeV. Table 5.6 also shows that the cross-section for ^{240}Np production increases more rapidly than the cross-section for ^{241}Np production over the same 27 to 37 MeV α particle energy range.

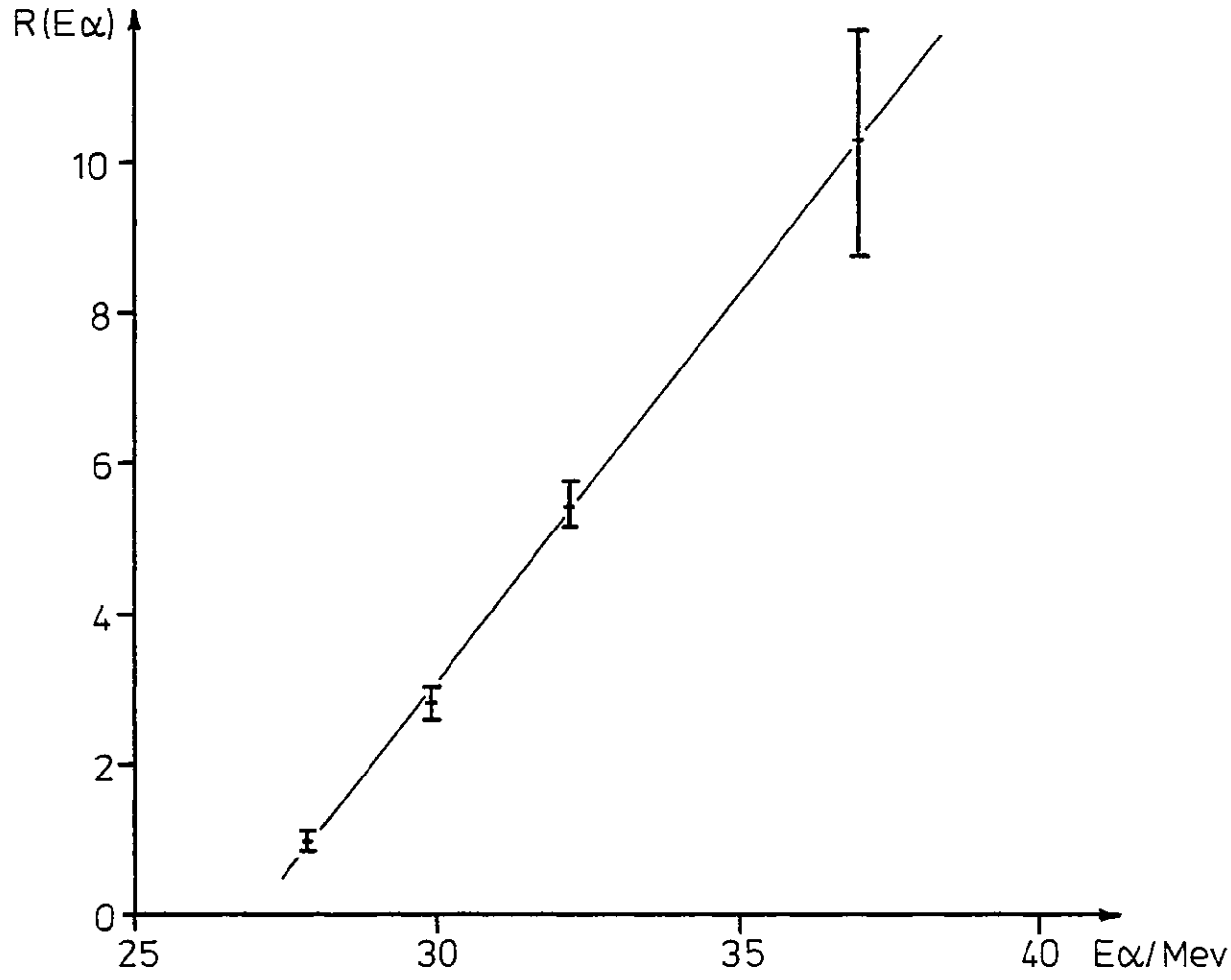

Fig. 5.7 Plot of $R(E_\alpha)$ vs E_α for the reaction $^{238}U(\alpha,p)^{241}Np$. $R(E_\alpha)$ is proportional to the cross-section for the production of ^{241}Np

Table 5.6 Experimental R Values (Proportional to Cross-Section) for α particle Induced Reactions on ^{238}U

E_α (MeV) \ Reaction Product / Peak used for analysis	(α,p) ^{241}Np		(α,pn) ^{240}Np
	Pu $K\alpha_1$ X-ray	175 keV γ	566.7 keV γ
27.87	1.00±0.04	1.00±0.08	-
29.88	3.06±0.30	2.60±0.30	0.05±0.02
32.17	5.24±0.20	5.73±0.32	0.19±0.04
37.01	10.13±1.31	10.47±1.71	1.48±0.24

5.4.4 Conclusions

A weighted mean ^{241}Np half-life of (13.6 ± 1.1)m is calculated from the results (reported in section 5.4.3) of the individual peak area decay curve analyses for the 133 and 175 keV γ-transitions and the associated Pu$K\alpha_1$ X-ray peak component arising from the internal conversion of weaker unobserved γ transitions following ^{241}Np β^- decay. The present half-life measurement is therefore in agreement with the most recent measurement of (13.9 ± 0.2)m reported by Parekh et al.[6] and thus the experimental data provide evidence for the successful production of ^{241}Np by the $^{238}U(\alpha,p)^{241}Np$ reaction over an incident 27 to 37 MeV α particle energy range. However the present investigation of ^{241}Np β^- decay has provided no further data on the excited level structure of ^{241}Np other than that it confirms the previously reported 133 and 175 keV γ transitions as the most intense within the ^{241}Pu level scheme.

Except at the lowest α beam energy considered here, the production of ^{241}Np is always accompanied by the production of ^{240}Np. The presence of ^{239}Np over the complete range of α beam energies considered here also implies that, on the experimental evidence available, there is no way to discriminate by suitable α beam energy selection against the production of this particular Np isotope. To obtain a high ^{241}Np yield for a given irradiation period then it is also necessary to select a high incident α beam energy (≥ 35 MeV, say) where the yield

is approximately one order of magnitude greater than that obtained at an E_α ~ 27 MeV. The factor of eight increase in ^{240}Np production over an incident E_α range of 32 to 37 MeV observed here, is approximately double the increase observed over the same energy range in earlier studies of α induced reactions in ^{238}U performed by Vandenbosch et al.[8]; however, the present studies are not able to confirm the decrease in the (α,pn) reaction cross-section observed by Vandenbosch et al. above an incident α beam energy of ~ 40 MeV.

Hence, on the evidence available, a suitable α beam energy for use in future in-beam ^{238}U(α,p)^{241}Np studies is approximately 37 MeV. The production of both ^{239}Np and ^{240}Np at this same incident α beam energy will require the use of particle identification techniques discussed in section 5.3.3 to identify those protons associated with the (α,p) reaction and which could be used as gating signals to build up a spectrum of coincident γ radiation.

For off-line measurements (and despite the extremely low ^{241}Np count rates achieved in the present experimental arrangement) more exhaustive chemical separations would help considerably in eliminating extraneous fission product activities which at present may be masking weak γ transitions from the decay of ^{241}Np (or any other Np isotope) produced during the α bombardment of ^{238}U. Attempts at using the other charged particle reactions discussed in section 5.3.3 may also lead to increases in the ^{241}Np yield, permitting a more comprehensive and accurate decay scheme analysis than is possible at present.

REFERENCES

1. R. Vandenbosch, Phys. Rev. 113, 259 (1959)

2. R.M. Lessler and M.C. Michel, Phys. Rev. 118, 263 (1960)

3. S.M. Qaim, Nucl. Phys. 88, 285 (1966)

4. F. Asaro, F.S. Stephens and I. Perlman, unpublished data (March 1957) quoted in E.K. Hyde, I. Perlman and G.T. Seaborg, (The Nuclear Properties of the Heavy Elements; Vol II: Detailed Radioactivity Properties (Prentice-Hall, New Jersey, 1964)

5. J.K. Dickens and J.W. McConnel, Phys. Rev. C22, 1344 (1980)

6. P.P. Parekh, E-M. Franz, S. Katcoff and L.K. Peker, Phys. Rev. C24, 2240 (1981)

7. P.P. Parekh, L.K. Peker, S. Katcoff and E-M Franz, Phys. Rev. C26, 2178 (1982)

8. R. Vandenbosch, T.D. Thomas, S.E. Vandenbosch, R.A. Glass and G.T. Seaborg, Phys. Rev. 111, 1358 (1958)

9. J.B.A. England, Techniques in Nuclear Structure Physics, Vol 2 (MacMillan, London, 1974) ch.5.

10. C.M. Lederer and V.S. Shirley, Table of Isotopes (7th ed., Wiley, New York, 1978)

APPENDIX 1

CALCULATION OF ^{239}U AND ^{239}Np YIELDS AND SPECIFIC ACTIVITIES PRODUCED BY REACTOR IRRADIATION OF ^{238}U

Inside the reactor neutrons are captured by the sample ^{238}U nuclei producing ^{239}U. The ^{239}U nuclei are destroyed by the capture of additional neutrons, and they are also removed by the process of radioactive β^- decay. The number of ^{238}U nuclei present is also being continuously reduced by the primary neutron capture process. The rate of build-up of ^{239}U nuclei, $\frac{dN_1}{dt}$, is therefore given by

$$\frac{dN_1}{dt} = -\lambda_1 N_1 + N\sigma_1\phi - N_1\sigma_2\phi \qquad \text{(A1.1)}$$

where λ_1 is the decay constant for ^{239}U

ϕ is the neutron flux

σ_1 is the ^{238}U neutron capture cross-section = 2.7 barns

σ_2 is the ^{239}U neutron capture cross-section = 22 barns

N is the number of ^{238}U nuclei present.

The rate of change of ^{238}U nuclei, $\frac{dN}{dt}$, is given by

$$\frac{dN}{dt} = -\sigma_1\phi N \qquad \text{(A1.2)}$$

The solution of the coupled differential eqns. A1.1 and A1.2 yield the ^{239}U activity, $A_1(t)$, where

$$A_1(t) = \frac{N_o\sigma_1\phi\lambda_1}{(\lambda_1 + \sigma_2\phi - \sigma_1\phi)}\left[e^{-\sigma_1\phi t} - e^{-(\lambda_1+\sigma_2\phi)t}\right] \qquad \text{(A1.3)}$$

N_o is the number of ^{238}U nuclei originally present in the sample, and t is the time elapsed since the beginning the irradiation.

Inside the 0^o Facility of the Imperial College 100 kW research reactor the maximum value of thermal neutron flux is quoted to be 1.8×10^{11} n $cm^{-2}s^{-1}$. Therefore, for the short irradiations carried out in this experiment the burn-up of the sample ^{238}U nuclei and removal of ^{239}U nuclei by further neutron capture can be neglected

and eqn. A1.3 can be rewritten as

$$A_1(t) = N_o\sigma_1\phi(1 - e^{-\lambda_1 t}) \qquad \text{(A1.4)}$$

The rate of change of ^{239}Np nuclei, $\frac{dN_2}{dt}$, during the irradiation period is given by the differential equation

$$\frac{dN_2}{dt} = -\lambda_2 N_2 + \lambda_1 N_1 - N_2\sigma_3\phi \qquad \text{(A1.5)}$$

where σ_3 is the ^{239}Np neutron capture cross-section $\simeq$ 45 barns. The solution of coupled eqns. A1.4 and A1.5 yields

$$N_2(t) = N_o\sigma_1\phi\left[\frac{1}{(\lambda_2 + \sigma_3\phi)} - \frac{e^{-\lambda_1 t}}{(\lambda_2 - \lambda_1 + \sigma_3\phi)} + e^{-(\lambda_2+\sigma_3\phi)t} \times \left\{\frac{1}{(\lambda_2 - \lambda_1 + \sigma_3\phi)} - \frac{1}{(\lambda_2 + \sigma_3\phi)}\right\}\right] \qquad \text{(A1.6)}$$

Again, the removal of ^{239}Np nuclei by neutron capture can be neglected and eqn. A1.6 can be rewritten as

$$N_2(t) = \frac{N_o\sigma_1\phi}{(\lambda_2 - \lambda_1)}\left[(1 - e^{-\lambda_1 t}) - \frac{\lambda_1}{\lambda_2}(1 - e^{-\lambda_2 t})\right] \qquad \text{(A1.7)}$$

from which $A_2(t) = \lambda_2 N_2(t)$.

Upon removal of the sample from the reactor the differential equations governing the rate of change of ^{239}U and ^{239}Np nuclei are given by eqns. A1.8 and A1.9 respectively;

$$\frac{dN_1}{dt} = -\lambda_1 N_1 \qquad \text{(A1.8)}$$

$$\frac{dN_2}{dt} = -\lambda_2 N_2 + \lambda_1 N_1 \qquad \text{(A1.9)}$$

For a reactor irradiation period T these equations have the solutions

$$N_1(t') = \frac{N_o \phi \sigma_1}{\lambda_1} (1 - e^{-\lambda_1 T}) e^{-\lambda_1 t'}$$

$$N_2(t') = \frac{N_o \phi \sigma_1}{(\lambda_2 - \lambda_1)} \left[(1 - e^{-\lambda_1 T}) e^{-\lambda_1 t'} - \frac{\lambda_1}{\lambda_2} (1 - e^{-\lambda_2 T}) e^{-\lambda_2 t'} \right]$$

where t' is the time elapsed since removal of the sample from the reactor. The ^{239}U and ^{239}Np activities follow immediately from $A_1(t') = \lambda_1 N_1(t')$ and $A_2(t') = \lambda_2 N_2(t')$.

APPENDIX 2

EFFECT OF BACKSCATTERING FROM THE ^{243}Am SOURCE SUPPORT

In the following calculation to estimate the magnitude of the effect of α particle backscattering from the stainless steel backing support only large-angle single scattered events will be considered as contributing to the total observed α particle counting rate. Such an approximation is valid for the case of a low-geometry counting system. Other approximations and simplifications made in the calculation are:-

(i) The source is approximated by a point source (of zero thickness) such that all scattering takes place in the source support. A point source approximation is valid for the geometry factors used in the course of the experiment.

(ii) The backing support is assumed to be nickel rather than stainless steel in order to simplify calculations of density of scattering centres and α-particle range.

(iii) All α particle scattering is assumed to take place at an energy $E_o/2$ where E_o is the full α particle energy; the differential Rutherford scattering cross-section is therefore independent of energy. For ^{243}Am $E_o \simeq 5.3$ MeV.

(iv) Corresponding to a mean energy $E_o/2$ the α particle has a maximum range of $R_o/2$ in the backing support where R_o is the full energy α particle range. $R_o \simeq 10$ mg cm^{-2} for 5.3 MeV α particles in nickel.

(v) For the scattered α particle to enter the detector the scattering angle ϕ (see fig. A2.1 is set equal to $(\pi - \theta)$.

In the absence of scattering the number of α particles, N_α, passing through the fractional solid angle Ω and being detected is given by

$$N_\alpha = N_o\Omega$$

where N_o is the absolute α activity of the source. If scattering occurs within the source backing then, using single scatter theory,

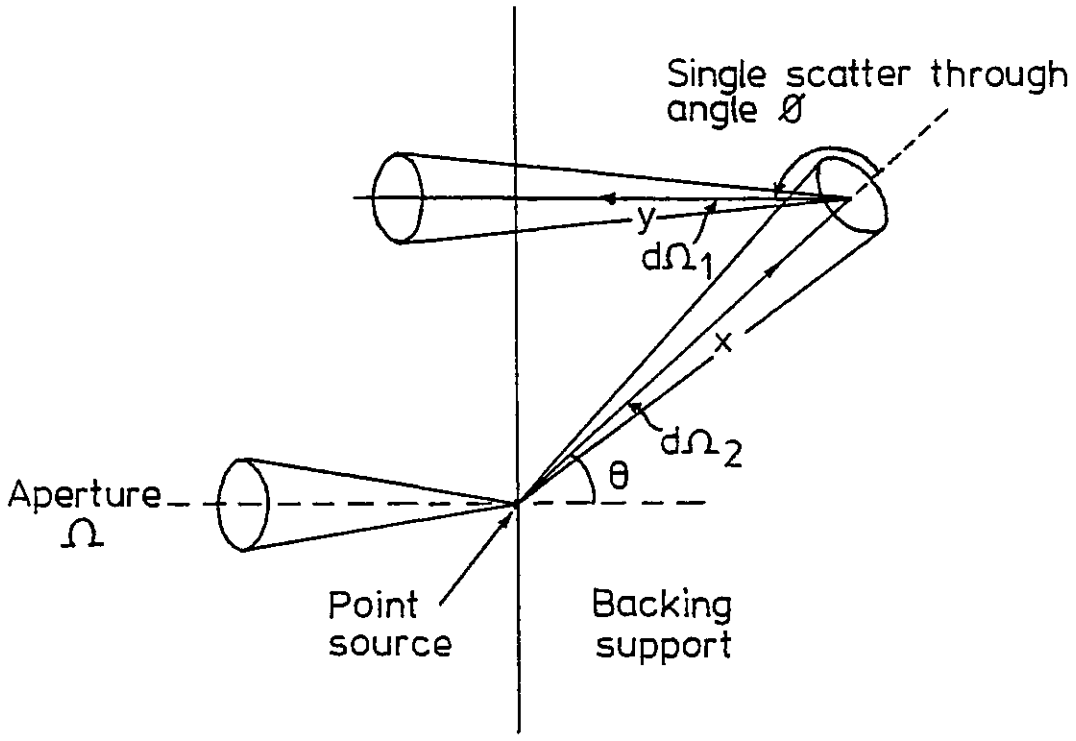

Fig. A2.1 Diagram of source support for large-angle backscattering corrections

the number of scattered α particles entering the detector, N'_α, can be expressed as (see fig. A2.1)

$$N'_\alpha = N_o \int_{\Omega_1} \int_{\Omega_2} \int_0^{x_{max}} n \, dx \left(\frac{d\sigma}{d\Omega}\right) d\Omega_2 d\Omega_1$$

Here $d\sigma/d\Omega$ is the differential Rutherford scattering cross-section and is given by

$$\frac{d\sigma}{d\Omega} = 1.296 \left(\frac{Z_1 Z_2}{E}\right)^2 \frac{1}{\text{Sin}^4(\phi/2)} \times 10^{-27} \text{ cm}^2/\text{atom (E in MeV)}.$$

Z_1 and Z_2 are the atomic numbers of the projectile and scattering (target) nuclei respectively and E is the energy of the projectile upon scattering. n is the density of scattering centres (= $N_A \rho/A$; N_A = Avogadro's number, ρ = density of backing support,

A = atomic weight of the support) and the constraint $x + y \leq R_o/2$ leads to a value of $x_{max} = R_o/\{2(1 + \cos\theta)\}$.

Using the approximation that after a single scattering event, the solid angle subtended by the aperture is still Ω, then the above expression for N'_α reduces to

$$N'_\alpha \simeq N_o \Omega n 2\pi \; 1.296 \left(\frac{Z_1 Z_2}{E}\right)^2 \times 10^{-27} \left(\frac{R_o}{2}\right) \times$$

$$\left[\int_{\theta=0}^{\pi/2} \frac{1}{(1 + \cos\theta)} \frac{1}{\cos^4(\theta/2)} \sin\theta \; d\theta\right]$$

The term in square parentheses is equal to 3/2. Substitution of numerical values into the above expression yields
$N'_\alpha \simeq (5.64 \times 10^{-4}) \; N_o \Omega$.

Hence $N'_\alpha/N_\alpha \simeq 5.6 \times 10^{-4}$ and a correction of the order of 0.06% must be applied to the measured absolute α disintegration rate to take into account those α particles backscattered from the source support.

APPENDIX 3

CORRECTIONS TO PEAK AREAS

A3.1 Coincidence summing

Whenever a decay scheme includes γ-rays that are in cascade, coincidence summing will affect the areas of the peaks observed in a γ spectrum. The magnitude of the effect depends on the specific features of the decay scheme and on the solid angle subtended by the detector from the source. Depending on whether each photon deposits its full energy (F) or only part of it (P) in the detector there are several possible consequences; for a simple cascade of two γ-rays the possible combinations are:

$F_1 + F_2$, which results in the "coincidence sum peak",

$F_1 + P_2$ or $P_1 + F_2$, which give rise to "peak loss" effects,

$P_1 + P_2$ which contribute only to the smooth background and does not influence intensities of full-energy peaks.

A cascade involving more than two γ-rays gives rise to further terms.

Consider the decay scheme shown in fig. A3.1. Levels 1 and 2 are populated with intensities N_1 and N_2; transitions from level i to j are assigned internal conversion coefficients α_{ij} and total branching ratios (i.e. γ-ray plus conversion) F_{ij}. The observed full-energy (photoelectric) peak (FEP) intensities S_{ij} are given by the following expressions:

$$S_{10} = \frac{N_1 \varepsilon_{10}}{(1 + \alpha_{10})} + N_2 F_{21} \frac{\varepsilon_{10}}{(1 + \alpha_{10})} \left(1 - \frac{\varepsilon_{21}^T \bar{W}_{21:10}}{(1 + \alpha_{21})}\right) \qquad \text{(A3.1)}$$

$$S_{21} = \frac{N_2 \varepsilon_{21}}{(1 + \alpha_{21})} F_{21} \left(1 - \frac{\varepsilon_{10}^T \bar{W}_{21:10}}{(1 + \alpha_{10})}\right) \qquad \text{(A3.2)}$$

$$S_{20} = N_2 \left[\frac{\varepsilon_{20} F_{20}}{(1 + \alpha_{20})} + F_{21} \frac{\varepsilon_{21} \varepsilon_{10} \bar{W}_{21:10}}{(1 + \alpha_{21})(1 + \alpha_{10})} \right] \qquad \text{(A3.3)}$$

The quantity ε_{ij} is the FEP detection efficiency for a γ-ray of energy E_{ij} and ε_{ij}^T is the corresponding total detection efficiency;

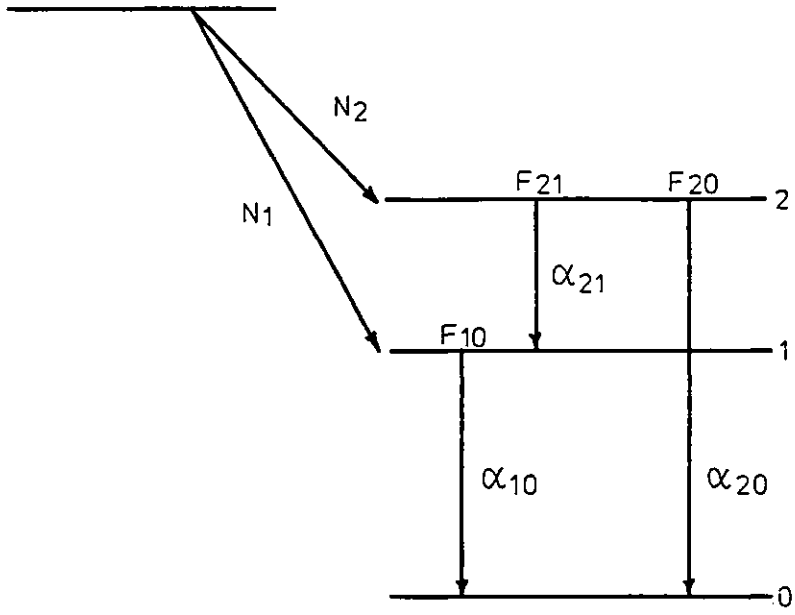

Fig. A3.1 A simple decay scheme. N_1 and N_2 are respectively the percentages of direct decays to levels 1 and 2; F_{21} is the "total" branching ratio (i.e. γ-ray plus conversion electron) for transitions from level 2 to 1, and α_{21} is the total conversion coefficient of this transition

$\bar{W}_{ik:lm}$ is the angular correlation function of cascade γ-rays of energy E_{ik} and E_{lm} taking finite geometry corrections into account. Terms containing two efficiency terms represent a correction due to coincidence summing. The X-rays produced by internal conversion can be taken into consideration in the calculation of the observed FEP intensities. Here it is assumed that corrections are important for only the most intense group of X-ray peaks arising from either K or L shell internal conversion. This is done simply by replacing ε^T_{ij} with $\varepsilon^T_{ij} + \alpha^{K(L)}_{ij}\omega_{K(L)}\varepsilon^T_{K(L)}$

$\alpha^{K(L)}_{ij}$ = the K(L) shell internal conversion coefficient for γ_{ij},

$\omega_{K(L)}$ = fluorescence yield for the daughter element, and

$\varepsilon^T_{K(L)}$ = total detection efficiency at the mean K(L) X-ray energy.

Therefore, if the transition γ_{21} in the above example is highly

internally converted, the expression for S_{10} (eqn. A3.1) is more accurately given by

$$S_{10} = \frac{N_1\varepsilon_{10}}{(1+\alpha_{10})} + N_2 \frac{F_{21}\varepsilon_{10}}{(1+\alpha_{10})}\left[1 - \frac{1}{(1+\alpha_{21})}\left\{\varepsilon_{21}^{T}\,\bar{W}_{21:10} + \alpha_{21}^{K(L)}\omega_{K(L)}\varepsilon_{K(L)}^{T}\bar{W}_{K(L):10}\right\}\right] \qquad (A3.4)$$

whilst the expressions for S_{21} and S_{20} remain unchanged. The term $\bar{W}_{K(L):10}$ represents the angular correlation between the K(L) X-ray and the unconverted γ in the cascade.

Similar expressions to those given for the simple example shown in fig. A3.1 have been developed for the major transitions occurring in the decay of the ^{57}Co, ^{133}Ba and ^{241}Am standard γ sources used to determine the Ge detector efficiency curve. In each case coincidence summing effects include terms arising from the summing of Cs K X-rays, Fe K X-rays and Np L X-rays with γ transitions occurring in the decay of ^{133}Ba, ^{57}Co and ^{241}Am respectively, as well as the usual γ-γ coincidence terms.

A3.2 Calculation of total detection efficiency

The total detection efficiency at the 105 mm source-detector separation was computed for a standard source γ-ray energy, E, using the relation[1]

$$\varepsilon_{\gamma}^{T}(E) = \frac{1}{4\pi}\sum_{i} e^{-\mu_i(E)x_i}\int\left[1 - e^{-\mu_{Ge}(E)t}\right] d\Omega \qquad (A3.5)$$

where $\mu_{Ge}(E)$ is the total absorption coefficient in Ge and t is the path length of the γ-ray in the detector. The integral is performed over the solid angle subtended by the detector (Ω). The term $\sum_i e^{-\mu_i(E)x_i}$ represents the attenuation of radiation by the 6 mm thick perspex absorber (used to stop electrons entering the detector) and the thin Be window of the Ge detector. For calculation purposes the required values of $\mu_{Ge}(E)$ were interpolated by expressing $\mu_{Ge}(E)$ in the polynomial form

$$\log_e[\mu_{Ge}(E)] = \sum_{i=1}^{4} a_i (\log_e E)^i \qquad \text{(A3.6)}$$

using a least-squares fitting procedure.

As the detector is cylindrically symmetric, eqn. A3.5 may be written in the form

$$\varepsilon_\gamma^T(\theta,E) = \frac{\sum_i e^{-\mu_i(E)x_i}}{2}\left[\int_0^{\theta''} \{1 - e^{-\mu_{Ge}(E)t(\theta)}\}\mathrm{Sin}\theta d\theta\right] \qquad \text{(A3.7)}$$

where, for the source - Ge crystal dimensions shown in fig. A3.2,

$$t(\theta) = h/\mathrm{Cos}\theta \qquad \text{for } 0 \le \theta \le \mathrm{Tan}^{-1}\left(\frac{r}{h+d}\right) = \theta'$$

$$t(\theta) = r/\mathrm{Sin}\theta - d/\mathrm{Cos}\theta \quad \text{for } \theta' \le \theta \le \mathrm{Tan}^{-1}(r/d) = \theta''$$

The values of absorption coefficients used in eqn. A3.6 are taken from the tabulated photon cross-section data of Storm and Israel[2]. The angles θ' and θ'' are calculated to be 10.76^o and 11.76^o respectively for the 15 cm^2 x 10 mm deep Ge detector used in this experiment.

A3.3 Angular correction factors

For a general γ-γ cascade (see fig. A3.3) the directional correlation assuming two point detectors (each gated to detect one or other of the cascade γ-rays) is given by the expression[3]

$$W_{\gamma 1:\gamma 2}(\alpha) = \sum_k A_k^{(1)} A_k^{(2)} P_k(\mathrm{Cos}\alpha) \qquad \text{(A3.8)}$$

The P_k are the even Legendre polynomials i.e. the summation is over the even integers including zero. The $A_k^{(1)}$ and $A_k^{(2)}$ depend only on the spins and multipolarities of the first and second transitions of the cascade, respectively. If the first transition proceeds from I_1' to I with a mixture of multipolarities L_1 and $L_1' = L_1 + 1$ (mixing ratio δ_1) then $A_k^{(1)}$ is given by[3]

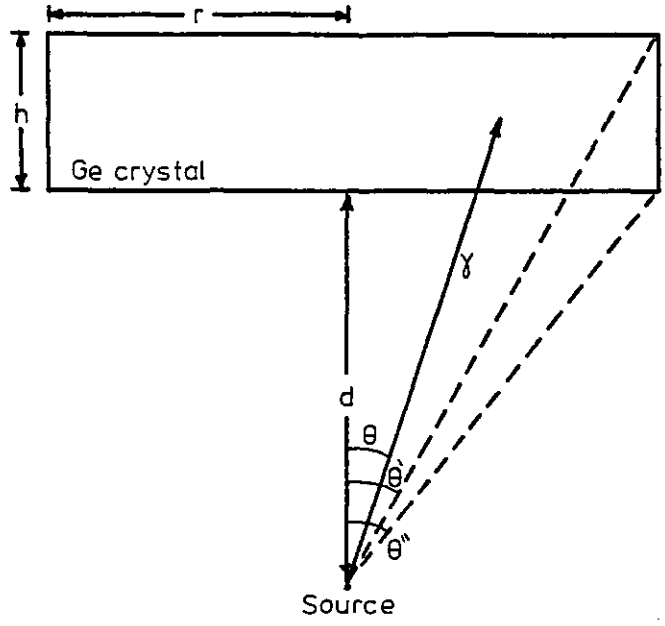

Fig. A3.2 Definition of angles θ',θ" for the case of a cylindrically symmetric detector (thickness h, radius r) located at a distance d from an axially mounted point source

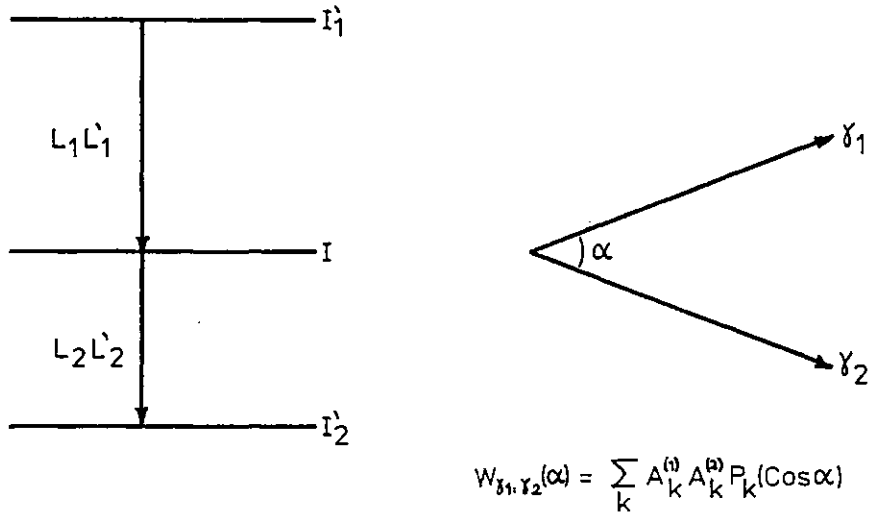

Fig. A3.3 Quantum numbers involved in a nuclear radiation cascade and which are required to calculate the angular correlation function $W_{\gamma 1:\gamma 2}(\alpha)$

$$A_k^{(1)} = \frac{F_k(L_1L_1I_1'I) + 2\delta_1 F_k(L_1L_1'I_1'I) + \delta_1^2 F_k(L_1'L_1'I_1'I)}{(1 + \delta_1^2)} \qquad (A3.9)$$

where

$$F_k(L_1L_1'I_1'I) = (-1)^{I_1'+I-1}\left[(2L_1 + 1)(2L_1' + 1)(2I + 1)(2k + 1)\right]^{\frac{1}{2}} x$$

$$\begin{pmatrix} L_1 L_1' & k \\ 1 & -1 & 0 \end{pmatrix} \begin{Bmatrix} L_1 L_1' k \\ I \; I \; I_1' \end{Bmatrix} \qquad (A3.10)$$

In the second line of the expression for $F_k(L_1L_1'I_1'I)$ () is a Wigner 3-j symbol[4,5] and can be expressed in terms of a Clebsch-Gordan coefficient representing the coupling of two angular momenta. {} is the Wigner 6-j symbol[4,5] and is related to the more familiar Racah W coefficient[4,5], which again can be expressed in terms of four Clebsch-Gordan coefficients representing the coupling of three angular momenta. For a pure multipole transition ($\delta_1 = 0$, $L_1 = L_1'$) $A_k^{(1)} = F_k(L_1L_1I_1'I)$.

Similarly for the second transition $I \rightarrow I_2'$ with L_2 mixed with $L_2' = L_2 + 1$ (mixing ratio δ_2):

$$A_k^{(2)} = \frac{F_k(L_2L_2I_2'I) + 2\delta_2 F_k(L_2L_2'I_2'I) + \delta_2^2 F_k(L_2'L_2'I_2'I)}{(I + \delta_2^2)} \qquad (A3.11)$$

The expression for F_k (eqn. A3.10) satisfies

$$F_o(L_1L_1'I_1'I) = \delta_{LL'}$$

and therefore eqn. A3.8 can be written in the form

$$W_{\gamma 1:\gamma 2}(\alpha) = 1 + A_2P_2(\mathrm{Cos}\alpha) + A_4P_4(\mathrm{Cos}\alpha) + \ldots$$

where $A_2 = A_2^{(1)}A_2^{(2)}$ and $A_4 = A_4^{(1)}A_4^{(2)}$.

In the case of coincidence summing $\alpha = 0$ and a single γ detector is used to register both cascade γ-rays. Restricting the series to $k = 0,2,4$ only (for practical reasons), the angular correlation function reduces to

$$W_{\gamma 1:\gamma 2}(0) = 1 + A_2 + A_4 \qquad \text{(A3.12)}$$

A3.4 Effect of finite γ detector size

The directional correlation of the γ-rays γ_1 and γ_2 averaged over the solid angle subtended by the detector is given by[3]

$$\bar{W}_{\gamma 1:\gamma 2}(\alpha) = \sum_k A_k Q_k P_k(\mathrm{Cos}\alpha) \qquad \text{(A3.13)}$$

where the coefficients $Q_k = Q_k^{(1)} Q_k^{(2)}$ are solid-angle correction factors expressed as a product of the individual correction factors for γ_1 (of energy E_1) and γ_2 (of energy E_2). The coefficients $Q_k^{(i)}$ are defined, in the case of cylindrical symmetry, by the equation[6]

$$Q_k^{(i)} = \frac{\int P_k(\mathrm{Cos}\theta)\varepsilon_\gamma^T(\theta,E_i)\mathrm{Sin}\theta d\theta}{\int \varepsilon_\gamma^T(\theta,E_i)\mathrm{Sin}\theta d\theta} \qquad \text{(A3.14)}$$

where $\varepsilon_\gamma^T(\theta,E_i)$ has been previously defined in eqn. A3.7 and the integrations are performed over the same θ limits for each E_i since only one detector is used to detect both cascade γ-rays. Therefore, taking into account the finite γ detector size, eqn. A3.12 can be rewritten in the form

$$\bar{W}_{\gamma 1:\gamma 2}(0) = 1 + A_2 Q_2 + A_4 Q_4 \qquad \text{(A3.15)}$$

Coefficients A_2, A_4 have been calculated for all relevant γ_1-γ_2 cascade transitions in the standard γ sources which give rise to coincidence summing effects. Coefficients Q_2, Q_4 have also been computed (by numerical integration of eqn. A3.14) to obtain values for $\bar{W}_{\gamma 1:\gamma 2}(0)$. To simplify the coincidence summing effect terms involving X-rays, the expression $\bar{W}_{X:\gamma}(0)$ has been set equal to 1.0. Where necessary triple cascade (γ_1 - γ_3) correlation functions have been calculated[7].

A3.5 Absorber corrections

The spherical, 1 mm diameter γ standard sources are sealed between clear polystyrene windows of 0.5 mm thickness each. Therefore the effects of absorption and scattering of radiation in the source window must be taken into account when determining the Ge detector efficiency in order that systematic errors in absolute γ-ray intensities from the unsealed ^{239}U and ^{243}Am sources be avoided.

An identical polystyrene window obtained from the manufacturer of the γ standard sources was used to determine experimentally the absorption effects as a function of incident γ-ray energy and the results compared with a theoretical prediction of the γ-ray attenuation in polystyrene using the known γ-ray absorption coefficients in carbon and hydrogen[2]. Within the limits of experimental and calculational error the γ transmission factors for the 0.5 mm polystyrene window were found to be in good agreement and the measured FEP efficiencies obtained from the standard sources were corrected by a factor derived from the mean of the experimental and calculated transmissions. Small adjustments to the mean transmission factors were made where poor peak area data precluded an accurate experimental measurement of the γ transmission in order to produce a consistent set of transmission factors which varied smoothly over the required energy range.

In a similar manner the γ absorption in the 6 mm perspex has been determined as a function of incident γ-ray energy using the tabulated absorption coefficients[2] in carbon, hydrogen and oxygen. The required values of $\mu_{Pe}(E)$ were interpolated by expressing $\mu_{Pe}(E)$ in the polynomial form given by eqn. A3.6. These values were used in the calculation of the overall total detector efficiency (eqn. A3.7) in which the γ attenuation effects in the 0.56 mm Be window of the Ge detector and the 0.5 mm polystyrene window of the standard source were assumed negligible compared with the attenuation caused by the 6 mm perspex absorber.

A3.6 Tabulated results of corrections to peak areas

Figures A3.4, A3.5 and A3.6 show simplified level scheme diagrams indicating the major γ transitions following the decay of the ^{57}Co, ^{133}Ba and ^{241}Am γ standard sources respectively. Tables A3.1-A3.5 list the relevant data discussed in sections A3.1-A3.5 required to calculate final coincidence summing corrections (table A3.6) for the γ-ray energies used in the detector efficiency calibration.

In the case of ^{133}Ba the 'theoretical' $\bar{W}_{\gamma 1:\gamma 2}(0)$ angular correlation values (table A3.5) have been calculated using the theoretical A_2, A_4 coefficients together with the experimental Q_2, Q_4 values (table A3.2); these values are found to be in good agreement with the tabulated 'experimental' $\bar{W}_{\gamma 1:\gamma 2}(0)$ values which have been derived from the previously measured A_2, A_4 coefficients and the same experimental Q_2, Q_4 coefficients.

At low energies ($\lesssim$ 80 keV) the photoelectric cross-section dominates and it is expected that the measured FEP efficiencies, ε_γ, be comparable with the calculated total detection efficiencies, ε_γ^T; the efficiency data of tables A3.1-A3.3 reflect this general trend although in some cases the total detection efficiencies are found to be slightly less than the corresponding measured FEP efficiencies. These differences reflect the rather simplified approach to the calculation of the γ detection efficiency within the Ge crystal and the γ attenuation in the 6 mm thick perspex absorber.

Coincidence summing corrections for major γ transitions have been determined using the measured full energy peak efficiencies*, the computed total detection efficiencies, the calculated angular correlation factors and I.C.C.'s, level branching fractions and level feeding intensities from the existing decay scheme data. The magnitude of the summing correction is determined by taking the difference between the FEP intensity calculated on the assumption of no coincidence summing effects within the level scheme and the calculated observed FEP intensity; this difference is then expressed as a percentage of the observed full-energy peak intensity to give a final % coincidence summing correction. A negative coincidence summing correction indicates that the measured γ-ray peak area must be reduced by the

*The correction to a peak area due to the effect of coincidence summing can be interpreted as a correction to the FEP efficiency. Therefore it is not strictly correct to use the measured FEP efficiencies to determine the coincidence summing corrections since the experimental efficiencies may each require correction to take into account similar summing effects. However, the production of a self consistent set of FEP efficiencies is beyond the scope of this work and therefore, to a first approximation, the magnitude of the coincidence summing corrections are assumed to be independent of any (small) change in the measured FEP efficiencies; for small summing corrections (say $\lesssim$ 3%) this is a valid approximation.

appropriate factor; this is equivalent to reducing the FEP efficiency at the γ-ray energy in question. A positive value of coincidence summing correction implies an increase in the FEP efficiency.

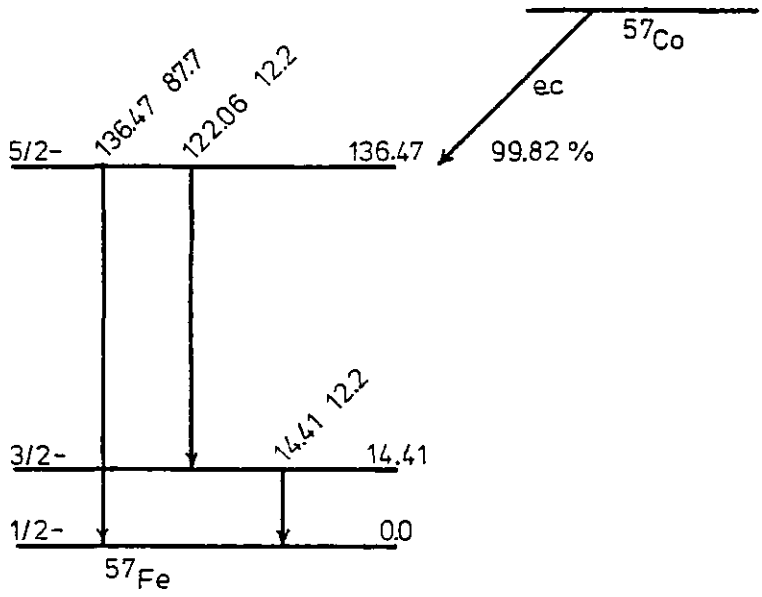

Fig. A3.4 Major γ transitions following decay of ^{57}Co standard source for which real coincidence summing effects must be taken into account. Transition intensities (γ + c.e per 100 source decays) are also given. Data taken from ref. 8

Table A3.1 ^{57}Co coincidence summing correction data

E (keV)	Transition type	δ	α	ε_γ a	ε_γ^T b	Q_2	Q_4
14.41	M1	0	8.2	3.733-3	3.565-3	0.968	0.898
122.06	M1 + E2	+0.120	0.0242	6.880-3	7.068-3	0.971	0.905
136.47	E2	0	0.147	5.676-3	6.115-3	0.971	0.904
Fe X-rays: $\bar{E}_{K\alpha} \simeq 6.4$ keV, $\bar{\varepsilon}^T_{K\alpha} \simeq 1.0\text{-}3$, $\omega_K = 0.32$							

a. Corrected for γ attenuation in 0.5 mm polystyrene window using data of table A3.4

b. Corrected for γ attenuation in 6 mm perspex using data of table A3.4

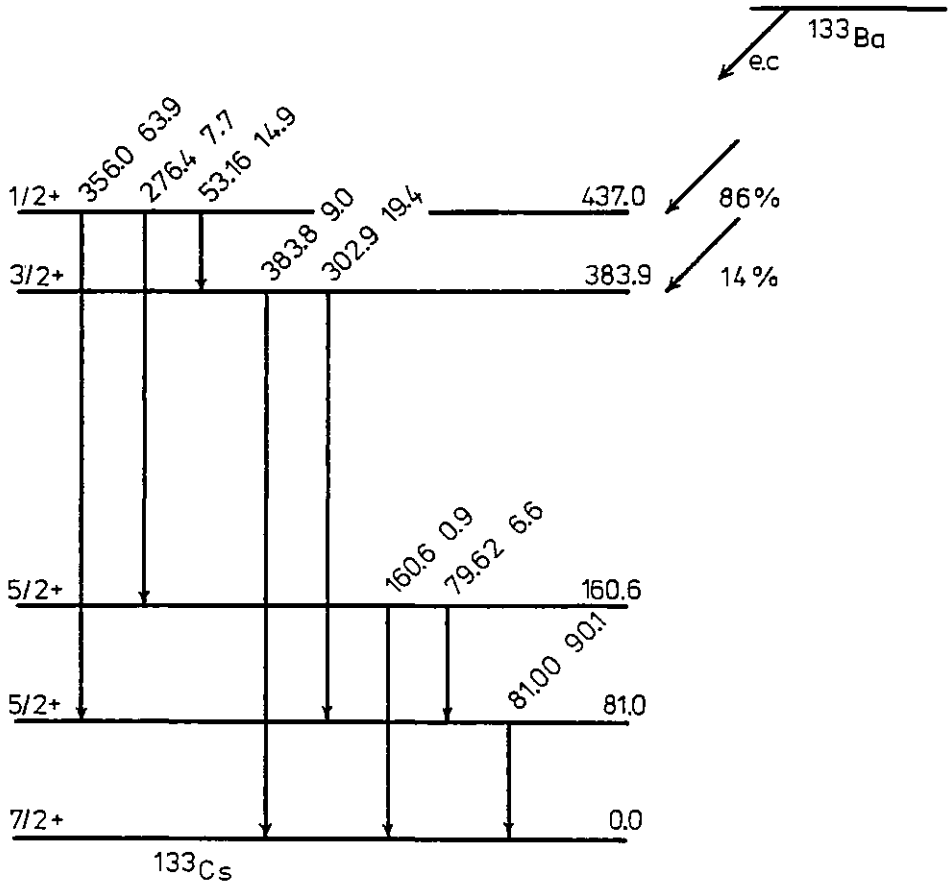

Fig. A3.5 Major γ transitions following decay of ^{133}Ba standard source for which real coincidence summing effects must be taken into account. Transition intensities (γ + c.e per 100 source decays) are also given. Data taken from ref. 9

Table A3.2 ^{133}Ba coincidence summing correction data

E (keV)	Transition type	δ	α	ε_γ [a]	ε_γ^T [b]	Q_2	Q_4
53.16	M1 + E2	+0.114	5.7	9.857-3	9.882-3	0.969	0.899
79.62	M1 + E2	+0.131	1.7	9.8 -3*	9.643-3	0.970	0.902
81.00	M1 + E2	-0.151	1.75	9.775-3	9.600-3	0.970	0.902
160.6	M1 + E2	+0.59	0.253	4.012-3	4.816-3	0.971	0.905
276.4	E2	0	0.0571	1.585-3	2.220-3	0.971	0.906
302.9	M1 + E2	-0.164	0.0431	1.327-3	2.004-3	0.971	0.906
356.0	E2	0	0.0256	9.896-4	1.725-3	0.971	0.906
383.8	E2	0	0.0205	8.6 -4*	1.630-3	0.972	0.906
Cs X-rays: $\bar{E}_{K\alpha} \simeq 32$ keV, $\bar{\varepsilon}^T_{K\alpha} \simeq 9.29\text{-}3$, $\omega_K = 0.895$							

a. Corrected for γ attenuation in 0.5 mm polystyrene window using data of table A3.4

b. Corrected for γ attenuation in 6 mm perspex using data of table A3.4

* Estimated

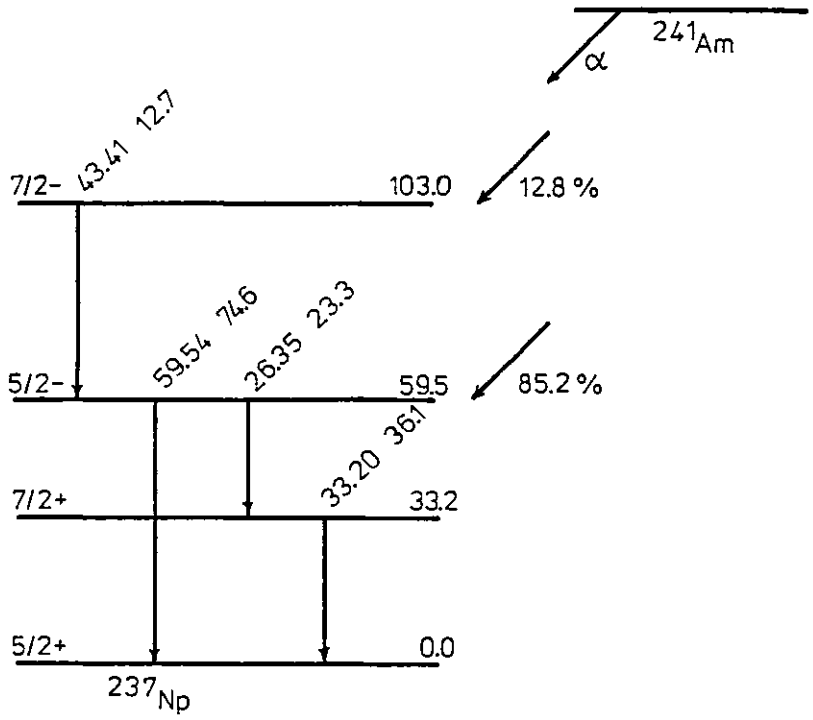

Fig. A3.6 Major γ transitions following decay of ^{241}Am standard source for which real coincidence summing effects must be taken into account. Transition intensities (γ + c.e per 100 source decays) are also given. Data taken from ref. 10

Table A3.3 ^{241}Am coincidence summing correction data

E_γ (keV)	Transition type	δ	α	ε_γ [a]	ε_γ^T [b]	Q_2	Q_4
26.35	E1	0	9.0	8.484-3	8.481-3	0.968	0.898
33.20	M1 + E2	0.134	188	1.051-2	9.301-3	0.968	0.899
43.41	M1 + E2	0.41	167	1.0 -2*	9.717-3	0.969	0.899
59.54	E1	0	1.15	1.053-2	9.889-3	0.969	0.900
Np X-rays: $\bar{E}_L \simeq 17$ keV, $\bar{\varepsilon}_L^T \simeq 5.46\text{-}3$, $\omega_L \simeq 0.445$							

a. Corrected for γ attenuation in 0.5 mm polystyrene window using data of table A3.4

b. Corrected for γ attenuation in 6 mm perspex using data of table A3.4

* Estimated

Table A3.4 γ transmission factors

E_γ (keV)	Mean$^+$ γ transmission factor for 0.5 mm polystyrene window	Calculated γ transmission factor for 6 mm perspex
14.41	0.95	0.34
26.35	0.975	0.81
32.20	0.982	0.89
43.41	0.986	0.94
53.16	0.989	0.96
59.54	0.989	0.96
81.00	0.990	0.97
122.06	0.991	0.97
136.47	0.991	0.97
160.6	0.991	0.97
276.4	0.992	0.97
302.9	0.993	0.97
356.0	0.994	0.97
383.8	0.994	0.97

$^+$average of experimental and calculated transmission factors

Table A3.5 Angular correlation factors

Source	Cascade	Calculated		Experimental		Calculated $\bar{W}_{\gamma 1:\gamma 2}(0)$	Exptl $\bar{W}_{\gamma 1:\gamma 2}(0)$
		A_2	A_4	A_2	A_4		
^{133}Ba	53γ -303γ	+0.194	0	+0.130	0	1.182	1.122
	53γ -384γ	-0.042	0	-0.034	0	0.961	0.968
	80γ -81γ	+0.037	-(1.7-5)	+0.037	-0.003	1.032	1.032
	276γ-80γ	+0.293	+ 0.004	-	-	1.280	-
	276γ-161γ	-0.423	- 0.019	-0.423	-0.030	0.586	0.576
	303γ-81γ	-0.044	+(4.8-5)	-0.043	+0.011	0.958	0.969
	356γ-81γ	+0.0357	- 0.0016	+0.0361	-0.0023	1.032	1.032
	276γ-81γ*	+0.023	+(2.3-4)	-	-	1.023	-
	53γ -81γ*	-0.015	0	-	-	0.986	-
^{57}Co	122γ-14γ	+0.122	0	-	-	1.115	-
^{241}Am	26γ -33γ	+0.023	0	-	-	1.022	-
	43γ -26γ	+0.087	0	-	-	1.082	-
	43γ -33γ*	+0.040	+(1.1-4)	-	-	1.038	-
	43γ -59γ	-0.278	0	-	-	0.739	-

*Denotes triple (γ_1-γ_3) cascade

Table A3.6 Coincidence summing corrections

Source	E_γ (keV)	Summing correction (%)
^{57}Co	14.41	0.78
	122.06	0.076
	136.47	-0.47
^{133}Ba	53.16	0.80
	81.00*	0.43**
	160.6	-2.84
	276.4	1.69
	302.9	1.34
	356.0	0.79
	383.8	-0.68
^{241}Am	26.35	0.28
	33.20	-0.80
	43.41	-3.07
	59.54	0.032

*Doublet consisting of unresolved 79.62 and 81.00 keV γ-ray peaks.

**Summing correction based on predicted 1.17 and 0.38% coincidence summing corrections for 79.62 and 81.00 keV γ-ray peaks respectively.

REFERENCES

1. R. Griffiths, Nucl. Instr. and Meth. 91, 377 (1971).

2. E. Storm and H. Israel, Nucl. Data Tables A7, 565 (1970).

3. H. Frauenfelder, R. M. Steffan, Alpha, Beta and Gamma-ray Spectroscopy (ed. K. Siegbahn, North Holland, Amsterdam, 1965) ch. 19.

4. D. M. Brink and G. R. Satchler, Angular Momentum (Oxford Univ. Press, London, 1962).

5. A. R. Edmunds, Angular Momentum in Quantum Mechanics (Princeton Univ. Press, New Jersey, 1957).

6. R. D. Gill, Gamma-ray Angular Correlations (Academic Press, London, 1975) ch. 3.

7. L. C. Biedenharn and M. E. Rose, Revs. Mod. Phys. 25, 729 (1953).

8. R. L. Auble, Nucl. Data Sheets 20, 327 (1977).

9. E. A. Henry, Nucl. Data Sheets 11, 495 (1974).

10. Y. A. Ellis, Nucl. Data Sheets 23, 123 (1978).

APPENDIX 4. BOUND STATE TRANSITION PROBABILITIES FOR ^{3}H AND ^{241}Pu

A4.1 Continuum and Bound Decay Transition Probabilities

The decay probability, P_C, for a continuum β^- transition is given by[1]

$$P_C = \frac{1}{2\pi^3} g^2 |M|^2 \left(\frac{c^4 m_e^5}{\hbar^7}\right) f(Z,W_o) \qquad (A4.1)$$

where g is the weak coupling constant, $|M|^2$ is the square of the nuclear matrix element and the quantity $f(Z,W_o)$ is an integral over the electron spectrum. $f(Z,W_o)$ is given by[1]

$$f(Z,W_o) = \int_1^{W_o} C_j(W) p W F(Z,W) (W_o - W)^2 dW \qquad (A4.2)$$

where $p(= p_e/m_e c)$ and $W(=E_e/m_e c^2)$ are the dimensionless electron momentum and total energy (i.e. including rest mass energy) and W_o is the corresponding maximum total electron energy. F(Z,W) is the Fermi factor equal to the ratio of the electron density at the daughter nucleus (of atomic number Z) to the density at infinity and $C_j(W)$ is a shape factor, dependent upon β^- transition type (e.g. j = 0,1,2 for allowed, first forbidden and second forbidden transitions respectively), which modifies the statistically predicted distribution of emitted electron energies.

The probability for bound state β^- decay, P_B, can be calculated using the time dependent formula[2]

$$P_B = \frac{2\pi}{\hbar} |H_{if}|^2 \rho(E) \qquad (A4.3)$$

where H_{if} is the matrix element of the weak interaction Hamiltonian operator between initial and final states i,f and $\rho(E)$ is the density of momentum states in the final system at the total energy E_o $(= W_o m_e c^2)$; $\rho(E)$ is defined in terms of the neutrino momentum, p_ν, accompanying the two body β^- decay process, and is given by

$$\rho(E) = \frac{4\pi p_\nu^2}{h^3 c} \quad . \qquad (A4.4)$$

If an electron is created in (say) the K shell following β^- decay then

$$|H_{if}|^2 = g^2|M|^2|\psi(0)|^2 \qquad \text{(A4.5)}$$

where $|\psi(0)|^2$ is the square of the s state wavefunction at the daughter nucleus. Eqns. A4.3, A4.4 and A4.5 combine to give

$$P_B = \frac{g^2}{\pi} |M|^2|\psi(0)|^2 \frac{E_\nu^2}{\hbar^4 c^3} \qquad \text{(A4.6)}$$

where E_ν is the emitted neutrino energy; since the binding energy of the created bound K-shell electron is much smaller than the total energy release then

$$E_\nu = (W_o - 1)m_e c^2 \qquad \text{(A4.7)}$$

and P_B becomes

$$P_B = \frac{g^2}{\pi} |M|^2|\psi(0)|^2 \left(\frac{m_e^2 c}{\hbar^4}\right)(W_o - 1)^2. \qquad \text{(A4.8)}$$

after substitution of eqn. A4.7 into A4.6. Therefore, the ratio of bound to continuum β^- decay transition probabilities is given, using eqns. A4.1 and A4.8, by the expression

$$\frac{P_B}{P_C} = 2\pi^2(\alpha a)^3|\psi(0)|^2 \frac{(W_o - 1)^2}{f(Z,W_o)} \qquad \text{(A4.9)}$$

where α = fine structure constant ($\sim 1/137$)

a = Bohr radius

A4.1.1 P_B/P_C for ^3H β^- decay

For ^3H (end point β^- energy $E_{\beta max}$ = 18.6 keV) the β^- transition is of the allowed type and the shape factor (C_o) is equal to unity; in this particular case $f(Z,W_o)$ may be integrated explicitly and, in the limit $(W_o - 1) << 1$, may be approximated by

$$f(Z,W_o) = \frac{16\sqrt{2}}{105} (W_o - 1)^{7/2}$$

Thus eqn. A4.9 becomes

$$(P_B/P_C)^3_H = \frac{105\pi^2}{8\sqrt{2}} (\alpha a)^3 |\psi(0)|^2 \left(\frac{m_e c^2}{E_{\beta max}}\right)^{3/2} \qquad (A4.10)$$

In this particular case $|\psi(0)|^2$ is the square of the $1s_{\frac{1}{2}}$ state wavefunction at the daughter nucleus and is given simply by $|\psi(0)|^2 = (1/\pi)(Z/a)^3$. Substitution into eqn. A4.10 yields

$$(P_B/P_C)^3_H = \frac{105\pi}{8\sqrt{2}} (\alpha Z)^3 \left(\frac{m_e c^2}{E_{\beta max}}\right)^{3/2} \qquad (A4.11)$$

The effective helium charge Z can be taken as 27/16[2] for a filled tritium shell and as 2 for an unfilled shell. Thus, from eqn. A4.11, the ratio $(P_B/P_C)^3H$ is $\sim 7.9 \times 10^{-3}$ for neutral tritium atom decay and $\sim 1.3 \times 10^{-2}$ for ionised tritium decay. (This calculation does not take into account the possibility of electron capture into an excited state of helium). Therefore the decay constant for ionised tritium is ~ 0.5% larger than the predicted decay constant for neutral tritium. This result agrees reasonably well with a 0.35% difference in decay constants predicted by Tikhonov and Chukreev.

The ratio $(P_B/P_C)^3H$ can also be calculated using the known experimental log ft value for the ^3H β^- decay transition; here f is equal to $f(Z,W_o)$ (defined in eqn.A4.2) and t is the partial half-life for the particular decay under consideration. Since ^3H decay proceeds via a 100% β^- branch to the ^3He ground state then the partial ^3H half-life is simply the total ^3H half-life of 12.35y. Hence, from the known log ft assignment[3] of 3.1, the value of $f(Z,W_o)$ is calculated to be $\sim 3.23 \times 10^{-6}$ s^{-1} and eqn.A4.9 predicts $(P_B/P_C)^3H$ $\sim 4.8 \times 10^{-3}$ for neutral tritium atom decay and $\sim 8.0 \times 10^{-3}$ for ionised tritium decay. The resulting 0.32% difference in total decay constants for the neutral and ionised tritium is now in closer agreement with the 0.35% difference predicted by Tikhonov and Chukreev.[4]

A4.1.2 P_B/P_C for ^{241}Pu β^- decay

To obtain an order of magnitude estimate of the ratio P_B/P_C for ^{241}Pu only electron capture into the $7s_{\frac{1}{2}}$ state of ^{241}Am has been considered. The ratio P_B/P_C for ^{241}Pu is given in terms of the

$(P_B/P_C)^{3}H$ ratio by the expression

$$\left(\frac{P_B}{P_C}\right)_{^{241}Pu} = \frac{|\psi_{7s_{\frac{1}{2}}}(0)|^2_{^{241}Am}}{|\psi_{1s_{\frac{1}{2}}}(0)|^2_{^{3}He}} \cdot \frac{f(Z,W_o)^{3}H}{f(Z,W_o)^{241}Pu} \cdot \frac{(E_{\beta max})^{2}{}^{241}Pu}{(E_{\beta max})^{2}{}^{3}H} \cdot \left(\frac{P_B}{P_C}\right)_{^{3}H} \qquad \text{(A4.12)}$$

The ^{241}Pu β^- transition to the ^{241}Am ground state (100%) is of 1st forbidden type; however, since ^{241}Pu has a low end-point β^- energy (i.e. $E_{\beta max} << m_e c^2$) the forbidden β^- spectrum shape can be approximated by an allowed shape for the decay and, for the purpose of estimating the ratio $(P_B/P_C)^{241}Pu$, eqn.A4.12 can be assumed to be insensitive to differences in spectrum shape factors for given transition types.

From the experimental log ft value of 5.8[3] for the ^{241}Pu β^- transition, $f(Z,W_o)^{241}Pu$ is calculated to be ~ 1.39×10^{-3} s^{-1}.

Assuming that the $7s_{\frac{1}{2}}$ and $1s_{\frac{1}{2}}$ wavefunctions can be approximated by hydrogenic forms with screening provided by the electrons inside the ones of interest and modified nuclear charges Z*, then the ratio of electron densities at the ^{241}Am and ^{3}He nuclei can be estimated from the expression

$$\frac{|\psi_{7s_{\frac{1}{2}}}(0)|^2_{^{241}Am}}{|\psi_{1s_{\frac{1}{2}}}(0)|^2_{^{3}He}} = \frac{(Z^*/n)^{3}{}^{241}Am}{(Z^*/n)^{3}{}^{3}He} \qquad \text{(A4.13)}$$

where $$Z^* = \frac{3a}{2\bar{r}} [\, n^2 - \ell(\ell+1)\,].^{(5)}$$

Here n, ℓ are the principal atomic quantum numbers for the particular electron under consideration ($\ell=0$ for s electrons), $\bar{r}$ is the corresponding mean orbital radius of the electron and a is the Bohr radius. For ^{241}Am, $\bar{r}/a$ for the $7s_{\frac{1}{2}}$ shell is ~4.2[6] and hence Z* for ^{241}Am is ~17.5; for ^{3}He Z* is equal to 27/16. Therefore the ratio of eqn.A4.13 is estimated to be ~ 3.3; substitution of this value into the expression for $(P_B/P_C)^{241}Pu$ (eqn. A4.12) yields

$$\left(\frac{P_B}{P_C}\right)_{^{241}Pu} \sim 10^{-2} \left(\frac{P_B}{P_C}\right)_{^{3}H}$$

Thus, since (P_B/P_C) for tritium is equal to ~ 1% (eqn.A4.11), then, according to the present calculation, the ratio (P_B/P_C) for ^{241}Pu is ~ 0.01%; this value is four orders of magnitude smaller than the corresponding ratio determined by Tikhonov and Chukreev[7] who obtained a value for $(P_B/P_C)^{241}Pu$ of ~ 100%. A similar order of magnitude estimate compared to the one calculated here for the ratio $(P_B/P_C)^{241}Pu$ has been obtained by Blin-Stoyle[8] using a parametric expression[9] to evaluate $f(Z,W_o)^{3}H$ and $f(Z,W_o)^{241}Pu$ assuming an allowed shape for the ^{241}Pu β^- decay.

Such large discrepancies in the calculated $(P_B/P_C)^{241}Pu$ ratio appear to be due to differences in the estimated ratio $|\psi_{7s}(0)|^2/|\psi_{1s}(0)|^2$; using tabulated (non-relativistic) Hartree-Fock wavefunctions[10,11] for ^{241}Am and ^{3}He this ratio is increased to ~ 5, less than a factor of two increase over than value obtained previously using simple screened hydrogenic wavefunctions. Relativistic corrections, particularly important for an atom as large as Pu, will certainly increase the value of $|\psi_{7s}(0)|^{2(12)}$ but would not account completely for the current factor of 10^4 difference between calculated $(P_B/P_C)^{241}Pu$ ratios of the present work and that value obtained by Tikhonov and Chukreev; at most the relativistic corrections would reduce the discrepancy by one, possibly two orders of magnitude. Thus, the $(P_B/P_C)^{241}Pu$ ratio derived here is still at least two orders of magnitude smaller than that proposed by Tikhonov and Chukreev.

REFERENCES

1. C.S. Wu and S.A. Moszkowski, Beta Decay (Wiley, New York, 1966) ch.2.

2. L.I. Schiff, Quantum Mechanics (3rd ed.,McGraw-Hill, Tokyo, 1968) ch.8

3. C.M. Lederer and V.S. Shirley, Table of Isotopes (7th ed., Wiley, New York, 1978)

4. V.N. Tikhonov and F.E. Chukreev, "Beta-decay of tritium into bound chemical states, and its effect on the accuracy of calorimetric measurements", INDC(CCP)-151/NE (1980)

5. S.W. Lovesey, C.D. Bowman and R.G. Johnson, Z. Phys. B47, 137 (1982)

6. I.M. Band and M.B. Trzhaskovskaya, CERN-Trans. 74-7

7. V.N. Tikhonov and F.E. Chukreev, "Comment on the half-life of ^{241}Pu", INDC(CCP)-ISI/NE (1980)

8. R.J. Blin-Stoyle. (Private communication)

9. D.H. Wilkinson and B.E.F. Macefield, Nucl. Phys. A232, 58 (1974)

10. E. Clements and C. Roetti, At. Data and Nucl. Data Tables 14, 177 (1974)

11. J.G. Snijders, P. Vernooijs and E.J. Baerends, At. Data and Nucl. Data Tables 26, 483 (1981)

12. A. Hibbert. (Private communication)